Physicochemical Studies on Amphiphilic Conjugates of Amino Alcohols

A thesis
Submitted for the degree of
DOCTOR OF PHILOSOPHY
in Chemistry

By
SUMAN KUMAR CHOUDHURY
Reg. No: 17CHPH57

Under the supervision of
Prof. Musti J. Swamy

School of Chemistry
University of Hyderabad
Hyderabad – 500 046
INDIA

April 2024

School of Chemistry
University of Hyderabad
Hyderabad – 500 046

CERTIFICATE

This is to certify that the thesis entitled "**Physiochemical Studies on Amphiphilic Conjugates of Amino Alcohols**" submitted by **Mr. Suman Kumar Choudhury** bearing the registration number 17CHPH57 in partial fulfillment of the requirements for the award of the Doctor of Philosophy (Ph.D.), is a bonafide work carried out by him under my supervision and guidance in the School of Chemistry, University of Hyderabad, India. This thesis is free from plagiarism and has not been submitted previously in part or in full to this or any other University or Institution for the award of any degree or diploma.

Parts of this thesis have been published/communicated for publication (or under preparation) as indicated below.

1. **Choudhury, S.K.;** Sivaramakrishna, D.; Swamy, M.J. Biophysical characterization of long chain *O*-acyl-β-alaninols and equimolar *O*-myristoyl-β-alaninol/sodium dodecyl sulfate complex, ***Colloids Surfaces A: Physicochem. Eng. Aspects*****.** 2024**,** 133483. **(Chapter 2)**

2. **Choudhury, S.K.;** Manasa, K.; Swamy, M.J. Long chain *O*-acyl-L-alaninols: Synthesis, biophysical characterization and formation of equimolar catanionic liposomes with sodium dodecyl sulfate. **(Manuscript under preparation) (Chapter 3)**

3. Sivaramakrishna, D.; **Choudhury, S.K.;** Swamy, M. J. Thermotropic phase behavior and supramolecular organization of *N, O*-diacyl-L-alaninols: effect on stratum corneum model membrane. ***J. Chem. Sci.*** 2021**,** 133, 91. **(Chapter 4)**

4. **Choudhury, S.K.;**[$] Sivaramakrishna, D.;[$] Swamy, M.J. Structure and supramolecular organization of *N*-acylserinols: agonists of the G-protein coupled receptor, GPR-119. ***J. Chem. Sci.*** 2023**,** 135, 1-9. ([$]These authors contributed equally) **(Chapter 5)**

The student has also made presentations at the following conferences:

1. Poster presentation at **"International Conference on Frontier Area of Science and Technology (ICFACT-2022)",** 12th India-Japan Science and Technology Seminar organized by Indian JSPS Alumni Association (IJAA), University of Hyderabad, Hyderabad.
2. Oral presentation at **"CHEMFEST-2023"** Annual in-house Symposium, organized by School of Chemistry, University of Hyderabad, Hyderabad.
3. Poster presentations at **"CHEMFEST-2020 and 2023"** organized by School of Chemistry, University of Hyderabad, Hyderabad.

Further, the student has passed the following courses towards the fulfillment of the coursework requirement for the Ph.D. degree:

Sl. No.	Course No.	Title of the Course	No. of Credits	Status
1	CY455	Biological Chemistry	3	Pass
2	CY801	Research Proposal	4	Pass
3	CY805	Instrumental Method-A	4	Pass
4	CY806	Instrumental Method-B	4	Pass

Hyderabad
April 2024

Prof. Musti J. Swamy
(Thesis Supervisor)

Prof. Musti J. Swamy
School of Chemistry
University of Hyderabad
Hyderabad – 500 046, India

Dean
School of Chemistry
University of Hyderabad

Dean
School of Chemistry
University of Hyderabad
Hyderabad-500 046.

School of Chemistry
University of Hyderabad
Hyderabad – 500 046

DECLARATION

I, **Suman Kumar Choudhury**, hereby declare that the thesis entitled "**Physiochemical Studies on Amphiphilic Conjugates of Amino Alcohols**," submitted by me under the guidance and supervision of **Prof. Musti J. Swamy,** is a bonafide research work which is free from plagiarism. Furthermore, I also declare that it has not been submitted previously in part or in full to this University or any other Institution for the award of any degree or diploma. By signing below, I agree that my thesis can be deposited with Shodganga/INFLIBNET.

A report on plagiarism from the University Library is enclosed.

Suman Kumar Choudhury

Suman Kumar Choudhury

Reg. No.: 17CHPH57

Prof. Musti J. Swamy

(Thesis Supervisor)

Prof. Musti J. Swamy
School of Chemistry
University of Hyderabad
Hyderabad – 500 046, India

DEDICATION

To my teachers, who have been my guiding light on the path of knowledge.

To my beloved family, whose love and care have been my constant source of strength and support.

To my friends, whose support and encouragement have continuously motivated and inspired me.

Contents

School of Chemistry
University of Hyderabad
Hyderabad – 500 046

STATEMENT

I hereby declare that the matter embodied in this thesis is the result of investigations I carried out at the School of Chemistry, University of Hyderabad, Hyderabad, under the supervision of **Prof. Musti J. Swamy**.

In keeping with the general practice of reporting scientific observations, due acknowledgments have been made whenever the work described is based on the findings of other investigators. Any omission that might have occurred due to oversight or error is regretted.

Hyderabad
April 2024

Suman Kumar Choudhury

Suman Kumar Choudhury

ACKNOWLEDGEMENT

This is a pleasant obligation to express my heartful thanks to all those who contributed in different ways to accomplish the thesis. It wouldn't be complete without thanking their contributions.

I would like to express my sincere gratitude to Prof. M. J. Swamy, my research supervisor, for his support and invaluable contributions throughout my PhD program. His guidance, encouragement, and freedom have allowed me to develop personally and professionally. I am deeply grateful for the opportunity to work under his guidance. Prof. Swamy's insightful suggestions have been instrumental in shaping my research and have provided me with a truly enriching and educational experience that I will always treasure. I am profoundly thankful for all he has done for me, and I am honored to have had him as my supervisor.

I extend my gratitude to Prof. Ashwini Nangia, the present dean, former dean(s), and faculty member at the School of Chemistry for their valuable suggestions at various stages and the infrastructure available at the school. I sincerely thank doctoral committee members Prof. Tushar Jana and Dr. Manju Sharma for their cooperation and support during the PhD journey.

I want to thank all the non-teaching staff of the SoC for being very helpful and supportive: Mr. Abraham, Mr. Gupta, Mr. Venkat, Mr. Durga Prasad, Mr. Anandam, Mr. Mahendra, Ms. Gita, Ms. Rani, and Ms. Radhika, in particular. I am also grateful to the School of Physics, UoH, for allowing an instrumentation facility for PXRD data collection. My special thanks to Dr. Durga Prasad, Dr. Rajesh, Mr. Kashilingam, Mr. Mahesh, Mr. Shyam, Mr. Durgesh, Mr. Mahendar, and Mr Vinaya for their assistance and cooperation during the TEM, AFM, single crystal XRD, DSC, DLS and NMR experiments.

I sincerely appreciate and thank my esteemed Master's Degree professors. My special thanks to Prof. K. Hanumae Gowd, Dr. Harish Holla, and Dr. N. S. Venkata Narayanan for their guidance, support, and insightful mentorship throughout my academic journey. Their dedication to teaching and relentless effort in demonstrating

research significance have profoundly influenced my perspective and approach to academic and scientific endeavors. Their motivation and encouragement have fueled my passion for research and instilled in me a desire to pursue my Ph.D. career. I am immensely thankful for their valuable contributions, which have played a pivotal role in shaping my academic trajectory. Their mentorship has been instrumental in my growth as a student and aspiring academic.

I extend my heartfelt gratitude and appreciation to all my degree lecturers, tutors, and school teachers, particularly Dr. Sarbeswar Mahapatra, Dr. Umakanta Dash, Mrs. Diptimayee Mohapatra, Sri Pradeep Kumar Panigrahi, Mr. Sahendra Kumar, Mr. Satyapriya Patel, Sri Lambodara Kalo, Sri Nilamani Tanti, Sri. Panchana Naik, Sri Bishnucharan Patel. Their collective efforts have been instrumental in shaping my career trajectory and nurturing my personal growth. Their influence has been invaluable from my early days of education to my current position as a research scholar. They instilled in me a passion for learning and ignited my enthusiasm for science, which continues to burn brightly in my pursuit of an academic career. Each educator's unique teaching style and insightful knowledge have left an indelible mark on my academic journey. I am deeply grateful for their efforts and contributions and aspire to carry forward their legacy by inspiring and nurturing the next generation of students. Thank you for being an integral part of my success story.

Acknowledging the immense significance of teamwork and camaraderie, I extend my heartfelt appreciation to my esteemed labmates and seniors. In particular, a special note of appreciation goes to Dr. D. Sivaramakrishna for his support, insightful suggestions, and mentorship, which significantly contributed to my research progress. I am also deeply thankful to Dr. Ravindar Chinapaka and Konga Manasa for their collaborative efforts in my research endeavors. I thank Dr. Mohini Suneel, Dr. SK Alim, Dr. Saradamoni Mandal, Sneha Banerjee, Guguloth Tejaswani, and Power S. Sonali, who have been steadfast companions on this arduous yet rewarding journey of being a Ph.D. Their support, intellectual collaboration, and willingness to share their expertise have been invaluable. Through countless hours spent together in the laboratory, we have collectively faced challenges, celebrated successes, and grown professionally and personally. Each one has contributed uniquely, fostering an environment of knowledge exchange and friendship that has enriched my academic experience. I am deeply grateful

for their friendship, guidance, and the sense of unity that we have fostered. Together, we have advanced our research and created lasting memories I will always treasure. I would also like to thank the M.Sc. project students and summer interns who worked in the laboratory, Madhu, Navin, Shalini, and Suman Mondal, for helping with my projects.

I extend my heartfelt gratitude and appreciation to my departmental seniors and friends, especially Dr. Rajendra Kumar Mallik, Dr. N Tanmaya Kumar, Dr. Sameeta Sahoo, Dr. Sipra Sucharita Sahoo, Dr. Soutrick Das, Dr. Mamina Bhol, Dr. B Gorachand, Dr. Smruti Pragya Dr. Subhalakshmi Ms. Suchismita, Dr. Manasi Dalei and Dr. Subham Datta who have played an instrumental role in guiding and supporting me throughout my PhD journey. Their valuable advice, shared experiences, and encouragement have been a beacon of light, illuminating the path through the intricate maze of research and academia. The countless discussions, both scholarly and casual, have broadened my perspective and enriched my academic pursuits. I am thankful for their patience, mentorship, and the genuine camaraderie we have built over the years. I would also like to thank my Odia juniors, Aradhana, Manoj, Sibani, Rajkiran, Aishwarya, Tapas, and Pragati for making my academic period beautiful and cheerful. Here's to the bonds we've formed and the knowledge we've gained – a treasure that will endure beyond these academic corridors.

I am thankful to all my Ph.D. batchmates (2018, January batch): Anand Sai, Sashikant, Arghadip, Praveen, Shyam, Vinod, Ramesh, Ajaya, Jhansi, Olivia, Kamala, Tabassum, Sneha, and Prasannatha for their support and encouragement.

I extend my heartfelt gratitude to my present and past hostel companions: Dillip Bhai, Hemadri Da, Dhirendra Bhai, Kali Kumar Bhai, Dhrub Bhai, Manas Bhai, Ashis Bhai, Ranjit Bhai, Abhaya Bhai, Dhaneswar, Soumya, and Dinesh. Additionally, I express my appreciation to my juniors, namely Sachi, Dhiren, Sambit, Bijaya, Bikram, Abhik and Sujit. I am also deeply thankful to my gym partner and fellow marathon runner, Debanath, as well as Prosperu, for their support and companionship. A special mention goes to Manas and Abhishek from my native place, whose constant support and friendship have been a source of strength for me, especially here in Hyderabad. Their presence has brought immense joy to my life, and I am deeply grateful for their constant help and support.

This thesis owes its completion to the unwavering support of my family members, who have been by my side through every phase of this journey. I am profoundly grateful to my beloved parents and my Choudhury family. I extend special thanks to my dear siblings, Anjan, Anita, Sarita, Sangita, and their entire families, including my adorable nieces and nephews. I am also indebted to my relatives for their invaluable moral support during my Ph.D. studies. My heartfelt gratitude goes to my cousins, Pramesh, Piush, Priyanka, Pragyan, and Priya. Furthermore, I express my gratitude to Shilpa, Samli, Sonali, and Karishma, who have always supported me as their own brother or uncle.

I extend my heartfelt gratitude to my village friends, Suraj, Thakur, Tanka, Ajit, Nikesh, Rukesh, Sunita, Amrita, Reshma, and others, for their enduring friendship since my childhood. I am deeply appreciative of the bond we share, which has been a source of strength and joy throughout the years. I am equally thankful to my high school companions, Abhilash, Sachin, Suman, Tulu, Happy, Lipan, Sony, Akankshya, Ankita, Jayashree, Manisha, Liva, Abhishek, Indra, Prabosh, Sumit, Rashmi, Lalit, Pranab, Silidevi, and Swagatika. Their friendship has enriched my life in countless ways. Furthermore, I express my gratitude to my intermediate friends, Banty, Rishi, Manish, Prasada, Akash, Bhabana, Chetana, and Dipali, for their companionship and support during that crucial phase of my education. The years spent pursuing my bachelor's degree were some of the most memorable, thanks to the friendship and support of individuals like Manas, Rudra, Sasmita, Saga, Suchi, Mihir, Ashis, and Rajesh. Your presence in my life has been invaluable, and I am truly grateful for everything you have done for me. I also extend my thanks to all my MSc friends, including Debajoti, Bhaskar, Sudipa, Kamala, Krishna, Shruti, Rilfa, Asha, Jai, Satendra, Ashis, Sourav, Basawa, Lokesh, and Amit. Your friendship and encouragement have been a source of motivation and inspiration throughout my academic journey.

I am deeply grateful to the Odisha Cultural Association at the University of Hyderabad for affording me the opportunity to be a part of this enriching community.

Through my involvement as both a leader and a participant, I have gained invaluable insights and experiences. This association has introduced me to remarkable individuals with diverse and inspiring personalities. I extend special thanks to the esteemed members of the association, including university faculties such as Panchanan Sir, Siddharth Sir, Pramod Sir, Debasis Sir, Meera Mam, Meena Mam, Prajna Mam, and Rukumani Mam. Their guidance and mentorship have been instrumental in my personal and academic growth. I am also grateful for the friendships formed with fellow students within the association, including Sikha Srichandan, Sabnam, Alibha, Atashi di, Rekha di, Subhashree, Reshma, Priyanka, and many others. Their support has enriched my experience within the community.

In the end, I extend my sincere gratitude to all the individuals who have supported and assisted me throughout this journey. Your contributions, whether big or small, have been immensely valued and appreciated. To those whom I may have inadvertently overlooked, I offer my apologies. Your kindness and generosity have not gone unnoticed, and I am deeply grateful for the role each of you has played in shaping my path. Thank you for being a part of this journey with me.

Above all, I thank Maa Samlei and Prabhu Jagannath for their eternal love and blessings in every moment of my life.

Once again, thank you, everyone!

Suman Kumar Choudhury

ABBREVIATION

ΔG_b	Gibbs free energy of binding
ΔH_b	Enthalpy of binding
ΔH_{inc}	Incremental contribution of each CH_2 group to transition enthalpy
ΔH_o	End contribution to transition enthalpy; ΔH_t, Transition enthalpy
ΔH_t	transition enthalpy
ΔS_b	Entropy of binding
ΔS_{inc}	Incremental contribution of each CH_2 group to transition entropy
ΔS_o	End contribution to transition entropy
ΔS_t	Transition enthalpy
^{13}C NMR	Carbon-13 nuclear magnetic resonance
^{1}H NMR	Proton nuclear magnetic resonance
Boc	Tert-butyloxycarbonyl
CCDC	Cambridge Crystallographic Data Center
CEs	Chemical enhancer
CMC	Critical micellar concentration
DAAOHs	*N, O*-diacyl-L-alaninols
DAE	N, O-diacylethanolamine
DCC	*N,N'*-dicyclohexylcarbodiimide
DCM	Dichloromethane
DLS	Dynamic light scattering
DMAP	4-Dimethylaminopyridine
DNA	Deoxyribonucleic acid
DSC	Differential scanning calorimetry
ESI-MS	Electrospray ionisation mass spectrometry
FTIR	Fourier transform infrared
GLP1	Glucagon-like peptide 1
GOF	Goodness of fit
GP	Generalized polarization
GPCRs	G protein-coupled receptors
GPR119	G protein-coupled receptors 119

HRMS	High-resolution mass spectrometry
I_1/I_3	Polarity ratio of pyrene
IPA	Ion pair amphiphiles
ITC	Isothermal titration calorimetry
K_b	Binding (association) constant
kV	Kilovolt
LCB	Sphingoid bases
mA	Milliampere
Me	Methyl
n	number of C-atoms in the acyl chain
n	Stoichiometry of binding
N15SOH	*N*-pentadecanoylserinol
N9SOH	*N*-nonanoylserinol
NAAA	NAE-hydrolyzing acid amidase
NAAEs	*N*-acyl-L-alanine alkyl esters
NAAOHs	*N*-acyl-L-alaninols
NAEs	*N*-acylethanolamines
NAGEs	*N*-acyl glycine alkyl esters
NAS	N-acyl synthase
NASEs	*N*-acyl serine alkyl esters
NASOHs	*N*-acylserinol
NAT	*N*-acyl tris
NLGLE	*N*-lauroyl glycine lauryl ester
NLSLE	*N*-lauroyl serine lauryl ester
NMEA	*N*-myristoylethanolamine
NMLAOH	*N*-myristoyl-L-alaninol
NPBAOH	*N*-pamitoyl-β-alaninol
OABAOHs	*O*-acyl-β-alaninols
OAE	*O*-acylethanolamine
OALAOHs	*O*-acyl-L-alaninols
ºC	Degree Celsius
OD	Optical density

OHDLAOH	*O*-heptadecanoyl-L-alaninol
OMBAOH	*O*-myristoyl-β-alaninol
OMEA	*O*-myristoylethanolamine
OMLAOH	*O*-myristoyl-L-alaninol
OMLAOH-SDS	*O*-myristoyl-L-alaninol-Sodium dodecyl sulfate complex
OPBAOH	*O*-palmitoyl-β-alaninol
OPDBAOH	*O*-pentadecanoyl-β-alaninol
OPDLAOH	*O*-pentadecanoyl-L-alaninol
OPLAOH	*O*-palmitoyl-L-alaninol
ORTEP	Oak ridged thermal-ellipsoid plot program
PDI	Polydispersity index
PXRD	Powder X-ray diffraction
RNA	Ribonucleic acid
rpm	Revolution per minute
SC	Stratum corneum
SCM	Stratum corneum model membrane
SDS	Sodium dodecyl sulfate
SI	Supporting information
SLs	Sphingolipids
TDD	Transdermal drug delivery
TEM	Transmission electron microscope
THF	Tetrahydrofuran
T_t	Transition temperature
T_t^{∞}	Transition temperature at infinite chain length
UV-Vis	Ultraviolet-visible
v	Volume
XRD	X-ray diffraction

Chapter 1

General Introduction

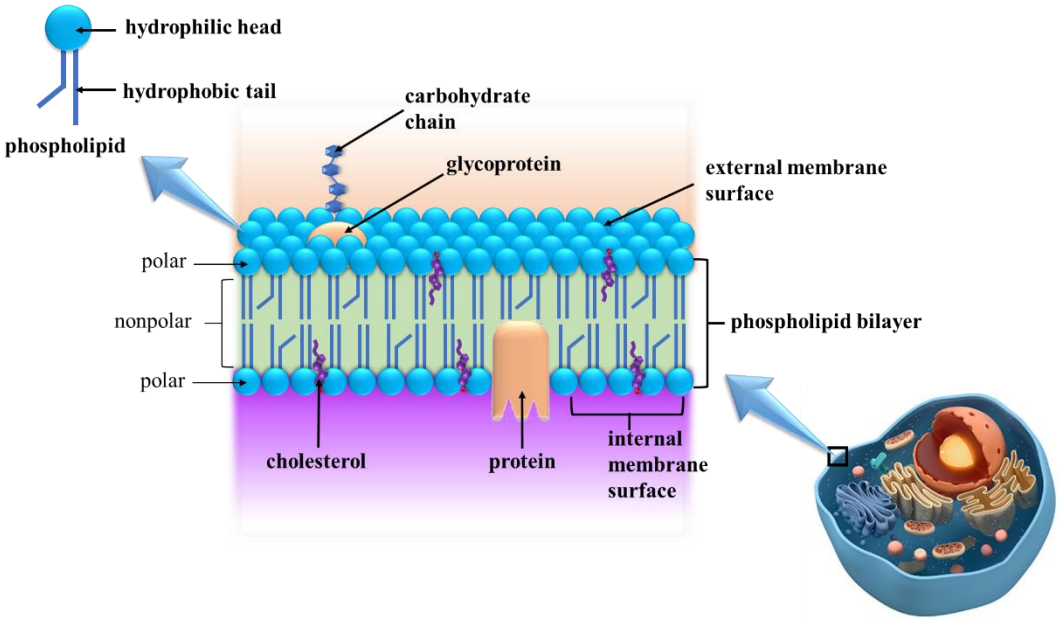

The origin of life is a mystery in the scientific community. How did something living arise from non-living matter? The boundary between chemistry and biology, between the abiotic and biotic, is still debated. Biochemistry helps to understand the unique properties of living organisms that result from combining thousands of non-living biomolecules. Life appeared as simple microorganisms that harnessed energy from organic compounds or sunlight four billion years ago. They used this to create a wide range of more complex biomolecules from Earth's basic elements and compounds (Nelson et al., 2017). The building blocks of life are biomolecules such as lipids, proteins, carbohydrates, and nucleotides. Studying these molecules helps us understand how living organisms interact to maintain and perpetuate life, guided only by the physical and chemical laws of the non-living universe. All living components are vital in biological systems and play important roles in *in vivo* and *in vitro* studies.

The current research focuses on lipids, an important cell component. Lipids are simple amphiphilic molecules lacking the complex structures of proteins and nucleic acids. However, when in contact with excess water, they form various supramolecular assemblies depending on their chemical structure, ionic strength, pH, and temperature. One of the most common assemblies is the bilayer, found in cell membranes and organelles. Historically, lipids have been considered less important than other biomolecules, such as proteins, which catalyze chemical reactions, and nucleic acids, which carry genetic information. However, in recent years, the importance of lipids as second messengers in cell signalling, cell function, and health has been recognized (Spiegel et al., 1996; Fernandis et al., 2007; Mouritsen, 2011). Lipidomics is the comprehensive study of lipids in the biological system, including their identification, quantification, and characterization. Lipidomics involves using advanced analytical techniques like liquid chromatography and mass spectrometry (Wenk, 2005). Lipids can be classified into different types based on their functions in biological systems, including energy storage, membrane structure, signalling, and insulation.

1.1. Fatty Acids

Fatty acids are a class of biomolecules important for various biological processes in living organisms. They are long-chain hydrocarbons with a carboxylic acid group at one end and are classified into saturated and unsaturated fatty acids. Saturated fatty acids

Table 1.1. Structure and nomenclature of some naturally occurring fatty acids

Carbon skeleton	Structure*	Systematic name†	Common name (derivation)
12:0	$CH_3(CH_2)_{10}COOH$	*n*-Dodecanoic acid	Lauric acid (Latin laurus, "laurel plant")
14:0	$CH_3(CH_2)_{12}COOH$	*n*-Tetradecanoic acid	Myristic acid (Latin Myristica, nutmeg genus)
16:0	$CH_3(CH_2)_{14}COOH$	*n*-Hexadecanoic acid	Palmitic acid (Latin palma, "palm tree")
18:0	$CH_3(CH_2)_{16}COOH$	*n*-Octadecanoic acid	Stearic acid (Greek stear, "hard fat")
20:0	$CH_3(CH_2)_{18}COOH$	*n*-Eicosanoic acid	Arachidic acid (Latin Arachis, legume genus)
24:0	$CH_3(CH_2)_{22}COOH$	*n*-Tetracosanoic acid	Lignoceric acid (Latin lignum, "wood" + cera, "wax ")
16:1 (Δ^9)	$CH_3(CH_2)_5CH{=}CH(CH_2)_7COOH$	cis-9-Hexadecenoic acid	Palmitoleic acid
18:1 (Δ^9)	$CH_3(CH_2)_7CH{=}CH(CH_2)_7COOH$	cis-9-Octadecenoic acid	Oleic acid (Latin oleum, "oil")
18:2 ($\Delta^{9, 12}$)	$CH_3(CH_2)_4CH{=}CHCH_2CH{=}CH(CH_2)_7COOH$	cis-,cis-9,12-Octadecadienoic acid	Linoleic acid (Greek linon, "flax")
18:3 ($\Delta^{9, 12, 15}$)	$CH_3CH_2CH{=}CHCH_2CH{=}CHCH_2CH{=}CH(CH_2)_7COOH$	cis-,cis-,cis-9,12,15-Octadecatrienoic acid	α-Linolenic acid
20:4 ($\Delta^{5, 8, 11, 14}$)	$CH_3(CH_2)_4CH{=}CHCH_2CH{=}CHCH_2CH{=}CHCH_2CH{=}CH(CH_2)_3COOH$	cis-,cis-,cis-,cis-5,8,11,14-Icosatetraenoic acid	Arachidonic acid

*All acids are displayed in their nonionized state. Every free fatty acid has an ionized carboxylate at pH 7. Note that the numbering of carbon atoms begins at the carboxyl carbon.

† The prefix *n*- indicates the "normal" unbranched structure. For instance, "dodecanoic" indicates 12 carbon atoms, which could be arranged in various branched forms; "*n*-dodecanoic" specifies the linear, unbranched form. For unsaturated fatty acids, the

configuration of each double bond is indicated; in biological fatty acids, the configuration is almost always cis

have no double bonds between the carbon atoms in their hydrocarbon chains, while unsaturated fatty acids have one or more double bonds. Fatty acids are essential components of cell membranes, serve as a major energy source, and are involved in synthesizing many important molecules, such as hormones and signalling molecules (Calder, 2015). Some examples of fatty acids are listed in Table 1.1.

One of the most biologically important fatty acids is omega-3 fatty acid. Unsaturated fatty acids of the omega-3 variety are crucial for human health. The human body cannot synthesize them, and they must be obtained through diet. Omega-3 fatty acids have been demonstrated to provide several health benefits, including lowering inflammation, increasing brain function, and lowering the risk of heart disease (Weylandt et al., 2015; Serhan and Levy, 2018). Another important fatty acid is arachidonic acid, an omega-6 fatty acid. Arachidonic acid is involved in many physiological processes, such as blood clotting and the inflammatory response. It is also a precursor to numerous signalling molecules, including prostaglandins, thromboxanes, and leukotrienes (Innes and Calder, 2018).

1.2. Storage Lipids

Storage lipids, also known as triacylglycerols, are a group of biomolecules that play a crucial role in the energy metabolism of living organisms. Triacylglycerols are made up of three fatty acids, each of which is ester-linked to a single glycerol molecule (Fig. 1.1), and are found in a wide range of organisms, from bacteria to mammals. Simple triacylglycerols are named after the fatty acid they contain and are those that have the same type of fatty acid in each of the three locations of glycerol. For instance, tripalmitin, tristearin and triolein are examples of straightforward triacylglycerols containing 3 chains each of 16:0, 18:0 and 18:1 fatty acids, respectively. The majority of triacylglycerols that exist in nature are mixed and contain two or more distinct fatty acids. It is necessary to identify the name and location of each fatty acid in order to label these molecules clearly. These lipids are stored in specialized organelles called lipid droplets, which are found in almost all eukaryotic cells (Martin and Parton, 2006). They act as a reserve of energy, providing a source of fuel for the cell during times of stress

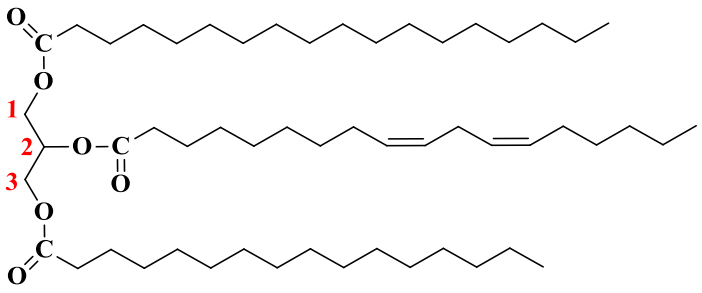

Fig. 1.1. Structure of 1-stearoyl, 2-linolwoyl, 3-palmitoyl glycerol, a mixed triacylglycerol.

or nutrient deprivation (Cushman, 1970). The accumulation of storage lipids in cells is tightly regulated, as excess lipids can lead to diseases such as obesity and diabetes (Xu et al., 2018). The study of storage lipids has important implications for understanding the regulation of energy metabolism in cells and the development of therapies for metabolic disorders (Welte, 2015). They are also used in various applications, such as in the food and cosmetics industry (Lísa and Holčapek, 2008).

1.3. Structural lipids

Structural lipids are a diverse group of biomolecules essential for the structural integrity and function of biological membranes in living organisms. Structural lipids are responsible for forming the lipid bilayer, which acts as a barrier, separating the cell's internal environment from the external environment. They include phospholipids, glycolipids, and cholesterol, which play critical roles in maintaining cell membranes' fluidity, permeability, and stability (van Meer et al., 2008). These lipids also participate in signalling pathways and cellular processes, such as vesicular trafficking and membrane fusion (Simons et al., 1997; 2000). The study of structural lipids is essential for understanding the organization and function of biological membranes and has implications for developing therapies for diseases that affect membrane integrity.

1.3.1. Phospholipids

Phospholipids are a class of lipids that are essential components of biological membranes in cells. They are composed of a glycerol backbone, two fatty acid chains, and a phosphate group that is often linked to another molecule, such as choline or ethanolamine. The unique structure of phospholipids allows them to form bilayer

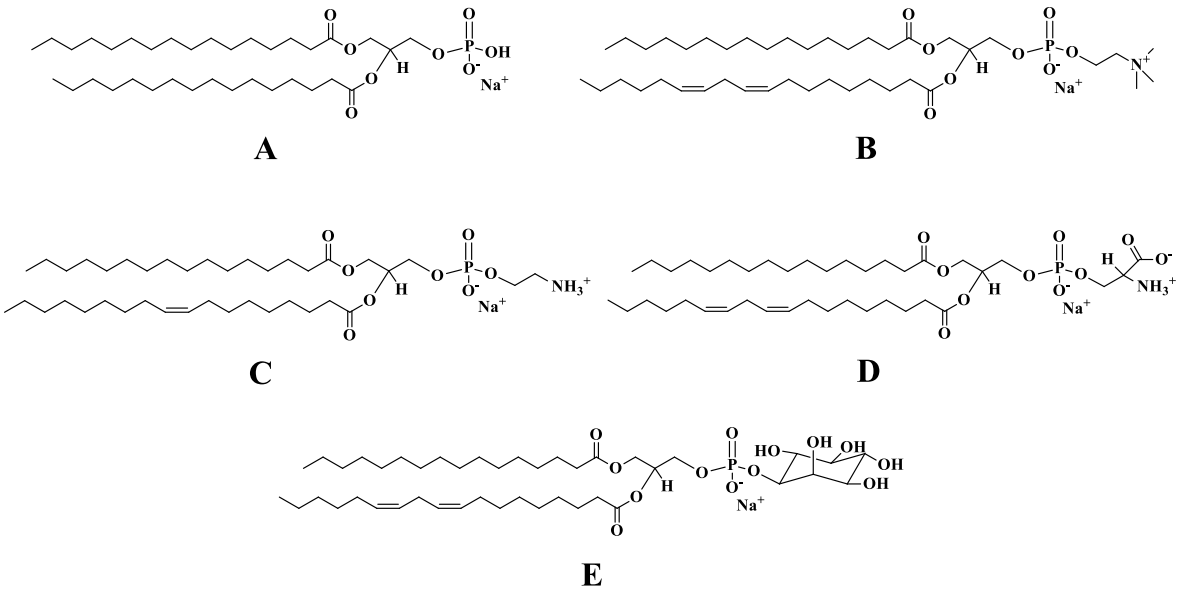

Fig. 1.2. Structures of phospholipids. (A) Phosphatidic acid mono sodium salt (DPPA-Na), (B) Phosphatidylcholine, (C) Phosphatidylethanolamine, (D) Phosphatidylserine, (E) Phosphatidylinositol.

membranes that serve as barriers and regulate the transport of molecules into and out of cells. Phospholipids are found in all living organisms and are essential for maintaining the integrity and function of cell membranes. In addition to their structural role, phospholipids also participate in cellular signaling and serve as precursors for the synthesis of other important molecules, such as prostaglandins and leukotrienes (Vance et al., 2002). Phospholipids are synthesized through a complex series of enzymatic reactions that involve the modification of the glycerol backbone and the attachment of various fatty acids and polar head groups. These reactions are tightly regulated and occur in different cellular compartments, including the endoplasmic reticulum and the Golgi apparatus.

Phospholipids can be classified into several different types based on their head group. The most common types of phosphoglycerides include phosphatidylcholine (PC), phosphatidylethanolamine (PE), phosphatidylserine (PS), and phosphatidylinositol (PI) (Figure 1.2). These lipids play critical roles in maintaining the structural integrity and functionality of cell membranes, as well as in signaling and other cellular processes. Research has shown that abnormalities in the composition and

metabolism of phosphoglycerides are associated with various diseases, including cancer, Alzheimer's disease, and metabolic disorders (Komoroski et al. 2001; Viader et al. 2015).

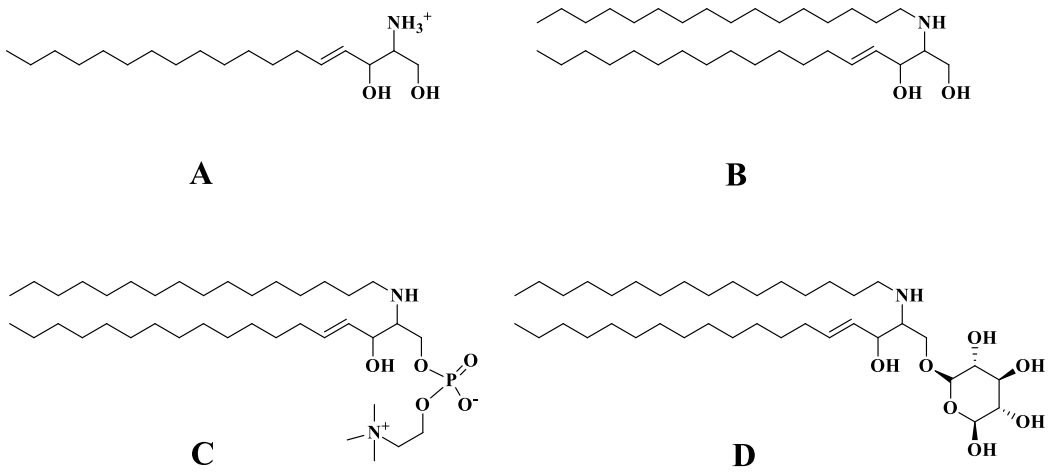

Fig. 1.3. Structures of sphingolipids (A) Sphingosine, (B) Ceramide, (C) Sphingomyelin, (D) Cerebroside.

1.3.2. Sphingolipids

Sphingolipids are generally found in eukaryotic cells. They comprise a long-chain amino alcohol called sphingosine, linked to a fatty acid by an amide bond. Sphingolipids are categorized into several classes based on their structure and function, including ceramides, sphingomyelins, and glycosphingolipids. The simplest sphingolipids are ceramides, which are made of sphingosine bonded to a fatty acid by an amide bond (Simons and Ikonen, 1997). Sphingomyelins are the most abundant sphingolipids in cell membranes and are composed of sphingosine, a fatty acid, and a phosphocholine or phosphoethanolamine head group. Glycosphingolipids are sphingolipids that have one or more sugars attached to the sphingosine backbone. Sphingolipids are also involved in lipid rafts, specialized membrane domains enriched in cholesterol, sphingolipids, and certain types of proteins (Simons and Toomre, 2000). Structures of various sphingolipids are shown in Fig. 1.3.

1.3.3. Sterols

Sterols are a class of organic molecules that contain a rigid four-ring structure, known as the sterane ring system, with a hydroxyl (-OH) group attached to one of the rings.

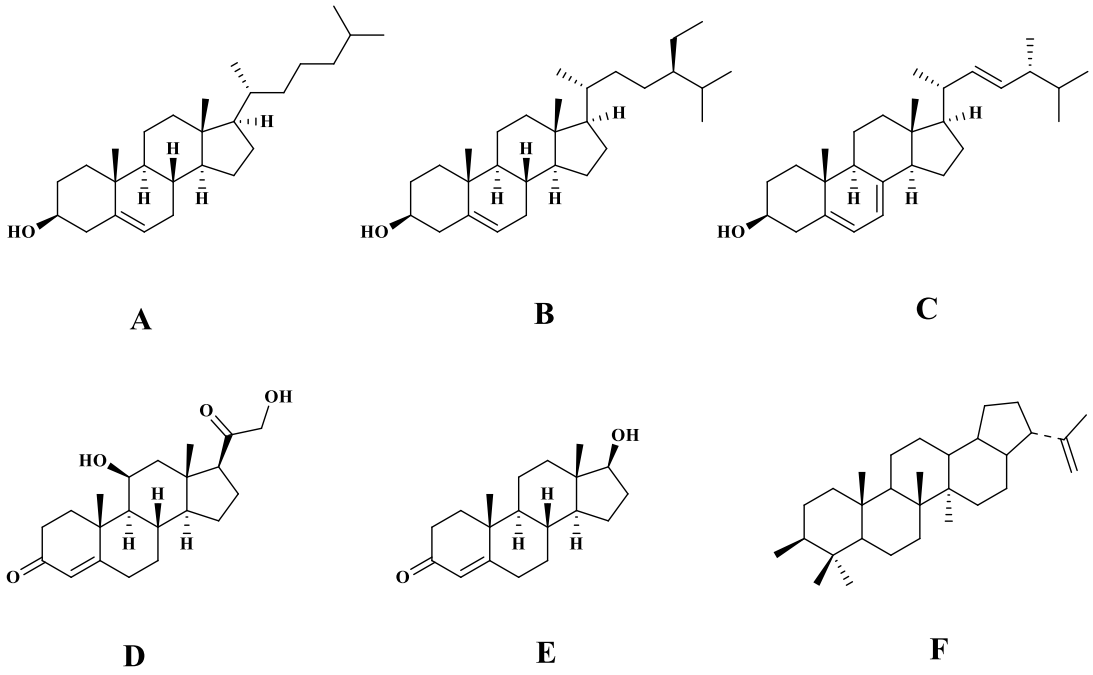

Fig. 1.4. Structure of sterols (A) Cholesterol (B) Sitosterol (C) Ergosterol (D) Corticosterone (E) Testosterone (F) Hopanoids

The most common sterol found in animal cells is cholesterol, which is present in the animal cell plasma membranes and other cell organs, such as lysosomes, endosomes, and Golgi complex. In contrast, plant cells contain a variety of sterols, including sitosterol, campesterol, and stigmasterol. Hopanoids are other kinds of sterol lipids are present in bacterial cell membranes. Sterols are also precursors for the biosynthesis of many essential hormones, including testosterone, estrogen, and cortisol, and they are involved in regulating lipid metabolism and transport (Chatuphonprasert et al., 2018). Furthermore, they have been shown to have potential therapeutic effects, such as reducing cholesterol levels in the blood and decreasing the risk of cardiovascular disease (Fassbender et al., 2008). Structures of different sterols are shown in the Fig. 1.4.

1.3.4. Glycolipids

Glycolipids generally comprise a lipid (fatty acid) and a carbohydrate (sugar) component. They are present on the surface of cells and are crucial for cell adhesion, cell signaling, and cell identification (Zhao et al. 2008; Boscher et al., 2011). There are two main types of glycolipids: sphingolipids and glycerolipids. Sphingolipids comprise

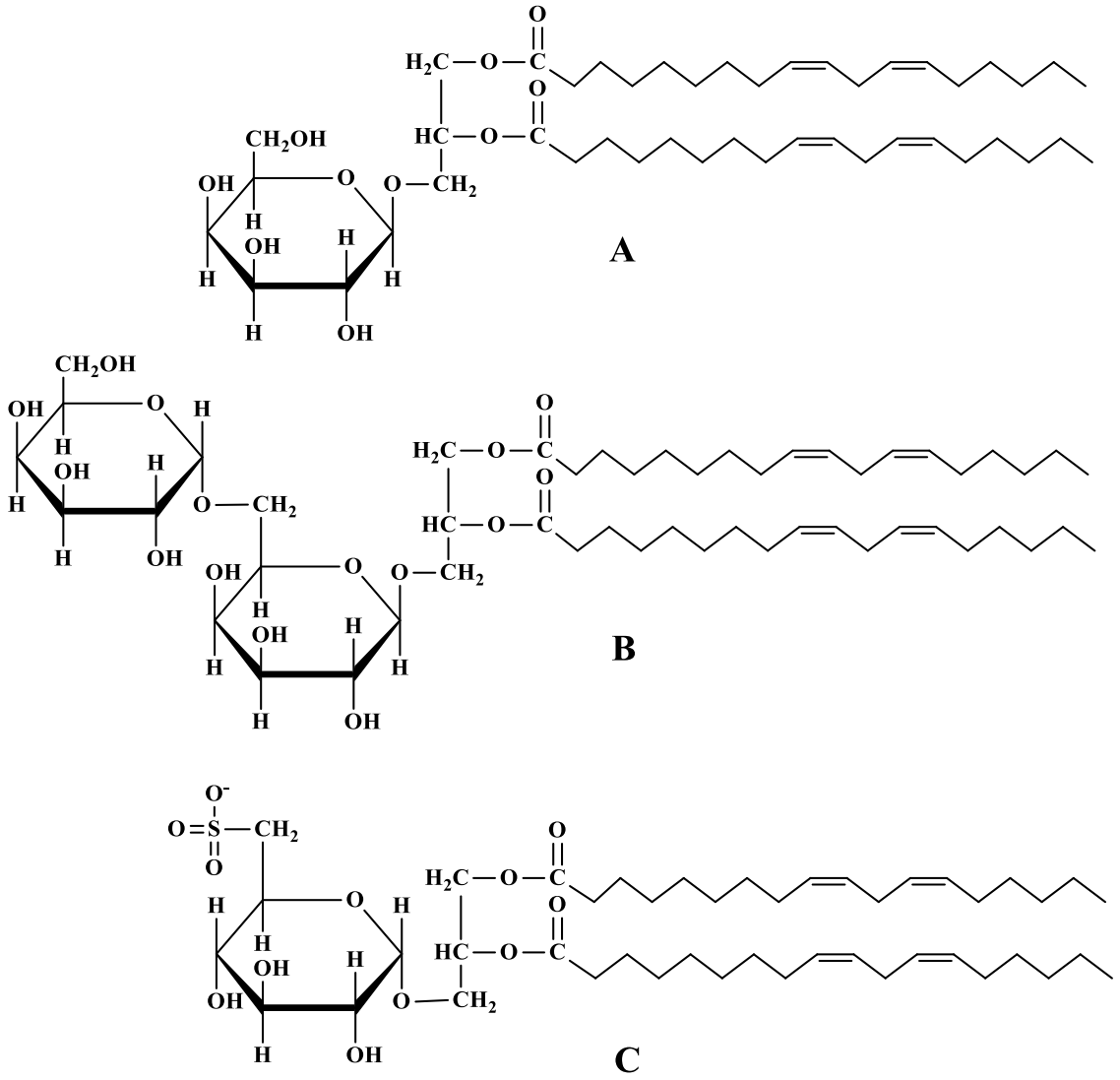

Fig. 1.5. Three glycolipids of chloroplast membranes. (A) Monogalactosyldiacylglycerols (MGDGs), (B) Digalactosyldiacylglycerols (DGDGs) and (C) 6-sulfo-6-deoxy-α-D-glucopyranosyldiacylglycerol.

of a sphingosine backbone and a fatty acid, while glycerolipids comprise a glycerol backbone and a fatty acid. Glycolipids are important for cell-cell communication and are involved in many biological processes, such as immune responses, cell development, and cellular differentiation (Nishimura et al., 2000; Fujii et al., 2006). They also play a role in the structure and function of the nervous system, as myelin, the insulating sheath around nerves, is composed largely of glycolipids (Jungalwala, 1994). Additionally, some glycolipids are known to act as receptors to toxins or pathogens in certain diseases.

Glycolipids are also found in chloroplast thylakoid membranes (internal membranes), where they account for 70% to 80% of a vascular plant's total membrane lipids. Additionally, sulfolipids, in which a diacylglycerol is linked to a sulfonated glucose residue via a glycosidic linkage, are found in plant membranes. The sulfonate on the head group of sulfolipids has a fixed negative charge, similar to the phosphate group in phospholipids (Fig. 1.5).

1.4. Waxes

These are long-chain fatty acid and long-chain alcohol esters, which are soluble in organic solvents like ether, chloroform, and benzene but insoluble in water. Waxes are found in many natural sources, such as plants, animals, and minerals. In plants, they serve as a protective coating on leaves and fruits, helping to reduce water loss and protect against pests and pathogens. In animals, waxes are found in fur, feathers, and the outer layer of skin, helping to repel water and maintain insulation. Waxes are also commonly used in various industrial applications, such as in producing candles, polishes, coatings, and lubricants. In the food industry, they are often used as a coating on fruits and vegetables to help preserve freshness and prevent spoilage (Krendlinger and Wolfmeier, 2022).

1.5. Classification of Lipids according to the charge on the head group

Lipids can be classified according to the charge in their head group. The two main categories are non-polar lipids and polar lipids.

1.5.1. Non-polar lipids

These lipids have a non-polar or hydrophobic head group, which means they do not have a charged or predominantly polar functional group in the head region. Examples of non-polar lipids include triglycerides, waxes, and steroids. Triglycerides, also known as triacylglycerols, are a type of storage lipid that provides energy to the cell. Waxes, such as wax esters and cholesterol esters, provide a waterproof barrier to the surface of the skin, hair, and feathers. Steroids, such as cholesterol and steroid hormones, are involved in the regulation of cell membrane functions and play a role in many physiological processes (Gimpl et al., 2002).

1.5.2. Polar lipids

These lipids have a polar head group, which means they have a charged or significantly polar functional group in the head region. Examples of polar lipids include phospholipids and glycolipids. Phospholipids like phosphatidylcholine and phosphatidylethanolamine have a charged phosphate group in the head region. Glycolipids, such as cerebrosides and gangliosides, have a carbohydrate group in the head region. These lipids are important for forming and stabilizing biological membranes and play crucial roles in cell signalling, cell recognition and communication (Cheng and Smith, 2019).

Recently, *N*-acyl conjugates of amino acids and neurotransmitters (NAANs), which belong to the anionic lipid group, have drawn increasing attention because of their functions in the nervous system, circulatory system, and immune system. NAAN are substances like glycine, γ-aminobutyric acid (GABA), or dopamine that have been coupled with long-chain fatty acids. There have been reports indicating the presence of more than 70 endogenous NAANs in mammalian brain and neuronal tissues. It is unclear what their physiological function is, however, NAANs interact with ion channels and G protein-coupled receptors (GPCRs) with modest affinities (Saghatelian et al. 2004; 2006; Milman et al. 2006; Chu et al. 2003; Huang et al. 2002; 2001; Tan et al. 2010; Bradshaw et al. 2009; Rimmerman et al. 2008). Pharmacologists are very interested in NAANs because of their promise as versatile tools for probing novel sites on GPCRs, transporters, and ion channels, regardless of their possible physiological function. Amphipathic NAANs can contain a range of different fatty acids and headgroup moieties. Through unique binding locations and processes, this combination offers a wealth of potential ligands for modulating membrane proteins like GPCRs, ion channels, and transporters (Connor et al., 2010). In recent years many *N*-acyl conjugates of fatty acids have been synthesized and characterized which show high potential for use in developing drug delivery vehicles (Ramakrishnan et al., 1997; 1998; 1999; Sivaramakrishna et al. 2015a; 2015b; 2016a; 2016b; 2018; 2019; 2021; Reddy et al., 2014; 2015; 2017; Kamlekar and Swamy 2006; Swamy et al., 2010).

On the other hand, cationic lipids have been recognized as highly versatile agents in drug delivery, particularly for transporting therapeutic molecules such as DNA and RNA (Zhi et al., 2013; 2018). They are particularly appealing due to their simplified

design, synthesis, and characterization process. Most cationic lipids have a basic structure consisting of the hydrophobic tail and hydrophilic cationic head groups connected by linker units (Niculescu-Duvaz et al., 2003). When the positively charged head group of cationic lipids reacts electrostatically with the negatively charged phosphate group of nucleic acids, condensed nucleic acid complexes can result in (Liu et al. 2017). The length and composition of the aliphatic chain can impact the fluidity of the bilayer, the temperature at which a phase shift takes place, and the stability of liposomes (Sardar et al. 2018; Hazra et al. 2022; Tarafdar and Swamy 2010). The length, number, type, and relative alignment of the linker bond that joins the polar head group and the hydrophobic tail domain substantially impact the transfection efficiency, biodegradability, stability, and cytotoxicity of cationic lipids (Karmali and Chaudhuri 2007; Srinivas et al., 2009; Zhi et al., 2018). Looking into the importance of cationic lipids and amphiphiles as nonviral nucleic acid carriers for gene therapy, our group has also studied the interaction of cationic lipid like L-alanine alkyl ester with DNA using ITC (Sivaramakrishna and Swamy 2015c).

Amino alcohols are reduced derivatives of amino acids and very important components in the structure of various biomolecules. Their multifaceted roles extend to the structural composition of cell membranes like choline. These amino alcohols are essential for maintaining membrane fluidity and permeability, thereby influencing vital cellular processes such as selective transport of molecules and signal transduction (Lodish et al., 2000). In mammalian tissues, sphingolipids (SLs) are of vital importance; SLs are derived from aliphatic amino alcohols called sphingoid bases (LCB) (Carreira et al., 2019). L-Alaninol (2-amino-1-propanol) is a reduced derivative of L-alanine. *N*-Acyl-L-alaninols (NAAOHs) are chiral homologs of *N*-acylethanolamines (NAEs) and reduced forms of *N*-acyl-L-alanines (NAAlas) and were reported to induce apoptosis in human lymphocytes (Ogura et al., 2000). Both D- and L- forms of *N*-acyl alaninols induce apoptosis in Jurkat cells (human lymphocytes), similar to that caused by C2-ceramide and anti-Fas antibodies. Similarly, β-alaninol is a reduced derivative of β-alanine and influences the phospholipid composition upon supplementation to *Tetrahymena* and L-cells (Kovács et al., 1997; Eidelman et al., 2002). Amphiphilic derivatives of β-alaninols have been reported in various biological applications (Suleman et al., 2015; Mangraviti et al.,2015: Kalhapure and Akamanchi, 2012).

Ethanolamine and certain other amino alcohols modulate the evoked release of synthesized acetylcholine in the rat hippocampus (Bostwick et al., 1992) Additionally, *O*-acylethanolamines (OAEs), structural isomers of the putative stress-fighting lipids, namely *N*-acylethanolamines (NAEs), putative stress-fighting lipids are present in biological membranes under physiological conditions (Tarafdar and Swamy, 2010)

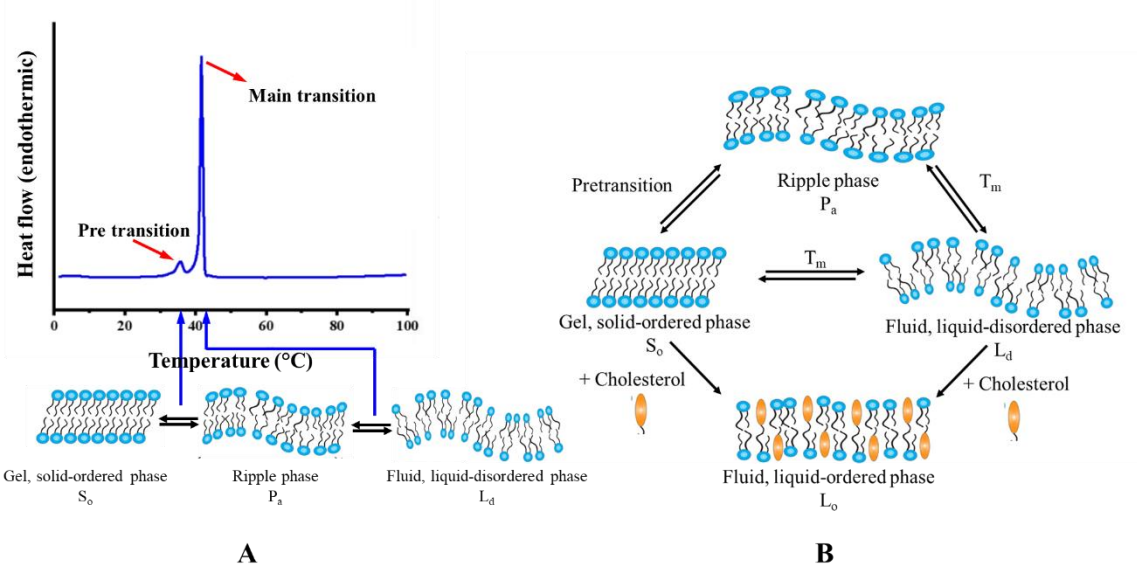

Fig.1.6. (A) Phase transition of DPPC. (B) Scheme showing various physical states that a lipid bilayer can take in an aqueous environment (https://popups.uliege.be/1780-4507/index.php?id=6568).

1.6. Physiochemical characterization of lipids

The physiochemical characterization of lipids is important for understanding the behaviour and properties of these molecules. This characterization can provide insights into the structural, dynamic, and thermodynamic properties of lipids, which are crucial for understanding the role of lipids in biological systems.

1.6.1. Phase transition

Lipid molecules can undergo phase transitions, which involve a change in their physical state from one phase to another, such as those from a solid-to-solid, solid to liquid or gel to liquid etc. The phase transition of lipids is a complex process which can be influenced by several factors, including temperature, pressure, lipid composition, and the presence of other molecules such as water or buffer. The phase transition

temperature (T_t) is the temperature at which a lipid transitions from one phase to another occurs. Lipids are relatively fluid and can move freely within the membrane when they are in a liquid phase. However, when the temperature decreases or pressure increases, the lipids may undergo a phase transition to a gel or solid phase, resulting in a decrease in membrane fluidity. Both the gel and liquid phases stabilize with the addition of cholesterol. Cholesterol stops the bilayer from becoming acidic in the gel phase and keeps the liquid disordered phase stable in the fluid phase. Compared to all other lipids, phosphatidylcholines exhibit a characteristic pre-transition in the hydrated state. Pretransition is the transition of lipids from their gel phase to their ripple phase, which is characterized by the formation of ripples on the surface of the lipid bilayer (Fig. 1.6). This change in fluidity can affect the function of the membrane and the biological processes that depend on it, such as ion transport and protein function (Bastiaanse et al., 1997).

Understanding the phase transition of lipids is important for numerous research fields, including biochemistry, biophysics, and pharmacology. For example, developing drugs that target the lipid phase transition may be used to treat diseases associated with changes in membrane fluidity, such as cancer and Alzheimer's disease.

Lipid phase transition is investigated using differential scanning calorimetry (DSC) for both hydrated and dry-state lipids. In addition to DSC, the phase transition of solid lipid samples can be studied using NMR, FTIR, PXRD, and optical microscopy. (AFM, TEM, and SEM). On the other hand, DSC and spectroscopic techniques including electron spin resonance, UV-visible, and fluorescence can be used to examine the phase transition of the hydrated lipids. Additionally, techniques for X-ray scattering and small-angle neutron scattering are utilized to examine the phase transition of hydrated lipids (Tardieu et al., 1973; Eeman and Deleu, 2010).

1.6.2. Fluidity and diffusion

Fluidity refers to the ability of the membrane to move and change shape. This movement is due to the presence of phospholipids, which comprise most of the plasma membrane. Phospholipids have a hydrophilic head and one or more hydrophobic tails, and usually arrange themselves in a bilayer when dispersed in aqueous media, with the heads facing outward and the tails facing inward. This bilayer allows for flexibility and

movement within the membrane. In contrast, diffusion describes the transfer of molecules from a region of high concentration to one of low concentration. The fluidity and diffusion of the plasma membrane are crucial for the functioning of cells. For example, the membrane's fluidity allows it to change shape and move in response to external stimuli, such as during phagocytosis (cellular ingestion of foreign particles) or endocytosis (cellular uptake of materials). The diffusion of molecules through the membrane allows cells to take in nutrients and remove waste products (Singer and Nicolson,1972).

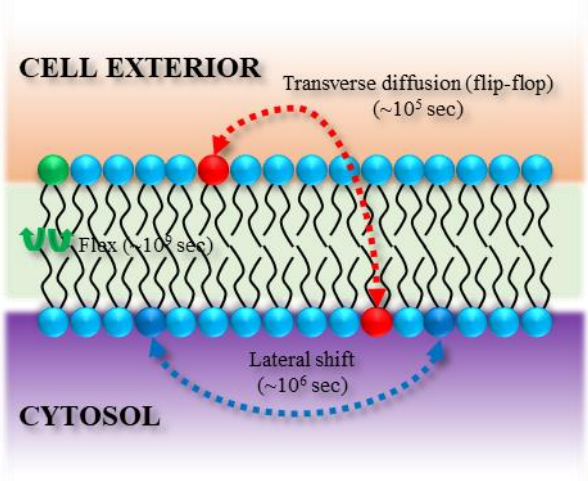

Fig. 1.7. Schematic representation of various translational and rotational in the cell membrane.

In the case of synthetic lipid membranes, lipids with short acyl chains are more fluid than those with long acyl chains due to increased kinetic energy and smaller surface area for van der Waal interactions between the acyl chains. The strong interactions between the acyl/alkyl chains in membranes composed of saturated fatty acids contribute to the membrane's stiffness. At room temperature, they are frequently in the gel phase. The kinks in the architecture of the unsaturated fatty acids reduce interactions between the side chains and increase membrane mobility. The amount of cholesterol in the membrane substantially impacts its fluidity; at low concentrations, cholesterol increases stiffness, whereas at larger quantities, it enhances fluidity. When added to a more fluid unstructured membrane, it decreases fluidity by increasing molecular interaction, however when applied to a saturated membrane, it increases fluidity (Bhattacharya et al., 2000; Rubenstein et al., 1979).

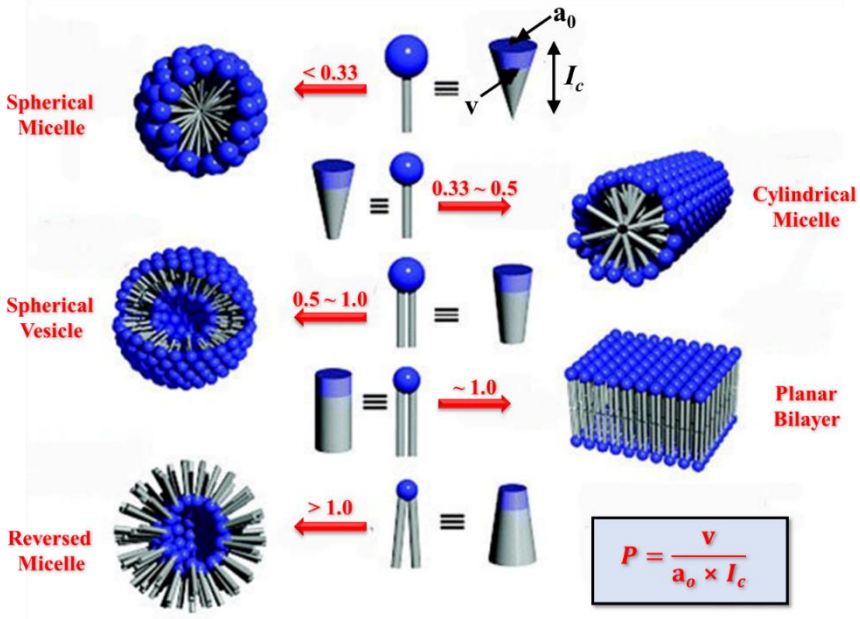

Fig. 1.8. Self-assembly of lipids: Morphology and analysis of the Cpp. (Figure taken from Shimizu et al., 2005).

Several factors can affect the fluidity and diffusion of the membrane, including temperature, lipid composition, and the presence of cholesterol. At higher temperatures, the membrane becomes more fluid, while at lower temperatures, it becomes more rigid. The lipid composition of the membrane can also affect its fluidity, as different lipids have different properties. Diffusion of lipid molecules within the same membrane is known as lateral diffusion. Transverse diffusion, also known as flip-flop motion, is the migration of lipid molecules from one layer of the bilayer membrane to the opposing layer. (Fig. 1.7). Transverse diffusion is slow and infrequent compared to lateral diffusion.

1.7. Self-assembly of lipids

Self-assembly of lipids refers to the spontaneous organization of lipid molecules into ordered structures without external forces or intervention. This process occurs due to the unique chemical and physical properties of lipids, which are amphiphilic in nature with a hydrophilic (water-loving) head and a hydrophobic (water-fearing) tail. In aqueous solutions, lipids form various self-assembled structures such as micelles, bilayers, and

liposomes, depending on the type of lipid, concentration, temperature, and other factors. The thermodynamic factors that influence self-aggregation are likewise under the control of the compound′s nature. The size of the head group, the charge on the molecule, and the length of the hydrocarbon chains in the tails all affect it. Based on physical characteristics, the crystal packing parameter, presented below in Fig. 1.8, can be used to estimate aggregate formation (Shimazu et al., 2005). These lipid structures have numerous applications in drug delivery, cosmetics, and biomaterials.

1.7.1. Micelles

Micelles are self-assembling aggregates of amphiphilic molecules in a solvent. They consist of a hydrophobic core and a hydrophilic shell, which allows them to form stable colloidal particles in aqueous solutions. Due to their unique properties and potential applications, micelles have attracted significant interest in various fields, including drug delivery, oil recovery, and surface science. The hydrophobic effect drives micelle formation by aggregating hydrophobic molecules and minimizing their interaction with water. The hydrophilic part of the molecules forms a shell around the hydrophobic core, stabilizing the micelle and allowing it to exist in solution. Micelles are typically spherical; however, depending on the chemical content, temperature, pH, and ionic strength, they can occasionally appear as cylindrical rods. Amphiphiles with small head groups in non-polar fluids are protected from the surface by their non-polar tail groups, which are exposed to the solvent. These micelles are referred to as reverse micelles.

The first observations of micelles, i.e., soap, has been made and used since ancient time in Mesopotamia (Spitz, 2004). However, it was much later that the structure and properties of micelles began to be studied in detail, thanks to the development of modern techniques such as electron microscopy, light scattering, and spectroscopy. Since then, numerous studies have been conducted on micelles, and their applications have been explored in various fields. For example, micelles can be used in drug delivery to encapsulate hydrophobic drugs and improve their solubility and bioavailability (Movassaghian et al., 2015). In oil recovery, micelles can be used to mobilize oil trapped in reservoirs and increase oil recovery efficiency (Gong et al., 2020). In surface

science, micelles can be used to study surface properties and as templates for synthesizing nanoparticles and other materials.

1.7.2. Liposomes or vesicles

Liposomes are spherical structures composed of a phospholipid bilayer are arranged in bilayer. Hydrophilic head groups are both externally and internally exposed to the water, while hydrophobic tails are facing one another. They can encapsulate and deliver a wide range of molecules, including drugs, vaccines, and genetic material. Bangham and colleagues first described them in 1965 (Bangham et al., 1965) and have since been extensively studied for their potential biomedical applications (Torchilin, 2005).

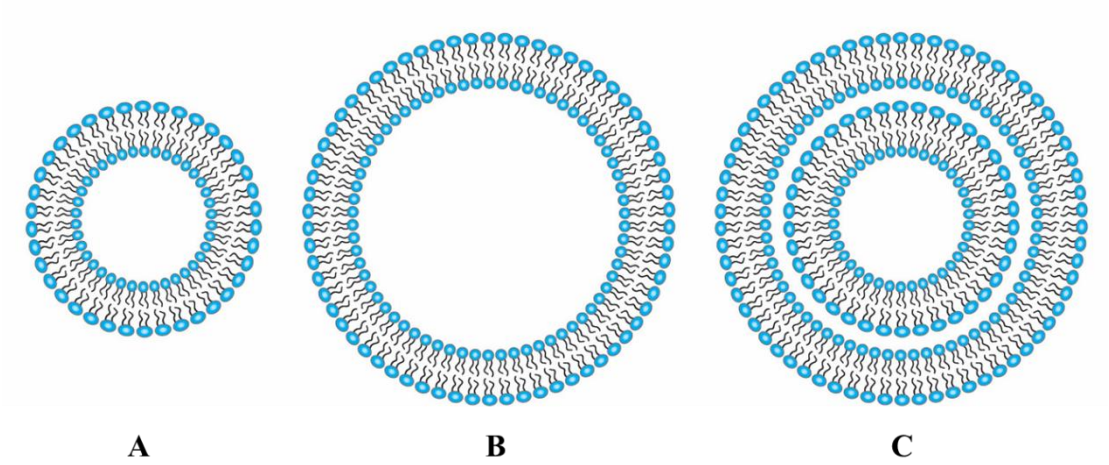

Fig. 1.9. (A) Small unilamellar vesicles (SUV), (B) large unilamellar vesicles (LUV), and (C) multilamellar vesicles (MLV).

Liposomes can be modified to improve their stability, targeting, and release properties (Allen and Cullis, 2013; Lukyanov et al., 2004). They can also be engineered to carry both hydrophilic and hydrophobic molecules, making them versatile carriers for drug delivery. Liposomal drug formulations have been approved for clinical use in cancer treatment (Barenholz, 2012) and other diseases (Al-Ahmady and Kostarelos, 2016). Additionally, liposomes have been explored for their potential in vaccine delivery, gene therapy, and diagnostic imaging (Aryasomayajula et al., 2016; Sharma et al., 2006; Ding et al., 2022). The size and number of lamellae serve as a general guide for classifying liposomes. Unilamellar Vesicles (ULV) which usually have a single bilayer and Multilamellar Vesicles (MLV) which have a multi bilayers are two different

types of bilayers that can be formed in a liposome (Fig. 1.9). ULV is further classified into three types: small unilamellar vesicles (SUV) have a diameter of 25-100 nm, large unilamellar vesicles (LUV) having a diameter of 100-400, and giant unilamellar vesicles, which are defined as having a diameter more than 1 μm. (GUV) (Drulis-Kawa, et al., 2006; Matosevic and Paegel, 2011).

1.7.3. Catanionic vesicles

In recent years, there has been a large shift in focus within the realm of liposomal applications from single-molecule formulations to surfactant mixtures. These mixtures are increasingly recognized for their adaptability and versatility, allowing easy optimization of composition for specific applications (Penfold and Thomas, 2019;

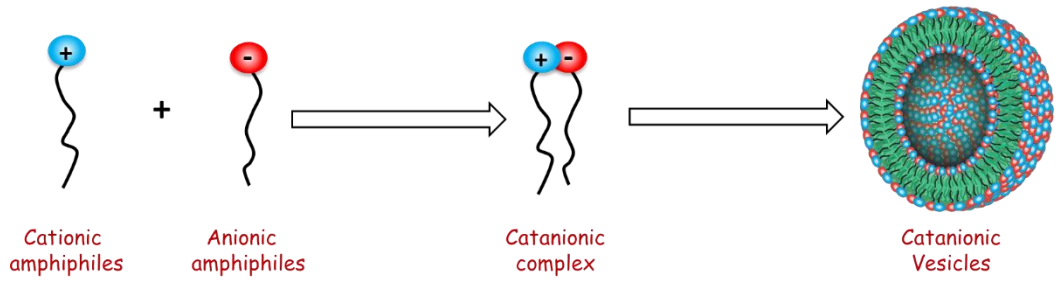

Fig. 1.10. Schematic representation of formation of catanionic vesicles.

Manga et al., 2021). Particularly, the exploration of catanionic systems, characterized by a mixture of cationic and anionic amphiphiles, has emerged as a compelling avenue of scientific exploration. Unlike single-molecule vesicles, aqueous solutions containing these mixtures spontaneously yield catanionic vesicles that exhibit heightened stability and enhanced efficiency in drug encapsulation (Hao et al., 2004, Marques et al., 2003; Kume et al., 2008; Ravindar et al., 2022; Choudhury et al., 2024). The multifaceted nature of these vesicles broadens their utility across a spectrum of disciplines encompassing oil recovery(Li et al., 2020), purification processes (Lioi et al., 2009), biomedical sciences, and pharmaceuticals (Dhawan et al., 2017; Ghosh et al., 2016; Bramer et al., 2007). Driven by concerns over biocompatibility and environmental sustainability, there is an escalating trend towards the development of catanionic aggregates employing natural and bio-derived constituents (Marquès et al., 2021). Examples include aggregates derived from bile salts (di Gregorio et al., 2018), sugars

(Mahle et al., 2018; Thomas et al., 2009; Soussan et al., 2008), fatty acids (Fameau et al., 2014), and modified amino acids (Oliveira et al., 2021).

1.8. Objectives

The synthesis and biophysical characterization of small amphiphilic molecules have gained significant attention in recent years due to their potential applications in various fields, including drug delivery, materials science, and biotechnology. The synthesis of these molecules involves the development of efficient and versatile synthetic strategies, which allow the introduction of functional groups at precise locations on the molecule while maintaining the amphiphilic nature of the molecule. Biophysical characterization of these molecules includes systematic investigations on their phase transition using differential scanning calorimetry (DSC), self-assembly using isothermal titration calorimetry (ITC) and fluorescence spectroscopy and supramolecular organization through single-crystal X-ray diffraction and powder X-ray diffraction (PXRD). The biophysical properties of these small amphiphilic molecules are critical in determining their biological and industrial applications. For example, the ability of these molecules to form self-assembled structures, such as micelles, vesicles, and liposomes, is crucial in drug and gene delivery applications, as they can encapsulate hydrophobic drugs, DNA and RNA and protect them from degradation.

Furthermore, the ability of these molecules to interact with cell membranes can be exploited in developing antimicrobial agents and other therapeutic molecules. Incorporating cholesterol in both model and intact membranes induces diverse changes in the bilayer properties. In addition to that, cationic lipids can interact with anionic lipids and form a catanionic mixed lipid system, which has been seen to exhibit higher stability and versatile physicochemical properties. In view of this, we have synthesized and characterized several novel, biocompatible amphiphiles such as *O*-acyl-β-alaninols (OABAOHs), *O*-acyl-L-alaninols (OAAOHs), *N, O*-diacyl-L-alaninols (DAAOHs) and and *N*-acyl serinols (NSOHs) which is an agonist of the G-protein coupled receptor, GPR-119. These liposomes will be useful in different drug delivery studies. With this main objective, the following investigations have been carried out in the present study, and the results obtained are presented in Chapters 2-5.

- Biophysical characterization of long chain *O*-acyl-β-alaninols and equimolar *O*-myristoyl-β-alaninol/sodium dodecyl sulfate complex
- Long chain *O*-acyl-*L*-alaninols: Synthesis, structure, biophysical characterization and formation of equimolar catanionic liposomes with sodium dodecyl sulfate
- Thermotropic phase behavior and supramolecular organization of *N*, *O*-diacyl-L-alaninols: effect on stratum corneum model membrane
- Structure and supramolecular organization of *N*-acylserinols: agonists of the G-Protein Coupled Receptor, GPR-119

Chapter 2

Biophysical characterization of long chain *O*-acyl-β-alaninols and equimolar *O*-myristoyl-β-alaninol/sodium dodecyl sulfate complex

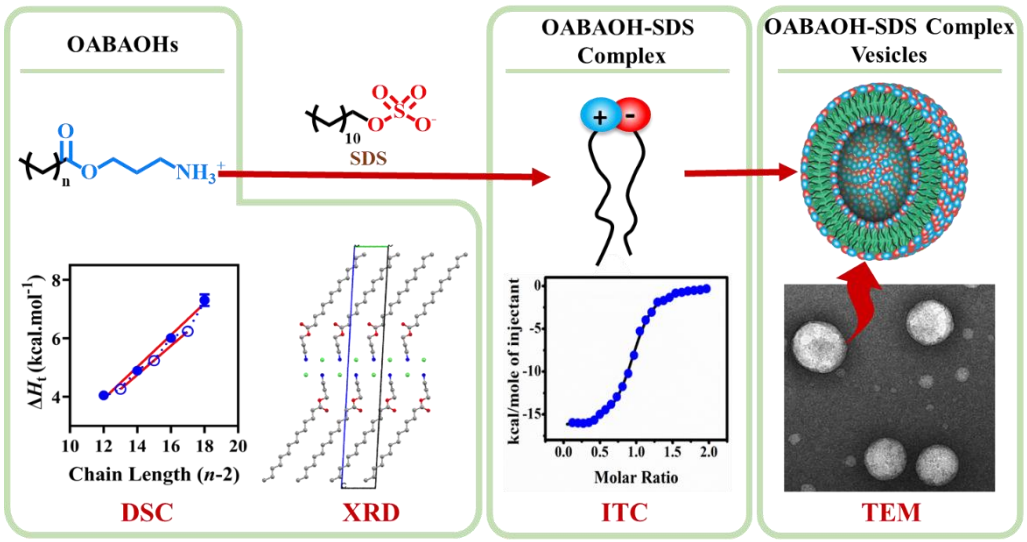

The work presented in this chapter was published in ***Colloid Surf. A: Physicochem. Eng. Asp.*** (2024) 133483

2.1. Summary

O-Acyl-β-alaninols (OABAOHs) are interesting amphiphiles in view of their ability to strongly inhibit *N*-acylethanolamine hydrolyzing acid amidase. In the present work, we synthesized and characterized long-chain OABAOHs bearing 14-20 C atoms in the acyl chain. Differential scanning calorimetric (DSC) studies showed that OABAOHs exhibit odd-even alternation in the solid-liquid phase transition enthalpies (ΔH_t) and entropies (ΔS_t). However, the odd- and even- chain length series independently showed linear dependence on the chain length (*n*) and values for the even chain length series are slightly higher than for the odd chain length series. Such odd-even alternation was not observed upon hydration, although ΔH_t and ΔS_t exhibited linear dependence on the chain length. Crystal structures of *O*-myristoyl-β-alaninol and *O*-palmitoyl-β-alaninol have been solved in triclinic crystal system with P-1 space group. In both structures, hydrocarbon chains of the amphiphiles are organized in a tail-to-tail format in a tilted bilayer. Powder X-ray diffraction data revealed odd-even alternation in the *d*-spacings of all OABAOHs, suggesting that the odd-even alternation observed in the thermodynamic properties most likely originates from differences in crystal packing. A number of C-H···O and N-H···Cl hydrogen bonds between OABAOH molecules from adjacent and opposite layers stabilize the overall supramolecular organization of the self-assembled bilayer system. In aqueous solution, turbidimetric and isothermal titration calorimetric studies established that *O*-myristoyl-β-alaninol and sodium dodecyl sulfate form an equimolar complex. Transmission electron microscopic, dynamic light scattering and DSC studies indicate that the complex forms unilamellar liposomes of ~150-160 nm diameter, which undergo a sharp thermotropic phase transition. These results provide a thermodynamic and structural basis for further investigations on OABAOHs including biomedical applications, e.g. in developing liposomal drug-delivery systems.

2.2. Introduction

3-Amino-1-propanol, or β-alaninol, is a compound derived from the reduction of β-alanine, a nonessential amino acid present in carnosine (a dipeptide of β-alanine and L-histidine). Supplementation of β-alaninol to *Tetrahymena* (a model organism used in biomedical research) led to the formation of phosphatidylpropanolamine and reduction of other phospholipids (Kovács et al., 1997; Smith and Barrows, 1988). Studies show that the *O*-acyl derivatives of β-alaninol, i.e., *O*-acyl-β-alaninols (OABAOHs), are potent inhibitors of *N*-acylethanolamine-hydrolyzing acid amidase (NAAA), which play a central role in the degradation of endogenous lipid mediators like *N*-acylethanolamines (NAEs) (Yamano et al., 2012; Ueda et al., 2010). Several derivatives (polymeric, dendritic, etc) of β-alaninol have been employed as drug carriers, non-viral gene carriers to treat brain tumours, and as antimicrobial agents (Jain et al., 2010; Mangraviti et al., 2015; Suleman et al., 2015).

Phospholipids form vesicular structures, and when they are kept for a long time, their metastable nature and thermodynamic instability often leads to precipitation as solid aggregates (Limin et al., 2001; Sakai et al., 2013). Conversely, the spontaneous formation of thermodynamically stable vesicles is observed in aqueous dispersions of mixed cationic and anionic single-chain lipids with simple structures (Sakai et al., 2013; Brady et al., 1984; Kaler et al., 1989; Tsuchiya et al., 2004; Yin et al., 2005; Brito et al., 2006). This phenomenon was observed across various single-tailed charged lipids and mixtures of cationic and anionic amphiphiles, which are also referred to as ion pair amphiphiles (IPA) or catanionic systems (Kaler et al., 1989; 2005; Dubois et al., 2001). Mixing aqueous solutions of cationic and anionic amphiphiles can result in spontaneous formation of catanionic vesicles, and these vesicles exhibit enhanced stability and improved efficiency in drug encapsulation compared to other types of vesicles. This is evidenced by numerous reports underscoring the versatility and promise of catanionic surfactant mixtures for various applications (Scamehorn, 1986; Šegota and Težak, 2006; Bramer et al., 2006; O′Driscoll et al., 2007; Kume et al., 2008; Lioi et al., 2009). Notably, these mixtures have demonstrated efficacy in diverse areas, including membrane applications, drug delivery, detergents, foaming processes, emulsions, wetting and others

(Bramer et al., 2006; Zhao et al., 2013; Rang, 2009; Stocco et al., 2010; Varade et al., 2011; Schelero et al., 2009; Wang et al., 2021).

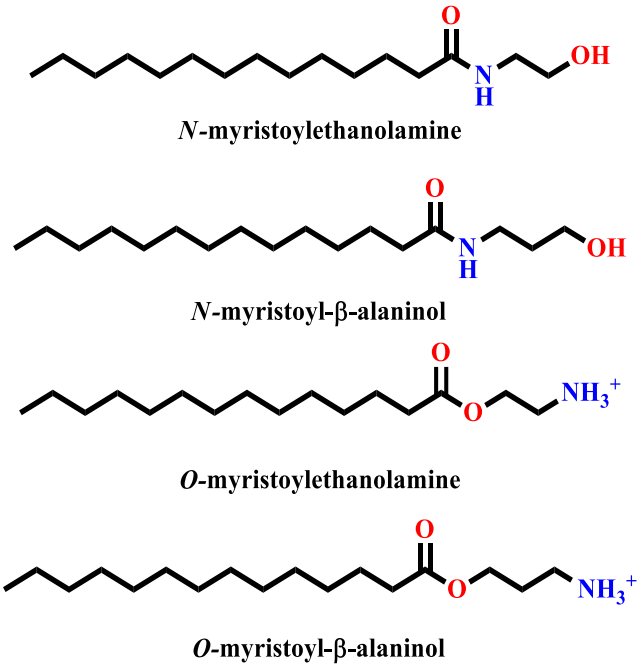

Fig. 2.1. Molecular structures of *N*-myristoylethanolamine, *N*-myristoyl-β-alaninol, *O*-myristoylethanolamine and *O*-myristoyl-β-alaninol.

OABAOHs are structural isomers of *N*-acyl-β-alaninols (NABAOHs) and share structural similarity with *O*-acylethanolamines (OAEs) (Sivaramakrishna et al., 2021a; Tarafdar et al., 2010a). While NABAOHs are non-ionic and contain an amide linkage, OABAOHs are cationic under physiological conditions and contain an ester linkage (Fig. 2.1). Cationic lipids have been recognized as highly versatile agents in drug delivery, particularly for transporting DNA and RNA in therapeutic applications as interaction of the positively charged head groups of cationic lipids with the negatively charged phosphate groups of nucleic acids results in the formation of condensed complexes (Zhi et al., 2013; Niculescu-Duvaz et al., 2003; Liu et al., 2017). The length and composition of the aliphatic chain in these amphiphiles can impact the fluidity of the hydrophobic region of the assembly (Sardar et al., 2018; Hazra et al., 2022; Tarafdar et al., 2010b). Transfection efficiency, biodegradability, stability, and cytotoxicity of cationic lipids depends on the length, number, type, and relative alignment of the linker bond that joins

the polar head group and the hydrophobic tail (Zhi et al., 2018; Karmali et al., 2007; Srinivas et al., 2009).

The foregoing shows that OABAOHs represent a novel family of amphiphiles with application potential in creating drug formulations and delivery systems. Direct interaction of these amphiphiles with membrane proteins may also affect their conformation and dynamics. Additionally, the ester linkage is base labile and can result in *O*- to *N*-acyl migration of the hydrocarbon chain, which could be used to design base labile nanocarriers for drug delivery applications (Sardar et al., 2018; Hazra et al., 2022). Cationic lipids can also interact with anionic lipids and form catanionic mixed lipid systems which exhibit high stability and versatile physicochemical properties (Reddy et al., 2017; Ravindar et al., 2022). In this context, it is imperative to conduct systematic investigations on their self-assembly, phase transition characteristics, molecular structure and supramolecular organization and the knowledge obtained from such studies will be highly useful in designing lipid-based drug delivery systems employing these amphiphiles. In this direction, in the present study, we have synthesized a homologous series of *O*-acyl-β-alaninols (n = 14–20) bearing saturated acyl chains and characterized their self-assembly, supramolecular organization and phase behavior using various spectroscopic, calorimetric and crystallographic techniques. Additionally, complex formation between *O*-myristoyl-β-alaninol with sodium dodecyl sulphate was investigated and the catanionic liposomes formed by the complex were characterized with respect to size, stability and polydispersity. The results obtained are discussed in this manuscript.

2.3. Materials and methods

2.3.1. Materials

Fatty acids, *N*, *N′*-dicyclohexylcarbodiimide (DCC), 4-dimethylaminopyridine (DMAP) and sodium dodecyl sulphate (SDS) were purchased from Sigma Aldrich (India). 3-(Tert-butoxycarbonylamino)-1-propanol was purchased from TCI Chemicals (India). 1,4-Dioxane, dichloromethane (DCM), chloroform and tetrahydrofuran (THF) were purchased from Sisco Research Laboratories (India). All other chemicals and solvents required in this work were obtained from local vendors and were of the highest purity available. Milli-Q water was used for preparing buffers and other aqueous solutions.

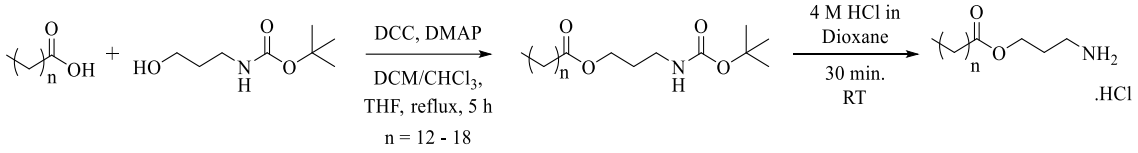

Scheme 2.1. Synthesis of *O*-acyl-β-alaninols.

2.3.2. Synthesis of O-acyl-β-alaninols

DCC (5.5 mmol), DMAP (1 mmol) and fatty acid of appropriate chain length (5 mmol) were dissolved in anhydrous DCM or chloroform. For reactions with C14-C16 fatty acids DCM was used as the solvent, whereas chloroform was used in reactions involving fatty acids bearing 17-20 C-atoms. After stirring for about 10 minutes, a solution of 3-(tert-butoxycarbonylamino)-1-propanol (5 mmol) in THF (5 mmol) was added to the reaction mixture. The reaction mixture was kept under reflux with stirring for 5 hours at 40°C and 60°C for compounds bearing acyl chains with 14-16 and 17-20 C-atoms, respectively. The mixture was then cooled, filtered through celite, and concentrated to yield a transparent oil that was purified using flash column chromatography. N-Boc protected *O*-acyl-β-alaninols were then deprotected using 4 M HCl in 1,4-dioxane for 30 minutes affording white coloured hydrochlorides of *O*-acyl-β-alaninols. The final product was refined through two recrystallizations at -18°C from DCM and chloroform for compounds with acyl chains bearing 14-16 and 17-20 C-atoms, respectively. The purified products were characterized by Fourier transform infrared (FTIR), ^{1}H NMR, and ^{13}C NMR spectroscopy and high-resolution mass spectrometry (HRMS).

2.3.3. Isothermal titration calorimetry

Critical micellar concentrations (CMC) of OABAOHs were determined by isothermal titration calorimetry. Experiments were carried out on a MicroCal PEAQ-ITC equipment from Malvern Instruments (Worcestershire, United Kingdom). In order to calculate the CMC of OABAOHs (C14–C16), small aliquots of the surfactant were injected into water from a 5–25 mM stock solution. A gap of 150 seconds was given between successive injections, with each 1.5 μL injection taking place over 3 sec. Throughout the titration, the solution in the reaction cell was constantly stirred at 750 rpm. As previously mentioned, an abrupt shift in enthalpy (ΔH_i) brought on by the injections was observed

and used to calculate the CMC (Heerklotz and Seelig, 2000; Tarafdar et al., 2010a). The first injection was usually found to be inaccurate, so the resulting point was eliminated before the rest of the data was analyzed to a "dissociation" model using the MicroCal PEAQ-ITC Analyser software provided by the ITC manufacturer.

The interaction between SDS and *O*-myristoyl-β-alaninol (OMBAOH) was investigated by ITC in the following manner. A 0.5 mM solution of OMBAOH in water was prepared. Using a rotating stirrer syringe, 1.5 µL aliquots of the solution were added sequentially to a sample cell containing 280 µL of a 50 µM aqueous solution of SDS. Concentrations of the cationic and anionic amphiphiles were kept well below their respective CMCs (Umlong and Ismail, 2007). Each injection was performed over a period of 3 seconds, and a time gap of 150 seconds was maintained between successive injections. Throughout the titration, the reaction cell contents were continuously stirred at 750 rpm. To address the potential inaccuracy of the first injection, a preliminary 1 µL injection was made, and the corresponding data point was excluded from the analysis. The remaining data were analyzed using the MicroCal PEAQ-ITC Analyser provided by MicroCal, as previously described. The analysis allowed the determination of the stoichiometry of binding (n), binding constant (K_b), and enthalpy of binding (ΔH_b). Additionally, based on these values, the free energy of binding (ΔG_b) and entropy of binding (ΔS_b) were calculated using the fundamental thermodynamic equations (2.1) and (2.2).

$$\Delta G_b = -RT \ln K_b \qquad (2.1)$$

$$\Delta G_b = \Delta H_b - T\Delta S_b \qquad (2.2)$$

2.3.4. Fluorescence spectroscopy

The CMCs of OABAOHs were also determined by fluorescence spectroscopy using pyrene as the fluorescent probe. A Horiba Jobin-Yvon Fluoromax-4 spectrofluorometer was used for the fluorescence measurements. In these experiments, small aliquots of OABAOHs from a 5–25 mM stock solution were added to a 1.0 mL solution of 2 µM pyrene. The fluorescence spectra were recorded between 350 and 500 nm keeping the excitation wavelength at 335 nm. The scan rate was set at 200 nm/min and 2.5 nm slits were used on both excitation and emission monochromators. The emission spectrum of

pyrene monomer displays five bands (Kalyanasundaram et al., 1977). Intensity ratio of bands one and three in the emission spectrum of pyrene (I_1/I_3), also known as the polarity ratio, was calculated for each spectrum and plotted as a function of amphiphile concentration. The concentration at which a clear break in the slope was observed was taken as the CMC.

2.3.5. Turbidimetry

The interaction between OMBAOH and SDS was also studied by turbidimetry using a JASCO V-750 UV-Vis spectrophotometer. Aqueous solutions of OMBAOH and SDS, each with a concentration of 0.2 mM (which is well below their critical micellar concentration), were mixed in various proportions and incubated for 30 minutes. The resulting turbidity was analysed at room temperature by measuring the optical density (OD) between 320 and 450 nm. Data was collected at a scanrate of 200 nm/min. The turbidity at 340 nm was selected for subsequent analysis.

2.3.6. Differential scanning calorimetry

A DSC-250 differential scanning calorimeter from TA instruments (New Castle, Delaware, USA) was used for studies on dry (solid) samples. Thermograms were collected between 25°C and 120°C with a scan rate of 2°/min by taking 2-3 mg of each sample in an aluminum sample pan, whereas the reference pan was prepared without any sample (Sivaramakrishna et al., 2021a). For each sample, three heating and two cooling scans were recorded in alternate heating and cooling cycles. All heating scans were reproducible with only minor decreases in the enthalpies in the second and third heating scans. Therefore, the first thermal scans were taken for further analysis.

For studies with hydrated samples, a lipid film was prepared on the inner walls of a test tube using 2-5 mg of each OABAOH dissolved in dichloromethane/methanol (1:1, v/v) followed by slow evaporation of the solvent and vacuum desiccation for several hours. The film was then hydrated with 1 mL of 150 mM NaCl and put through 5–6 freeze-thaw cycles. A Nano-DSC differential scanning calorimeter from TA instruments (New Castle, Delaware, USA) was used to perform DSC studies on these samples. The sample compartment was filled with 0.3 mL of the lipid suspension and the reference cell was filled with 150 mM NaCl. Three heating and two cooling thermograms were recorded

for each sample between 0 and 100°C at a scan rate of 60°/h. Although the temperature and enthalpy of the major transition peak were reproducible in repeat scans, the minor transition peaks were not seen in the subsequent heating cycles. Therefore, the second heating thermogram was considered for further analysis.

DSC measurements on hydrated OMBAOH-SDS equimolar catanionic mixtures were also performed by preparing a thin film of the sample on the inner walls of a test tube by evaporation from a solution in dichloromethane/methanol (1:1, v/v) and hydrating it with water to yield a 10 mM concentration of OMBAOH and SDS (20 mM total surfactant concentration). The sample was then subjected to a couple of freeze-thaw cycles (heating to ~60 °C) after which it was loaded into the DSC sample cell. Each sample was subjected to three heating and two cooling scans. Data obtained from repeat scans were found to be essentially identical and data obtained from the first heating scan were used for further analysis.

For all DSC experiments peak area under the transition curve was integrated to obtain the enthalpy of the phase transition (ΔH_t) and peak point of the transition curve was taken as the transition temperature (T_t). Transition entropy (ΔS_t) values were derived from transition enthalpyies and transition temperatures under the assumption of a first-order transition (Marsh, 1990):

$$\Delta S_t = \Delta H_t / T_t \qquad (2.3)$$

where T_t, ΔH_t and ΔS_t refer to the transition temperature, enthalpy and entropy, respectively.

2.3.7. Crystallization, structure solution and refinement

Thin plate type, colourless single crystals of OMBAOH and *O*-palmitoyl-β-alaninol (OPBAOH) were grown at room temperature from dichloromethane containing trace amounts of methanol. X-Ray diffraction data was collected at room temperature (~293 K) on a Xtlab Synergy Rigaku Oxford diffractometer with HyPix – 3000 detector, equipped with a graphite monochromator giving Mo Kα radiation (λ =0.7107 Å). The 2θ range for data collection was 2-25° for both samples. CrysAlisPro, Xtlab Synergy Rigaku Oxford Diffraction, Version 171.39.exe, and absorption correction based on the multi-scan approach were used to analyze the data interpretations. Olex2-1.2 programme was

used to solve and refine the crystal structures. Both structures were solved in P-1 space group in the triclinic crystal system. For OMBAOH the refinement was carried out using 3500 observed [>2σ (F0)] reflections, which converged into final R_1 = 0.1262, wR_2 = 0.3742 and goodness of fit = 1.065. For OPBAOH the refinement was carried out using 7677 observed [>2σ (F0)] reflections, which converged into final R_1 = 0.1295, wR_2 = 0.3317 and goodness of fit = 1.086.

2.3.8. Powder X-ray diffraction studies

Powder X-ray diffraction (PXRD) patterns of all OABAOHs (C14-C20) were captured using a Bruker SMART D8 Advance powder X-ray diffractometer (Bruker-AXS, Karlsruhe, Germany) with Cu-K radiation (λ = 1.5406 Å) at 40 kV and 30 mA as described earlier (Sivaramakrishna et al., 2015b). The circular spinning disk of the instrument sample holder was loaded with fine powders of the OABAOHs. A LynxEye PSD data collector was used to record diffraction patterns at room temperature over a 2θ range of 5-50° with a step size of 0.0198° and a measurement duration of 1.5s for each step. *d*-Spacings were determined using Bragg's equation from the diffraction peaks.

2.3.9. Dynamic light scattering

Dynamic light scattering (DLS) experiments were conducted to investigate the particle size and stability of catanionic vesicles made up of OMBAOH and SDS, prepared as described in Section 2.3.5, with minor modifications as indicated below. The lipid film containing the two amphiphiles in equimolar ratio was hydrated with water, sonicated in a bath sonicator at room temperature (~25 °C) for ~2 minutes, and then incubated at 10 °C for 12 hours to facilitate vesicle formation.

For DLS measurements, the samples were taken in a 1 mL quartz cuvette and placed securely in the sample chamber of a Horiba SZ-100 nanoparticle analyser (Ravindar et al., 2022). Multiple measurements were performed for each sample, and average values from three independent measurements are reported. The acquired data were analyzed using the built-in software of the instrument, which utilizes autocorrelation analysis to determine the particle size distribution and polydispersity index (PDI) of the vesicles. To ensure reliability of the results, the entire experiment was repeated with different batches

of OMBAOH–SDS catanionic vesicles, and the measurements were found to be consistent and reproducible.

2.3.10. Transmission electron microscopy

The morphology of OMBAOH-SDS vesicles was investigated using transmission electron microscopy (TEM) with the aid of a JEOL JEM-F200/F2 multipurpose electron microscope (Ravindar et al., 2022). A 0.5 mM catanionic vesicle suspension was prepared for TEM analysis following the same procedure as described above for DLS studies. A microsyringe was employed to load a 5-10 µL sample volume onto a carbon-coated copper grid, and any excess solution was removed by blotting with a filter paper. Subsequently, the sample on the grid was air-dried, and a stratified layer of 1.0% uranyl acetate solution was applied. Excess solution was removed with the aid of a blotting paper. The samples were then allowed to dry at room temperature (~25 °C) for a few minutes before examination by TEM.

2.4. Result and discussion

In the current study, a homologous series of OABAOHs have been synthesized by condensation of 3-(tert-butoxycarbonylamino)-1-propanol with fatty acids bearing saturated acyl chains (with 14-20 C atoms), followed by deprotection with the help of 4 M HCl in 1,4-dioxane. The structure and purity of the products obtained were characterized by FTIR, ^{1}H NMR and ^{13}C NMR spectroscopy and HRMS.

2.4.1. Spectroscopic characterization of OABAOHs

A representative FTIR spectrum of *O*-myristoyl-β-alaninol hydrochloride (OMBAOH) is shown in Fig. 2.2 as a representative example. Very similar IR spectra were obtained for the other OABAOHs. In general, OABAOHs showed absorption bands of the ester carbonyl group at ~1732-1739 cm^{-1}, C-H stretching bands at ~2846-2955 cm^{-1}, stretching bands for the two C-O bonds at ~1160-1170 cm^{-1} and ~1063-1070 cm^{-1}. The methylene scissoring and rocking bands are seen at ~1461-1471 cm^{-1} and ~717-729 cm^{-1}, respectively. The important IR resonances obtained for the homologous series of OABAOHs are listed in Table S1 of Chapter 2 (see supporting information)

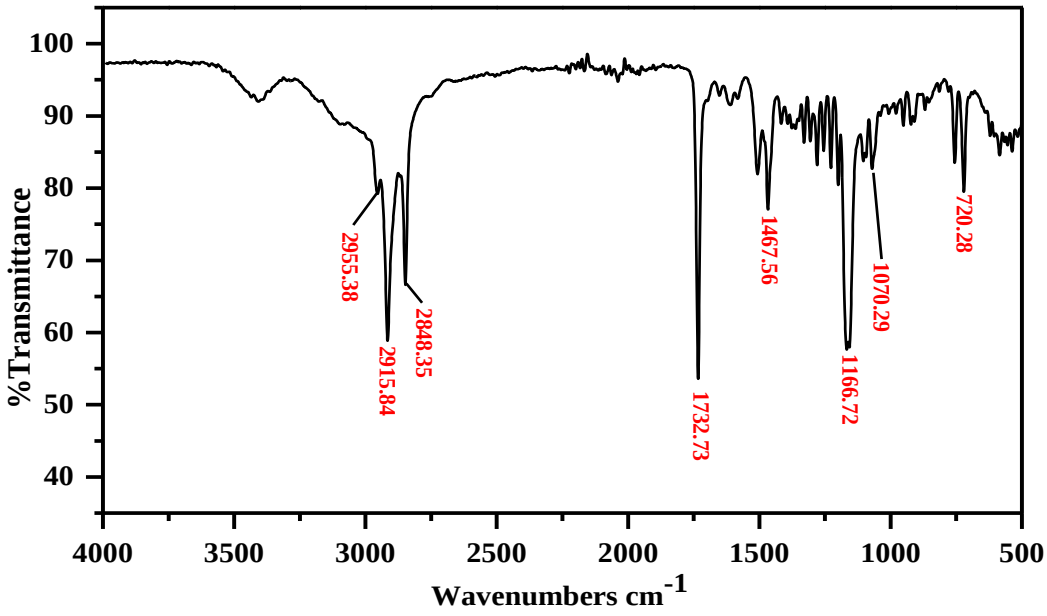

Fig. 2.2. FTIR spectrum of *O*-myristoyl-β-alaninol recorded at room temperature.

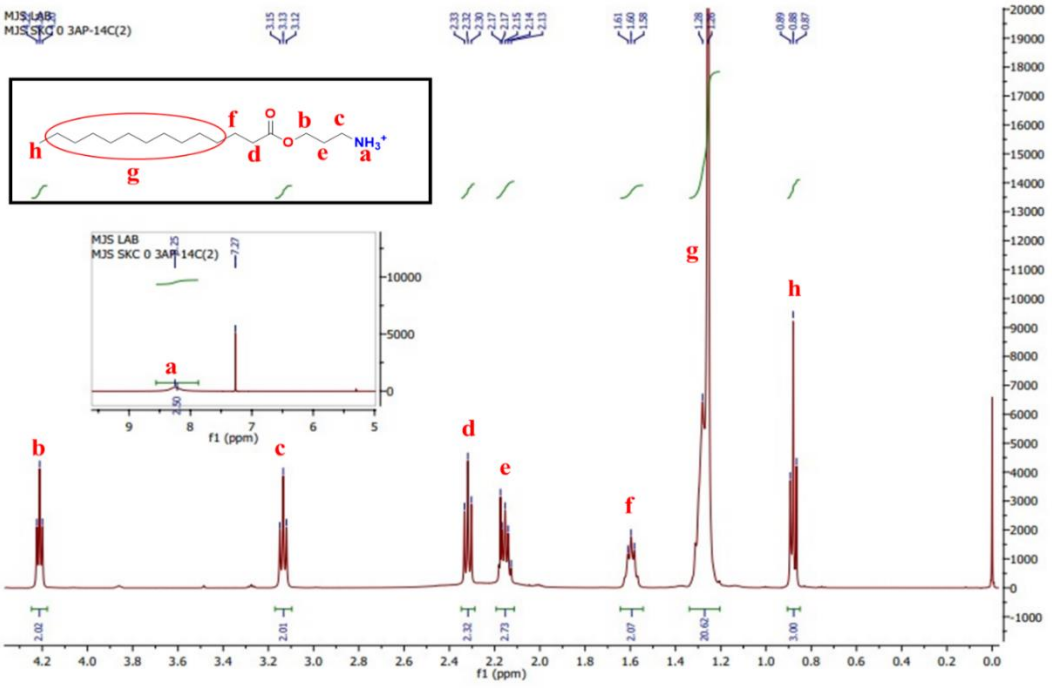

Fig. 2.3. ^{1}H-NMR spectrum of *O*-myristoyl-β-alaninol recorded at room temperature (solvent $CDCl_3$).

The ^{1}H-NMR spectrum of OMBAOH, taken as a typical example, is given in Fig. 2.3. The ^{1}H NMR spectra were recorded in $CDCl_3$ (in some cases with added DMSO-d_6/methanol-d_4) as the solvent. Proton NMR spectra of OABAOHs showed the following resonances: 0.52-0.88 δ (3H, t) corresponding to acyl chain terminal methyl group; 0.89-1.26 δ (nH, m) for acyl chain methylene groups except the α, β methylenes w.r.t. the acyl carbonyl; 1.23-1.60 δ (2H, m) for the β-methylene w.r.t. the carbonyl; 1.74-2.15 δ (2H, t) for the α-methylene w.r.t. the carbonyl; 2.63-3.13 δ (2H, t) for the methylene attached to the amide nitrogen; 1.19-2.32 δ (2H, t) for the β-methylene w.r.t. the hydroxyl group, 3.78-4.21 δ (2H, t) corresponding to methylene attached to the oxygen; 8.01-8.30 δ (3H, bs) corresponding to the amide hydrogens. The ^{1}H-NMR chemical shifts obtained for the OABAOHs with different acyl chains are listed in Table S2 of Chapter 2 (see supporting information)

The ^{13}C-NMR spectrum of OMBAOH is given in Fig. 2.4. The OABAOHs gave the following resonances: 13.53-14.32 δ, 21.99-22.90 δ and 28.64-29.92 δ for terminal methyl, α, β methylenes of the acyl chain. Resonance of C-atoms at the β and α positions w.r.t. the carbonyl were observed at 24.20-25.10 δ and 33.45-34.40 δ, respectively. Resonances for the C-atoms at α and β positions w.r.t. the ester oxygen were seen at 60.50-60.98 δ and 31.22-32.14 δ, respectively. Resonance of the C-atom at α position w.r.t. the amide N-H was seen at 36.33-37.31 δ. Finally, the resonance of carbonyl carbon was seen at 172.95-174.34 δ. The ^{13}C-NMR chemical shifts obtained for all the OABAOHs investigated here and bearing different acyl chains are listed in Table S3 of Chapter 2 (see supporting information)

A high-resolution mass spectrum of OMBAOH is presented in Fig. 2.5. The intense peak at m/z = 286.2756 matches well with the calculated mass of the molecular ion $[M+H]^+$, The additional peak seen at m/z = 571.5350 have been assigned as $[2M+H]^+$. All OABAOHs with (*n* = 14-20) acyl chains also show essentially similar mass spectrometric data and they are listed in Table S4 of Chapter 2 (see supporting information)

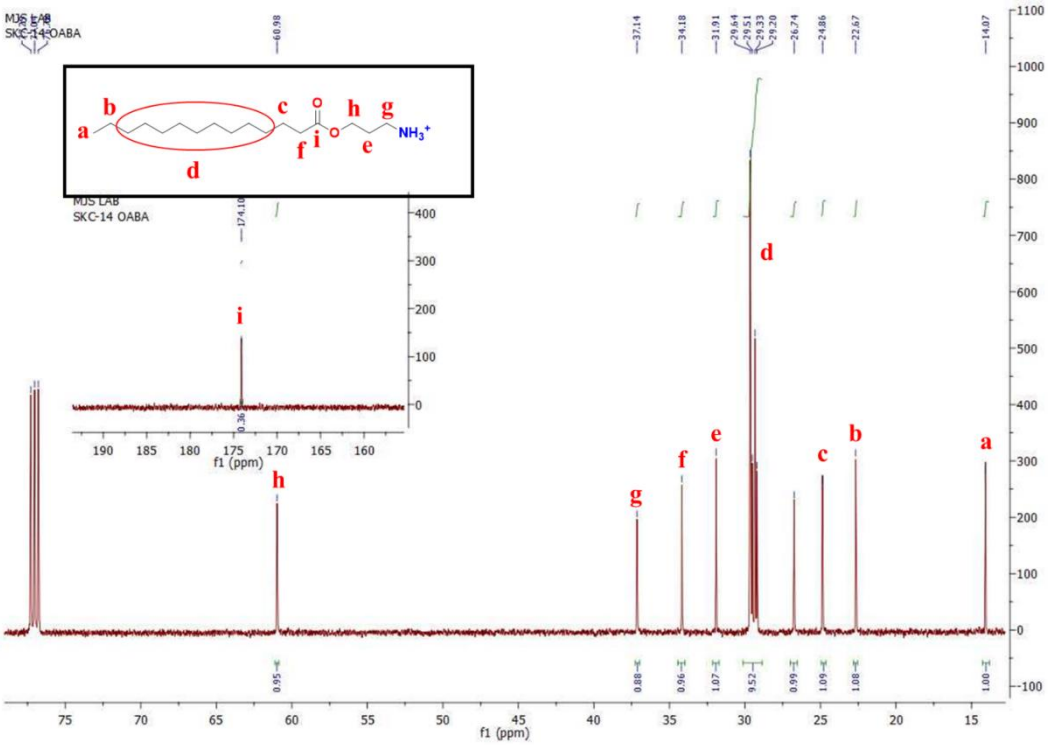

Fig. 2.4. ^{13}C-NMR spectrum of *O*-myristoyl-β-alaninol recorded at room temperature (solvent $CDCl_3$).

Fig. 2.5. ESI mass spectrum of *O*-myristoyl-β-alaninol.

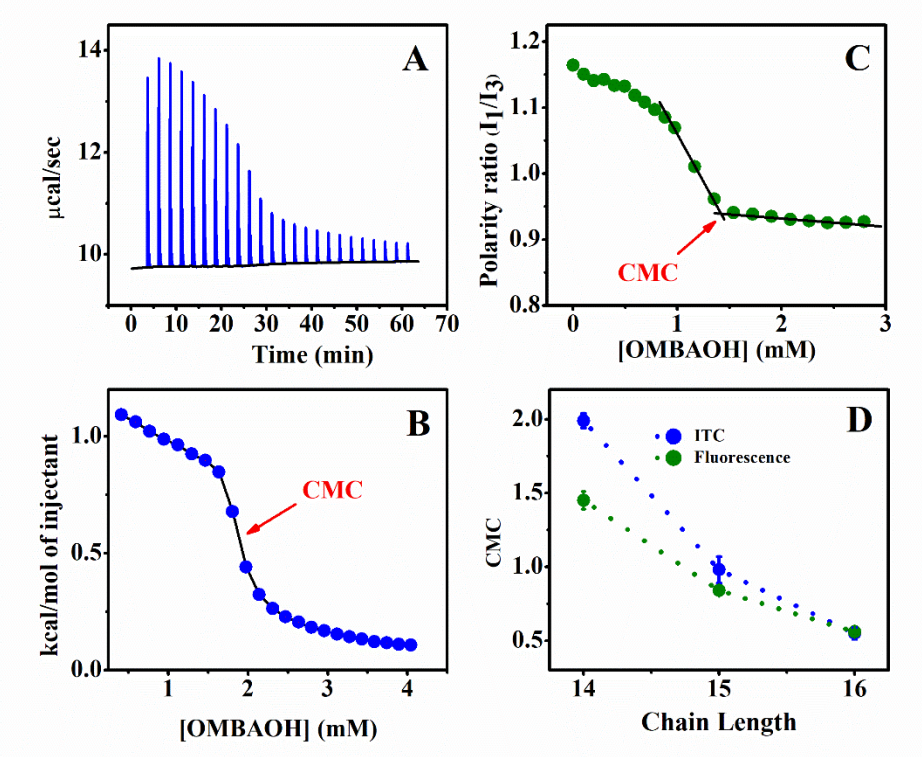

Fig. 2.6. Determination of the CMC of OMBAOH. (**A**) ITC profile obtained when aliquots were injected from a concentrated OMBAOH solution into water. (**B**) Integrated heats of dilution from the raw data shown in **A**. The CMC is obtained as 2.0 (±0.1) mM from the midpoint of the steeply decreasing part of the ΔH_i *vs* [OMBAOH] plot shown in **B**. (**C**) Determination of CMC by fluorescence spectroscopy using pyrene as a probe. The plot depicts the variation of the pyrene polarity ratio as a function of added OMBAOH concentration. The CMC is determined as 1.5 (±0.1) mM from the intercept of two linear fits. (**D**) Chain-length dependence of CMC.

2.4.2. Critical micellar concentration of OABAOHs

To determine the CMCs of OABAOHs (C14-C16) from ITC measurements, change in the enthalpy is monitored when each OABAOH was added from a stock solution (5-25 mM) to water. The top panel of Fig. 2.6A shows an ITC profile depicting the heat changes caused by the injection of small aliquots of OMBAOH from a 25 mM stock solution. Fig. 2.6B shows a plot of incremental heat changes as a function of surfactant concentration. The heat changes decrease gradually for successive injections, but display a steep decrease after about 7-8 injections, and after another 4-5 injections the heat changes again become gradual. Since this is a thermodynamically favourable process, the endothermic

changes must be accompanied by positive entropy changes, which most likely result from the disruption of water structure around the micelles (Tarafdar et al., 2010a; Bijma et al., 1997). The steep drop in the peak height observed in the middle of the titration indicates that the surfactant concentration in the reaction cell exceeded the CMC and that the micelles added subsequently to the reaction cell do not dissociate further. Therefore, the only cause of the enthalpy shift above the CMC is the effects of micelle dilution. From the inflection point in the ΔH_i versus lipid concentration plots, the CMC of OMBAOH, OPDBAOH, and OPBAOH was determined as 2.0 (±0.1) mM, 1.0 (±0.1) mM, and 0.55 (±0.04) mM, respectively.

Fluorescence spectroscopy was also used to estimate the CMC of OABAOHs by following changes in the fluorescence emission properties of pyrene probe when the concentration of the amphiphiles is altered (Sivaramakrishna et al., 2015b). The polarity ratio of the probe showed a steady decrease when the OABAOH concentration in solution was increased, but showed a steep change in the slope at a particular point. The CMC was calculated from the intercept of the linear least squares fits of the two sections of such plots. Such a plot for the determination of CMC of OMBAOH is shown in Fig. 2.6C. The CMC values obtained by this approach for OMBAOH, *O*-pentadecanoyl-β-alaninol (OPDBAOH) and OPBAOH are 1.5 (±0.1) mM, 0.84 (±0.02) mM and 0.56 (±0.01) mM, respectively. While the values for C14 and C15 compounds show 20-25% variation with the CMC values obtained from the ITC studies, the values obtained for C16 compound by both methods are nearly identical (Fig. 2.6D). Similar observations were made in earlier studies where ITC and fluorescence techniques were employed for estimating the CMC of other amphiphiles (Reddy et al., 2017; Ravindar et al., 2022).

2.4.3. DSC of dry and hydrated OABAOHs

First heating thermograms for dry OABAOHs with even and odd numbers of C-atoms in the acyl chain are shown in Figs. 2.7A and 2.7B, respectively. Each thermogram displays a prominent transition peak corresponding to the capillary melting point of the compound. In addition, one or two minor transitions are seen before the major transition peak and these can be interpreted as arising from solid−solid transitions, indicating polymorphism. In most cases these minor transitions were reproduced in repeat scans. Similar minor transitions have also been observed in other homologous series of single-chain

amphiphiles such as *N*-acylethanolamines (NAEs) and *N*-acyl-β-alaninols (NABAOHs) (Ramakrishna et al., 1997; Sivaramakrishna et al., 2021a). In the case of NAEs, the crystal structures of two different polymorphs of *N*-palmitoylethanolamine were solved and it was shown that a simple 180° rotation of a lipid layer in one polymorph could yield the other polymorph (Kamlekar and Swamy, 2006). It is possible that the minor transitions observed in OABAOHs also arise due to the presence of different polymorphic structures in the solid state. Thermograms that are essentially indistinguishable were obtained in the second and third heating scans. Thus, data obtained from the initial heating scans were selected for further analysis, and the transition temperature (T_t), transition enthalpy (ΔH_t) and transition entropy (ΔS_t) values are presented in Table 2.1.

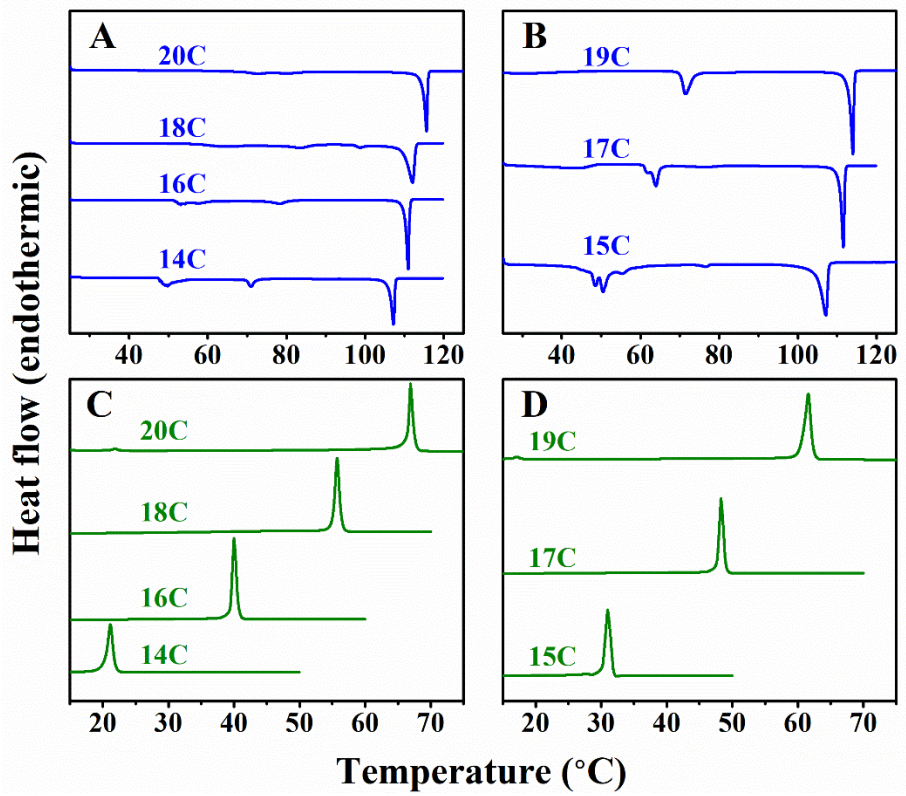

Fig. 2.7. DSC thermograms of dry and hydrated OABAOHs. (**A**, **B**) dry samples; (**C**, **D**) hydrated samples. The left panels (**A**, **C**) correspond to compounds with an even number of C atoms in the acyl chains, and the right (**B**, **D**) panels correspond to those with an odd number of C atoms. The number of carbon atoms in the acyl chain is indicated against each thermogram.

Table 2.1. Average values of transition temperatures (T_t), transition enthalpies (ΔH_t) and transition entropies (ΔS_t) of OABAOHs in dry and hydrated states. Samples were hydrated in 150 mM NaCl. Values in parentheses correspond to standard deviations from three independent measurements.

Acyl chain length	Dry OABAOHs			Hydrated OABAOHs		
	T_t (°C)	ΔH_t (kcal.mol^{-1})	ΔS_t (cal.mol^{-1}.K^{-1})	T_t (°C)	ΔH_t (kcal.mol^{-1})	ΔS_t (cal.mol^{-1}.K^{-1})
14	108.4 (0.1)	4.07 (0.01)	14.45 (0.05)	20.2 (0.6)	3.78 (0.19)	12.90 (0.66)
15	109.0 (0.1)	4.25 (0.14)	15.08 (0.49)	30.9 (0.1)	4.09 (0.09)	13.45 (0.31)
16	111.9 (0.1)	4.88 (0.08)	17.12 (0.27)	40.0 (0.1)	5.04 (0.10)	16.08 (0.32)
17	112.4 (0.1)	5.23 (0.19)	18.32 (0.66)	48.4 (0.1)	5.39 (0.56)	16.76 (1.74)
18	114.4 (0.1)	6.03 (0.01)	20.94 (0.03)	55.6 (0.4)	5.47 (0.24)	16.65 (0.71)
19	113.6 (0.1)	6.19 (0.01)	21.61 (0.01)	61.8 (0.2)	6.01 (0.47)	17.95 (1.42)
20	115.9 (01)	7.19 (0.07)	25.14 (0.22)	66.8 (0.1)	7.15 (1.11)	21.03 (3.26)

In a previous study it was shown that the presence of salt, such as NaCl stabilizes the lamellar structure of *O*-stearoylethanolamine even at elevated temperatures (Tarafdar et al., 2010b). To investigate the effect of salt on the phase transitions of OABAOHs, we hydrated OABAOHs with 150 mM NaCl and carried out DSC studies on them. The thermograms obtained with the even and odd chain-length compounds are shown in Fig. 2.7C and 2.7D, respectively. The values of transition temperature T_t, transition enthalpy (ΔH_t) and transition entropy (ΔS_t) for hydrated OABAOHs are presented in Table 2.1.

2.4.4. *Chain length dependence of transition enthalpy and entropy*

Figs. 2.8A and 2.8B present the relationship between acyl chain length of the OABAOHs in the solid state and the transition enthalpy (ΔH_t) and transition entropy (ΔS_t), respectively. The corresponding plots for the hydrated samples are shown in Figs. 2.8C and 2.8D, respectively. For solid OABAOHs, a linear dependence of ΔH_t and ΔS_t on the chain length is independently seen for the even and odd acyl chain length compounds, with the enthalpy and entropy values for the odd acyl chain length compounds being slightly lower than those for the even acyl chain length ones. Thus, when the data obtained for the entire series are examined together, a zig-zag pattern is observed. On the other hand, for the hydrated samples a linear dependence was observed for the transition enthalpies and entropies for the entire chain length series. The chain length dependent

ΔH_t and ΔS_t values could be fit to expressions 2.4 and 2.5, respectively (Larsson et al., 1986):

$$\Delta H_t = \Delta H_o + (n - 2)\, \Delta H_{inc} \quad (2.4)$$

$$\Delta S_t = \Delta S_o + (n - 2)\, \Delta S_{inc} \quad (2.5)$$

where ΔH_o and ΔS_o are the end contributions to ΔH_t and ΔS_t resulting from the terminal methyl group and the polar component of the molecule, and n is the number of C atoms in the acyl chains. The average incremental contributions of each CH_2 group to the overall ΔH_t and ΔS_t are ΔH_{inc} and ΔS_{inc}, respectively. It was previously noted that the transition enthalpies and entropies of several homologous series of single/double chain amphiphiles with saturated acyl/alkyl chains including diacyl phosphatidylcholines and phosphatidylethanolamines with matched, saturated acyl chains fit well to equations 2.4 and 2.5 (Ramakrishna et al., 1997; Tarafdar et la., 2012; Reddy et al., 2015; Marsh et al., 1991; 2000; Kamlekar et al., 2010). The incremental values (ΔH_{inc} and ΔS_{inc}) and end contributions (ΔH_o and ΔS_o) obtained from the linear least-squares analysis of ΔH_t and ΔS_t for the OABAOHs investigated here (for both solid samples and hydrated suspensions) are given in Table 2.2.

Table 2.2: Incremental values (ΔH_{inc} and ΔS_{inc}) of chain length dependence and end contributions (ΔH_o and ΔS_o) of the phase transition enthalpy and entropy of OABAOHs.

Thermodynamic parameter	**Dry OABAOHs**		**Hydrated OABAOHs**
	Even chain length	**Odd chain length**	**(odd- & even chain lengths)**
ΔH_{inc} (kcal/mol)	0.54 (0.02)	0.49 (0.02)	0.64 (0.03)
ΔH_o (kcal/mol)	-2.59 (0.30)	-2.18 (0.29)	-4.03 (0.46)
ΔS_{inc} (cal/mol/K)	1.82 (0.07)	1.66 (0.07)	1.59 (0.09)
ΔS_o (cal/mol/K)	-7.92 (1.07)	-6.60 (1.04)	-6.54 (1.42)

[a]Average values of ΔH_t and ΔS_t given in Table 2.1 have been used for linear fitting of the data. Errors shown in parentheses are fitting errors obtained from the linear least-squares analysis.

The fact that both transition entropy and enthalpy are linearly dependent on chain length suggests that the solid-state structures of OABAOHs with various even chain lengths exhibit high similarity. Similarly, the results indicate that structures of all odd-chain OABAOHs are also likely to be very similar. This conclusion is supported by the molecular packing and intermolecular interactions observed in the 3-dimensional structures of OMBAOH and OPBAOH, which will be further discussed below.

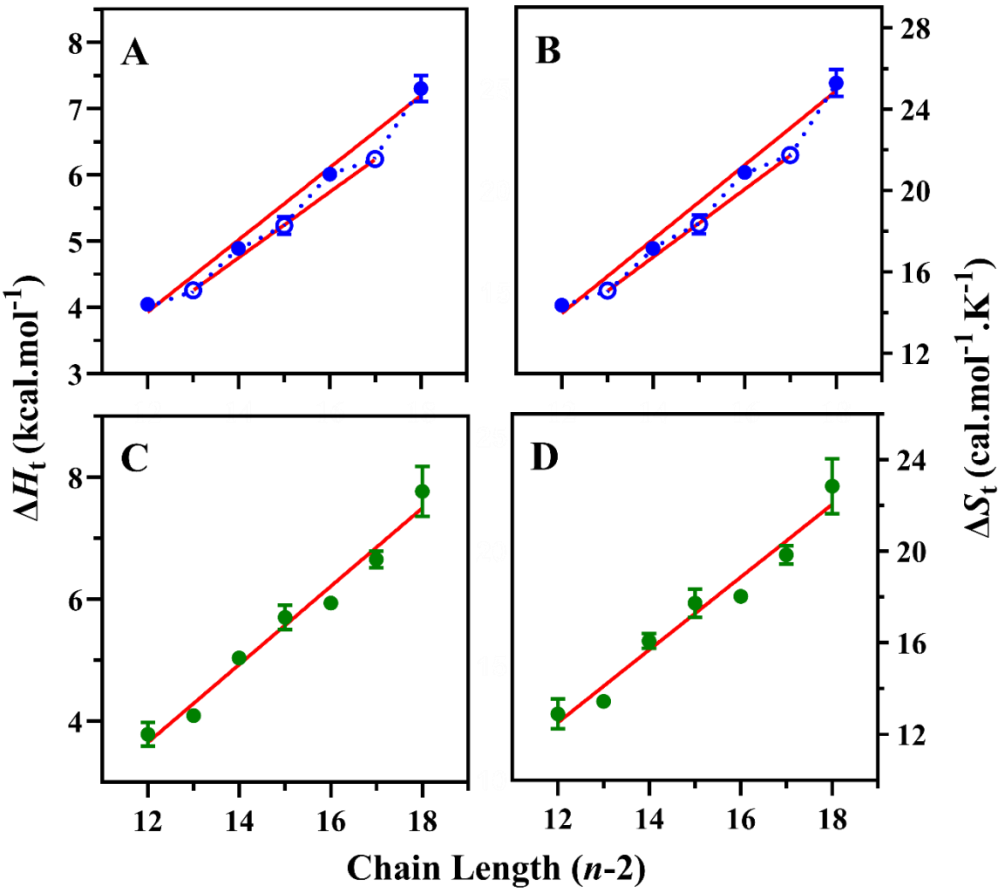

Fig. 2.8. Chain length dependence of transition enthalpy and transition entropy of OABAOHs in the dry state (**A**, **B**) and upon hydration with water (**C**, **D**). (**A**, **C**) Transition enthalpy; (**B**, **D**) transition entropy. For dry samples: open circles, (○) odd chain length; filled circles (●) even chain length. For hydrated samples: filled circles (●) both even- and odd- chain length. Values of ΔH_t and ΔS_t were plotted against the number of methylene (CH_2) units in the *N*-acyl chain (*n*-2). The solid lines in **A** and **B** represent linear least squares fits of the data for even and odd chain length series separately. The solid line in **C** and **D** represents the linear least-squares fit of the data.

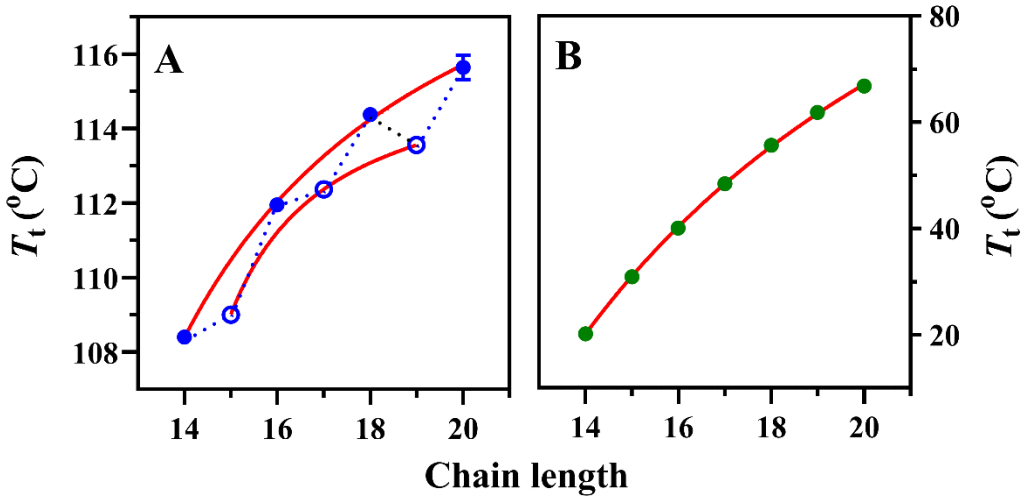

Fig. 2.9. Chain length dependence of chain-melting phase transition temperatures of OABAOHs. (**A**) Dry samples: (●) even chain-length compounds; (○) odd chain-length compounds. (**B**) Fully hydrated samples. The solid lines correspond to nonlinear least-squares fits of the transition temperatures to equation 6.

2.4.5. Chain length dependence of transition temperature

The transition temperatures of dry and hydrated OABAOHs increase with chain length (Fig. 2.9). However, in both situations, the magnitude of the shift gets smaller as the chains get longer. Fig. 2.9A shows that compounds in the even chain length series exhibit slightly higher transition temperatures than the odd chain length compounds. This alternation was not seen with the hydrated samples (Fig. 2.9B). A similar trend was observed previously for several long-chain amphiphiles such as *N*-acylethanolamines, *N*-acyldopamines, *N*-acylserotonins, and *N*, *O*-diacylethanolamines (Reddy et al., 2013; 2015; Kamlekar et al., 2010; Ramakrishna et al., 1998). However, in a few cases, e.g., *N*-acyl-L-alanines, *N*-acyl-L-alanine alkyl esters with matched chains, and L-alanine alkyl esters, the T_t values for the odd chain length series were found to be greater than those for the even chain length series (Sivaramakrishna et al., 2015a; 2015b; 2015c).

For a range of single-chain amphiphiles and two-chain lipids that exhibit linear dependence of ΔH_t and ΔS_t on the chain length, it has been shown that the values of ΔH_t and ΔS_t could be fitted to the equation below (Marsh, 1982):

$$T_t = \Delta H_t/\Delta S_t = T_t^{\infty} [1 - (n_o\text{-}n_o')/ (n\text{-}n_o')] \qquad (2.6)$$

Table 2.3. Crystallographic data for OMBAOH and OPBAOH.

Crystal parameter	**OMBAOH**	**OPBAOH**
Formula	$C_{17}H_{35}NO_2$. HCl	$C_{19}H_{40}NO_2$. HCl
Formula wt.	321.92	349.97
Crystal system	Triclinic	Triclinic
T, K	295.9(8)	297(1)
Space group	P-1	P-1
a (Å)	4.4857(4)	4.4763(2)
b (Å)	5.5889(8)	5.5917(2)
c (Å)	39.797(4)	87.300(3)
α	92.847(12)	90.768(3)
β	92.314(9)	90.651(3)
γ	95.143(29	95.270(4)
z	2	4
V (Å3)	991.47(19)	2175.52(14)
Dx (g cm-3)	1.078	1.068
μ (mm^{-1})	0.198	0.185
F(000)	356.0	776.0
Reflections collected	3500	7677
Independent reflections	2108	2412
Parameters	192	419
GOF	1.065	1.086
R indices (all data)	R_1 = 0.1671, wR_2 = 0.4004	R_1 = 0.2365, wR_2 = 0.4064
Final R indices	R_1 = 0.1262, wR_2 = 0.3742	R_1 = 0.1295, wR_2 = 0.3317

where n_o(= - ΔH_o/ ΔH_{inc}) and n_o' (= - ΔS_o/ ΔS_{inc}) are the values of n at which the ΔH_t and ΔS_t extrapolate to zero. Fig. 2.9A and 2.9B show that the T_t values of dry OABAOHs with even and odd acyl chains independently fit rather well to Eq. (2.6). The nonlinear least-squares fitting of T_t values of all the hydrated OABAOHs to Eq. (2.6) was quite satisfactory, as is evident in Fig. 2.9B. The T_t^{∞} values for even and odd OABAOHs in the dry state were 398 and 389 K, respectively, and 432 K, for the hydrated OABAOHs.

2.4.6. Description of structure

ORTEPs presented in Fig. 2.10A and Fig. 2.11A depict the molecular structures of OMBAOH and OPBAOH determined by single-crystal X-ray diffraction. The atom numbering for all non-hydrogen atoms is shown in these ORTEPs. Table 2.3 lists the crystal parameters for these two compounds, and Tables S5-S7 (OMBAOH) and S8-S10 (OPBAOH) provide the corresponding atomic coordinates, equivalent isotropic displacement parameters, bond lengths and torsion angles.

These results demonstrate that hydrocarbon portion of the acyl chains of OMBAOH (C2-C14) and OPBAOH (C2-C16) exist in an *all-trans* conformation (Fig. 2.10A and Fig. 2.11A) with all the torsion angles being ~180°. The torsion angle corresponding to the O2-C1-C2-C3 linkage in OMBAOH and OPBAOH is 169.1° (see Fig. 2.10B) and -169.4°(see Fig. 2.11B), respectively. The molecular structures of OMBAOH and OPBAOH are very similar. The torsion angles observed for C17-C16-C15-O2 and O2-C17-C18-C19 linkage in OMBAOH and OPBAOH are -69.7° (see Fig. 2.10B) and -71.7° (see Fig. 2.11B), respectively. The gauche conformation at the C15-C16 bond in OMBAOH and C17-C18 bond in OPBAOH results in a bending of the molecule, giving it an ice hockey stick like shape. In NAEs bearing saturated acyl chains such as *N*-myristoylethanolamine, *N*-palmitoylethanolamine and *N*-stearoylethanolamine similar bending of the molecule due to gauche conformation at a single C-C bond was reported earlier which gave them a bent structure resembling the letter ‘L’ (Kamlekar and Swamy, 2006; Dahlén et al., 1977; Ramakrishnan and Swamy, 1999). Interestingly, in the isomeric *O*-acylethanolamines (OAEs) such as *O*-stearoylethanolamine a significant difference is observed in the acyl chain conformation, due to which the molecular

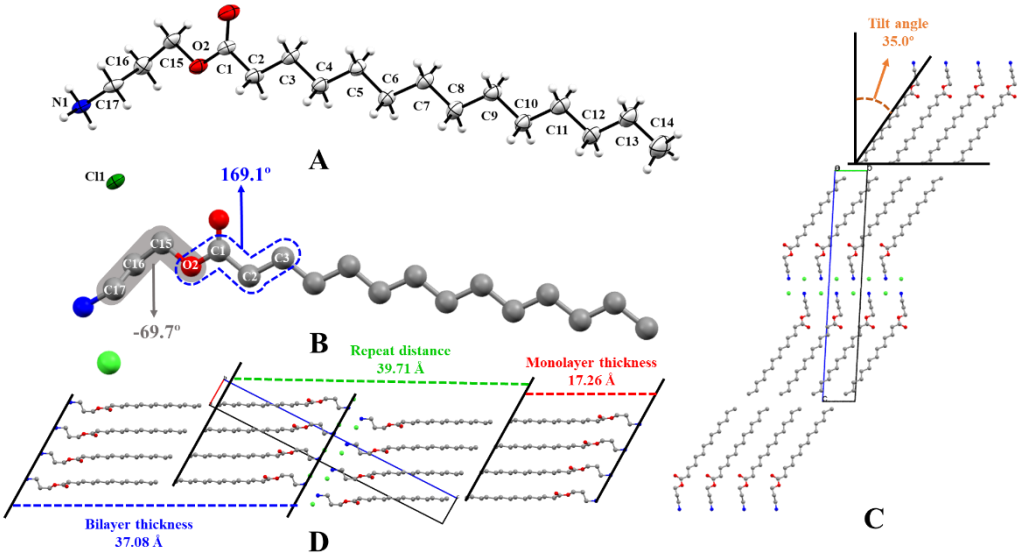

Fig. 2.10. Molecular and crystal structures of *O*-myristoyl-β-alaninol. (**A**) ORTEP; (**B**, **C**) packing diagrams along the *a*-axis and *b*-axis, respectively. Hydrogen atoms were omitted in the packing diagrams for clarity.

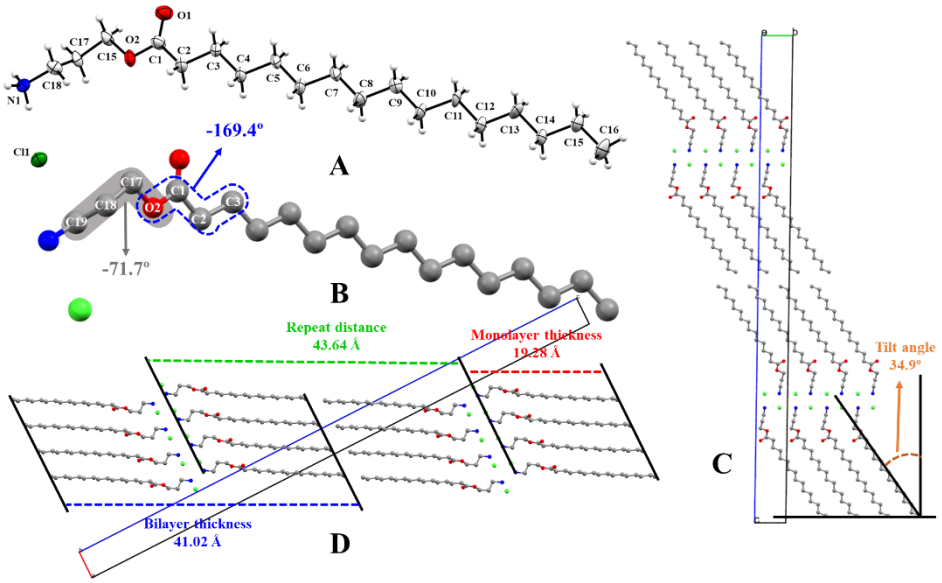

Fig. 2.11. Molecular and crystal structure of *O*-pamitoyl-β-alaninol. (**A**) ORTEP of OPBAOH. (**B**, **C**) Packing diagrams along the *a*-axis and *b*-axis, respectively. Hydrogens were omitted in the packing diagrams for clarity.

geometry changes from a bent structure in the NAEs to an essentially linear structure in OAEs (Tarafdar et al., 2010b; Kamlekar et al., 2006; Ramakrishnan and Swamy, 1999). It is pertinent to note here that OAEs are also structural homologues of OABAOHs. Similarly, the acyl chain conformations in NPBAOH exhibits distinct differences from its isomer OPBAOH (Sivaramakrishna et al., 2021a).

2.4.7. Molecular packing

Packing diagrams of OMBAOH, viewed along the *a*-axis and *b*-axis, are shown in Figs. 2.10C and 2.10D, respectively. Similarly, the packing diagrams of OPBAOH, viewed along the *a*-axis and *b*-axis, are shown in Figs. 2.11C and 2.11D, respectively. These diagrams show that in OMBAOH, each unit cell contains two molecules, whereas in OPBAOH, each unit cell contains four molecules. In both cases the molecules are packed in a head-to-head (and tail-to-tail) manner in stacked bilayers. The hydrocarbon chains in the two leaflets of the bilayer are at an angle of 180° with each other, resulting in a collinear arrangement of the chains, similar to that seen in NAEs (Kamlekar and Swamy, 2006; Dahlén et al., 1977; Ramakrishnan and Swamy, 1999). The methyl ends of the stacked bilayers are in van der Waals contact, with the closest methyl-methyl contact distance (C14-C14 in OMBAOH and C16-C16 in OPBAOH) between the opposing layers and within the same layer being 3.84 Å and 4.49 Å for OMBAOH and 3.83-3.88 and 4.48 Å for OPBAOH, respectively. The bilayer thickness (i.e., Me − Me distance) in the crystal lattices of OMBAOH and OPBAOH are 37.08 Å and 41.02 Å, respectively, and the monolayer (single leaflet) thickness (O3 − C12 distance) for OMBAOH is 17.26 Å. For OPBAOH (O3-C14 distance), it is 19.28 Å. The repeat distance (*d*-spacing) is 39.71 Å and 43.64 Å for OMBAOH and OPBAOH, respectively. Area per molecule of OMBAOH and OPBAOH is 25.1 $Å^2$ and 25.0 $Å^2$, respectively. The *O*-acyl chains are tilted by 35.0° in OMBAOH (Fig. 2.10D) and 34.9° in OPBAOH (Fig. 2.11D) with respect to the bilayer normal.

2.4.8. Subcell packing

The different lateral packing modes observed in hydrocarbon chains of lipid crystal are usually described in terms of subcells which specify the relations between equivalent

positions within the chain and its neighbours. Such chain packing modes have been classified into a small number of subcells on the basis of symmetry considerations such as triclinic, monoclinic etc. Further, within each category, the polymethylene planes of the chains can be parallel or perpendicular with respect to their neighbours (Abrahamsson et al., 1978; Maulik et al., 1990). Analysis of the acyl chain packing in OMBAOH and

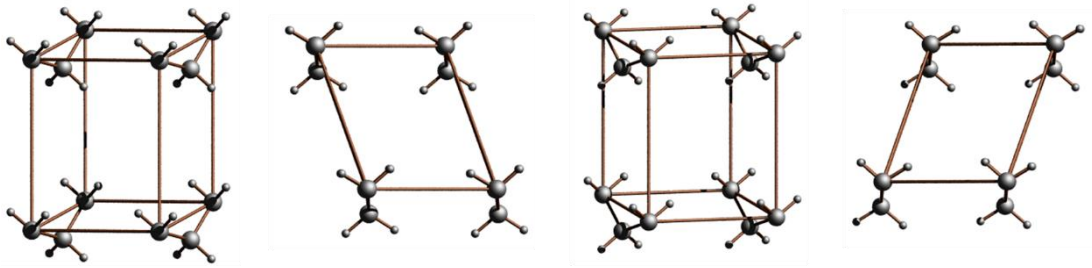

Fig. 2.12. Subcell packing of (**A**, **B**) OMBAOH and (**C**, **D**) OPBAOH. Both subcells belong to the classic triclinic parallel ($T_{//}$) type.

OPBAOH indicated that the subcells in their crystals belong to the classic triclinic parallel ($T_{//}$) type (Fig. 2.12). The unit cell dimensions of these subcells are given in Table 2.4.

Table 2.4. Subcell dimensions of OMBAOH and OPBAOH.

Cell parameter	OMBAOH	OPBAOH
a (Å)	5.59	5.59
b (Å)	4.48	4.47
c (Å)	2.53	2.55

2.4.9. Hydrogen bonding and intermolecular interaction

Close examination of the molecular packing in the crystal structure of OMBAOH and OPBAOH revealed that the intermolecular interactions in these compounds involve two types of hydrogen bonds: C-H···O and N-H···Cl. The H-bonds in OMBAOH and OPBAOH are shown in Fig. 2.13A and 2.13B, respectively and the bond distances and angles are listed in Table 2.5. Each ammonium group forms hydrogen bonds with three chloride ions, with two of these N-H···Cl hydrogen bonds bridging adjacent molecules in the same leaflet, whereas the third N-H···Cl H-bond connects the molecules from opposite

layers. Details of the three types of N–H···Cl H-bonds observed in the crystal structures of OMBAOH and OPBAOH are listed in Table 2.5, including the hydrogen bond distance (H···Cl), donor-acceptor distance, and bond angle at the H atom.

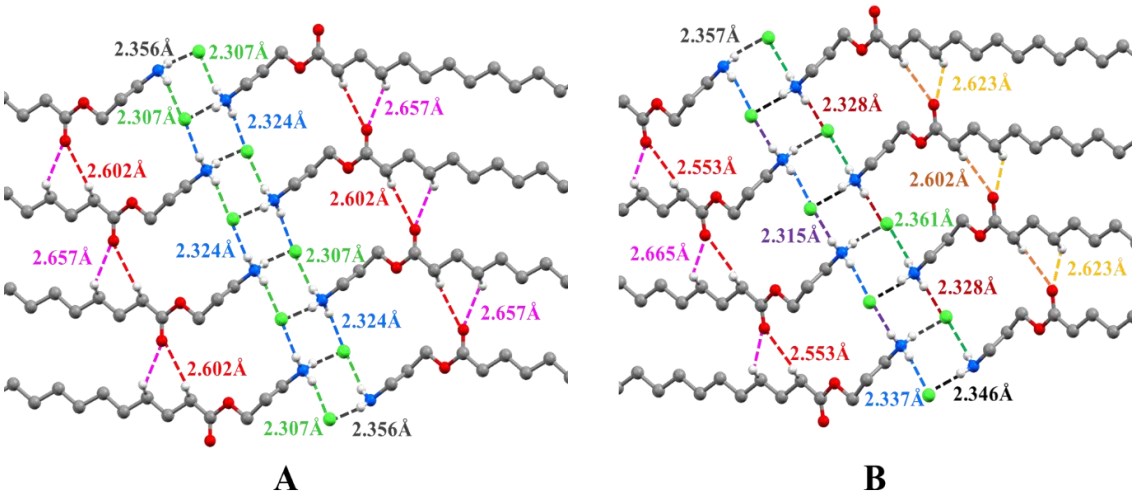

Fig. 2.13. Hydrogen bonding pattern in the crystal lattice of OMBAOH (**A**) and OPBAOH (**B**). Similar colours have been used for similar bonds. Colour code for atoms: grey, carbon; red, oxygen; blue, nitrogen. Hydrogen atoms not involved in H-bonds have been omitted for clarity.

In addition to the N–H···Cl interactions, a C-H···O interaction was also seen between a carbonyl oxygen (O1) from a neighbouring molecule and an H-atom on the C2 and C4 carbon atoms (at α- and γ- positions with respect to the ester carbonyl) (Figs. 2.13A and 2.13B). Two types of C–H···O bonds are seen in the crystal structure of OMBAOH and OPBAOH. In OPBAOH, same kind of C-H···O and N-H···Cl bonds in opposite layers show minor differences in the H-bond characteristics. The corresponding H-bond distance, donor-acceptor distance and the bond angle at 'H' atom are given in Table 2.5.

2.4.10. Powder X-ray diffraction studies

Powder X-ray diffraction (PXRD) experiments provided additional details on the molecular packing of OABAOHs with various acyl chain lengths. Figs. 2.14A and 2.14B display the PXRD data obtained at room temperature for OABAOHs with even and odd chain lengths, respectively. All OABAOHs (n = 14–20) produced a number of distinct

peaks in the 2θ range of 5−50°. The *d*-spacing was determined from the position of these diffraction peaks. For each compound, the *d*-spacing was estimated using 4−5 peaks and the values obtained are presented in Table 2.6. Fig. 2.14C displays a plot of the *d*-spacings of OABAOHs as a function of acyl chain length. From this plot it is seen that the even

Table 2.5. Details of hydrogen bond distances and angles in the crystal structures of OMBAOH and OPBAOH.

Bond	H-bond distance (Å)	Donor-acceptor distance (Å)	Bond angle at 'H' (°)
C14-BAOH			
C-H···O	2.602	3.425	142.79
„	2.657	3.441	138.17
N-H···Cl	2.324	3.208	172.29
„	2.356	3.235	169.40
„	2.307	3.164	161.48
C16-BAOH			
C-H···O	2.553	3.374	142.52
„	2.665	3.433	136.42
„	2.623	3.415	138.92
„	2.602	3.436	144.27
N-H···Cl	2.315	3.201	173.46
„	2.346	3.234	175.20
„	2.328	3.207	169.37
„	2.337	3.186	159.72
„	2.361	3.171	151.37
„	2.357	3.239	170.98

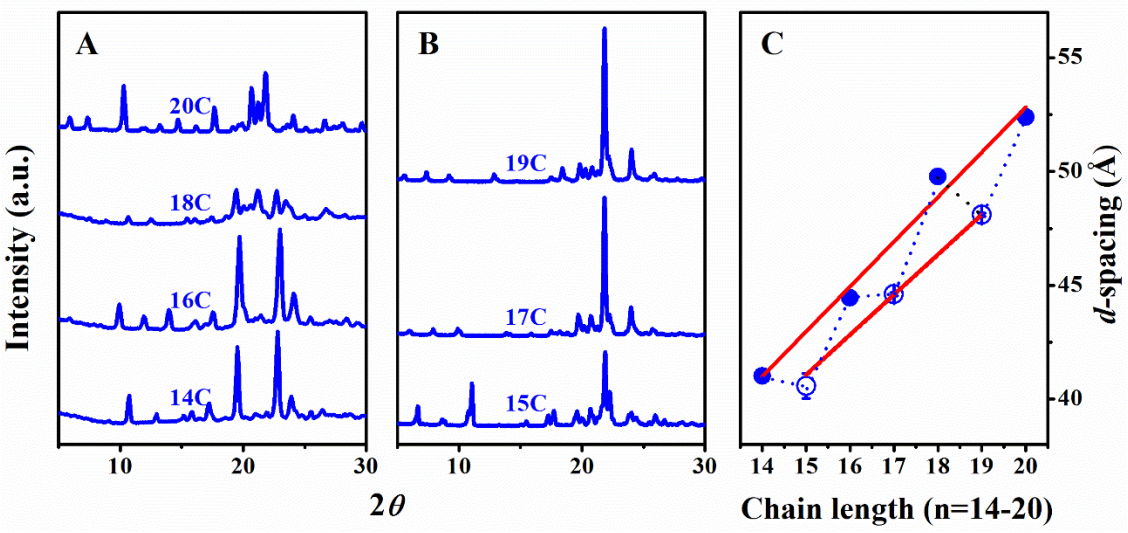

Fig. 2.14. Powder X-ray diffraction patterns of OABAOHs. Data for compounds with even acyl chain length (**A**) and odd acyl chain length (**B**) are shown. (**C**) Dependence of *d*-spacing on the acyl chain length. The number of C-atoms in the saturated, unbranched acyl chains is indicated against each PXRD profile. Solid lines in C represent linear fits of the data for even- and odd-chain length series, separately. Filled circles (●), even chain length; open circles (○), odd chain-length.

chain-length OABAOHs exhibit higher *d*-spacings than the odd chain-length ones, indicating a clear odd-even alternation.

The slopes of the two separate linear dependences seen for the even and odd acyl chain length series in Fig. 2.14C are 1.974 and 1.882 Å/CH_2, respectively, and indicate increases of 0.987 and 0.941 Å per additional CH_2 moiety. Since in a typical bilayer with all-trans acyl chains oriented perpendicular to the bilayer plane, increase in the acyl chain length by one CH_2 unit raises the *d*-spacing by 1.27 Å for each layer (2.54 Å for the bilayer), the incremental increase in the *d*-spacings estimated here indicate that the acyl chains must be tilted with respect to the bilayer normal. The larger deviation of the incremental *d*-spacing observed with the odd chain-length OABAOHs from the ideal value indicates that they are more tilted as compared to those with even chain lengths. From the incremental *d*-spacings the tilt angles (with respect to the bilayer normal) could be estimated as 39° and 42.2° for the even- and odd chain-length series, respectively. The value obtained for the even chain length series is in fairly good agreement with the value of 35° determined from the crystal structures of OMBAOH and OPBAOH (*n* = 14, 16).

Table 2.6. Lamellar *d*-spacings of OABAOHs with different acyl chain lengths (*n* = 14–20), derived from the powder X-ray diffraction data.

Chain length	d-spacing
14	40.1 (0.5)
15	40.6 (0.5)
16	45.5 (0.5)
17	44.6 (0.1)
18	48.9 (0.1)
19	48.1 (0.1)
20	55.4 (0.3)

2.4.11. Interaction between OMBAOH and SDS: Turbidimetric, ITC and DSC studies

The investigation of several systems of catanionic mixed amphiphiles revealed that they form unilamellar liposomes with considerable potential for application in developing drug delivery systems (Zhao et al., 2013; Tarafdar et al.,2010a; Reddy et al., 2017; Ravindar et al., 2022; Sivaramakrishna et al., 2015c). In this study, we focused on examining the interaction between the cationic amphiphile OMBAOH and sodium dodecyl sulphate (SDS), using turbidimetry, isothermal titration calorimetry and DSC. The results obtained from all three methods consistently indicate the formation of an equimolar complex between these two surfactants.

OMBAOH forms an optically clear solution in water. Upon the addition of small aliquots of SDS solution, the optically clear sample becomes turbid, suggesting the formation of larger aggregates. This can be attributed to the interaction between the cationic OMBAOH and the negatively charged dodecyl sulfate, leading to the formation of larger aggregates compared to those formed by OMBAOH or SDS alone. To investigate this phenomenon, we carried out turbidimetric experiments according to Job's method. The total surfactant concentration was held constant throughout the experiments, and the optical density at 340 nm, of the mixtures are presented in Fig. 2.15A. The plot reveals that the turbidity of the mixed surfactant solution initially increases with increasing SDS content until an X_{SDS} value of 0.5, but decreases with further increase in

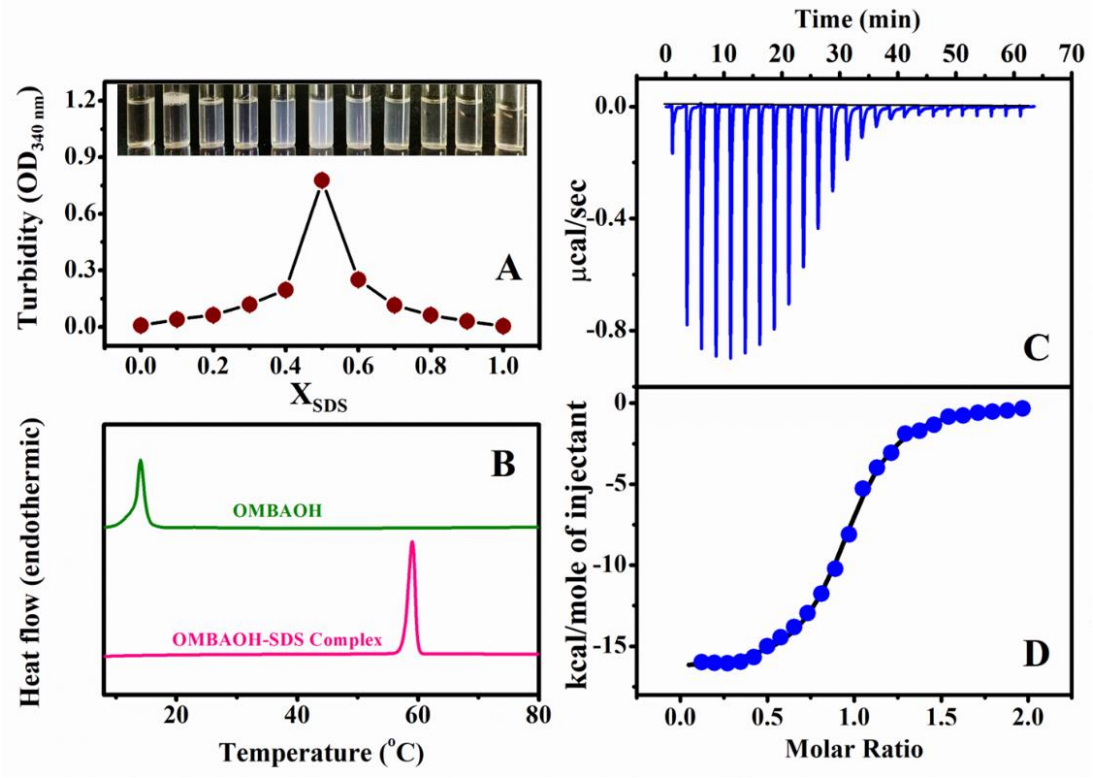

Fig. 2.15. Interaction of OMBAOH with SDS studied by Job's method and ITC. (**A**) Job's experiment measuring the turbidity of various mixtures of OMBAOH and SDS. The photo at the top shows turbidity of the samples and the plot below shows the optical density of the individual samples at 340 nm. (**B**) DSC thermograms of the OMBAOH and equimolar OMBAOH-SDS complex in water. (**C**, **D**) Interaction of OMBAOH and SDS studied by ITC. (**C**) Raw heats released for successive injections. (**D**) Integrated heats obtained from the titration data shown in **C** after correcting for dilution effects. The solid line represents the best curve fit of the experimental data to the 'one set of sites' binding model in MicroCal PEAQ-ITC data analysis software.

SDS content. The higher turbidity observed at $X_{SDS} = 0.5$ suggests the formation of large aggregates comprising the two components in an equimolar ratio.

Thermodynamic factors governing the interaction between OMBAOH and SDS were characterized by ITC, and the results are presented in Figures 2.15C and 2.15D. Concentrations of the two surfactants were kept well below their CMC in order to avoid complications from the presence of micelles. Fig. 2.15C shows that the exothermic heat of binding remains relatively constant for the initial injections of OMBAOH, but gradually decreases as more OMBAOH is added until saturation is achieved. Fig. 2.15D

depicts a plot of incremental heat changes against the OMBAOH/SDS ratio, and analysis of this data employing the 'one set of sites' binding model (solid line in the lower panel) yielded the following thermodynamic parameters. Stoichiometry of binding (n) = 0.94 ± 0.01, the binding (association) constant (K_b) = 9.74 (± 1.27) × 10^5 M^{-1}, enthalpy of binding (ΔH_b) = -17.4 ± 1.1 kcal.mol^{-1}, entropy of binding (ΔS_b) = -29.9 ± 3.5 cal.mol^{-1} K^{-1}. From these values the free energy of binding (ΔG_b) was estimated to be -8.30 kcal mol^{-1}. The stoichiometry of binding (n = 0.94) obtained from the ITC analysis is in excellent agreement with the results obtained from Job's experiment, further confirming that the interaction between OMBAOH and SDS leads to the formation of an equimolar complex between the two surfactants.

The thermal stability of the OMBAOH-SDS catanionic mixed system in water was investigated by differential scanning calorimetry. DSC thermograms of equimolar complex of OMBAOH and SDS exhibited a single, well-defined endothermic peak centered at 59.0 °C indicating that the complex undergoes a clear-cut phase transition (Fig. 2.15B). Repeat scans confirmed the reversibility and reproducibility of the thermal behavior. The transition enthalpy (ΔH_t) and entropy (ΔS_t) were found to be 14.84 (±0.14) kcal.mol^{-1} and 44.70 (±0.42) cal.mol^{-1}.K^{-1} respectively. In comparison, OMBAOH alone displayed a single, sharp endothermic peak centered at 14.1 °C with a transition enthalpy (ΔH_t) of 3.51 (±0.17) kcal.mol^{-1} and transition entropy (ΔS_t) of 12.3 (±0.64) cal.mol^{-1}.K^{-1}. On the other hand, SDS did not exhibit any thermal transition under similar conditions (not shown), which is consistent with its existence as micelles under these conditions (Rajkhowa et al., 2017). In the mixture, the samples appeared turbid at room temperature but became optically clear above the phase transition temperature, indicating that the mixture most likely exists in a micellar form above T_t. These observations indicate that the equimolar mixture of NMBAOH and SDS forms stable liposomes, which undergo a reversible transition from a lamellar gel phase to a micellar phase.

2.4.12. Characterization of the size and charge of liposomes by TEM and DLS

The above observations indicate that catanionic aggregates are formed by mixing OMBAOH and SDS in equimolar ratio. The morphology and size of these ensembles

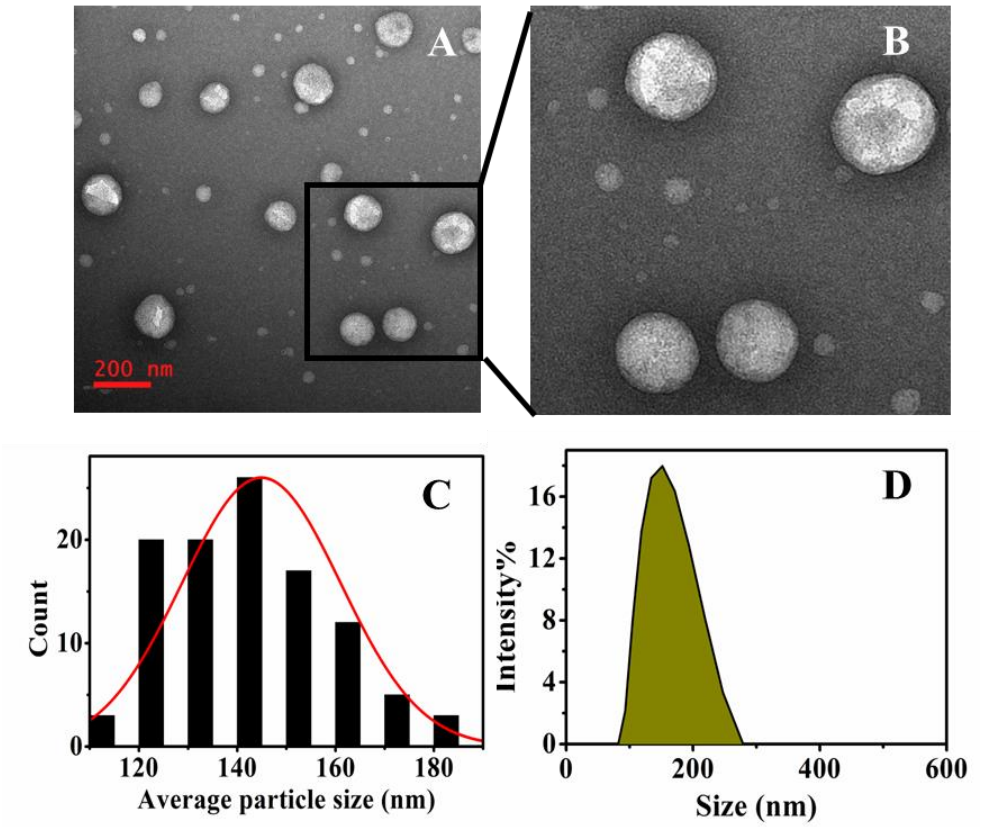

Fig. 2.16. Characterization of liposomes formed by OMBAOH-SDS equimolar mixture. (**A**) A TEM image of vesicles consisting of OMBAOH-SDS equimolar mixture. (**B**) A zoomed-in image of some of the vesicles shown in **A**. (**C**) A graphical representation of the average particle size measured from the TEM images. (**D**) Graphical representation of the particle-size distribution obtained from DLS measurements.

were further investigated by transmission electron microscopy (TEM). TEM image of the equimolar mixture is shown in Fig 2.16A and an enlarged view of a part of this image is shown in Fig. 2.16B. These images provide evidence for the spherical morphology of the ensembles, which are most likely catanionic vesicles. The average size of these vesicles was estimated as 144 (±16) nm (Fig. 2.16C). Size of the OMBAOH-SDS catanionic vesicles was also measured using dynamic light scattering (DLS), which yielded the vesicle size as 160 (±11) nm (Fig. 2.16D). The minor difference (~10%) in the size obtained from these two techniques could possibly be due to the fact that in TEM studies, the sample is dried whereas vesicles that are fully hydrated in aqueous medium are used in the DLS measurements. Previous TEM and DLS studies have shown that catanionic

vesicles made up of equimolar complexes of SDS with lauryl sarcosinate (~300 nm), lauryl alaninate (300–600 nm) and lauroyl glycinate (700–1000 nm) are about 2-6 times larger in size (Reddy et al., 2017; Ravindar et al., 2022; Sivaramakrishna et al., 2015c).

Long chain *O*-acyl-L-alaninols: Synthesis, structure, biophysical characterization and formation of equimolar catanionic liposomes with sodium dodecyl sulfate

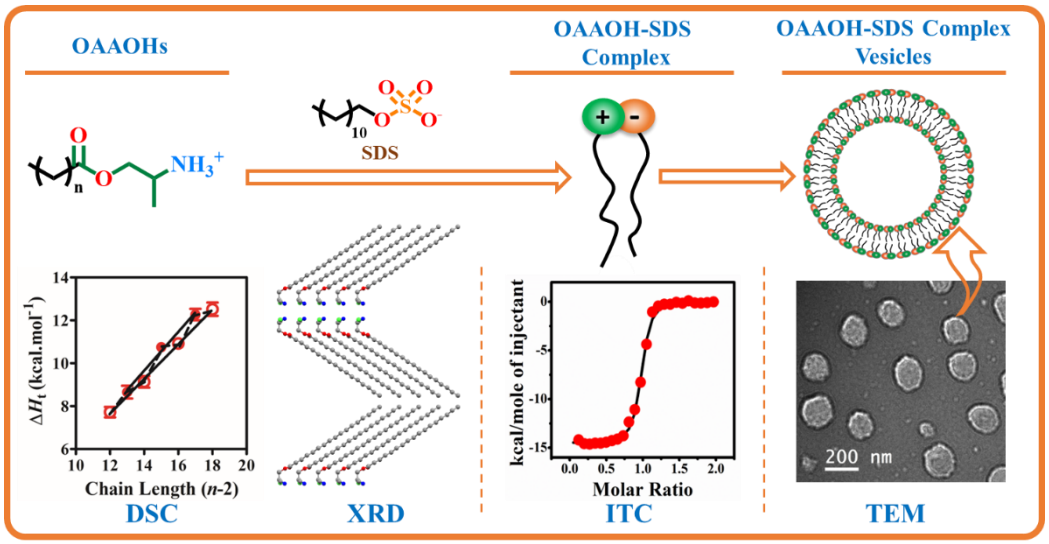

3.1.Summary

L-Alaninol and its derivatives display interesting biological and pharmacological properties, suggesting potential use in biomedical applications. This study presents the synthesis and characterization of *O*-acyl-L-alaninols (OAAOHs) bearing long, saturated acyl chains (n = 14-20). The investigation focuses on examining their thermotropic phase behavior, supramolecular organization, and interaction with sodium dodecyl sulfate (SDS), with the objective of preparing novel catanionic amphiphiles. Results from differential scanning calorimetry and powder XRD studies revealed an odd-even alteration in the transition enthalpies (ΔH_t), transition entropies (ΔS_t) and *d*-spacings of OAAOHs. A linear dependence was observed in the values of ΔH_t and ΔS_t on the acyl chain length, independently for compound with even and odd acyl chains in the dry state (solid-liquid phase transition), wherein the odd chain length molecules exhibited higher values than the even chain length series. Crystal structure analysis of *O*-palmitoyl-L-alaninol and *O*-heptadecanoyl-L-alaninol, solved in monoclinic system in the C2 space group, showed a tilted bilayer structure organised in a head-to-head (and tail-to-tail) fashion, although their molecular conformation within the bilayer differed. Odd-even alternation in the *d*-spacings was observed in powder XRD of all OAAOHs, which could be correlated with that observed in the thermodynamic parameters ΔH_t and ΔS_t, indicating a variation in the molecular arrangement in the crystal. Single-crystal XRD analysis on *O*-palmitoyl- and *O*-heptadecanoyl-L-alaninols revealed that OAAOHs bearing odd- and even-chain length compounds pack differently. However, both compounds exhibit significant similarities in their supramolecular organization, stabilized by number of C-H···O and N-H···Cl H-bonds across adjacent and opposing layers. Exploration of the interaction between *O*-myristoyl-L-alaninol and SDS revealed the formation of an equimolar catanionic complex, leading to the generation of liposomes with diameters of 150-190 nm.

3.2. Introduction

Amino alcohols, reduced derivatives of amino acids, play crucial roles in various cellular processes. One prominent function involves their contribution to the structural makeup of cell membranes, particularly in substances like choline (Lodish et al., 2008). Within mammalian tissues, sphingolipids (SLs) hold paramount importance, deriving from aliphatic amino alcohols known as sphingoid bases (Carreira et al., 2019).

Recently, much interest has focused on investigating amino alcohol derivatives in biomedical/pharmaceutical applications. For instance, both D- and L-forms of *N*-acyl alaninols were reported to exhibit apoptosis-inducing properties in Jurkat cells, similar to the effects caused by C2-ceramide and anti-Fas antibodies (Hannun et al., 1997; Ogura and Handa, 2000). Amino alcohols also demonstrated an ability to suppress the proliferation of mouse B16 melanoma cells (Landau et al., 1993). *N*-Myristoyl-phenylamino alcohol was found to inhibit alkaline ceramidases, effectively preventing HL-60 leukemia cell growth (Bielawska et al., 1992; 1996). Reports further highlight that *N*-acyl derivatives of serinol induce apoptosis in various cancer cell types, including neuroblastoma, glioma, medulloblastoma, and adenocarcinoma cells (Bieberich et al., 2000; 2002). In the area of infectious diseases, ceramide analogs, such as *d,l*-threo-1-phenyl-2-acylamino-3-morpholino-1-propanol compounds, emerge as potent inhibitors of *Plasmodium falciparum* growth in culture (Labaied et al., 2004). Additionally, amphiphilic derivatives of β-alaninols have found application in various biological contexts (Sivaramakrishna et al., 2021a; Suleman et al., 2015; Mangraviti et al., 2015; Kalhapure and Akamanchi, 2012). Ethanolamine and certain other amino alcohols have been identified as modulators of the release of synthesized acetylcholine in the rat hippocampus (Bostwick et al., 1993). Additionally, admixtures containing equimolar quantities of *N*-myristoyl-L-alaninol (NMAOHs) and dimyristoyl phosphatidycholine (DMPC) formed liposomes which can potentially be used in drug delivery applications (Sivaramakrishna and Swamy, 2016). It has also been reported that *N, O*-diacyl-L-alaninols affect the stratum corneum model membrane, which may find application in transdermal drug delivery (Sivaramakrishna et al., 2021b).

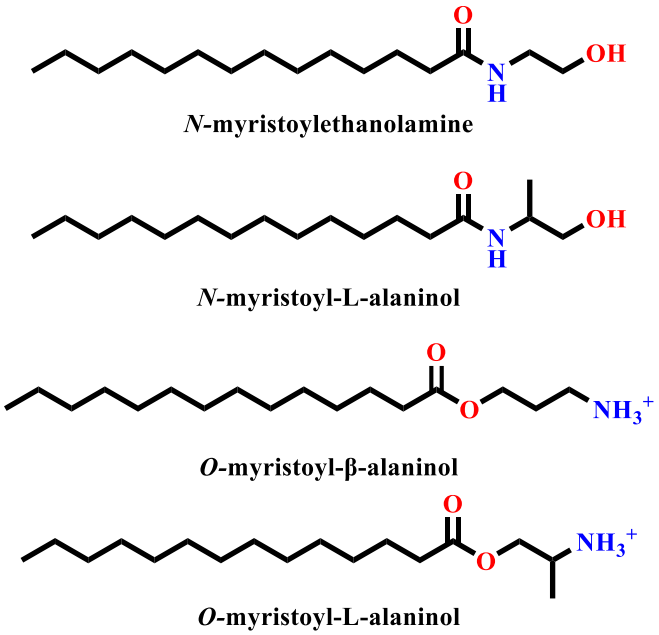

Fig. 3.1. Molecular structures of *N*-myristoylethanolamine (NMEA), *N*-myristoyl-L-alaninol (NMAOH), *O*-myristoyl-β-alaninol (OMBAOH) and *O*-myristoyl-L-alaninol (OMAOH).

Looking into the notable evolution in various applications of amphiphiles, researchers are now very much interested in synthetic amphiphiles. While applications of liposomes composed of single amphiphile have been well-known for a long time, the recent spotlight has shifted toward surfactant mixtures. These mixtures are gaining prominence due to their versatility, allowing easy optimization of composition for specific applications (Penfold and Thomas, 2019; Manga et al., 2021). The investigation of catanionic systems, comprising surfactant mixtures of cationic and anionic amphiphiles, has become a prominent area of scientific inquiry. When compared to single molecule vesicles, aqueous solutions of these mixtures spontaneously produce catanionic vesicles that are more stable and efficient in drug encapsulation (Hao et al., 2004, Marques et al., 2003; Kume et al., 2008; Ravindar et al., 2022; Choudhury et al., 2024). The versatility of these vesicles extends their application across diverse fields, including oil recovery (Li et al., 2020), purification processes (Lioi et al., 2009), biomedicine, and pharmaceutics (Dhawan et al., 2017; Ghosh et al., 2016; Bramer et al., 2007).

Driven by concerns over biocompatibility and eco-sustainability, there is a growing trend towards designing catanionic aggregates using natural and bio-derived compounds (Marquès et al., 2021). Examples include aggregates based on bile salts (di

Gregorio et al., 2018), sugars (Mahle et al., 2018; Thomas et al., 2009; Soussan et al., 2008), fatty acids (Fameau et al., 2014), and modified amino acids (Oliveira et al., 2021). In the current investigation, we have synthesized a series of *O*-acyl-L-alaninols (n = 14–20) bearing saturated acyl chains with focus on a thorough examination of their self-assembly, supramolecular organization, and phase behavior utilizing a range of spectroscopic, calorimetric, and crystallographic techniques. Furthermore, we explored the interaction between *O*-myristoyl-L-alaninol (OMAOH) (Fig 3.1) and sodium dodecyl sulfate (SDS), delving into the complex formation. The catanionic liposomes formed by this complex were characterized for size, stability, and polydispersity, and a detailed discussion of the findings is presented in this manuscript.

3.3. Materials and methods

3.3.1. Materials

We purchased fatty acids, *N, N′*-dicyclohexylcarbodiimide (DCC), 4-dimethylaminopyridine (DMAP), and sodium dodecyl sulfate from Sigma Aldrich (India). Additionally, 3-(tert-butoxycarbonylamino)-L-alaninol (t-Boc-L-alaninol) was procured from TCI Chemicals (India). The solvents, namely 1,4-dioxane, dichloromethane (DCM), chloroform, and tetrahydrofuran (THF), were obtained from Sisco Research Laboratories (India). Other chemicals and solvents were acquired from local vendors, ensuring the highest available purity. Milli-Q water was used for the preparation of buffers and other aqueous solutions.

3.3.2. Synthesis of DAAOHs

O-acyl-L-alaninols were synthesized following the protocol outlined in our previous study, which involved a two-step process (Choudhury et al., 2024). In the first step, a condensation reaction was carried out, wherein the BOC-protected L-alaninol (3-(tert-butoxycarbonylamino)-L-alaninol) underwent condensation with a fatty acid, facilitated by the coupling reagent DCC. A catalytic amount of DMAP was employed to

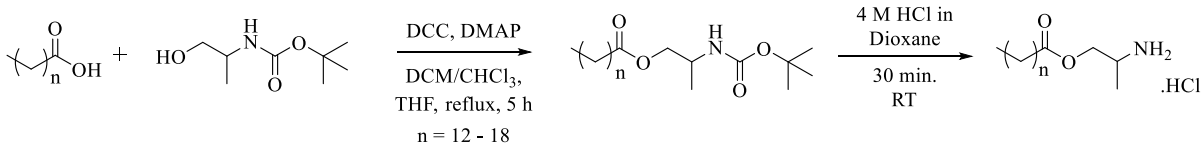

Scheme 3.1. Synthes of *O*-acyl-L-alaninols

accelerate the DCC-activated esterification of the carboxylic acid. Subsequently, in the second step, the BOC-protected ester underwent deprotection through treatment with 4M HCl in 1,4-dioxane, yielding the hydrochloride salt of *O*-acyl-L-alaninols. Purity of the synthesized products was thoroughly characterized using Fourier transform infrared (FTIR), ^{1}H NMR and ^{13}C NMR spectroscopy, complemented by high-resolution mass spectrometry (HRMS) analysis (Scheme 3.1).

3.3.3. Fluorescence spectroscopy

Fluorescence spectroscopy, employing pyrene as a fluorometric probe, was utilized to determine the critical micelle concentrations (CMC) of OAAOHs. Experimental measurements were conducted using a Horiba Jobin-Yvon Fluoromax-4 spectrofluorometer. During the experiments, incremental additions of OAAOHs were introduced from a 5–25 mM stock solution following the methodology described in (Choudhury et al. 2024) Pyrene is a spatially sensitive probe that displays a set of five monomeric fluorescence emission peaks between 375 and \405 nm (Kalyanasundaram and Thomas, 1977). The polarity ratio, represented as the intensity ratio (I_1/I_3) of bands one and three in the pyrene emission spectrum, was calculated for each spectrum. The resultant values were plotted against the amphiphile concentration, and the CMC was taken as the concentration at which a noticeable change in slope was observed.

3.3.4. Differential scanning calorimetry

Differential scanning calorimetric (DSC) investigations on solid/dry OAAOHs were conducted using a DSC-250 differential scanning calorimeter from TA Instruments (New Castle, Delaware, USA). Precise quantities of dry OAAOH samples, ranging from 2 to 5 mg, were meticulously weighed and placed in aluminium sample pans. Subsequently, each sample was covered with an aluminium lid and hermetically sealed through crimping. A corresponding reference pan was prepared in a similar fashion, devoid of any sample material. The DSC analyses encompassed heating and cooling scans initiated from 25°C to around 120°C, employing a scan rate of 2° C/min. Each individual sample underwent a series of three heating scans and two cooling scans, ensuring comprehensive thermal characterization.

Differential scanning calorimetry (DSC) investigations involving hydrated samples were conducted utilizing a Nano DSC differential scanning calorimeter procured

from TA Instruments (New Castle, Delaware, USA). Lipid samples, precisely weighed, were dissolved in dry dichloromethane/methanol (1:1, v/v), followed by the removal of the solvent under a stream of dry nitrogen gas. The resultant lipid film underwent vacuum desiccation for 5-6 hours to eliminate residual traces of the solvent. Prior to heating, the lipid was thoroughly hydrated with 150 mM NaCl. Each sample underwent three heating and two cooling thermograms in the temperature range of 0 to 100°C, employing a scan rate of 60° C/h.

In all DSC experiments, the enthalpy (ΔH_t) was obtained by integrating the area of the peak, while the transition temperature (T_t) was identified as the peak point of the transition curve. Transition entropy (ΔS_t) values were computed from transition enthalpies and transition temperatures, assuming first-order transitions (Marsh, 1990).

$$\Delta S_t = \Delta H_t / T_t \qquad (3.1)$$

3.3.5. Crystallization, structure solution and refinement

Colourless single crystals of *O*-palmitoyl-L-alaninol (OPAOH) hydrochloride and *O*-heptadecanoyl-L-alaninol (OHDAOH) hydrochloride having thin-plate morphology were grown at room temperature from a DCM solution containing 2-5% of methanol. XRD data were collected at ~298 K utilizing an Xtlab Synergy Rigaku Oxford diffractometer, which was equipped with a HyPix-3000 detector and a graphite monochromator providing Mo-Kα radiation (λ = 0.7107 Å). Data collection spanned a 2θ range of 2-25° for both samples. The subsequent data analysis and interpretation were performed using CrysAlisPro, Xtlab Synergy Rigaku Oxford Diffraction, Version 171.39.exe, and absorption correction was implemented utilizing the multi-scan approach. The Olex2-1.2 program was employed for the solution and refinement of the crystal structures, and the resulting crystal parameters are comprehensively presented in Table 2.

3.3.6. Powder X-ray diffraction studies

Powder X-ray diffraction (PXRD) analyses of the entire OAAOHs series (C14-C20) were conducted employing a Bruker SMART D8 Advance powder X-ray diffractometer from Bruker-AXS in Karlsruhe, Germany. Cu-K radiation (λ = 1.5406 Å) was utilized at 40 kV and 30 mA for data collection. Fine powders of the OAAOHs were loaded onto the circular spinning disk of the instrument sample holder. Diffraction patterns were

measured at room temperature by a LynxEye PSD data collector, with a step size of 0.0198° and a measurement duration of 1.5 seconds for each step. We determined *d*-spacings by analyzing the observed diffraction peaks employing the Bragg's equation.

3.3.7. Turbidimetry

Investigation of the interaction between *O*-myristoyl-L-alaninol (OMAOH) and SDS was carried out through turbidimetry, employing a JASCO V-750 UV-Vis spectrophotometer. Various proportions of OMAOH and SDS (0.5 mM concentration, which is below their respective CMCs) were mixed and incubated for 30 minutes. Subsequently, turbidity of the resulting samples was determined by collecting optical density (OD) over the wavelength range of 330-450 nm at room temperature. The turbidity at 370 nm was specifically chosen for subsequent analytical investigations.

3.3.8. Isothermal titration calorimetry

Exploration of the interaction between OMAOH and SDS was extended through Isothermal Titration Calorimetry (ITC). Using a rotating stirrer syringe, 1 mM OMAOH solution was added in successive 1.5 µL aliquots to a sample cell with 280 µL of 0.1 mM aqueous SDS solution. Each injection, executed over a 3-second period, was separated by a 150-second interval, maintaining continuous stirring at 750 rpm throughout the titration. The acquired data were then analyzed using the PEAQ-ITC Analyser software supplied by MicroCal. This analysis facilitated the determination of binding stoichiometry (n), binding constant (K_b), and enthalpy of binding (ΔH_b). Additionally, leveraging these parameters, the free energy of binding (ΔG_b) and entropy of binding (ΔS_b) were computed using the following fundamental thermodynamic equations:

$$\Delta G_b = -RT \ln K_b \tag{3.2}$$

$$\Delta G_b = \Delta H_b - T\Delta S_b \tag{3.3}$$

3.3.9. Dynamic light scattering

Catanionic vesicles (made up of OMAOH and SDS) were analysed for particle size and stability using Dynamic Light Scattering (DLS) experiments. Sample preparation for DLS involved hydrating a thin film containing an equimolar OMAOH-SDS mixture. This thin film was generated by evaporating the solvent from a solution containing the two

amphiphiles in equal proportion in dichloromethane/methanol (1:1, v/v). The resulting vesicles were formed through sonication, followed by a 6-hour incubation in a refrigerator (3-6°C). DLS measurements were performed using a Horiba SZ-100 nanoparticle analyzer. Samples were measured multiple times, and the reported values represent averages from three independent measurements. The instrument's built-in software, utilizing autocorrelation analysis, was employed for data analysis, enabling the determination of the polydispersity index (PI) and particle size distribution of the vesicles.

3.3.10. Transmission electron microscope

The morphology of OMAOH and SDS catanionic vesicles was assessed by Transmission Electron Microscopy (TEM) using a JEOL JEM-F200/F2 multipurpose electron microscope (Ravindar et al., 2022; Choudhury et al., 2024). A 1 mM suspension of catanionic vesicles was prepared for TEM analysis following the previously described protocol for DLS studies. Subsequently, a drop of the sample was meticulously deposited on the carbon-coated side of a copper grid and allowed to settle for approximately 10 minutes. The excess solution was carefully removed using a piece of filter paper. Following this, a single drop of 1.0% uranyl acetate solution was applied for 30 seconds, and the excess solution was removed. The sample was then left to air-dry at room temperature overnight. The resulting dried sample was utilized for TEM data collection.

3.4. Result and discussion

In the current study, a series of *O*-acyl-L-alaninols bearing n-alkyl chains have been synthesized, and their structural integrity and purity have been systematically characterized through Fourier transform infrared (FTIR), ^{1}H- and ^{13}C nuclear magnetic resonance (NMR) spectroscopy, and high-resolution mass spectrometry (HRMS). This was followed by an extensive characterization of their biophysical properties and the interaction of *O*-myrstoyl-L-alaninol with SDS. Finally, the catanionic liposomes from the OMAOH-SDS catanionic complex were characterized by size and morphology. The results of these investigations are discussed below.

3.4.1. Spectroscopic characterization of OAAOHs

A representative FTIR spectrum of OMAOH is given in Fig. 3.2, which shows the absorption band of ester carboxyl group at ~1742-1730 cm^{-1}, C-H stretching bands at

~2958-2848 cm^{-1}, stretching bands for C-C-O functionalities at ~1151-1148 cm^{-1}. Methylene scissoring and rocking bands are seen at ~1471-1460 cm^{-1} and ~720-717 cm^{-1}, respectively. The IR resonances obtained for the homologous series of OAAOHs are listed in Table S1 of Chapter 3 (see supporting information).

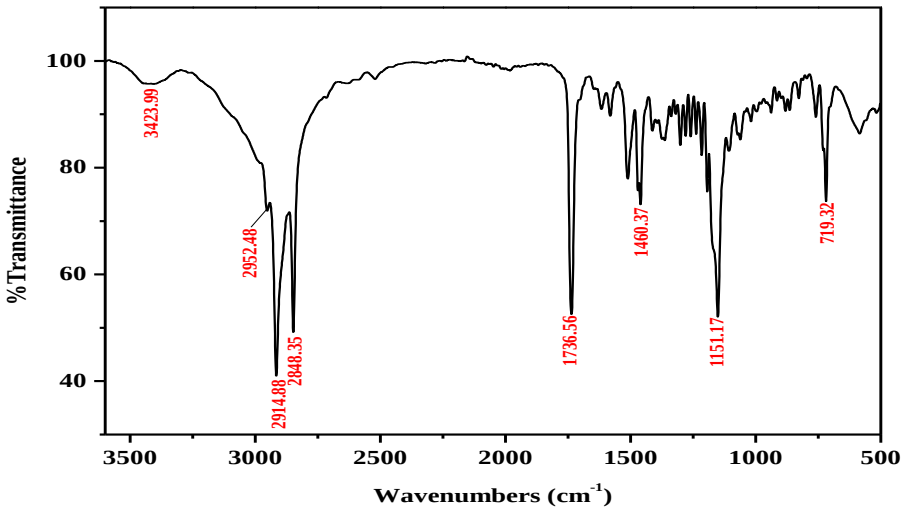

Fig 3.2. FTIR spectrumof *O*-myristoyl-L-alaninol recorded at room temperature.

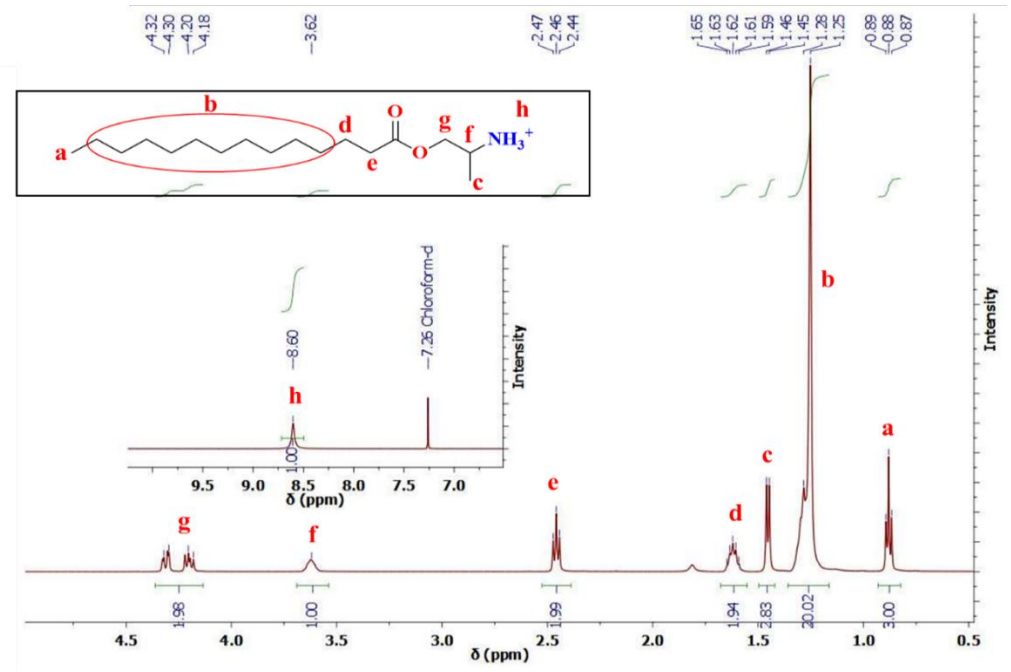

Fig. 3.3. ^{1}H-NMR spectrum of *O*-myristoyl-L-alaninol recorded at room temperature (solvent $CDCl_3$).

A representative ^{1}H-NMR spectrum of OMAOH in $CDCl_3$ is given in Fig 3.3. OMAOH shows the following resonances: ~0.80-0.90 δ (3H,t) corresponds to myristoyl terminal methyl group, ~1.18-1.27 δ (nH,m) myristoyl chain methylene group except α- and β- methylene groups with respect to acyl carbonyl, ~1.55-1.64 δ (2H,m) for β-methylene to carbonyl, ~2.33-2.47 δ (2H,t) of α-methylene to carbonyl, ~3.48-3.64 δ (1H,m) methine attached to the amine, ~1.31-1.47 δ(3H,d) methyl group attached to methine of L-alaninol, ~4.12-4.28 δ (2H,m) corresponding to methylene attached to the oxygen, ~8.20-8.61 δ corresponding to protons on amine nitrogen. The ^{1}H-NMR data obtained for the homologous series of OAAOHs are listed in Table S2 of Chapter 3 (see supporting information).

A representative ^{13}C-NMR spectrum of OMAOH is given in Fig. 3.4, which shows the following resonances: 13.92-14.12 δ, 22.56-22.70 δ, and 31.81-31.96 δ for the terminal methyl group of the acyl chain and α, β-methylene groups with respect to it, respectively. Resonance of β- and α- methylene groups with respect to the carbonyl are seen at 24.59-24.81 δ and 33.72-34.02 δ, respectively. Resonances corresponding to the remaining methylene groups are seen at 29.03-29.78 δ. Resonance of the methylene group at β position with respect to the amino group is seen at 64.31-64.53 δ, and resonance of the methine group is seen at 46.65-47.52 δ. The methyl group connected to the methine carbon shows a resonance at 14.96-15.25 δ. The carbonyl carbon shows a resonance at 173.51-173.78 δ. The ^{13}C-NMR data obtained for the homologous series of OAAOHs are listed in Table S3 of Chapter 3 (see supporting information).

A high-resolution mass spectrum of OMAOH is presented in Fig. 3.5. The intense peak at m/z = 286.2748 matches well with the compound molecular ion $[M+H]^+$. The additional peaks at m/z = 571.5338 have been assigned as $[2M+H]^+$. The HRMS obtained for the homologous series of OAAOHs are listed in Table S4 of Chapter 3 (see supporting information).

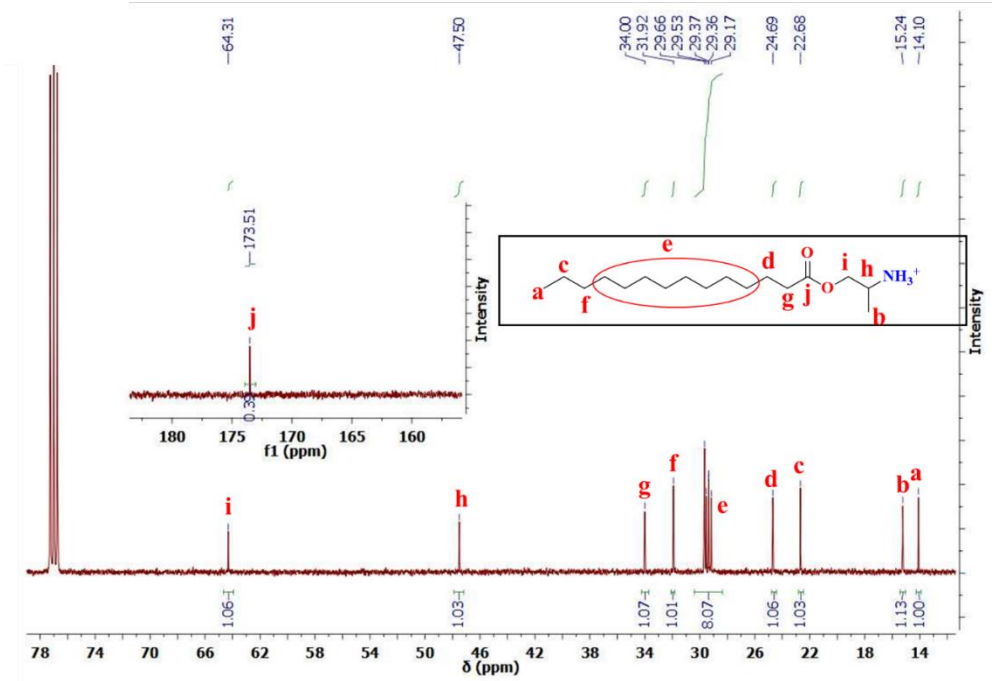

Fig. 3.4. ^{13}C-NMR spectrum of *N*-myristoyl-L-alaninol recorded at room temperature (solvent $CDCl_3$).

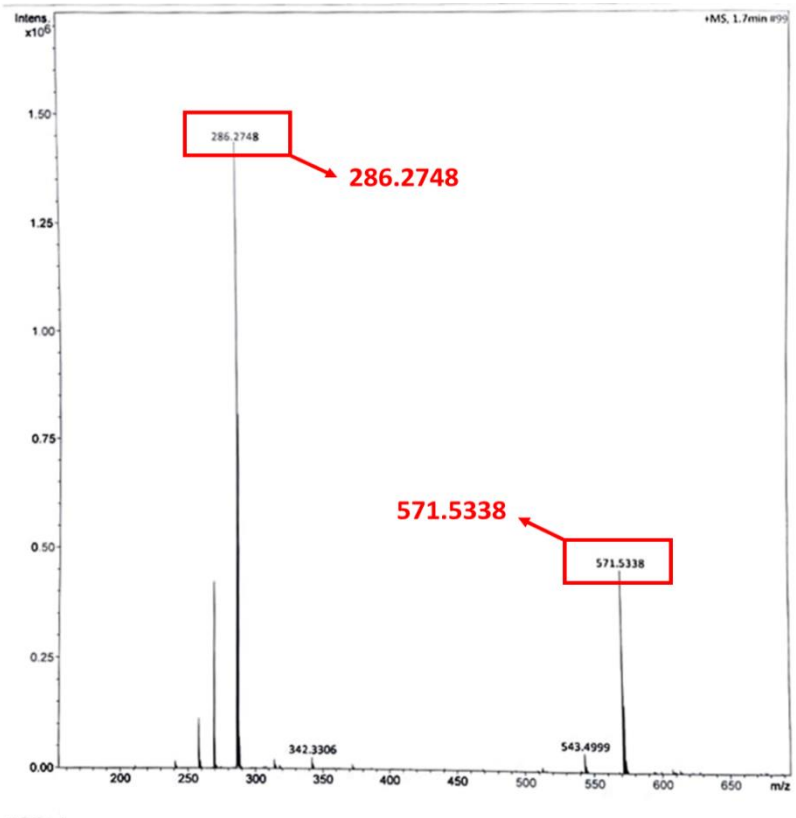

Fig. 3.5. ESI mass spectrum of *O*-myristoyl-L-alaninol.

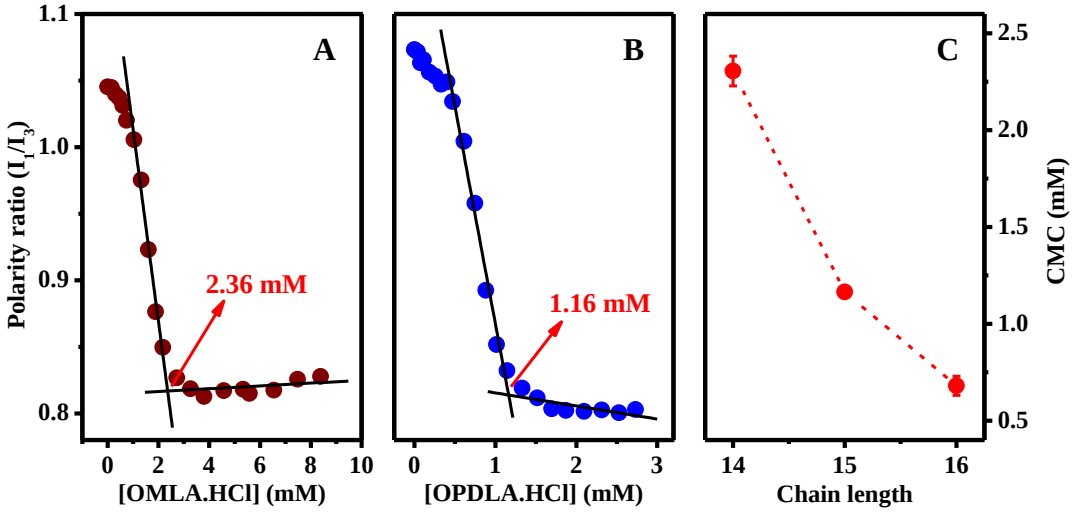

Fig. 3.6. Determination of the CMC of (**A**) *O*-myristoyl-L-alaninol and (**B**) *O*-pentadecanoyl-L-alaninol in water. (**C**) A plot of chain length versus CMC.

3.4.2. Critical micellar concentration of OAAOHs

CMC values of OAAOHs with different acyl chains were determined by monitoring changes in the fluorescence emission properties of the pyrene probe, a method well-established in the literature (Kalyanasundaram & Thomas, 1977; Sivaramakrishna and Swamy, 2015). The polarity ratio (I_1/I_3) of pyrene exhibited a gradual decrease with increasing OAAOH concentration in the solution, with a marked change in slope at a specific threshold. The CMC was determined by identifying the interception point of two linear least squares fits applied to specific sections of the plots of I_1/I_3 against [OAAOH]. Fig. 3.6A and 3.6B show representative plots for the determination of CMC for OMAOH and *O*-pentadecenoyl-L-alaninol (OPDAOH), respectively. The CMC values estimated for OMAOH, OPDAOH, and *O*-palmitoyl-L-alaninol (OPAOH) employing this methodology were 2.30 (±0.08) mM, 1.16 (±0.01) mM, and 0.68 (±0.05) mM, respectively (Fig. 3.6C).

3.4.3. DSC studies on dry and hydrated OAAOHs

The DSC heating thermograms for solid/dry OAAOHs having acyl chains of both even and odd number of carbon atoms are shown in Fig. 3.7A and 3.7B, respectively. Evidently, each OAAOH exhibits a significant transition, corresponding to the capillary melting point of the respective compound. Intriguingly, OAAOHs with even acyl chains

exhibit an additional minor transition before the major transition. Both major and minor peaks

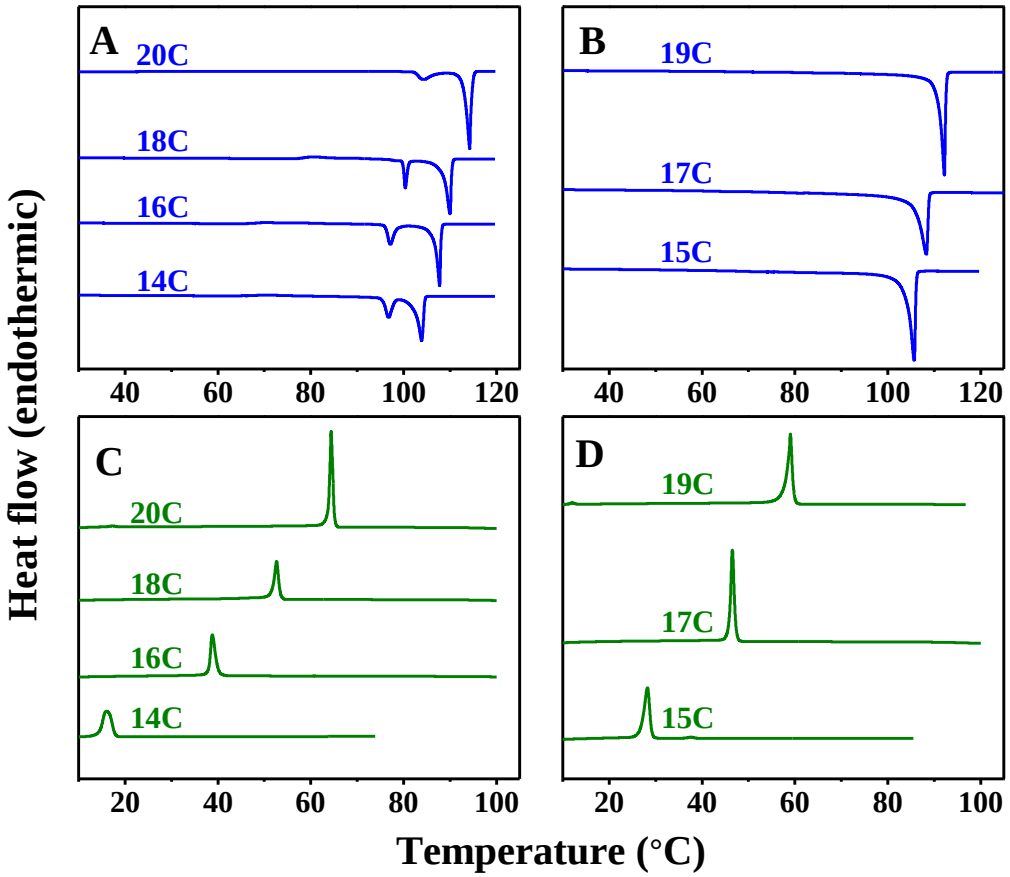

Fig. 3.7. DSC heating thermograms of dry and hydrated *O*-acyl-L-alaninols. (**A, B**) Dry (solid) samples; (**C, D**) hydrated samples. In the left panels (**A, C**), thermograms of compounds with an even number of C atoms in the acyl chain are shown, while in the right panels (**B, D**), thermograms of compounds with odd numbers of C atoms are shown. In each thermogram, the number of carbon atoms in the acyl chain is indicated.

exhibit pronounced sharpness, mitigating concerns regarding the minor peak's origin from significant impurities. These observations strongly indicate the potential polymorphic nature of OAAOHs. Analogous minor transition peaks before major transition have been documented in other single-chain amphiphiles, including *N*-acylethanolamines (NAEs) and *N*-acyl-β-alaninols (NABAOHs) (Ramakrishna et al., 1997; 1998; Sivaramakrishna et al., 2021a). For NAEs, a prior study established the molecular packing of two distinct polymorphs of *N*-palmitoylethanolamine and demonstrated that the lipid layer in one polymorph can undergo a 180º rotation, which results in the formation of the other

polymorph (Kamlekar and Swamy, 2006). The observed minor transitions in even-chain OAAOHs may also be attributed to the presence of two different polymorphs with different molecular packing in the solid state, undergoing interconversion upon heating.

Upon subjecting the samples to second and third heating scans, a slight drop in transition enthalpies was observed; however, the minor peaks remained reproducible. As a result, the first heating scan was chosen for further research, and the area beneath the significant transitions was taken to calculate the transition enthalpies. Table 3.1 shows the transition temperatures, enthalpies, and entropies estimated by analysing the DSC thermograms.

A previous study demonstrated that the introduction of salt, such as NaCl, preserves the lamellar structure of *O*-stearoylethanolamine even at elevated temperatures (Tarafdar and Swamy, 2010). To explore the impact of salt on the phase transitions of OAAOHs, we hydrated them with 150 mM NaCl and conducted DSC experiments. Thermograms for compounds with even and odd acyl chains are presented in Fig. 3.7C and 3.7D, respectively. Relevant transition temperatures, enthalpies, and entropies are detailed in Table 3.1.

Table 3.1. Average values of transition temperatures (T_t), transition enthalpies (ΔH_t) and transition enthalpies (ΔS_t) of OAAOHs in dry and hydrated states. Samples were hydrated in 150 mM NaCl. Values in parentheses correspond to standard deviations from three independent measurements.

Acyl chain length	**Dry OAAOHs**			**Hydrated OAAOHs**		
	T_t (°C)	ΔH_t (kcal.mol^{-1})	ΔS_t (cal.mol^{-1}.K^{-1})	T_t (°C)	ΔH_t (kcal.mol^{-1})	ΔS_t (cal.mol^{-1}.K^{-1})
14	104.4 (0.1)	7.72 (0.42)	20.45 (1.11)	15.8 (0.2)	3.19 (0.27)	10.95 (0.78)
15	106.2 (0.1)	8.65 (0.51)	22.81 (1.35)	28.2 (0.2)	3.55 (0.04)	11.85 (0.07)
16	108.1 (0.0)	9.14 (0.47)	23.96 (1.22)	38.4 (0.5)	3.61 (0.26)	11.60 (0.85)
17	109.4 (0.1)	10.75 (0.16)	28.10 (0.43)	46.4 (0.2)	4.13 (0.23)	12.47 (1.05)
18	110.5 (0.2)	10.92 (0.34)	28.46 (0.88)	52.7 (0.6)	4.41 (0.30)	13.67 (1.01)
19	112.8 (0.2)	12.27 (0.46)	31.79 (1.19)	59.3 (0.2)	4.84 (0.02)	14.53 (0.06)
20	113.9 (0.2)	12.52 (0.54)	32.34 (1.39)	64.5 (0.1)	5.25 (0.29)	15.53 (0.85)

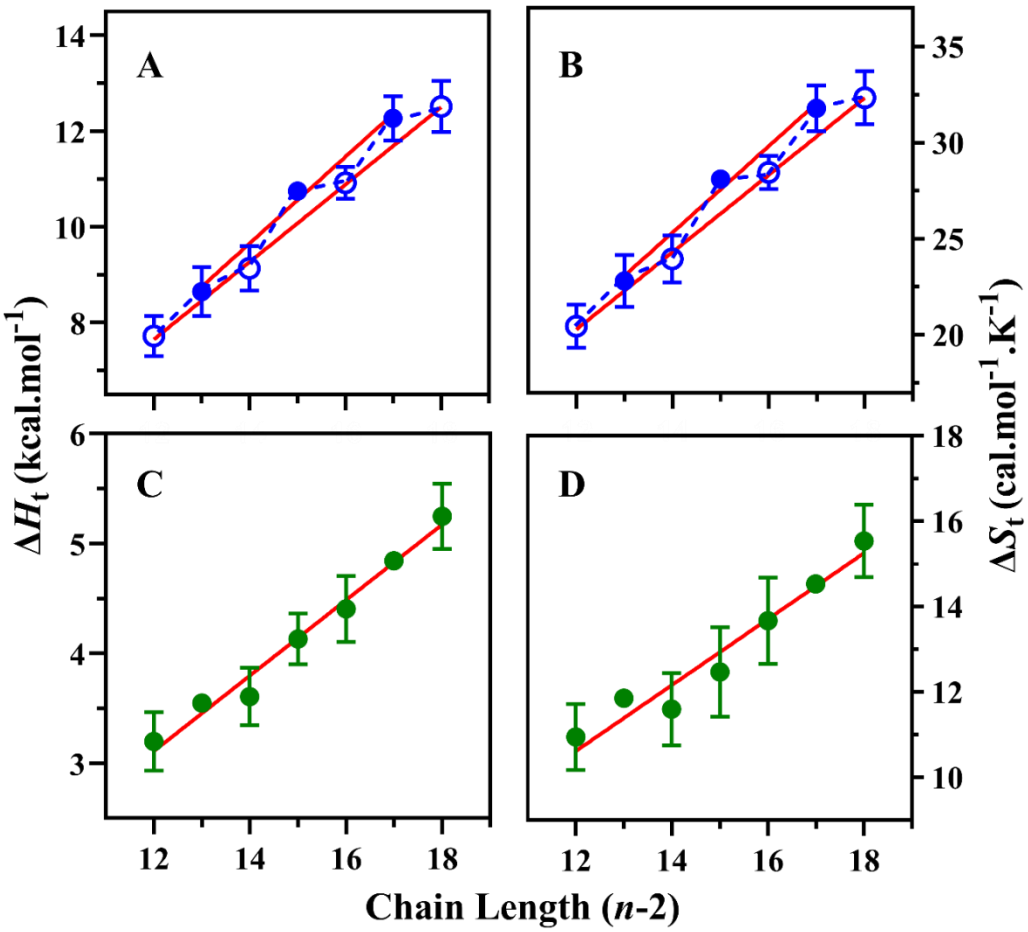

Fig. 3.8. Chain length dependence of ΔH_t and ΔS_t of OAAOHs for dry samples (**A**, **B**) and for hydrated samples (**C**, **D**). (**A**, **C**) ΔH_t; (**B**, **D**) ΔS_t. Symbol code in **A**, **B**: (○), odd chain length; (●), even chain length. Linear least squares fits are shown in **A** and **B** for even and odd chain length series, respectively. Data are fitted using linear least squares in **C** and **D**. Dash lines connecting adjacent points in A and B indicate odd-even alternation of transition enthalpies and entropies in the dry state.

3.4.4. Chain length dependence of transition enthalpy and entropy

The chain length dependence of transition enthalpy (ΔH_t) and transition entropy (ΔS_t) for OAAOHs featuring both even and odd acyl chains in both dry and fully hydrated states is shown in Fig. 3.8. In the case of dry samples, individual analysis of even and odd chain length series revealed a linear correlation between calorimetric parameters and acyl chain length. However, when combining data from both series, a discernible zig-zag pattern emerged, with ΔH_t and ΔS_t values for the even chain length series being distinctly lower than the values observed for the odd chain length series. In contrast, hydrated OAAOHs

showed a linear dependence for ΔH_t and ΔS_t across the whole series. The chain length-dependent ΔH_t and ΔS_t values may be fitted with expressions 3.4 and 3.5, respectively (Larsson, 1986):

$$\Delta H_t = \Delta H_o + (n - 2)\, \Delta H_{inc} \quad (3.4)$$

$$\Delta S_t = \Delta S_o + (n - 2)\, \Delta S_{inc} \quad (3.5)$$

Table 3.2: Thermodynamic parameters deduced from the DSC studies on dry and hydrated OAAOHs. ΔH_o and ΔS_o are end contributions to phase transition enthalpy and entropy, respectively, whereas ΔH_{inc} and ΔS_{inc} are the corresponding incremental values.

Thermodynamic parameter	**DSC of Dry OAAOHs**		**DSC of hydrated OAAOHs** (***both odd and even chain lengths***)
	Even chain lengths	**Odd chain lengths**	
ΔH_{inc} (kcal/mol)	0.81 (0.05)	0.90 (0.08)	0.34 (0.03)
ΔH_o (kcal/mol)	-2.05 (0.79)	-3.00 (1.26)	-1.02 (0.40)
ΔS_{inc} (cal/mol/K)	2.01 (0.14)	2.23 (0.22)	0.77 (0.09)
ΔS_o (cal/mol/K)	-3.81 (2.09)	-6.12 (3.32)	1.34 (1.42)

[#]Average values of ΔH_t and ΔS_t given in Table 3.1 have been used for linear fitting of the data. Error shown in parentheses are fitting errors obtained from the linear least-squares analysis.

The expressions for transition enthalpy (ΔH_t) and transition entropy (ΔS_t) are given as functions of the number of carbon atoms (n) in the acyl chains, incorporating end contributions ΔH_o and ΔS_o due to the terminal methyl group and the polar component of the molecule. The average incremental contributions of each CH_2 group to ΔH_t and ΔS_t are denoted as ΔH_{inc} and ΔS_{inc}, respectively. Eq. 3.4 and 3.5 have demonstrated a strong correspondence with the data acquired from analogous single-chain amphiphiles, such as *N*-acylethanolamines, *N*, *O*-diacylethanolamines, diacylphosphatidylcholines, diacylphosphatidylethanolamines, and *N*-acyl phosphatidylethanolamines, each characterized by saturated acyl chains of equivalent length (Sivaramakrishna et al. 2021a; Ramakrishnan et al., 1997; Tarafdar et al., 2012; Reddy et al., 2015; Marsh et al., 1991; 2000; Kamlekar et al., 2010). The incremental values (ΔH_{inc} and ΔS_{inc}) and end contributions (ΔH_o and ΔS_o) for both solid and hydrated samples were derived from the

linear least-squares analysis of ΔH_t and ΔS_t for the OAAOHs. The obtained data are provided in Table 3.2.

The observed linear dependence of both transition enthalpy and entropy on chain length suggests a notable degree of structural similarity in the molecular organization of OAAOHs of different acyl chain lengths in the solid state, regardless of whether the compounds feature even- or odd-numbered acyl chains. Furthermore, the odd-even alternation signifies distinct differences in molecular packing and intermolecular interactions between the odd- and even-chain length series. This interpretation is further supported by the results of single-crystal and powder X-ray diffraction studies, which are discussed in subsequent sections (3.4.6 to 3.4.10).

3.4.5. Chain length dependence of transition temperature

The transition temperatures of both dry and hydrated OAAOHs exhibit an upward trend with increasing chain lengths, as depicted in Fig. 3.9. Notably, in hydrated samples, it is evident that the extent of this temperature shift diminishes as the acyl chain length increases. This observed behavior in hydrated samples aligns with similar trends reported earlier for other single long-chain amphiphiles, for example, *N*-acyldopamines and *N*-acylglycines (Reddy et al., 2013; 2014).

For a range of amphiphiles bearing 1-3 acyl chains that exhibit linear dependence of ΔH_t and ΔS_t on the chain length, previous investigations have demonstrated that the values of ΔH_t and ΔS_t in this range of amphiphiles can be effectively fitted to equation 3.6 (Marsh, 1982):

$$T_t = \Delta H_t/\Delta S_t = T_t^{\infty} [1 - (n_o\text{-}n'_o)/ (n\text{-}n'_o)] \qquad (3.6)$$

where n_o (= - ΔH_o/ ΔH_{inc}) and n'_o (= - ΔS_o/ ΔS_{inc}) represent the values of n at which ΔH_t and ΔS_t extrapolate to zero, the T_t values of dry OAAOHs featuring both even and odd acyl chains demonstrate a good fit to Eq. 3.6, as illustrated in Figs. 5A and 5B. The nonlinear least-squares fitting of T_t values for all hydrated OAAOHs to Eq. 3.6 also exhibits a satisfactory agreement, as depicted in the same figures. The extrapolated T_t^{∞} value for OAAOHs in the dry state is estimated to be approximately 486 K, while for the hydrated OAAOHs, the corresponding value is ~407 K.

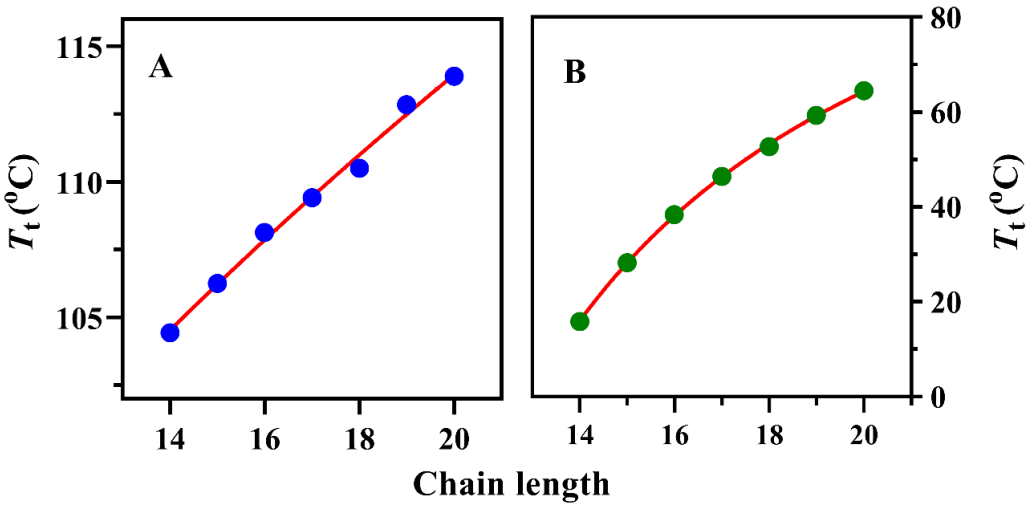

Fig. 3.9. Chain length dependence of chain-melting phase transition temperatures of OAAOHs. (**A**) Dry samples; (**B**) samples hydrated with 150 mM NaCl. The solid lines correspond to nonlinear least-squares fits of the transition temperatures to equation 3.6.

3.4.6. Description of structure

The molecular structures of OPAOH and OHDAOH are displayed in ORTEPs shown in Fig. 3.10A and Fig. 3.11A, respectively. Both figures reveal an all-*trans* conformation of the hydrocarbon segment in the acyl chain, with torsion angles of ~180°. In OPAOH, the torsion angle of the N1-C18-C17-O2 linkage is 54.6° (see Fig. 3.10B), while in OHDAOH, the corresponding angle for the N1-C19-C18-O2 linkage is -71.2° (see Fig. 3.11B). Additionally, the torsion angle of the C19-C18-C17-O2 portion in OPAOH is 173.5° (see Fig. 3.10B), whereas, in OHDAOH, the corresponding dihedral angle (C20-C19-C18-O2) is 52.7° (see Fig. 3.11B). These differences lead to distinctly different molecular packing arrangements, although the two molecules have essentially identical chemical structures, with the only difference being the presence of an additional CH_2 moiety in the acyl chain of OHDAOH. The implications of this difference are further discussed below.

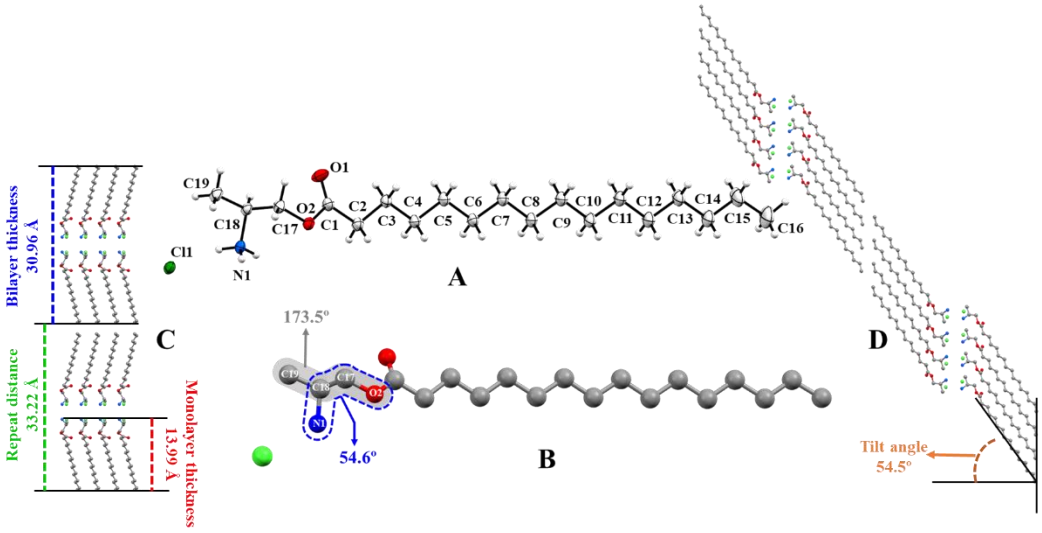

Fig 3.10. Molecular and crystal structure of *O*-pamitoyl-L-alaninol. (A) ORTEP of OPAOH. (B) Two torsion angles in the head region of OPAOH. (C, D) Packing diagrams along the *a*-axis and *b*-axis, Hydrogens were omitted for clarity.

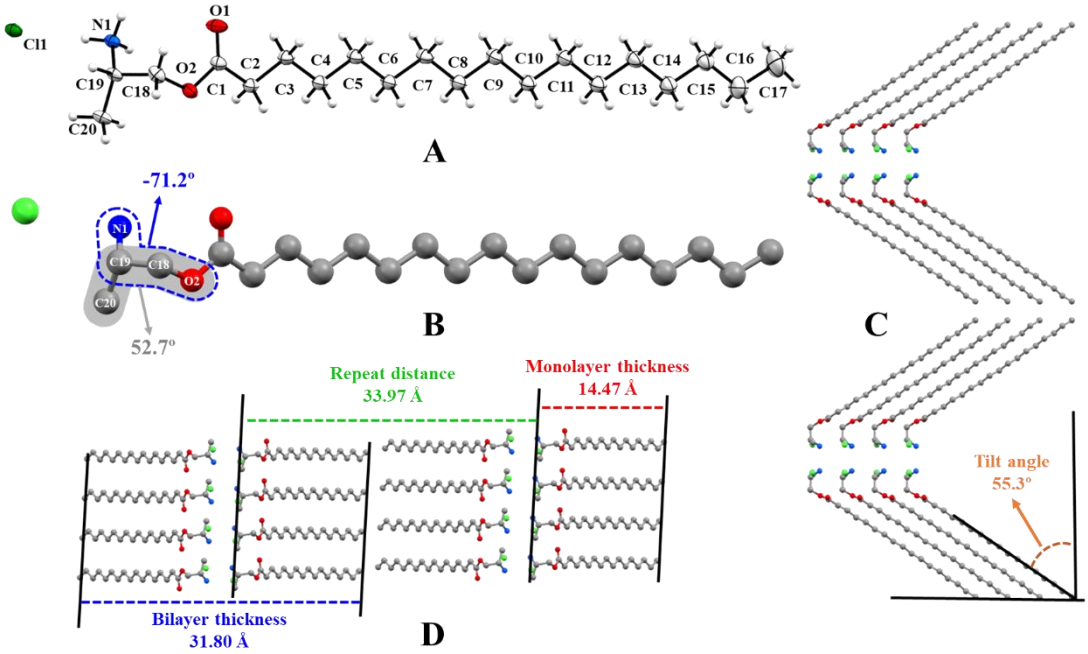

Fig. 3.11. Molecular and crystal structure of *O*-heptadecanoyl-L-alaninol. (**A**) ORTEP of OHDAOH. (**B**) Two torsion angles in the head region of OHDAOH. (**C, D**) Packing diagrams along the *a*-axis and *b*-axis. Hydrogens were omitted for clarity.

Table 3.3. Crystallographic data for OPAOH and OHDAOH.

Crystal parameter	**OPAOH**	**OHDAOH**
Formula	$C_{19}H_{39}NO_2$. HCl	$C_{20}H_{41}NO_2$. HCl
Formula wt.	349.97	364.00
Crystal system	Monoclinic	Monoclinic
T, K	295	298
Space group	C2	C2
a (Å)	8.7109(5)	9.0658(5)
b (Å)	7.5919(5)	7.4023(4)
c (Å)	33.2317(18)	34.118(3)
α	90.000	90.000
β	91.246(5)	95.383(6)
γ	90.000	90.000
z	4	4
V (Å3)	2197.2(2)	2280.2(3)
Dx (g cm-3)	1.058	1.060
μ (mm-1)	0.183	0.179
F(000)	776.0	808.0
Reflections collected	14232	9743
Independent reflections	4323	4286
Parameters	211	224
GOF	0.993	0.997
R indices	R_1 = 0.0906,	R_1 = 0.1005,
(all data)	wR_2 = 0.1857	wR_2 = 0.1637
Final R indices	R_1 = 0.0652,	R_1 = 0.0638,
	wR_2 = 0.1546	wR_2 = 0.1429

3.4.7. Molecular packing

The packing diagram of OPAOH and OHDAOH, as observed along the *a*-axis, are shown in Fig. 3.10C and 3.11C, respectively. Additionally, views along the *b*-axis are presented in Fig. 3.10D and 3.11D, respectively. These diagrams reveal a head-to-head (and tail-to-

tail) arrangement of the lipid molecules in the crystal lattice, with each unit cell accommodating two molecules. Further, a closer examination of multiple layers constituting the packed structure, it is seen that OPAOH is arranged in an extended tilted bilayer form (Fig. 3.10), while OHDAOH adopts a zig-zag packing arrangement (Fig. 3.11). The dissimilarity in molecular packing is attributed to the difference in molecular conformation in the head group region.

Van der Waals' contacts between methyl ends in stacked bilayers play an important role in the packing arrangements in lipid bilayers. The closest methyl-methyl distances between opposite layers are 3.71 Å and 4.33 Å in the crystal lattices of OPAOH and OHDAOH, respectively. Van der Waals' distances between methyl groups of the same leaflets are 5.78 Å and 5.85 Å for OPAOH and OHDAOH, respectively. The bilayer thickness (Me−Me distance) in the crystal lattices of OPAOH and OHDAOH is 30.96 Å and 31.80 Å, respectively. Furthermore, molecular packing also provides the monolayer (single leaflet) thickness, represented by the N1-C16 distance for OPAOH and N1-C17 distance for OHDAOH, which is measured at 13.99 Å and 14.47 Å, respectively. The repeat distance (*d*-spacing) in the molecular packing is 33.22 Å and 33.97 Å for OPAOH and OHDAOH, respectively. The area per molecule obtained from the crystal packing parameters of OPAOH and OHDAOH is 66.1 $Å^2$ and 67.0 $Å^2$, respectively. Additionally, the *O*-acyl chains exhibit a tilt of 54.5° in OPAOH (Fig. 3.10D) and 55.3° in OHDAOH with respect to the bilayer normal (Fig. 3.11D).

3.4.8. Subcell packing

The examination of various lateral modes of packing arrangements in the hydrocarbon chains of amphiphile crystals can be examined by characterizing the of subcells, outlining the relationships between identical positions within a hydrocarbon chain and those in neighboring molecules. These chain-packing modes are typically classified into distinct categories, such as triclinic, monoclinic, and others, based on symmetry considerations. Furthermore, within each class, the orientation of polymethylene planes within the hydrocarbon chains may vary, aligning either parallel or perpendicular to their neighboring chains (Abrahamsson et al., 1978; Maulik et al., 1990). A careful and systematic examination of the acyl chain arrangement in OPAOH and OHDAOH revealed that the subcells within their crystalline structures conform to the conventional

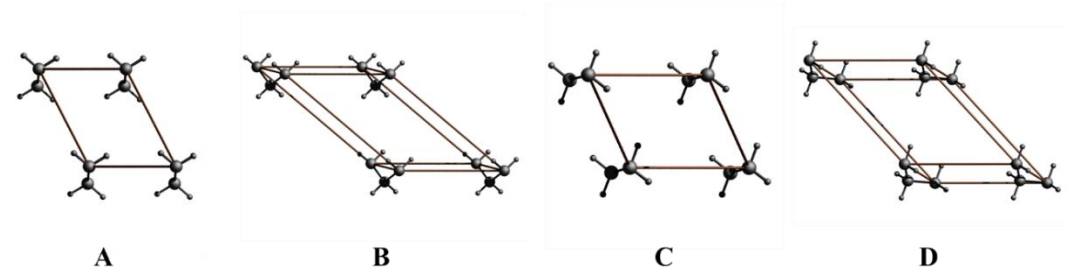

Fig. 3.12. (**A, B**) OPAOH and (**C, D**) OHDAOH. Both subcells belong to the classic triclinic parallel ($T_{//}$) type.

triclinic parallel ($T_{//}$) orientation, as shown in Fig. 3.12. The corresponding unit cell dimensions for these subcells are detailed in Table 3.4.

Table 3.4. Subcell dimensions of CPAOH and CHDAOH.

Cell parameter	CPAOH	CHDAOH
a (Å)	8.71	7.40
b (Å)	5.78	5.85
c (Å)	2.53	2.53

3.4.9. Hydrogen bonding and intermolecular interaction

The crystal structures of OPAOH and OHDAOH reveal two distinct types of hydrogen bonds (H-bond): C-H···O and N-H···Cl. Figs. 3.13A and 3.13B illustrate the hydrogen bonding patterns for OPAOH and OHDAOH, respectively. Table 3.5 lists the related bond distances and angles. In these compounds, each ammonium group from the head region forms H-bonds with three counter ions (chloride ions). Among these, two N-H···Cl hydrogen bonds join molecules within the same leaflet, while a third N-H···Cl H-bond links molecules from different layers. Table 3.5 provides detailed information on all three types of N-H···Cl H-bonds identified in OPAOH and OHDAOH. This includes H-bond distances (H···Cl), donor-acceptor distances (N···Cl), and bond angles at the hydrogen atom.

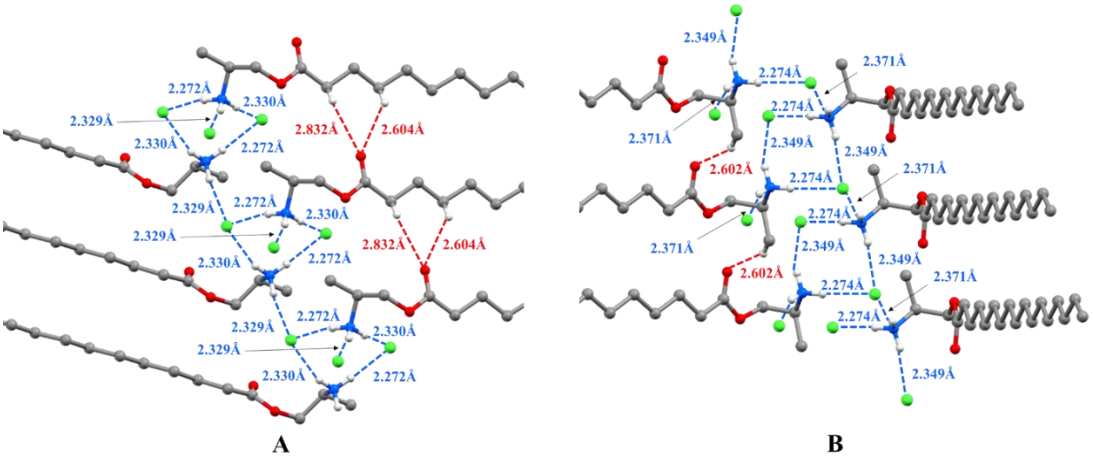

Fig. 3.13. Hydrogen bonding pattern in the crystal lattice of (**A**) OPAOH and (**B**) OHDAOH. Blue dashed lines (----), N-H····Cl H-bonds; red dashed lines (----), C-H····O H-bonds. Hydrogens not involved in H-bonds were omitted for clarity.

Table 3.5. The distances and angles between hydrogen bonds in the crystal structures of OPAOH and OHDAOH.

Bond	H-bond distance (Å)	Donor-acceptor distance (Å)	Bond angle at 'H' (°)
OPAOH			
C-H···O	2.832	3.404	118.62
„	2.604	3.289	127.77
N-H···Cl	2.272	3.148	166.98
„	2.329	3.209	169.81
„	2.330	3.177	159.09
OHDAOH			
C-H···O	2.602	3.495	155.10
N-H···Cl	2.349	3.203	160.75
„	2.274	3.150	168.09
„	2.371	3.224	160.67

Besides the above N-H···Cl interactions, C-H···O hydrogen bonds have also been identified in the crystal structures of OAAOHs. In OPAOH, such hydrogen bonds were

observed between the carbonyl oxygen atom (O1) of each molecule with the H-atoms on the C2 and C4 carbon atoms of a neighboring molecule (see Fig. 3.13A). On the other hand, in OHDAOH, a single C-H···O hydrogen bond was observed between the carbonyl oxygen atom (O1) and an H-atom on C20 (side chain methyl group of the alaninol moiety), as shown in Fig. 3.13B. The corresponding details, related to the H-bond distance (H···O), donor-acceptor distance (C···O), and the bond angle at the hydrogen atom (C-H···O angle), are presented in Table 3.5.

3.4.10. Powder X-ray diffraction studies

Additional information about the molecular packing of OAAOHs featuring acyl chains of various lengths was acquired through powder X-ray diffraction (PXRD) experiments. The PXRD data of OAAOHs with both even and odd matching acyl chains (n = 14-20) was acquired at room temperature, as shown in Fig. 3.14A and 3.14B. In the 2θ range of 5-50°, all OAAOHs exhibited several distinct peaks. The *d*-spacing, indicative of the distance between crystal planes, was determined by analysing the positions of these diffraction peaks. The estimation of *d*-spacing for each compound involved analyzing 4-5 peaks from the PXRD profile, and the resulting values are compiled in Table 3.6. Fig. 3.14C presents a graphical representation of the dependence of the *d*-spacing of OAAOHs on their acyl chain lengths. A notable observation emerging from the analysis revealed a consistent trend wherein the *d*-spacing for even chain-length OAAOHs is more than that of their odd chain-length counterparts. This observation suggests the existence of an odd-even alternation in *d*-spacing concerning acyl chain length, shedding light on the intricate structural difference in the packing arrangement of OAAOHs.

Fig. 3.14C shows different linear dependence for even and odd acyl chain lengths, with slopes of 1.331 and 1.308 Å/CH_2, respectively. These figures show incremental increases in *d*-spacing of 0.665 and 0.654 Å per extra CH_2 moiety. For a normal bilayer, the increment in *d*-spacing of one CH_2 unit is found at 1.27 Å for each layer, translating to 2.54 Å for the bilayer, in instances where acyl chains are oriented perpendicularly to the plane. The observed steady rise in *d*-spacing indicates that the hydrocarbon acyl chains are distinctly tilted with respect to the bilayer normal. The incremental *d*-spacings yielded tilt angles (w.r.t. the bilayer normal) of 59.4° and 59.0° for the even and odd acyl chain

length series, respectively. These values are broadly consistent with the tilt angles of 54.5° and 55.3° calculated from the crystal structures of OPAOH and OHDAOH, respectively.

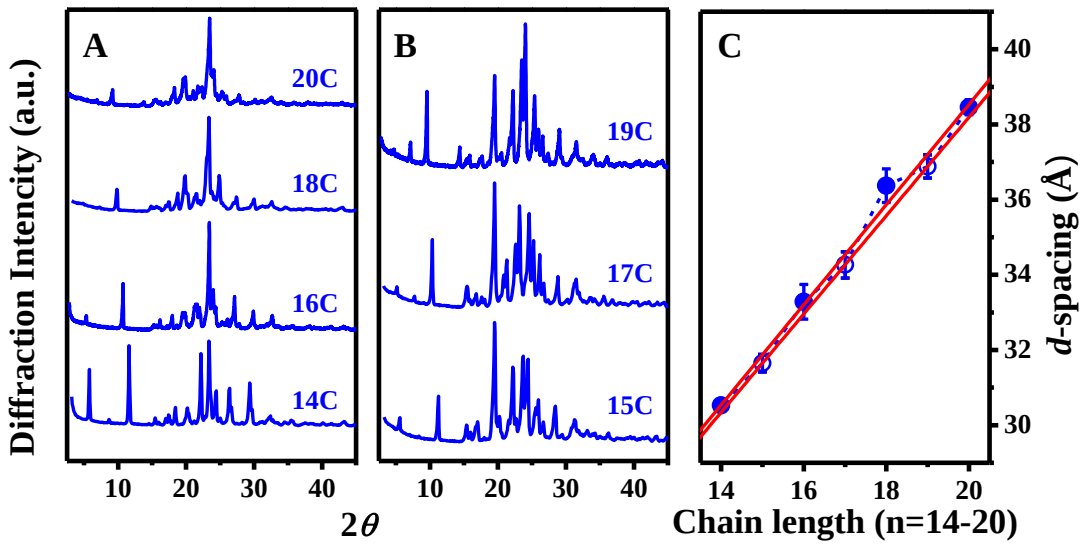

Fig. 3.14. PXRD patterns of OALAOHs. (**A**) Compounds with even number of C atoms in the acyl chain; (**B**) compounds with odd number of C atoms in the acyl chain; (**C**) Dependence of *d*-spacing on the acyl chain length. The number of carbon atoms in the acyl chain is indicated against each PXRD pattern. Solid red lines in **C** represent linear least squares fits for compounds with even (●) and odd (○) carbon atoms in the acyl chain.

Table 3.6. Lamellar *d*-spacings of OAAOHs with different acyl chain lengths (*n* = 14–20), derived from the powder X-ray diffraction data.

Chain length	*d*-spacing
14	30.5 (0.1)
15	31.6 (0.2)
16	33.3 (0.4)
17	34.3 (0.3)
18	36.4 (0.4)
19	36.9 (0.3)
20	38.4 (0.2)

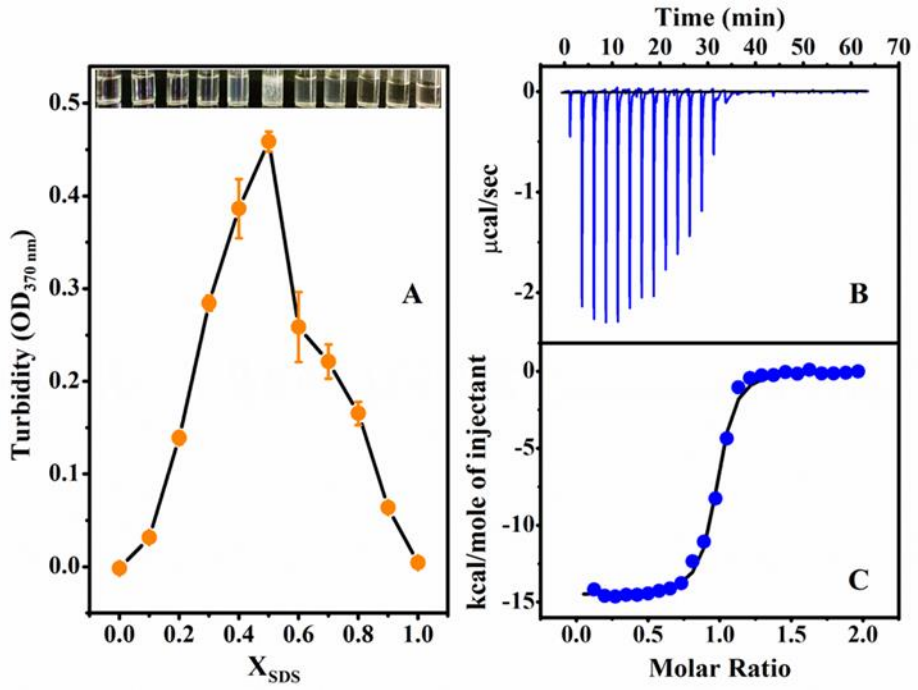

Fig. 3.15. OMAOH-SDS interaction studied by turbidimetry and ITC. (**A**) Job's experiment measuring turbidity in OMAOH-SDS mixtures. Top, a photo depicting the turbidity of samples; bottom, a plot of optical density at 370 nm for individual samples. (**B**, **C**) Results of ITC experiment: **B** Raw heats released during successive injections of 1 mM OMAOH into 0.1 mM SDS; **C** Integrated heat from titration data in **B**, corrected for dilution effects. Solid line: best curve fit using the *'one set of sites*' binding model in MicroCal PEAQ-ITC data analysis software.

3.4.11. Interaction between OMAOH and SDS: Turbidimetry and ITC studies

The interaction between cationic OMAOH and anionic SDS was initially studied using turbidimetry employing Job's method. The experiment was carried out by mixing 0.5 mM solutions of OMAOH and SDS in different proportions to give a final volume of 1.0 mL. This concentration was below the CMC of the two surfactants individually and the solutions were optically clear. When the optical density at 370 nm (OD_{370nm}) of samples containing OMAOH and SDS in different proportions was plotted as a function of the fraction of SDS it was observed that samples containing a low fraction of one of the surfactants gave low turbidity which increased with increase in its relative proportion till

the two components were present in equal proportion (Fig. 3.15A). The highest turbidity observed at X_{SDS} = 0.5 suggests the formation of an equimolar complex of the two amphiphiles, which is driven by the electrostatic attraction between the cationic OMAOH and the anionic SDS. In an aqueous medium, the catanionic complex or the ion pair, would then associate to form large supramolecular assemblies, which appear as turbid suspensions to the naked eye (Fig. 3.15A).

Thermodynamic factors governing the OMAOH-SDS interaction were investigated employing ITC, with results presented in Fig. 3.15B and 3.15C. To avoid problems caused by the presence of micelles in the reaction system, samples of the two amphiphiles were taken at concentrations well below their CMC. In Fig. 3.15B, titration data reveals a consistent exothermic heat of binding during initial OMAOH injections into SDS. However, it subsequently decreases rather steeply over the next few injections and becomes negligible afterwards, indicating saturation binding. In Fig. 3.15C, the plot of incremental heat changes against the OMAOH ratio suggests a good fit to the 'one set of sites' binding model, represented by the black solid line shown in the lower panel. This study resulted in the following thermodynamic parameters for the OMAOH-SDS interaction: The binding stoichiometry (n) is 0.96 (± 0.04), the binding constant (K_b) is 3.1 (± 0.5) × 10^6 M^{-1}, the binding enthalpy (ΔH_b) is -14.5 (± 0.3) kcal.mol^{-1}, and the binding entropy (ΔS_b) is -18.8 (± 1.1) cal.mol^{-1} K^{-1}. Using these data, the free energy of binding (ΔG_b) was calculated as -8.85 kcal mol^{-1}. The binding stoichiometry (n = 0.96) obtained from the ITC study is consistent with the data acquired earlier through Job's experiment, demonstrating that OMAOH and SDS interact to form an equimolar complex.

3.4.12. Characterization of the size and morphology by TEM and DLS

The findings from turbidimetric and ITC studies, as discussed earlier, strongly suggest the formation of an equimolar complex between OMAOH and SDS, leading to its subsequent assembly followed by the formation of catanionic vesicles. To gain further insights into the morphology and size of the OMAOH-SDS catanionic vesicles, TEM was employed. The TEM image presented in Fig. 3.16A shows the spherical morphology of the equimolar vesicles. An estimation of the average vesicle size revealed dimensions of 154 ± 17 nm (Fig. 3.16B). Additionally, DLS measurements of OMAOH-SDS catanionic

vesicles showed an average size of 188 (± 10) nm (Fig. 3.16C). Previous studies employing TEM and DLS techniques on catanionic vesicles formed by equimolar complexes of SDS with lauryl sarcosinate (~300 nm), lauryl alaninate (300–600 nm), and lauroyl glycinate

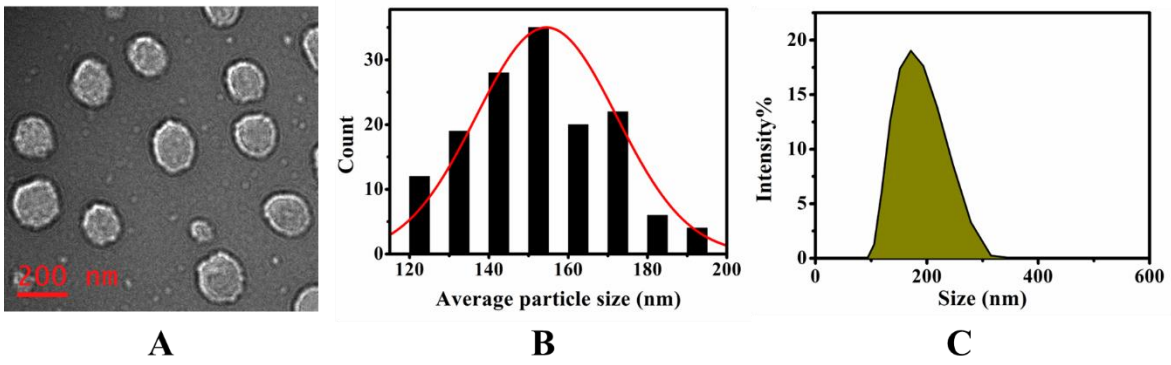

Fig. 3.16. Characterization of liposomes formed by OMAOH-SDS equimolar mixture. (**A**) TEM image of vesicles, (**B**) histogram of average particle size from TEM, and (**C**) graphical representation of particle-size distribution from DLS measurements.

(700–1000 nm) have reported sizes approximately 2-5 times larger in size (Reddy et al., 2017; Ravindar et al., 2022; Sivaramakrishna et al., 2015).

3.4.13. Comparative biophysical analysis of OABAOHs and OAAOHs and their catanionic vesicles formed in complex with SDS

A comparative analysis of the biophysical properties between OABAOHs and OAAOHs is expected to be of considerable relevance, given their relationship as structural isomers. This significance arises from the fact that OABAOHs are achiral, while OAAOHs (*O*-acyl-L-alaninols) are chiral analogues and hence are expected to exhibit distinct variations in biophysical characteristics. Differences in the biophysical properties have been previously seen in the case of NABAOHs and NAAOHs. Notably, these differences extend to the magnitude of interaction observed with other membrane lipids, such as phosphatidylcholines (Sivaramakrishna et al., 2016; 2021a). This comparison aims to elucidate the effect of isomeric variations on the biophysical behavior of these amphiphilic compounds.

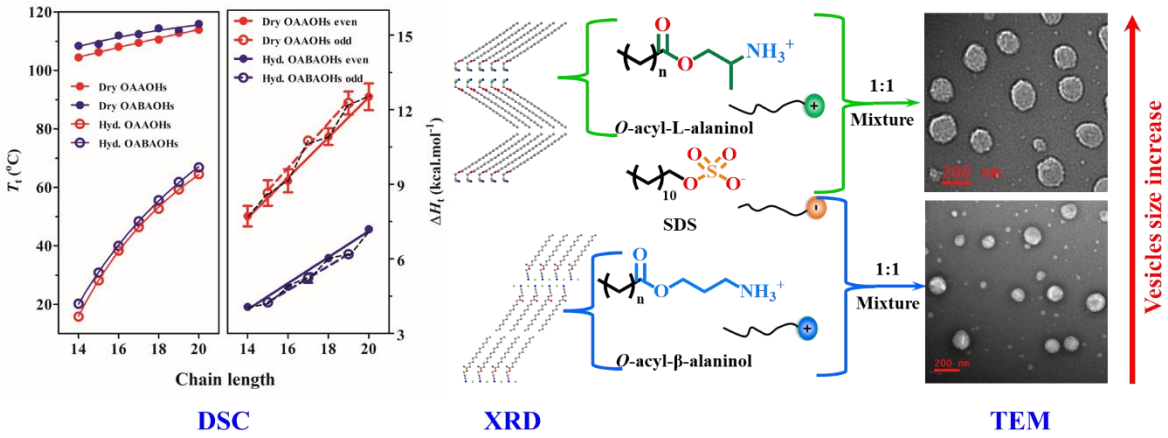

Fig. 3.17. Comparative biophysical representation of OAAOHs and OABAOHs by DSC and single crystal XRD and their catanionic vesicles formed with SDS by TEM.

Phase behaviour: The DSC study reveals notable differences in the transition temperatures (T_t) of achiral OABAOHs compared to chiral OAAOHs, with the T_t of OABAOHs (Choudhury et al., 2024) being higher in both dry and hydrated states. Analysis of the chain length-dependence of the transition enthalpy (ΔH_t) and entropy (ΔS_t) for dry OABAOHs as well as OAAOHs revealed an intriguing odd-even alternation pattern. Very interestingly, while in OABAOHs the even chain length compounds exhibit higher ΔH_t and ΔS_t values than their odd counterparts (Choudhury et al., 2024), OAAOHs display the reverse trend, with odd chain length compounds showing higher ΔH_t and ΔS_t values compared to the even acyl chain length compounds.

To comprehend this discrepancy, an examination of the incremental contributions (ΔH_{inc} and ΔS_{inc}) and the end contributions (ΔH_o and ΔS_o) for both systems becomes imperative. In the case of OABAOHs, the even chain length compounds exhibit higher ΔH_{inc}, ΔS_{inc}, ΔH_o, and ΔS_o values compared to odd chains (Choudhury et al., 2024). Conversely, for OAAOHs, the opposite trend is observed, with odd chain length compounds displaying higher ΔH_{inc}, ΔS_{inc}, ΔH_o and ΔS_o values than even chains. This detailed investigation sheds light on the intricate interplay of chain length and molecular contributions governing the thermal behavior of these achiral and chiral amphiphilic compounds.

Structure and supramolecular organization: The determination of the area per molecule for OPAOH and OHDAOH yielded values of 66.1 $Å^2$ and 67.0 $Å^2$, respectively. Notably,

these values exhibit a substantial increase compared to OABAOHs featuring acyl chains of 14 and 16 carbon atoms, which have molecular areas around 25 $Å^2$ (Choudhury et al., 2024). Previous research has established that head group size exerts a discernible influence on both molecular packing and tilt angle (Choudhury et al., 2023). In this context, it is of particular interest to investigate the impact of transitioning from an achiral to a chiral head group on molecular packing and tilt angle. Examination of achiral OABAOHs reveals that, in comparison to chiral OAAOHs, there is a minimal disparity in molecular packing. However, a significant reduction in tilt angle to 35º is observed for OABAOHs, resulting in molecules adopting an L-shaped geometry and thereby inducing a tilted orientation of the acyl chain with respect to the bilayer normal (Choudhury et al., 2024). This investigation underscores the intricate interplay between head group structure and molecular arrangement, providing valuable insights into the conformational characteristics of chiral amphiphilic compounds in lipid bilayer environments.

Size and morphology of equimolar complex of OMBAOH and OMAOH with SDS: The size and morphology of equimolar complexes formed by OMBAOH and OMAOH with SDS were investigated through TEM and DLS analyses. The aggregates resulting from equimolar OMBAOH-SDS and OMAOH-SDS mixtures were examined to discern their size and morphology. Both TEM and DLS experiments consistently revealed that equimolar OMAOH-SDS mixtures give rise to slightly larger unilamellar spherical vesicles (~150-190 nm) compared to their OMBAOH-SDS counterparts (~150-160) (Choudhury et al., 2024). This distinction in vesicle size is attributed to variations in the crystal packing parameters of the amphiphiles, with the primary difference lying in the head group of the cation. This systematic exploration of size and morphology offers valuable insights into the self-assembly behaviour of these amphiphilic compounds in combination with SDS, shedding light on the impact of structural nuances on aggregate formation.

Thermotropic phase behavior and supramolecular organization of *N*, *O*-diacyl-L-alaninols: effect on stratum corneum model membrane

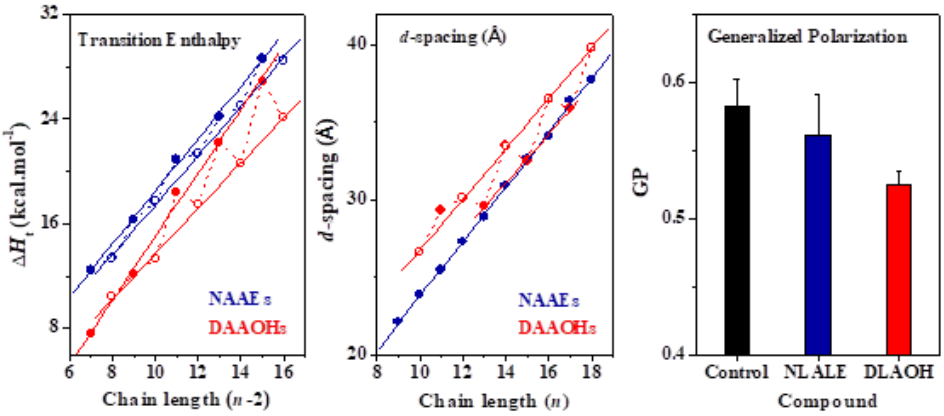

The work presented in this chapter was published in ***J. Chem. Sci.*** (2021) 233:91

4.1. Summary

In recent years, chemical enhancers that increase the permeability of stratum corneum (SC) attracted the attention of clinicians and researchers due to their utility in developing transdermal drug delivery systems. *N*-Lauroyl glycine lauryl ester (NLGLE) was reported to induce higher SC permeability than *N*-lauroyl serine lauryl ester (NLSLE). Earlier, we proposed a similar activity could be obtained by *N*-acyl-*L*-alanine esters (NAAEs) towards SC, which are homologous to NLGLE. In this study, we synthesized a homologous series of *N, O*-diacyl-*L*-alaninols (DAAOHs) (which are isomers of NAAEs) with saturated acyl chains. We investigated their thermotropic phase behavior and supramolecular organization, and the results are discussed with the properties of isomeric NAAEs. Most DAAOHs exhibited one polymorphic phase transition (solid-solid transition) before the melting transition in the first heating thermogram. The solid-solid transition disappeared in further heating thermograms. Odd chain length DAAOHs exhibited higher transition enthalpy and transition entropy values than even chain length DAAOHs. Interestingly, the even chain length DAAOHs exhibited higher transition temperature and *d*-spacing values than odd chain length DAAOHs. Further, Laurdan fluorescence studies revealed that *N, O*-dilauroyl-*L*-alaninol increases the fluidity of SC model membrane more efficiently as compared to NLGLE, suggesting that DAAOHs can potentially be used as chemical enhancers in developing transdermal drug delivery systems.

4.2. Introduction

Transdermal drug delivery (TDD) is a convenient and safe approach compared to conventional drug delivery methods, e.g. subcutaneous/intravenous injection, and oral administration. TDD avoids the hepatic first-pass effect, especially for drugs with low bio-availability through conventional administration, and when high doses of medication are necessary for a longer duration to get effective bioavailability (Kailash et al., 2013). Several anti-dermal, anti-ischemic, anti-hypertensive and hypoglycemic drugs, as well as some others are widely delivered in a transdermal form (Kailash et al., 2013; Meera et al., 2020). However, due to low permeability of drugs through the stratum corneum (SC), use of TDD is considerably restricted. SC or epidermis is the outer layer of skin, which serves as the primary barrier between the environment and the body. SC consists of dead cells (Corneocytes) without nuclei and cell organelles and contains cytoplasm with filamentous keratin. The major lipid components of the SC are ceramides (40-60%), sterols (20-33%), and fatty acids (7-13%), whereas cholesterol-3-sulphate and cholesteryl esters are minor components (Elias, 1983; Sahle et al., 2015; Bonte et al., 1995). However, the lipid composition varies based on a variety of parameters, e.g., location (depth of the skin), age, sex, race, and health of the individual. The ceramides in SC are complex and contain primarily saturated fatty acids, due to which permeability of drugs through SC is rather low (Sahle et al., 2015; Holleran et al., 2006).

Several chemical enhancers (CEs) have been investigated with the objective of improving the permeability of SC to drugs and therapeutic agents. These CEs include short and long-chain alcohols, propylene glycol and its esters, benzoic acid esters, fatty acid esters, cyclic amides, unsaturated fatty acids etc. However, the exact mechanism of how CEs enhance SC's permeability is not well understood. It is assumed that most CEs enhance the permeability by changing the SC lipid organization and protein hydration by their bent structure, hydration capabilities and partition differences (Haque et al., 2018; Pham et al., 2016; Karande et al., 2009). Earlier, *N*-acyl glycine alkyl esters (NAGEs) and *N*-acyl serine alkyl esters (NASEs), which are structurally similar to ceramides, have been reported to enhance the permeability of SC. NAGEs have shown a significant enhancement of permeability as compared to NASEs. The reduced/low ability of NASEs

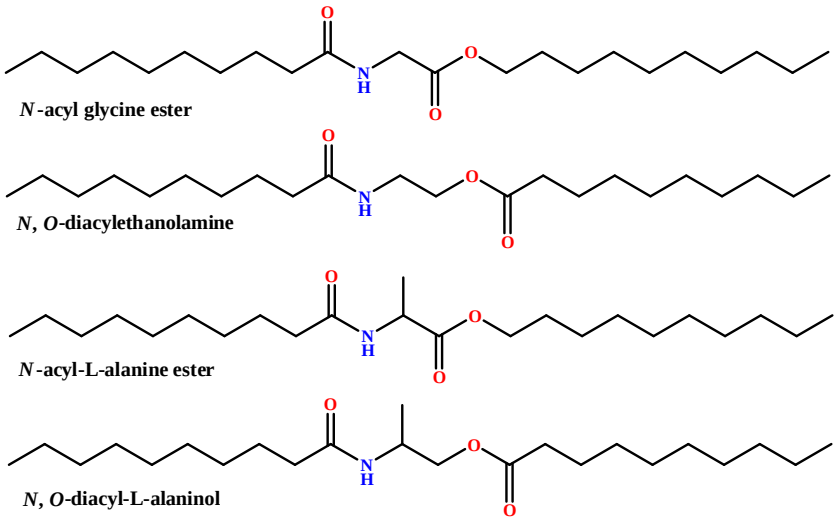

Fig. 4.1. Molecular structure of *N*-acyl glycine ester (NAGE), *N, O*-diacylethanolamine (DAE), *N*-acyl-L-alanine ester (NAAE), and *N, O*-diacyl-L-alaninol (DAAOH) with matched acyl-alkyl/acyl-acyl chains.

has been explained as due to the higher hydrophilic nature of the head group, which improves hydrogen bonding between adjacent lipid molecules, which results in improved resistance to the passage of the drug through SC (Vavrova et al., 2003). In previous work, we synthesized and characterized *N*-acyl-L-alanine alkyl esters (NAAEs), which are homologous to NAGEs and hydrophobic analogs of NASEs, and proposed them as potential CEs for enhancing the permeability of SC in view of their reduced hydrogen bonding capacity (Sivaramakrishna and Swamy, 2015b). With the objective of identifying other CEs for application in TDD, in the present study we synthesized and characterized a homologous series of *N, O*-diacyl-L-alaninols (DAAOHs) (see Fig. 4.1 for the structures of the above classes of compounds). The ability of these 4 classes of compounds to modulate the fluidity of stratum corneum model membrane (SCM) was investigated by monitoring Laurdan fluorescence properties, considering that membrane fluidity provides a good correlation to membrane permeability (Lande et al., 1995). The results obtained have been presented here and their potential for use in developing transdermal drug delivery systems has been discussed.

The above introduction indicates that *N*-acyl amino acid esters are a new class of compounds that may find use as CEs in formulating TDD systems. Recent studies on the structure and supramolecular organization of NAGEs revealed that these amphiphilic

molecules are packed in an untitled, normal bilayer mode (Reddy and Swamy, 2017). This raised a question as to how the untilted NAGEs improve the permeability of the tightly packed SC lipid membrane? Further, how do the *N*, *O*-diacylethanolamines (DAEs), which adopt a bent structure (Kamlekar et al., 2010), influence the SC permeability? Additionally, how do isomeric NAAEs and DAAOHs differ from one another with respect to modulating SC permeability? How isomeric NAGEs and DAEs, and homologous NAAEs and DAAOHs show their impact on SCM? We attempt to address these questions in the present study.

4.3. Materials and methods

4.3.1. Materials

Fatty acids (C9-C18) and L-alaninol were obtained from Sigma-Aldrich (Bangalore, India). Oxalyl chloride was purchased from Merck (Germany), and the remaining chemicals and solvents were obtained from Sisco Research Laboratories (Mumbai, India).

4.3.2. Synthesis of DAAOHs

DAAOHs of matched acyl chains were synthesized by a two-step procedure (Scheme 1). In the first step, *N*-acyl-L-alaninols (NAAOHs) were prepared as described earlier (Sivaramakrishna and Swamy, 2016b). In the second step, the NAAOHs were *O*-acylated to yield DAAOHs. Briefly, the fatty acid (1 mmol) was converted to the acid chloride by mixing with oxalyl chloride (4 mmol) in dichloromethane (DCM) under a dry N_2 atmosphere. After two hours, excess oxalyl chloride was removed by passing dry N_2 gas. The acid chloride thus obtained was added to L-alaninol (4 mmol) in DCM at low temperature (0-5 ºC), and the mixture was kept under stirring for 3 h. The crude NAAOH obtained after removing the excess DCM was then O-acylated as follows. Acid chloride of matched acyl chain length, prepared as mentioned above (1.1 mmol), was added to NAAOH (1 mmol) in DCM at room temperature, and the reaction mixture was kept under

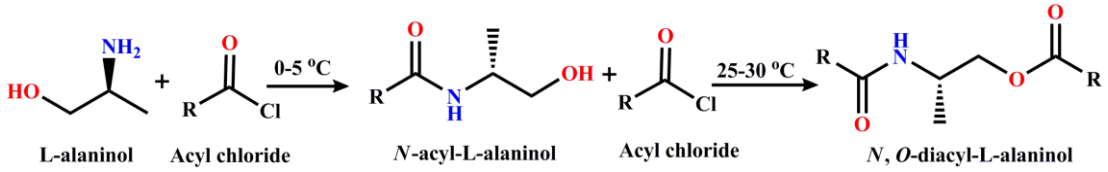

Scheme 4.1: Synthesis of *N*, *O*-diacyl-L-alaninols

continuous stirring overnight. After removing excess solvent, the reaction mixture was washed with water and brine solution, which yielded the crude DAAOH. Crude DAAOHs thus obtained were purified by silica gel column chromatography. Ethyl acetate/n-hexane mixtures of varying ratios were used for elution. Finally, pure products were obtained in 70-80% yield after recrystallization from DCM containing trace amounts of acetone as the solvent at low temperature (ca. -20 ºC). The purified DAAOHs were characterized using FTIR, NMR (^{1}H and ^{13}C), and high-resolution mass spectrometry (HRMS)

4.3.3. Differential scanning calorimetry

DSC experiments with dry DAAOHs were carried out on a Perkin Elmer Diamond differential scanning calorimeter as described earlier (Sivaramakrishna and Swamy, 2015b). About 2 mg of each dry DAAOH was weighed accurately into an aluminum sample pan, covered with an aluminum lid and sealed with the aid of a crimper. Another pan, prepared similarly but without any sample in it was used as the reference. For every sample, alternate heating (3) and cooling (2) scans were collected at a scan rate of 2 ºC/min. Most of the compounds showed minor transitions in the first heating scan which disappeared in the subsequent heating scans; therefore, the first heating scans were considered for further analysis. Transition temperatures (T_t) were determined from the peak of the transition curve and transition enthalpies (ΔH_t) were determined by integrating the area under the transition curve, whereas transition entropies (ΔS_t) were obtained from the ΔH_t values, assuming a first order transition, as indicated by Eq. (4.1) (Marsh, 1990):

$$\Delta S_t = \Delta H_t / T_t \qquad (4.1)$$

4.3.4. Powder X-ray diffraction studies

Powder X-ray diffraction measurements on DAAOHs were carried out using a Bruker SMART D8 Advance powder X-ray diffractometer (Bruker-AXS, Karlsruhe, Germany) with Cu-Kα radiation operating at 40 kV and 30 mA. Finely powdered samples were placed in the instrument sample holder and diffraction data were collected using a LynxEye PSD data collector over a 2θ range of 1–50º at room temperature with a step size of 0.0198º and a measuring time of 1.5 s for each step. Peaks corresponding to $2\theta \leq$ 20º were used to calculate *d*-spacings employing Bragg's equation.

4.3.5. Stratum corneum model membrane preparation and Laurdan fluorescence

Stratum corneum model membrane (SCM) was prepared from *N*–acetyl ceramide (C2-ceramide) (60 mol%), cholesterol (30 mol%), and palmitic acid (10 mol%). Twenty mol% of *N, O*-dilauroyl-L-alaninol (DLAOH), *N*-lauroyl-L-alanine lauryl ester (NLALE), *N, O*-dilauroylethanolamine (DLE), and *N*-lauroyl glycine lauryl ester (NLGLE) were added to the above lipid mixture in separate experiments to check their ability to modulate the fluidity of SCM. The final lipid composition in these samples was C2-ceramide (50 mol%), cholesterol (25 mol%), palmitic acid (8.3 mol%), DLAOH/DLE/NLGLE/NLALE (16.7 mol%). Stock solutions of C2-ceramide, cholesterol, palmitic acid, DLAOHs, NLALE, DLE, and NLGLE were prepared by dissolving in a mixture of chloroform and methanol (1:1, v/v). Samples with the above-mentioned lipid composition were obtained by mixing appropriate aliquots of the stock solutions of each lipid component. Similarly, a stock solution of the fluorescent dye laurdan was prepared in ethanol, and an aliquot from it was added to the lipid mixture in chloroform-methanol to give a final probe concentration of 1 μM [1 mM lipid and 1 μM probe (0.1 probe concentration)]. Then the solvent was evaporated by gently blowing dry nitrogen gas over the sample, and the remaining traces of solvent were removed by vacuum desiccation. Each sample was hydrated with 20 mM sodium phosphate buffer (pH 7.4) and subjected to 4-5 freeze-thaw cycles to get a homogeneous mixture. Laurdan fluorescence spectra were collected as reported earlier (Sivaramakrishna et al., 2019), and generalized polarization (GP) values were calculated using Equation 4.2 (Parasassi et al., 1998).

$$GP = (I_{433}-I_{503})/ (I_{433}+I_{503}) \qquad (4.2)$$

where I_{433}, I_{503} are the emission intensities at 433 and 503 nm, respectively.

4.4. Results and discussion

The homologous series of DAAOHs synthesized in the current study were characterized comprehensively by FTIR, ^{1}H- and ^{13}C-NMR spectroscopy and by high-resolution mass spectrometry. Details of the spectral data and their analysis are given in Supporting Information (Tables S1-S4 (SI) and Figs. 4.2-4.5). These data are fully consistent with the structures of DAAOHs and show that they are all highly pure.

4.4.1. Spectroscopic characterization of DAAOHs

An FTIR spectrum of *N, O*-dilauroyl-L-alaninol (DLAOH) is given in Fig. 4.2. The spectral data obtained for other DAAOHs were qualitatively comparable. IR spectra of DAAOHs contained absorption bands due to the ester carbonyl group at 1720-1741 cm^{-1} and amide carbonyl at 1625-1648 cm^{-1}. The N-H stretching and bending bands were observed at 3302-3309 cm^{-1} and 1533-1549 cm^{-1}, respectively. The C-H stretching bands were observed at 2848-2964 cm^{-1}. C-H scissoring and rocking bands were observed at 1463-1478 cm^{-1} and 717-723 cm^{-1}, respectively. The IR resonances of all DAAOHs (C9-C18) are listed in Table S1 of Chapter 4 (see supporting information).

The ^{1}H-NMR spectrum of DLAOH is shown in Fig. 4.3. All DAAOHs (C9-C18) are chemically much related and vary only in the number of methylene units in the acyl/alkyl chain. Their NMR spectra were nearly identical apart from the integration value of the peak corresponding to polymethylene moiety. The ^{1}H NMR spectra of the DAAOHs gave the following resonances: 0.84-0.90δ (6H, t), 1.12-1.17δ (3H, d), 1.22-1.27δ (nH, m), 1.58-1.62δ (4H, m), 2.11-2.18δ (2H), 2.28-2.34δ (2H), 3.98-4.02δ (1H, dd), 4.01-4.14δ (1H, dd), 4.12-4.31δ (1H, m), and 5.57- 5.88δ (1H, d). These resonances match well with the chemical structure of DAAOHs. The ^{1}H NMR chemical shifts obtained for all DAAOHs (C9-C18) are listed in Table S2 of Chapter 4 (see supporting information).

^{13}C NMR spectrum of DLAOH is shown in Fig. 4.4. The ^{13}C NMR resonances for the *N*-acyl and *O*-acyl chains are seen at:14.03-14.12δ (both terminal methyl groups), 17.31-17.40δ (C-atom of L-alaninol methyl), 4-5 closely spaced resonances of varying intensity between 22.62-31.93δ for the methylene groups (C-atoms except α-CH_2 to ester/amide in *N*-acyl and *O*-acyl chains), 34.13-34.20δ (C-atom α to the ester carbonyl), 36.78-36.92δ (C-atom α to the amide carbonyl), 44.27-44.53δ (C-atom of chiral carbon of L-alaninol), and 66.66-66.74δ (C-atom attached to the hydroxyl group of L-alaninol). The ester and amide carbonyl resonances are seen at 172.64-172.88δ and 173.86-174.05δ, respectively. The ^{13}C NMR spectra of other DAAOHs were qualitatively very similar and matched the expected chemical structures. The ^{13}C NMR chemical shifts for other DAAOHs (C9-C18) are listed in Table S3 of Chapter 4 (see supporting information).

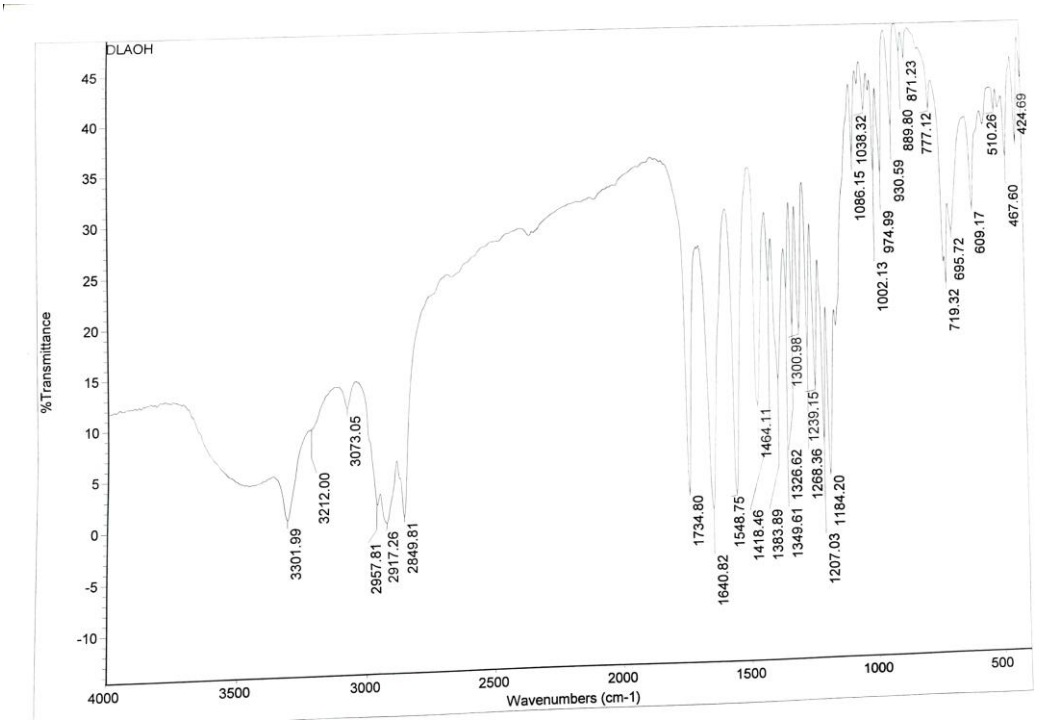

Fig. 4.2. FTIR spectrum (KBr pellet) of DLAOH recorded at room temperature.

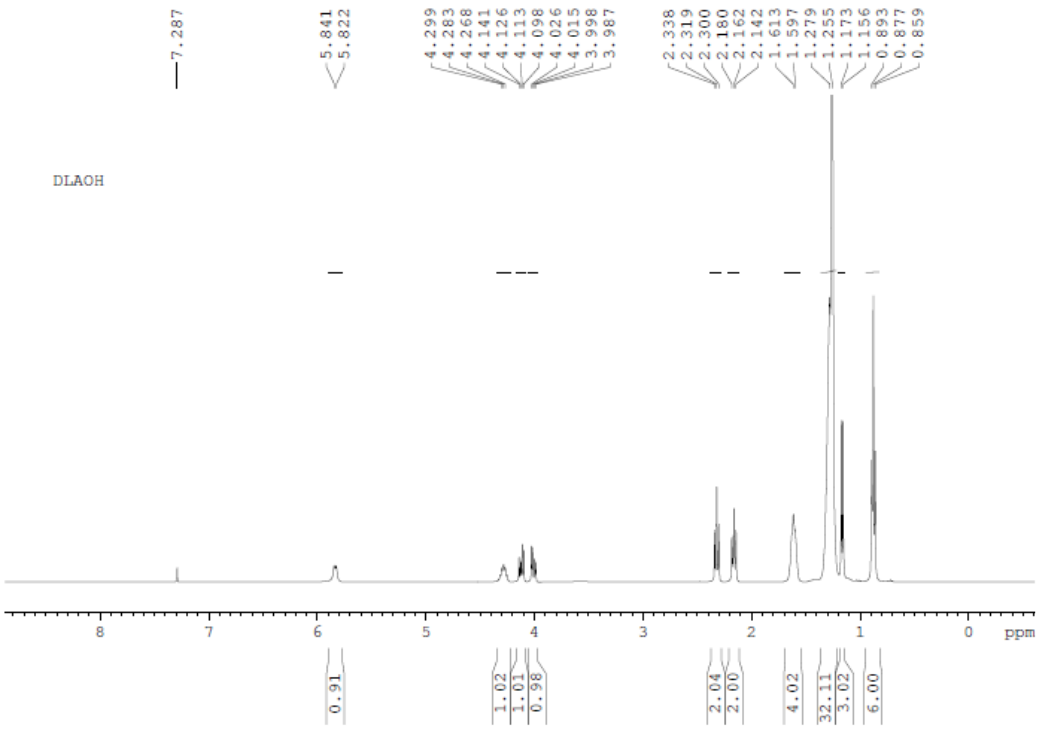

Fig. 4.3. ^{1}H NMR spectrum of DLAOH recorded at room temperature (solvent $CDCl_3$).

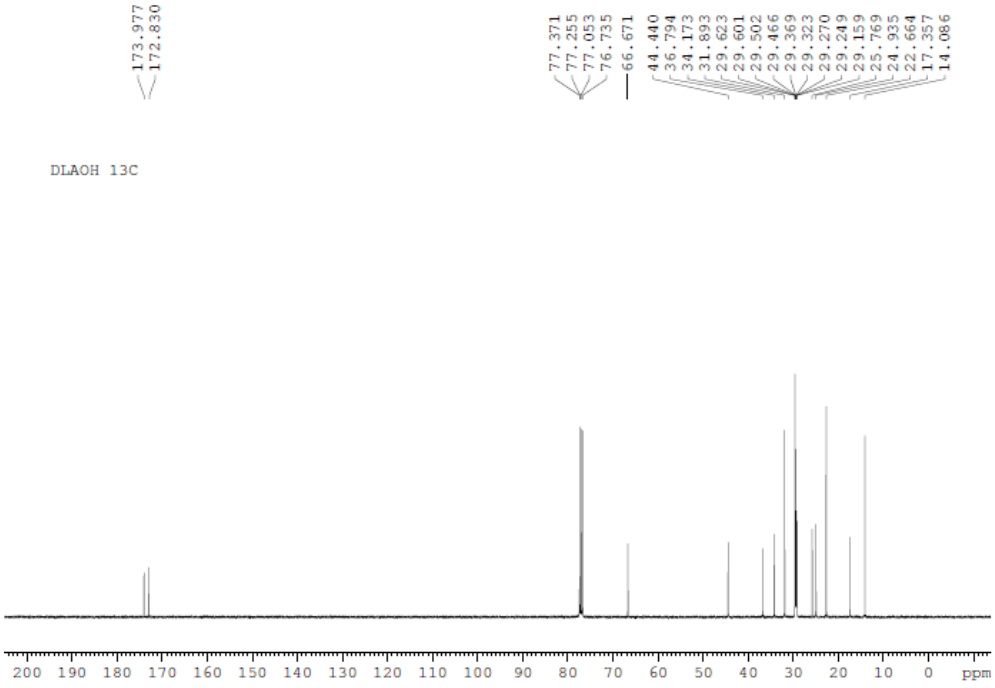

Fig. 4.4. ^{13}C-NMR spectrum of DLAOH recorded at room temperature (solvent $CDCl_3$).

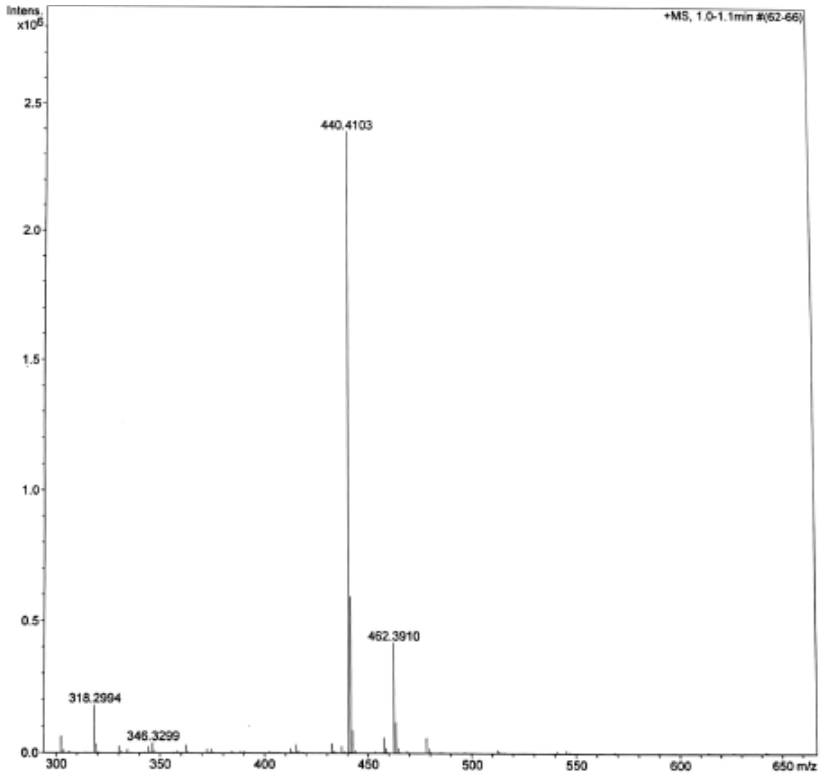

Fig. 4.5. ESI mass spectrum of DLAOH. Peaks at m/z values of 440.4103 $(M + H)^+$ and 462.3910 $(M + Na)^+$ correspond to the molecular ion.

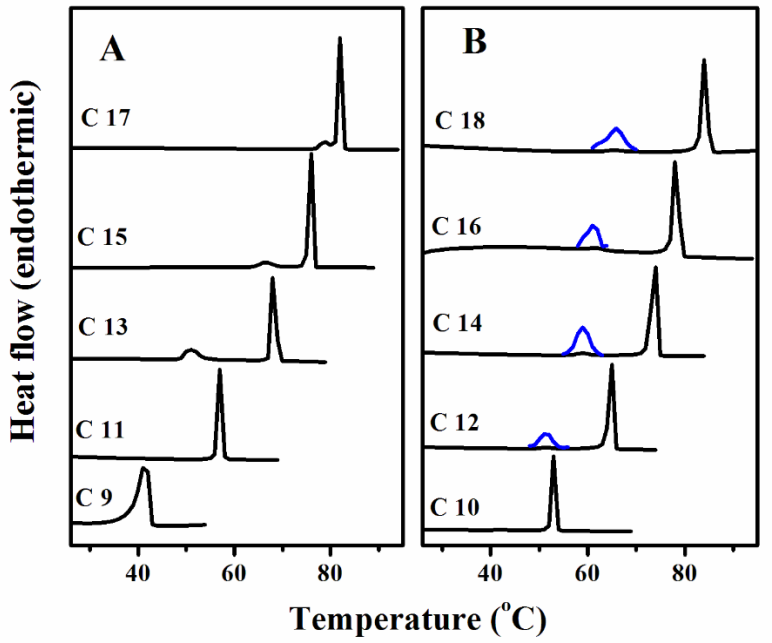

Fig. 4.6. DSC first heating thermograms of dry DAAOHs with odd (**A**) and even (**B**) number of C-atoms in the acyl chain. The number of C-atoms is indicated against each thermogram. Less-intense minor transitions of even-chain DAAOHs are vertically expanded 15 times and shown in blue color.

A high-resolution mass spectrum of DLAOH is presented in Fig. 4.5. The two most intense peaks seen at m/z = 440.4103 and 462.3910 match well with the molecular ion of the compound $[M+H]^+$ (calculated mass = 440.4104) and its sodium adduct $[M+Na]^+$ (calculated mass = 462.3923). All DAAOHs with different matched acyl chains also yielded essentially similar results, and the mass spectrometric data for them are listed in Table S4 of Chapter 4 (see supporting information).

4.4.2. Thermotropic phase behavior of DAAOHs

Heating thermograms of dry DAAOHs bearing matched odd- and even acyl chains are given in Figs. 4.6A and B, respectively, and the corresponding cooling thermograms are shown in Figs. 4.7A and B. DAAOHs bearing different acyl chains (12-18 C-atoms) show two transitions, whereas those with 9-11 C-atoms show a single transition (Fig. 4.6). The minor transitions most likely correspond to solid-solid phase transitions and suggest polymorphism in the solid-state structures of the compounds. The minor transition in even-chain DAAOHs are relatively less intense than those observed with odd-chain

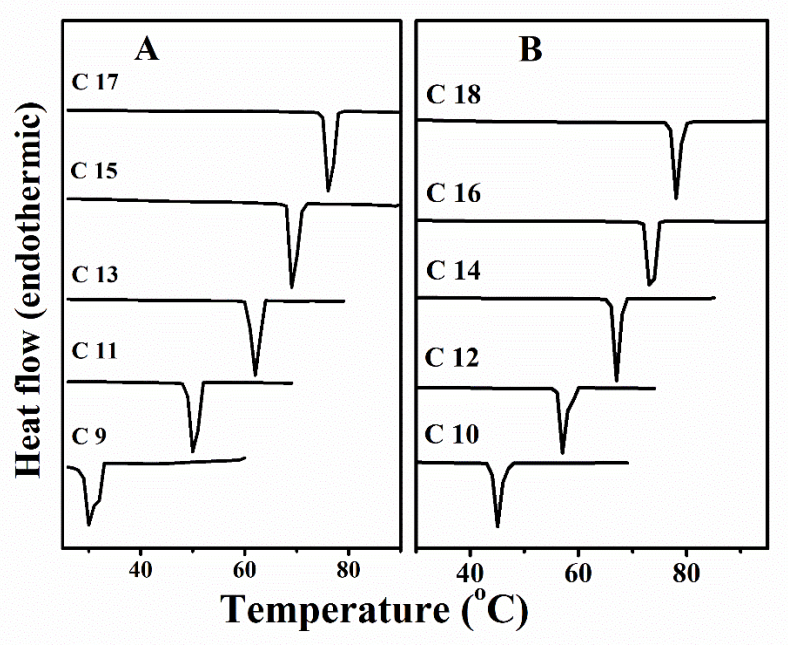

Fig. 4.7. DSC first cooling thermograms of dry DAAOHs with odd (**A**) and even (**B**) number of C-atoms in the acyl chain. The number of C-atoms is indicated against each thermogram.

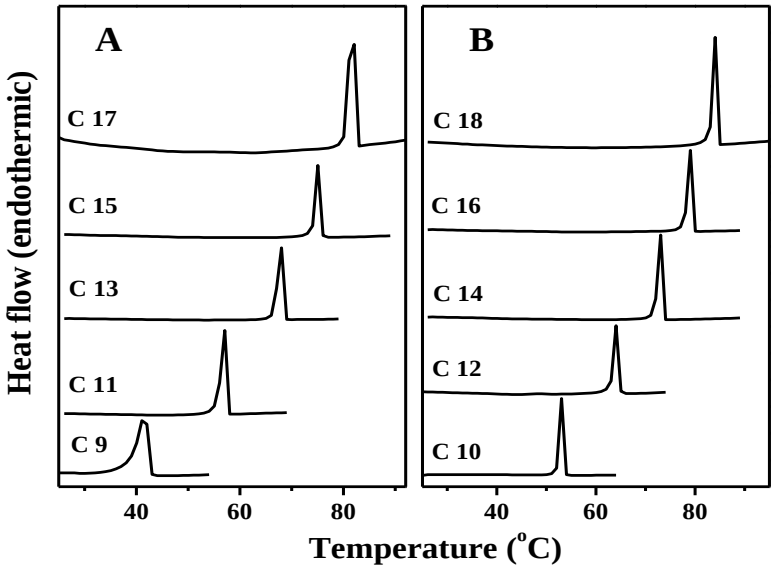

Fig. 4.8. DSC second heating thermograms of DAAOHs with odd (**A**) and even (**B**) number of C-atoms in the acyl chain. The number of C-atoms is indicated against each thermogram.

DAAOHs. The minor transition of C15 DAAOH is shifted towards major transition compared to C13 DAAOH, whereas it is partially merged with a major transition in C17 DAAOH. It is interesting to note that minor transitions are not observed in the case of NAAEs and NAGEs (which are structural analogs and homologs of (DAAOHs), while homologous DAEs showed minor transitions in the first heating thermograms (Sivaramakrishna and Swamy, 1015b; Reddy and Swamy, 2017; Kamlekar et al., 2010). *N*-Acyl derivatives of alanine and alaninol, namely *N*-acyl-L-alanines (NAAs) and *N*-acyl-L-alaninols (NAAOHs) also did not show any minor transitions, whereas even-chain ester derivatives of L-alanine (AEs) showed one minor transition in the first heating thermogram (Sivaramakrishna et al., 2015a; 2015c; 2016b).

Table 4.1. Average values of transition temperatures (T_t), transition enthalpies (ΔH_t), and transition entropies (ΔS_t) of DAAOHs from first and second heating thermograms. Values in parentheses correspond to standard deviations from three independent measurements.

Acyl chain length (n)	1st Heating			2nd Heating		
	T_t (°C)	ΔH_t (kcal.mol^{-1})	ΔS_t (cal.mol^{-1}.K^{-1})	T_t (°C)	ΔH_t (kcal.mol^{-1})	ΔS_t (cal.mol^{-1}.K^{-1})
9	41.8 (0.1)	7.55 (0.19)	24.0 (0.6)	41.8 (0.1)	7.55 (0.19)	24.0 (0.6)
10	53.2 (0.1)	10.39 (0.13)	31.8 (0.4)	53.1 (0.1)	10.31 (0.12)	31.6 (0.4)
11	57.4 (0.1)	12.17 (0.22)	36.8 (0.7)	56.9 (0.1)	11.39 (0.22)	34.5 (0.7)
12	64.8 (0.2)	13.28 (0.09)	39.3 (0.2)	64.7 (0.2)	13.19 (0.46)	39.1 (1.4)
13	68.4 (0.1)	18.37 (0.36)	53.7 (1.1)	67.6 (0.1)	14.64 (0.32)	43.0 (0.9)
14	73.5 (0.3)	17.43 (0.27)	50.3 (0.8)	73.3 (0.2)	16.29 (0.33)	47.0 (1.0)
15	76.0 (0.1)	22.17 (0.35)	63.5 (0.9)	75.3 (0.1)	17.65 (0.32)	50.7 (0.9)
16	79.4 (0.1)	20.64 (0.35)	58.5 (1.0)	78.9 (0.1)	19.55 (0.39)	55.5 (1.1)
17	82.5 (0.2)	26.91 (0.66)	75.8 (1.9)	81.8 (0.1)	21.09 (0.60)	59.2 (1.8)
18	84.8 (0.1)	24.06 (1.04)	67.2 (2.9)	84.2 (0.1)	22.39 (0.71)	62.7 (2.0)

The sharp transition temperatures of DAAOHs matched very well with the capillary melting points of the compounds. When the same samples were subjected to further heating scans, minor transitions for both even- and odd DAAOHs (C12-18) completely disappeared in the second and subsequent heating cycles and a slight decrease in the transition enthalpies was noticed in the second heating scan onward (Fig. 4.8, Table 4.1). The minor transition were not seen in the first cooling scans also (Fig. 4.7). Similar

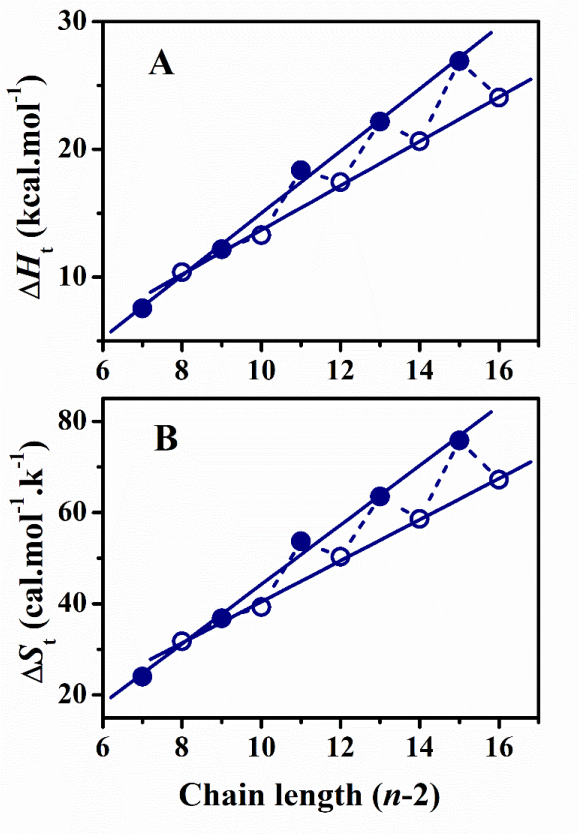

Fig. 4.9. Chain length dependence of transition enthalpy (A) and transition entropy (B) of dry DAAOHs from the first heating scans. Values of ΔH_t and ΔS_t were plotted against the number of methylene units (n-2). Filled symbols, odd chain length compounds; open symbols, even chain length compounds. Solid lines correspond to linear least-squares fits of the data.

behavior was noticed earlier in several single-chain and double-chain amphiphiles (Kamlekar et al., 2006, 2010; Sivaramakrishna et al., 2015c, 2019; Ramakrishnan and Swamy, 1998; Reddy et al., 2014; Tarafdar et al., 2012). Interestingly, the minor transitions were also seen in the second heating scans in the case of *N*-acyl-β-alanines (Sivaramakrishna and Swamy, 2016a). Values of T_t, ΔH_t, and ΔS_t of DAAOHs determined from the first and second heating thermograms are given in Table 4.1.

4.4.3. *Chain length dependence of* ΔH_t *and* ΔS_t

The chain length dependence of ΔH_t and ΔS_t corresponding to the phase transitions of DAAOHs in the first and second heating thermograms is shown in Figs. 4.9A and B, and Figs. 4.10A and B, respectively. In Fig. 4.9, the ΔH_t and ΔS_t values of odd chain length

DAAOHs are somewhat higher as compared to the even chain length compounds, except for the C10 compound. A similar pattern was observed earlier in NAAEs, which are structural isomers of DAAOHs. Besides, a similar pattern was noticed in the case of NAAs, while such pattern is missing in NAAOHs (Sivaramakrishna et al., 2015a; 2015b; 2016b). The values of ΔH_t and ΔS_t obtained for odd- and even chain length DAAOHs independently exhibit linear dependence on the chain length. In contrast, ΔH_t and ΔS_t of second heating thermograms (Fig. 4.10) show linear dependence for all DAAOHs, except C9 DAAOH. The ΔH_t and ΔS_t values of first and second heating scans could be fit well to expressions (4.3) and (4.4).

$$\Delta H_t = \Delta H_o + (n\text{-}2)\,\Delta H_{inc} \qquad (4.3)$$

$$\Delta S_t = \Delta S_o + (n\text{-}2)\,\Delta S_{inc} \qquad (4.4)$$

where ΔH_o and ΔS_o are the end contributions to ΔH_t and ΔS_t resulting from the terminal methyl group and the polar component of the molecule, and n is the number of C atoms in the acyl chains. The average incremental contributions of each CH_2 group to the overall ΔH_t and ΔS_t are ΔH_{inc} and ΔS_{inc}, respectively. It has been seen that similar linear dependence of the transition enthalpies and entropies was observed previously in several single- and double-chain amphiphiles such as NAAEs, NAAOHs, NAGEs, DAEs, and NAAs (Sivaramakrishna et al., 2015b; 2016b; Lande et al., 1995; Reddy and Swamy, 2017; Kamlekar et al., 2010; Tarafdar et al., 2012). The linear fits yielded values ΔH_{inc} and ΔS_{inc} from polymethylene groups, as well as end contributions ΔH_o and ΔS_o arising from the terminal methyl group of the acyl chains and the head group. These values obtained from first and second heating thermograms are given in Table 4.2.

The linear chain length dependence of ΔH_t and ΔS_t values, observed here, indicates that molecular packing of the compounds with odd- and even chains would be similar initially (obtained after crystallization from the solvent) within each group, whereas upon going through the melting transition, all DAAOHs (even chain compounds as well as odd chain compounds) might adopt a similar molecular packing. Therefore, molecular packing and intermolecular interactions in the solid state of all the even-chain DAAOHs are likely to be somewhat similar (initially), and determination of the 3-dimensional structure of any one of them can give a reasonably good idea of the molecular packing and intermolecular interactions present in the crystal lattice of DAAOHs in the

particular series. Interestingly, incremental and end contribution values obtained from second heating thermograms are significantly lower compared to the incremental and end contributions of first heating thermograms (both odd- and even chain length compounds), which could be due to changes in the molecular packing after the first heating cycle.

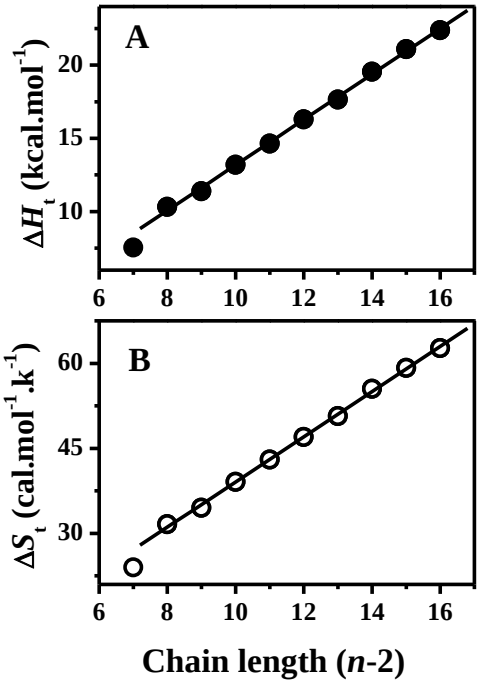

Fig. 4.10. Chain length dependence of transition enthalpy (A) and transition entropy (B) of dry DAAOHs from second heating. Values of ΔH_t and ΔS_t were plotted against the number of methylene (CH_2) units (n-2). Solid lines correspond to linear least squares fits of the data.

4.4.4. *Chain length dependence of T_t*

The variation in the melting phase transition temperatures (T_t) of DAAOHs with chain length for the first heating thermograms is given in Fig. 4.11. The even chain length DAAOHs have higher T_t values as compared to the odd chain length compounds and within each series the T_t of DAAOHs increases in a smooth progression with the acyl chain length, but the differences between the two series decrease with increasing chain length and after C15 the differences become very small such that the odd-even alternation is not detectable. In general, for many single-chain amphiphiles, T_t values of even chain

length compounds were found to be higher than the odd chain length compounds (Ramakrishnan and Swamy, 1998; Reddy et al., 2013; Larsson, 1986), although some exceptions were reported, e.g., NAAs and L-alanine alkyl ester (AEs) (Sivaramakrishna et al., 2015a; 2015c). The odd-even alternation in the T_t values and enthalpies and entropies in DAAOHs is unusual in that while the even chain length compounds have higher T_t values, the ΔH_t and ΔS_t values are higher for the odd chain length compounds. Similar unusual behavior was noticed earlier in AEs (Sivaramakrishna et al., 2015c).

Table 4.2. Incremental values (ΔH_{inc}, ΔS_{inc}) and end contributions (ΔH_o, ΔS_o) arising from the phase transition enthalpies and entropies of DAAOHs. Values in parentheses correspond to fitting errors obtained from the least-squares analysis.

Thermodynamic parameter	1st Heat		2nd Heat
	Odd chain length	Even chain length	
ΔH_{inc} (kcal/mol)	2.44 (0.09)	1.74 (0.05)	1.55 (0.02)
ΔH_o (kcal/mol)	-9.36 (1.11)	-3.66 (0.59)	-2.35 (0.28)
ΔS_{inc} (cal/mol/k)	6.52 (0.30)	4.50 (0.14)	3.98 (0.05)
ΔS_o (cal/mol/k)	-20.91 (3.46)	-4.62 (1.69)	-0.77 (0.62)

For compounds with very long acyl chains, the end contribution from terminal methyl and the polar head group can be neglected compared to the polymethylene chain portion towards ΔH_t and ΔS_t. Thus, at infinite acyl chain length, Eqs. (4.3) and (4.4) can be reduced to Eqs. (4.5) and (4.6), respectively:

$$\Delta H_t = (n\text{-}2)\, \Delta H_{inc} \qquad (4.5)$$

$$\Delta S_t = (n\text{-}2)\, \Delta S_{inc} \qquad (4.6)$$

Then the T_t for infinite chain length, T_t^{∞}, can be obtained from Eq. 4.7:

$$T_t^{\infty} = \Delta H_{inc}/\Delta S_{inc} \qquad (4.7)$$

T_t^{∞} values for the NAAOHs have been estimated from the ΔH_{inc} and ΔS_{inc} values presented in Table 4.2. The obtained T_t^{∞} for odd- and even chain length DAAOHs are 101.2 °C (374.2 K) and 113.7 °C (386.7 K), respectively, whereas the T_t^{∞} values obtained for the second heating scans is 116.4 °C (389.4 K).

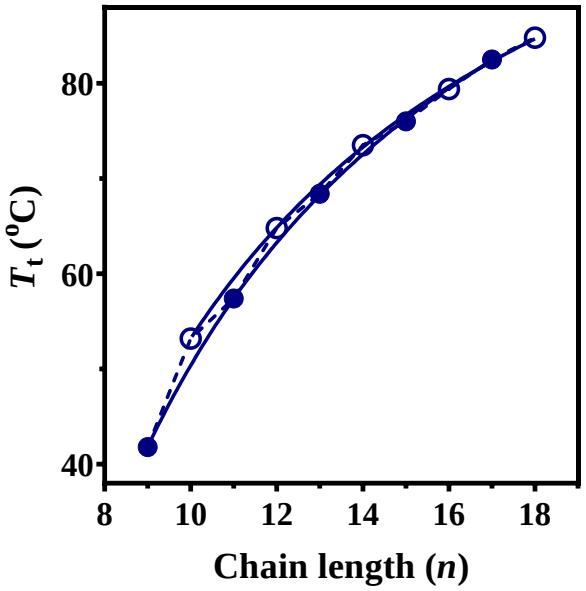

Fig. 4.11. Chain length dependence of solid-liquid phase transition temperatures (T_t) of DAAOHs. Dotted lines correspond to a nonlinear least-squares fit of the transition temperatures to Eq. 4.8. Filled symbols, odd chain length compounds; open symbols, even chain length compounds.

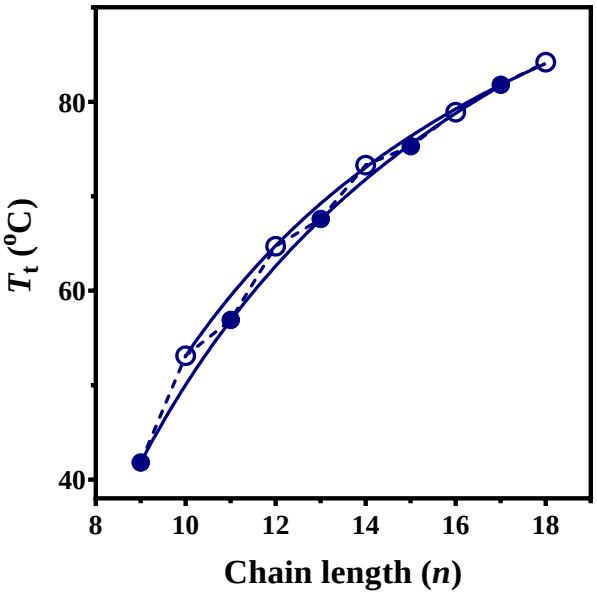

Fig. 4.12. Chain length dependence of chain-melting phase transition temperatures (second heating) of DAAOHs. Closed circles (●), odd chainlength compounds; (○), even chainlength compounds. Solid lines correspond to nonlinear least-squares fit of the transition temperatures to Eq. 4.8.

For many single- and double chain amphiphiles, which show a linear dependence of ΔH_{inc} and ΔS_{inc} on the chain-length, it has been shown that the ΔH_t and ΔS_t values can be fit to the following equation (Marsh, 1982):

$$T_t^{\infty} = \Delta H_t/\Delta S_t = T_t\,[1- (n_o–n'_o)/(n–n_o)] \qquad (4.8)$$

where n_o (= $-\Delta H_o/\Delta H_{inc}$) and n'_o (= $-\Delta S_o/\Delta S_{inc}$) are the values of n at which the ΔH_t and ΔS_t are extrapolated to zero. Fig. 4.11 indicates that the first heating T_t values of both odd- and even chain length DAAOHs fit well to Eq. (4.8). The T_t^{∞} values obtained for odd- and even chain DAAOHs are 128.9 °C (401.9 K) and 126 °C (399 K), respectively. Similarly, the T_t^{∞} values obtained for odd- and even-chain DAAOHs from second heating T_t values are 130.6 ºC (403.6 K) and 122.2 ºC (395.2 K), respectively. The T_t^{∞} values obtained for both first and second heating scans of DAAOHs from fitting to Eq. (4.8) are in good agreement with the T_t^{∞} values estimated using Eq. (4.7).

4.4.5. Comparison of thermodynamic properties of DAAOHs with other diacyl compounds

It is instructive to compare the thermodynamic parameters associated with the phase transitions of DAAOHs with isomeric NAAEs, as well as with those of homologous DAEs and their isomers, namely the NAGEs. The ΔH_t values of isomeric pair DAAOHs and NAAEs are shown in Fig. 4.13A, and those of the other isomeric pair, namely NAGEs and DAEs are given in Fig. 4.13B. As can be seen from this figure, ΔH_t values of DAAOHs and DAEs are low as compared to the isomeric NAAEs and NAGEs, respectively (although minor differences are observed in even chain length DAEs at higher chain length). This indicates that the functional group position plays a key role in the phase transition properties between the isomeric compounds. The ΔH_t values show clear distinction among the four series at lower chain length. However, the distinction is reduced at higher chain length due to partial overlap. This complex nature can be understood by comparing their incremental values (ΔH_{inc}) and end contributions (ΔH_o) given in Table 4.3. If the partial overlap at higher chain lengths is ignored, the ΔH_t values of four series follows the order: NAGEs > $DAEs_{even}$ = $NAAEs_{odd}$ > $NAAEs_{even}$ > $DAAOHs_{odd}$ > $DAEs_{odd}$ > $DAAOHs_{even}$.

Similarly, comparison of T_t values of the four series is shown in Fig. 4.14. Chain length dependence of T_t values of isomeric NAAEs and DAAOHs is shown in Fig. 4.14A, whereas the corresponding plots of NAGEs and DAEs are given in Fig. 4.14B. Similar to the transition enthalpies, the transition temperatures of NAGEs and NAAEs are higher compared to isomeric DAEs and DAAOHs. The difference in T_t values is more distinct at all chain lengths between NAGEs and DAEs, but less so between NAAEs and

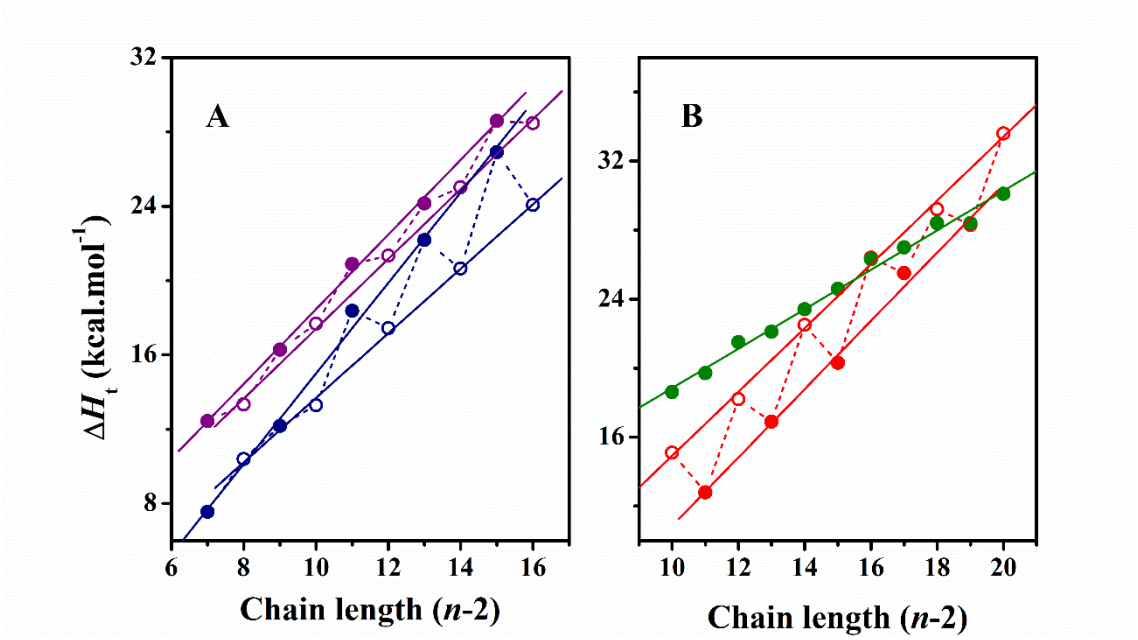

Fig. 4.13. Chain length dependence of transition enthalpies. (**A**) NAAEs (●) and DAAOHs (●). (**B**) NAGEs (●) and DAEs (●). Filled circles, odd chain length compounds; open circles, even chain length compounds. Values of ΔH_t were plotted against the number of CH_2 groups in the acyl chains (*n*-2). Solid lines correspond to linear least-squares fits of the data. For more details, see the text.

DAAOHs. The T_t values of four series will follow the following order: NAGEs > $DAEs_{even}$ > $DAEs_{odd}$ > $NAAEs_{odd}$ > $DAAOHs_{even}$ = $NAAEs_{even}$ = $DAAOHs_{odd}$. The noticed differences could be due to the differential contributions arising from polyethylene chains and end contributions. The T_t^{∞} calculated from Equations 4.7 and 4.8 are given in Table 4.3. Although the T_t^{∞} obtained show good agreement with the order mentioned above, few limitations are observed in $DAEs_{odd}$ (Eq. 4.7) and $DAAOHs_{odd}$ (Eq. 4.8). These exceptions can be rationalized in terms of molecular packing and

intermolecular interactions if crystal structures of several compounds (of both odd and even chain lengths) are determined from each series.

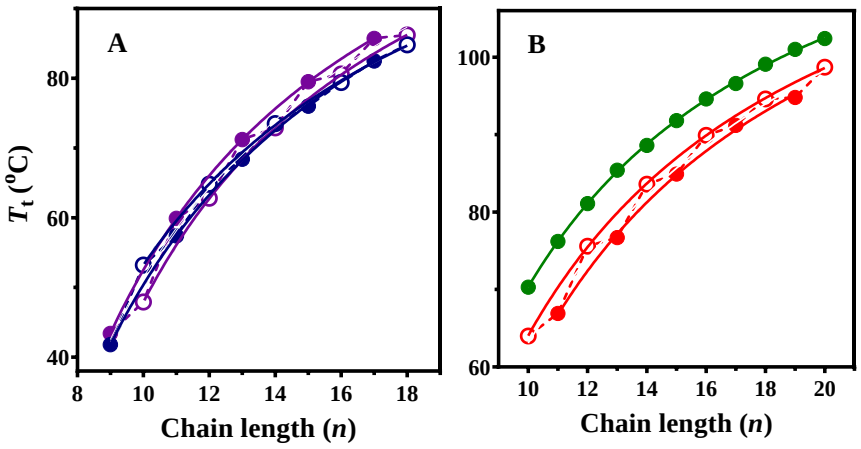

Fig. 4.14. Chain length dependence of transition temperatures, (T_t) of different two-chain amphiphiles. (**A**) NAAEs (●) and DAAOHs (●). (**B**) NAGEs (●) and DAEs (●). Filled symbols, odd chain length compounds; open symbols, even chain length compounds. Solid lines correspond to nonlinear least-squares fits of the data. For more details, see the text.

Further, odd-even alternation in ΔH_t (as well as ΔS_t and T_t) of homologous series of single and double chain lipids was explained by differences in the packing of terminal methyl groups of odd- and even chain length compounds (Larsson, 1986). If the hydrocarbon chains are aligned perpendicular to the plane of the terminal methyl groups, such alteration is not observed. On the other hand, if the acyl/alkyl chains are tilted with respect to the plane of the terminal methyl groups, the packing is different for the odd- and even-chain compounds and thus leads to changes in the physical properties. This can be seen in Table 4.3, where end contribution (ΔH_o) is much different for the four series. Although incremental values of NAGEs are low as compare to isomeric DAEs, due to the significant contribution of terminal methyl groups and the central polar moiety of NAGEs (0-1° tilt angle-untilted bilayer packing), NAGEs have shown higher ΔH_t than isomeric DAEs (32-33° tilt angle-tilted bilayer packing) (Reddy and Swamy, 2017; Kamlekar et al., 2010). Similarly, though incremental values of NAAEs and DAAOHs are

comparable, due to smaller end contributions in DAAOHs, NAAEs have higher ΔH_t than isomeric DAAOHs.

Table 4.3. Incremental values of transition enthalpies (ΔH_{inc}), end contribution (ΔH_o), and transition temperature at infinite chain length (T_t^{∞}) for NAGEs, DAEs, NAAEs, and DAAOHs.

Lipid	**ΔH_{inc} (kcal/mol)**	**ΔH_o (kcal/mol)**	**T_t^{∞} (K)**		**Reference**
			Eq. 6	**Eq. 7**	
NAGEs	1.19 (0.03)	10.16 (0.38)	442.4	409.8	(Reddy et al., 2017)
DAEs (even chain length)	1.84 (0.04)	0.13 (0.66)	402.6	407.2	(Kamlekar et al., 2010)
DAEs (odd chain length)	1.98 (0.09)	−4.98 (1.19)	396.0	407.2	(Kamlekar et al., 2010)
NAAEs (odd chain length)	2.01 (0.05)	−1.64 (0.59)	400.4	404.8	(Sivaramakrishna et al., 2015)
NAAEs (even chain length)	1.88 (0.05)	−1.39 (0.57)	406.9	402	(Sivaramakrishna et al., 2015)
DAAOHs (odd chain length)	2.44 (0.09)	-9.36 (1.11)	374.2	401.9	Present study
DAAOHs (even chain length)	1.74 (0.05)	-3.66 (0.59)	386.7	399	Present study

4.4.6. PXRD and molecular packing

Since we could not obtain crystals of DAAOHs that are suitable for single-crystal X-ray diffraction studies, we carried out PXRD studies to derive structural information on these compuounds. The PXRD data obtained for odd- and even-chain DAAOHs are shown in Figs. 4.15A and B, except for the C9 compounds. All the other DAAOHs (C10−C18) gave several sharp diffraction peaks in the 2θ range of 1−30°. From the diffraction peak positions, the average *d*-spacings were calculated using 3−4 peaks of each DAAOH. The average *d*-spacings obtained are given in Table 4.4, and the chain length dependence of the *d*-spacing is shown in Fig. 4.15C. The *d*-spacing data exhibit a linear dependence on the chain length, independently for the even- and odd acyl chain length series with slopes of 0.82 and 0.79Å/CH_2, respectively. The C11 compound which is an outlier was omitted from the fit of the odd chain length series. Since the estimated increment in the *d*-spacing for each C−C bond in an untilted chain is 1.27 Å/CH_2, the smaller incremental values

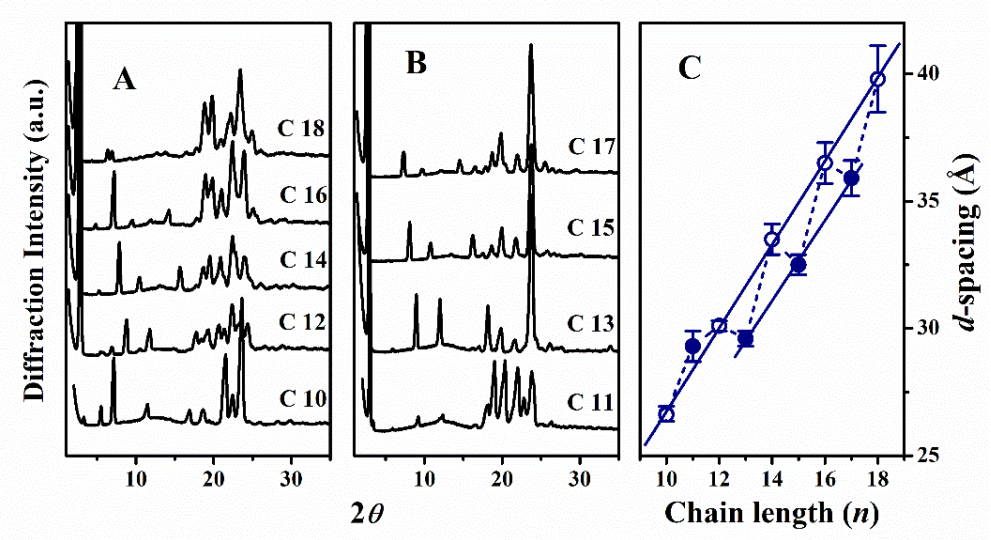

Fig. 4.15. Powder X-ray diffraction patterns of DAAOHs with different saturated acyl chains (**A**, **B**) and dependence of *d*-spacings on the chain length (**C**). The number of C-atoms in the acyl chain is indicated against each PXRD profile. Filled symbols, odd chain length compounds; open symbols, even chain length compounds. The solid line in C represents a linear least-squares fit of the data. Data corresponding to C11 compound was omitted from the linear fit as it seems to be an outlier.

Table 4.4. Average *d*-spacings of DAAOHs determined from PXRD data. Values in parentheses correspond to standard deviations estimated from the analysis of 4-5 reflections.

Acyl chain length	***d*-spacing (Å)**
10	26.6 (0.3)
11	29.3 (1.1)
12	30.1 (0.2)
13	29.6 (0.3)
14	33.5 (0.6)
15	32.5 (0.4)
16	36.5 (0.8)
17	35.9 (0.7)
18	39.8 (1.3)

obtained for DAAOHs suggest that the acyl chains are tilted with respect to the bilayer normal. The value of 0.82 Å for an increase in *d*-spacing per CH_2 for DAAOH is lower than the value of 0.88 Å/CH_2 obtained for the isomeric NAAEs (Sivaramakrishna and Swamy, 2015b), and suggests that the acyl chains in DAAOHs are more tilted as compared to the chains in NAAEs. While NAGEs are packed in a normal, untilted bilayer format with the *d*-spacing increment of 1.28 Å/CH_2 (Reddy and Swamy, 2017), the isomeric DAEs are packed in a tilted bilayer (Kamlekar et al., 2010). Similar to DAAOHs, DAEs, and NAAEs, dimyristoylphosphatidylglycerol (DMPG) and cerebroside also have tilted bilayer packing (Pascher et al., 1987; 1977).

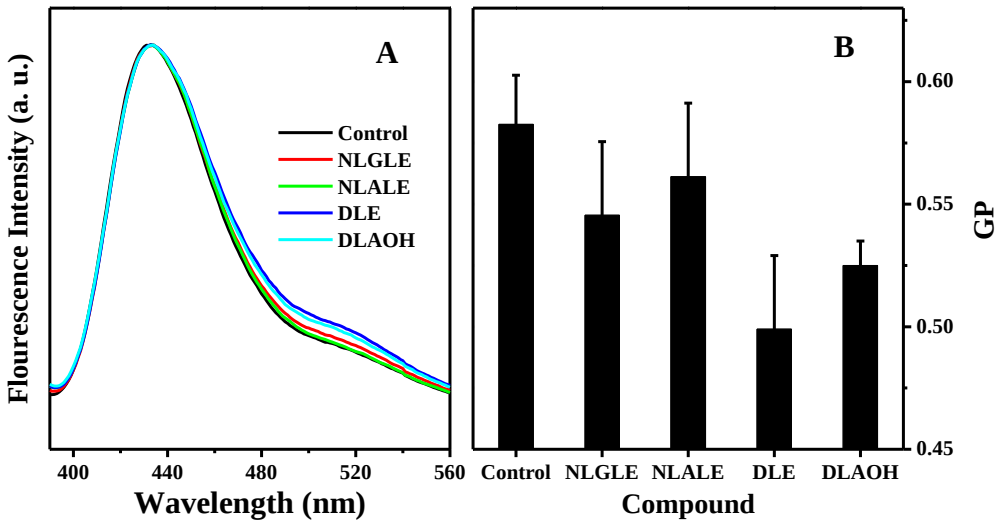

Fig. 4.16. (**A**) Emission spectra of Laurdan in stratum corneum model (SCM) lipid mixture and SCM lipid mixture containing 20 mol% NLGLE, NLALE, DLE, or DLAOH. (**B**) Comparison of Laurdan GP values for the different samples. See text for details.

4.4.7. Laurdan GP studies on stratum corneum model membranes

To monitor the change in fluidity, we determined the generalized polarization (GP) of the fluorescent probe laurdan for SCM lipid mixture and SCM lipid mixtures to which 20 mol% of DLAOH or DLE or NLALE, or NLGLE was added, which results in 16.7% mol% of the added lipid while the relative proportion of the SCM lipids remains constant. Laurdan is a phase-sensitive dye and shows distinct emission maxima in the gel phase (430-440 nm) and fluid phase (>470 nm) (Parasassi et al., 1998). Decrease in GP indicates fluidity change, which correlates with the permeability of the membrane. In the present

case, SCM and SCM containing DLAOH, DLE, NLALE, or NLGLE have shown emission maximum at 433 nm (Fig. 4.16A). Addition of any of these to the SCM lipid mixture, we noticed a small to moderate decrease in emission maximum at ~473 nm in both cases. Values of laurdan GP calculated from the fluorescence spectral data using Eq. 4.1 are shown in Fig. 4.16B. The results presented in Figs 4.16A and 4.16B reveal that the SCM fluidity is lower for membranes containing DLE and DLAOH compared to isomeric NLGLE and NLALE, respectively. Although, as discussed above, the general trends in the physical properties of these four classes of compounds are broadly similar, the present results on their interaction with stratum corneum model membranes suggest that they may exhibit important differences in their specific interaction with other membrane lipids, which in turn modulate the membrane fluidity. Importantly, these results also indicate that membranes containing *N*, *O*-diacylethanolamines (DAEs) and *N*, *O*-diacyl-L-alaninols (DAAOHs) exhibit a higher potential as chemical enhancers for increasing the permeability of SC membranes.

Chapter 5

Structure and supramolecular organization of *N*-acylserinols: agonists of the G-Protein Coupled Receptor, GPR-119

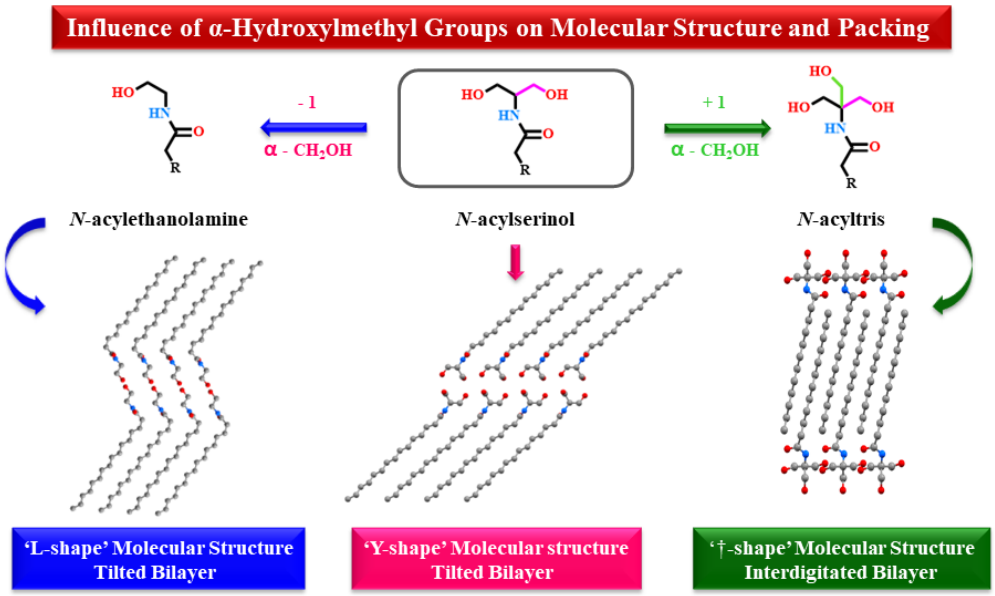

The work presented in this chapter was published in ***J. Chem. Sci.*** (2023) 135, 1-9

5.1.Summary

N-acyl serinols, the amphiphilic molecules produced by gastrointestinal bacteria regulate metabolic hormone production and glucose homeostasis in the host species, and also exhibit anti-cancer activity. In this study, molecular structure, supramolecular organization and intermolecular interactions of two *N*-acylserinols (NASOHs), viz., *N*-nonanoylserinol (N9SOH) and *N*-pentadecanoylserinol (N15SOH), are determined by single-crystal X-ray diffraction. The molecular structure and packing are compared and discussed with the structurally related molecules, *N*-acylethanolamine (NAE) and *N*-acyl tris (NAT) as NASOHs and NATs are derived by substituting one/two α-hydrogen(s) (with respect to amide N-H) of NAE with hydroxymethyl group(s). Structures of N9SOH and N15SOH were solved in the triclinic system in the *P-1* space group and both molecules are organized in a tilted head-to-head (and tail-to-tail) manner, resembling a bilayer membrane. The acyl chains in N9SOH and N15SOH are tilted by 20.43º and 18.12º, respectively, with respect to the bilayer normal. Several N─H···O, O─H···O, and C─H···O hydrogen bonds between the hydroxyl and amide moieties of the head groups of NASOH molecules belonging to adjacent and opposite layers stabilize the overall supramolecular organization. These results suggest that the α-hydroxymethyl groups exhibit considerable influence on the crystal structure, molecular packing, and phase structure of these amphiphiles.

5.2. Introduction

Mammals have co-evolved along with diverse microbial species that colonize cutaneous and mucosal surfaces of gastrointestinal tract, which are supported by diet (Ley et al., 2008a; 2008b). Many (patho)physiological processes of the mammalian hosts are profoundly affected by the gut microbiota, such as mucosal immunity, vitamin biosynthesis, inflammatory bowel disease and colorectal cancer (Bäckhed et al., 2005; Packey et al., 2008; O'Keefe 2008; Peterson et al., 2008; Neish, 2009). Recently, the expression of *N*-acyl amide synthase genes has been reported in gastrointestinal bacteria, and the lipids encoded by these genes interact with G protein-coupled receptors (GPCRs) that regulate the physiology of the gastrointestinal tract (Bäckhed et al., 2010). *N*-acylserinols are one of the six *N*-acyl amide families isolated from gastrointestinal bacteria (Cohen et al., 2017; Milshteyn et al., 2018).

In an interesting study, Brady and co-workers discovered that bacterial lipid products can modulate the activity of host GPCRs: for instance, *N*-oleoyl serinol is a GPR119 agonist able to modulate glucagon-like peptide 1 (GLP1) secretion and glucose homeostasis (Cohen et al., 2017). They also identified several *N*-acyl synthase (NAS) genes and cloned and expressed them in *E. coli*. *N*-oleoyl serinol derived from bacteria such as *Gemella spp*. was shown to activate GPR119 with similar potency to the endogenous ligand, oleoylethanolamide. In this direction, Hu and co-workers identified a new bacterial NAS that could effectively synthesize *N*-acylserinols, which exhibit GPR119 agonist activity in the bacterium *E. coli* Nissle1917 (Jia et al., 2021). GPR119 is an attractive therapeutic target for diabetes and obesity because this receptor affects, among others, glucose homeostasis through the release of GLP1.

In recent times, synthetic single-tailed amphiphiles have gained importance due to their ability to form various supramolecular assemblies, including vesicles with high application potential in various fields (Kunitake, 1992; Petkau-Milroy and Brunsveld, 2013; Gong et al., 2022). The bilayer thickness or mode of packing in these assemblies can be affected by both the head and tail groups of amphiphiles and modulated by various additives. Researchers have observed differences in bilayer thickness for amphiphiles, which differ in the head group structure but have identical hydrocarbon chains. Similarly, changes in the head group may affect the molecular packing by modulating the chain tilt

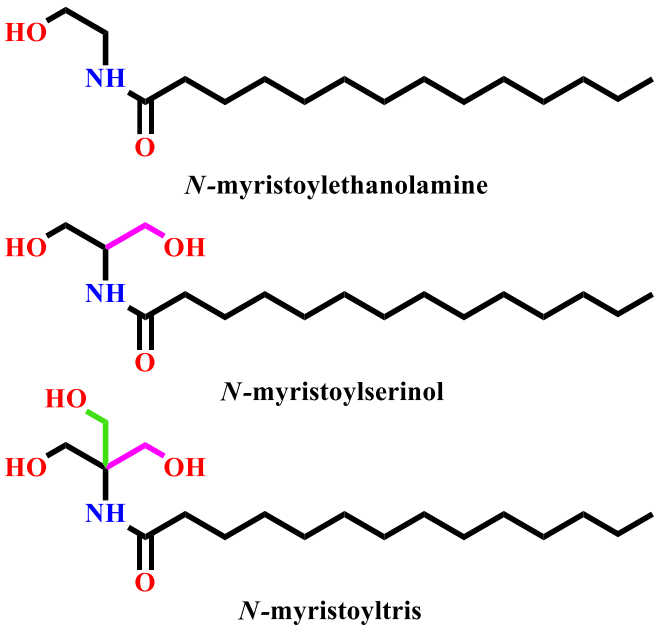

Figure 5.1. Structures of *N*-myristoylethanolamine, *N*-myristoylserinol and *N*-myristoyltris.

and/or adopting interdigitated chain packing (Sivaramakrishna et al., 2015a, 2015b, 2016a, 2016b, 2018, 2019, 2021a, 2021b; Reddy et al., 2014, 2015, 2017, 2021; Tarafdar et al., 2010, 2013; Kamlekar et al., 2010; Swamy et al., 2010). In this study, we discuss the structural analysis of two *N*-acylserinols (with 9 and 15 C-atoms in the acyl chain) and compare the results with those obtained with *N*-acylethanolamines (Ramakrishnan and Swamy, 1999) and *N*-acyltris (Sivaramakrishna et al., 2018) with the objective of understanding the influence of α-hydroxymethyl groups on the molecular structure and supramolecular organization (Fig. 5.1). Previous work on the preparation and characterization of niosomes containing NASOHs suggests that these compounds could be useful in developing nanocarriers for the delivery of drugs and therapeutics (Sivaramakrishna et al., 2019). In view of this, the precise structure of NASOHs at the atomic level will be helpful for a better understanding of the physicochemical properties and molecular assembly of these bioactive amphiphiles with potential applications.

5.3.Materials and methods

5.3.1. Materials

Serinol and long-chain fatty acids (n = 9, 15), were purchased from Sigma-Aldrich (St. Louis, MO, USA). Oxalyl chloride was purchased from Merck (Mumbai, India). Solvents and other reagents were obtained from Sisco Research Laboratories (Mumbai, India) and were of the highest purity.

5.3.2. Synthesis of N-acylserinols

N-nonanoylserinol (N9SOH) and *N*-pentadecanoylserinol (N15SOH) were prepared as reported in our previous study (Sivaramakrishna et al., 2019). Briefly, the fatty acids were converted to corresponding acid halides by reacting with oxalyl chloride. Then, the acid chloride was added to the solution containing serinol (1.1 mmol) and triethylamine (1.1 mmol) in a mixture of methanol:dichloromethane (1:3 v/v) at 0 °C and the reaction mixture was stirred continuously for 3 h. The solvent was removed by rotary evaporation under reduced pressure, and the final product was obtained by recrystallization followed by column chromatography. The purified products were characterized by various spectroscopic techniques (FT-IR, ^{1}H and ^{13}C-NMR) as well as by high-resolution mass spectrometry, and the results were consistent with those reported in our previous study (Sivaramakrishna et al., 2019).

5.3.3. Crystallization

Thin plate-type, colorless single crystals of N9SOH and N15SOH were grown at room temperature from dichloromethane containing a trace of methanol. X-ray diffraction data was collected at liquid nitrogen temperature (~112 K) for N9SOH and at room temperature (~293 K) for N15SOH on an Xtlab Synergy Rigaku Oxford diffraction system equipped with a HyPix – 3000 CCD plate detector. Mo-Kα radiation (λ = 0.7107 Å) was used, and the diffraction data were collected in the 2θ range of 2-27° for both samples.

5.3.4. Structure solution and refinement

The X-ray diffraction data of N9SOH and N15SOH were processed using CrysAlisPro Version 171.39, XtLAB Synergy Rigaku Oxford Diffraction, and absorption correction

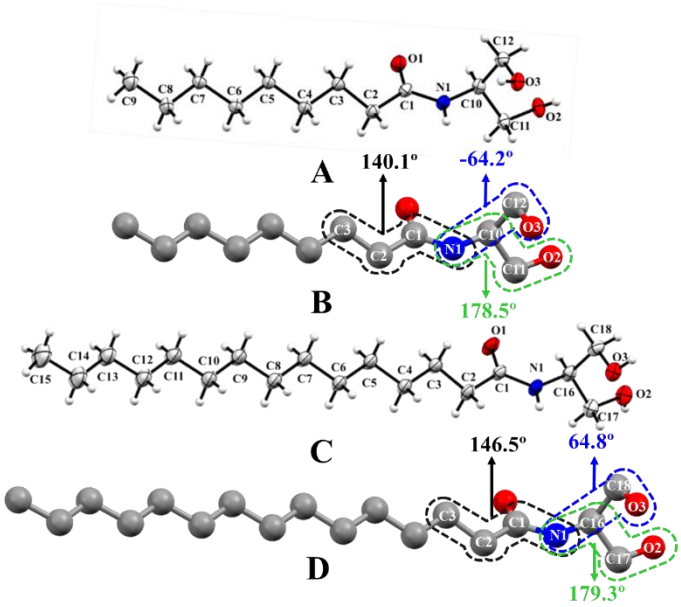

Fig. 5.2. ORTEP diagrams showing the structures of N9SOH (**A**) and N15SOH (**B**).

was done based on the multiscan method. The crystal structures were solved and refined using the Olex21.3/1.2 program. Both structures were solved in the triclinic crystal system with the *P-1* space group. For N9SOH the refinement was carried out using 3006 observed [>2σ (F0)] reflections, which converged into final R_1 = 5.19, wR_2 = 16.51 and goodness of fit = 1.018. For N15SOH the refinement was carried out using 3465 observed [>2σ (F0)] reflections, which converged into final R_1 = 9.63, wR_2 = 33.49 and goodness of fit = 0.973. The corresponding CIF files (deposition numbers 2243212 and 2243213) have been deposited in the Cambridge Crystallographic Data Centre (CCDC).

5.4. Result and discussion

Given the interesting biological properties of *N*-acylserinols and their potential in developing lipid-based drug delivery systems such as niosomes, as mentioned in the Introduction, we have taken up biophysical and structural investigations on these amphiphiles. In this direction, in a previous study, we reported on the thermotropic phase behaviour of a homologous series of *N*-acylserinols and the preparation and characterization of niosomes containing these non-ionic lipids (Sivaramakrishna et al., 2019). In this study, we report the crystal structures of two *N*-acylserinols, namely N9SOH and N15SOH, and the molecular packing and intermolecular interactions in the solid state.

5.4.1. Description of the structure

Molecular structures of N9SOH and N15SOH, determined by single-crystal X-ray diffraction, are shown in the ORTEPs given in Fig. 5.2A and 5.2C, respectively, along with the atom numbering for all non-hydrogen atoms. Crystal parameters for these two compounds are given in Table 5.1. The corresponding atomic coordinates, equivalent isotropic displacements, bond lengths, bond angles, and torsion angles are given in Tables S1-S3 (N9SOH) and S4-S6 (N15SOH).

Table 5.1. Crystallographic data for N9SOH and N15SOH.

Crystal parameter	**N9SOH**	**N15SOH**
Formula	$C_{12}H_{25}NO_3$	$C_{18}H_{37}NO_3$
Formula wt.	231.33	315.49
Crystal system	triclinic	triclinic
T, K	112 (18)	300 (3)
Space group	P-1	P-1
a (Å)	4.8800 (1)	4.8994 (3)
b (Å)	5.9777 (1)	5.9650 (6)
c (Å)	24.1131 (7)	35.1240 (3)
α	88.925 (2)	88.322 (7)
β	86.003 (2)	89.359 (5)
γ	72.207 (2)	72.914 (7)
Z	2	2
V ($Å^3$)	668.13 (3)	980.77 (14)
D_{calc} (g cm^{-3})	1.150	1.065
μ (mm^{-1})	0.081	0.071
F(000)	256	352
Total Reflections	3006	3465
Used Reflections	2161	1460
Parameters	148	202
GOF	1.018	0.973
R indices	R1 = 7.69	R1= 18.04
(all data)	wR2 = 18.52	wR2 = 33.49
Final *R* indices	R1 = 5.19	R1 = 9.63
	wR2 = 16.51	wR2 = 33.49

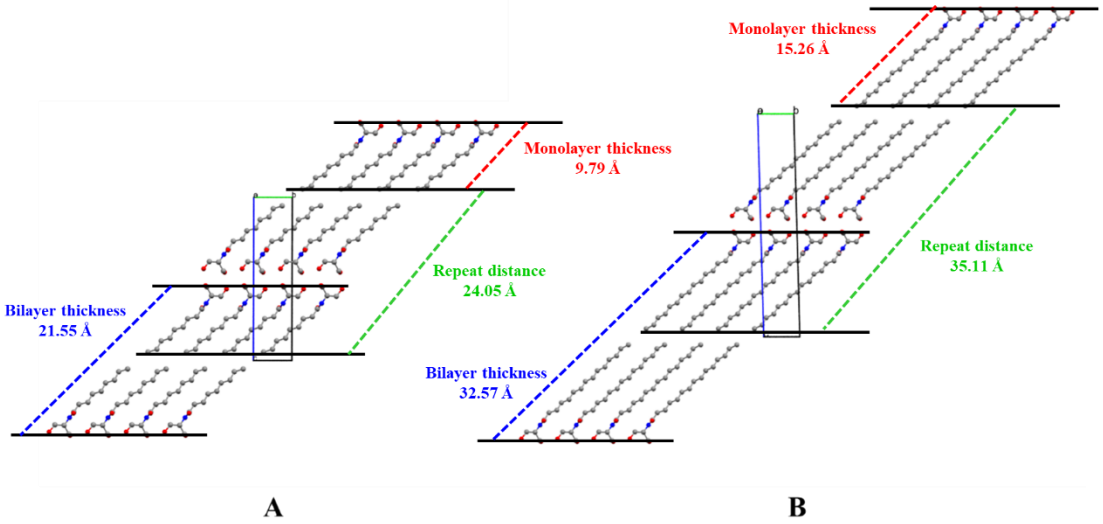

Fig. 5.3. Molecular packing diagrams of N9SOH (**A**) and N15SOH (**B**) viewed along the *a*-axis.

These data show that the hydrocarbon portions of the acyl chains of both N9SOH (C2-C9) and N15SOH (C2-C15) are in *all-trans* conformation (Fig. 5.2A and 5.2C), with all the torsion angles being ~180°. The torsion angles corresponding to the N1-C1-C2-C3 unit in N9SOH and N15SOH are 140.1° and 146.5° (see Figs. 5.2B and D), respectively. The amide N–H and carbonyl groups are also in trans geometry. The molecular structures of N9SOH and N15SOH are very similar to each other. In the structure of N9SOH, the torsion angles of C1-N1-C10-C11 and C1-N1-C10-C12 linkage are 128.8^{o} and 107^{o}, respectively, and the torsion angles for N1-C10-C11-O2 and N1-C10-C12-O3 units are 178.5^{o} and -64.2^{o} (see Fig. 5.2B), respectively. Similarly, torsion angles for C1-N1-C16-C17 and C1-N1-C16-C18 linkage in N15SOH are -131^{o} and 104.6^{o}, respectively, and for N1-C16-C17-O2 and N1-C16-C18-O3 units are 179.3^{o} and 64.8^{o} (see Fig. 5.2D), respectively. This suggests that the additional hydroxymethyl groups of N9SOH (C12-O3) and N15SOH (C18-O3) adopt a particular conformation, resulting in a "Y-like" shape by the NASOHs, whereas NAEs (which do not have any α-hydroxymethyl moiety) adopt an "L-shaped" structure, and NATs (which have two α-hydroxymethyl moieties) have a "dagger (†) shaped" structure (Ramakrishnan and Swamy, 1999; Sivaramakrishna et al., 2018).

5.4.2. Molecular packing

Packing diagrams of N9SOH and N15SOH, viewed along the *a*-axis are shown in Fig. 5.3A and 5.3B, respectively, and those viewed along the *c*-axis are given in Fig. 5.4A and 5.4B, respectively. Corresponding diagrams viewed along the *b*-axis, are given in Fig. 5.5A and 5.5B. These diagrams show that N9SOH and N15SOH are packed in a head-to-head (and tail-to-tail) format in stacked bilayers, with each unit cell containing two molecules. Several O-H····O and C-H····O hydrogen bonds that connect adjacent bilayers, as well as and N-H····O, O-H····O and C-H····O hydrogen bonds between adjacent molecules stabilize the molecular packing (see Fig. 5.8 and Figure 5.9; discussed in detail in Section 5.4.4). The methyl ends of stacked bilayers are in van der Waals' contacts, with the closest methyl − methyl distance between opposite layers being 3.915 and 3.786 Å in the crystal lattices of N9SOH and N15SOH, respectively. The van der Waals' distances between the methyl groups in the same leaflet are 4.880 and 4.899 Å for N9SOH and N15SOH, respectively. The bilayer thickness in the crystal lattices of N9SOH and N15SOH are 21.55 Å and 32.57 Å, respectively, and the monolayer (single leaflet) thickness for N9SOH is 9.79 Å, and for N15SOH it is 15.26 Å. The repeat distance (*d*-spacing) is 24.05 Å and 35.11 Å for N9SOH and N15SOH, respectively (Fig. 5.3). The *N*-acyl chains are tilted by 20.43° in N9SOH and 18.13° in N15SOH with respect to the bilayer normal (Fig. 5.6). The *N*-acyl/*O*-acyl chains of several other single-chain amphiphiles such as *N*-acyl-β-alanines, *N*-acyl-β-alaninols, and *O*-stearoylethanolamine were also found to be tilted with respect to the bilayer normal (Sivaramakrishna et al., 2016b, 2021a; Tarafdar et al., 2010). Interestingly, in the crystal structures of *N*-myristoylglycine and *N*-palmitoylglycine, the acyl chains were found to be essentially parallel to the bilayer normal with tilt angles <1°, which was attributed to the very small head group size in *N*-acylglycines (Reddy et al., 2014).

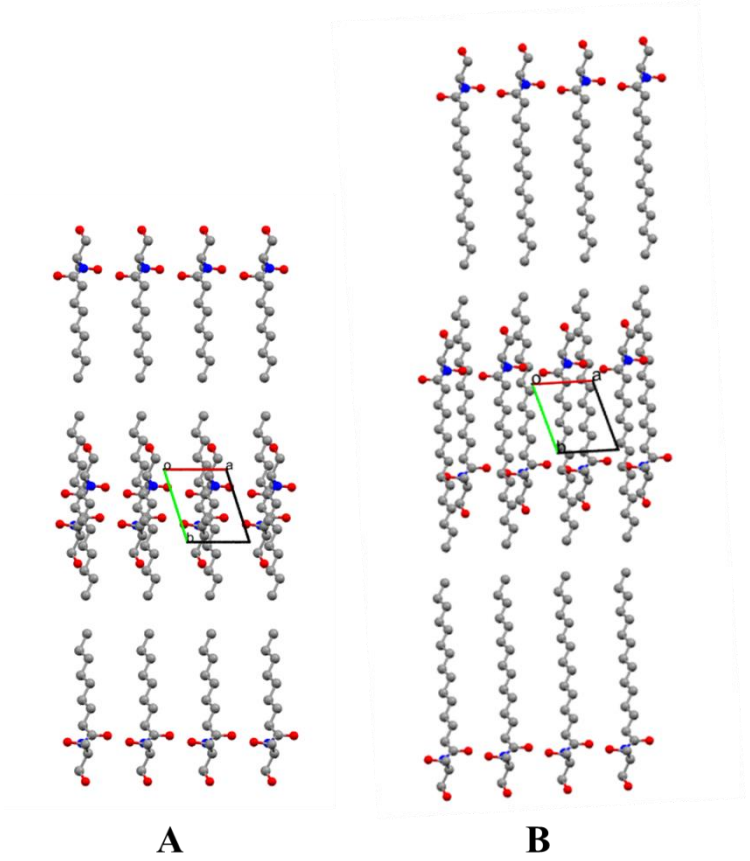

Fig. 5.4. Molecular packing of N9SOH (**A**) and N15SOH (**B**) along *c*-axis.

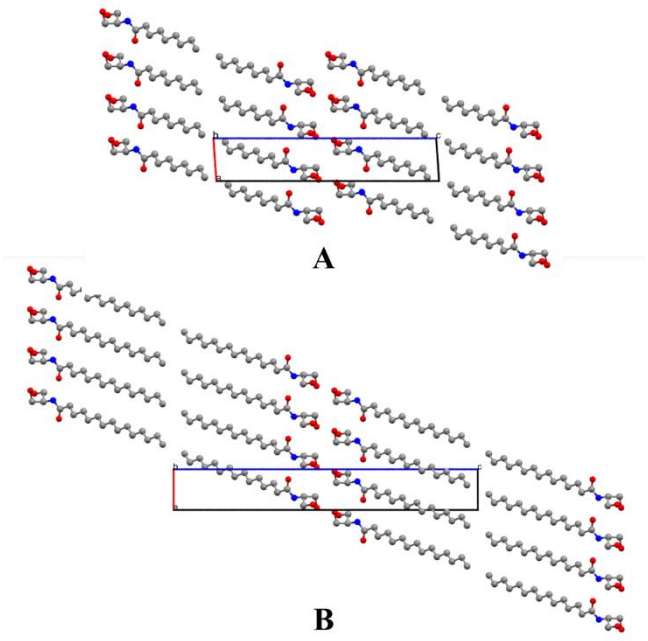

Fig. 5.5. Molecular packing diagrams of N9SOH (**A**) and N15SOH (**B**) along *b*-axis.

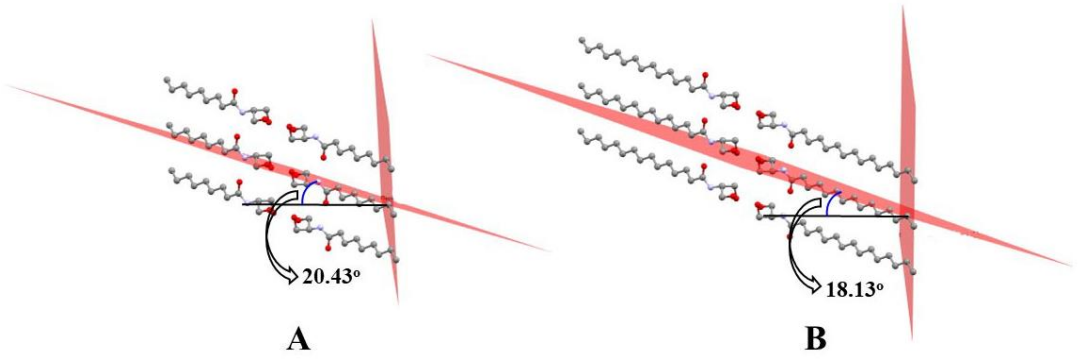

Fig. 5.6. Diagram showing the tilt angle of the acyl chain with respect to the bilayer normal in (**A**) N9SOH and (**B**) N15SOH.

5.4.3. Subcell structure and area per molecule

Hydrocarbon chains in lipid crystals adopt different lateral packing modes, generally described in subcells that specify the relations between equivalent positions within the chain and its neighbors. Based on symmetry considerations, the modes of chain packing have been classified into a small number of subcells: triclinic, monoclinic, orthorhombic, and hexagonal. Within each of these categories the polymethylene planes of the chains can be mutually parallel or perpendicular with respect to their neighbors (Abrahamsson et al., 1978; Maulik et al., 1990). Careful examination of the acyl chain packing in N9SOH and N15SOH revealed that the subcells in the crystals of both these compounds are of the classic triclinic parallel ($T_{//}$) type (Fig. 5.7). The unit cell dimensions of these subcells are given in Table 5.2.

Table 5.2. Subcell dimensions of N9SOH and N15SOH.

Cell parameter	N9SOH	N15SOH
a (Å)	6.46	6.51
b (Å)	5.98	5.96
c (Å)	2.54	2.53

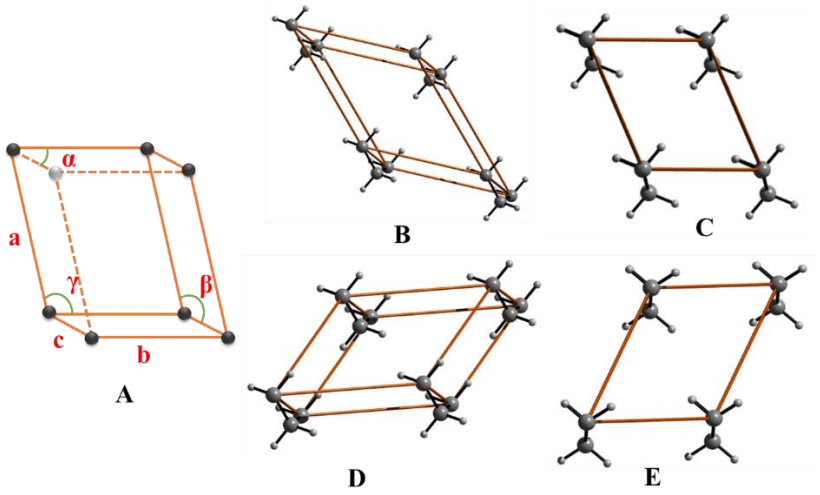

Fig. 5.7. (A) General representation of triclinic unit cell. Subcell packing of (**B, C**) N9SOH and (**D, E**) N15SOH. Both subcells belong to the classic triclinic parallel (T//) type.

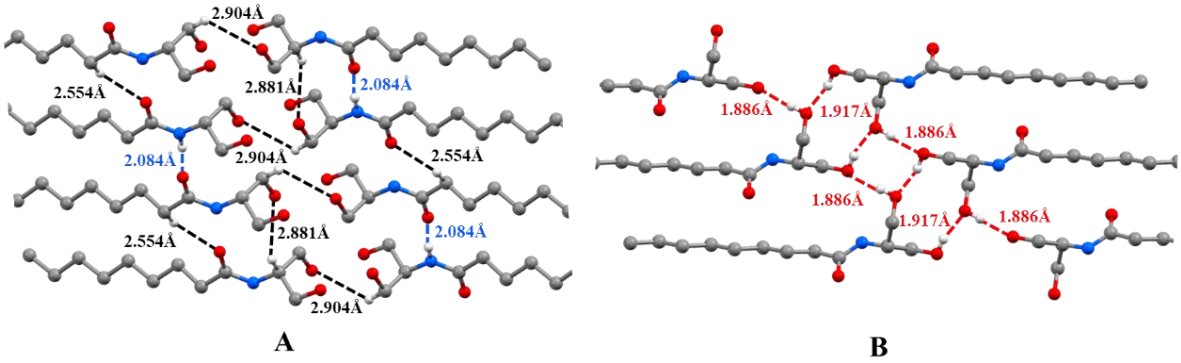

Fig. 5.8. Hydrogen bonding pattern in the crystal lattice of N9SOH. (**A**) N-H···O (----) and C-H···O (----) hydrogen bonds; (**B**) O-H···O (----) hydrogen bonds. In **A**, only alternate N-H···O and C-H···O hydrogen bonds are shown for the sake of clarity. Color code for atoms: gray, carbon; red, oxygen; blue, nitrogen. Hydrogen atoms not involved in H-bonds have been omitted for clarity.

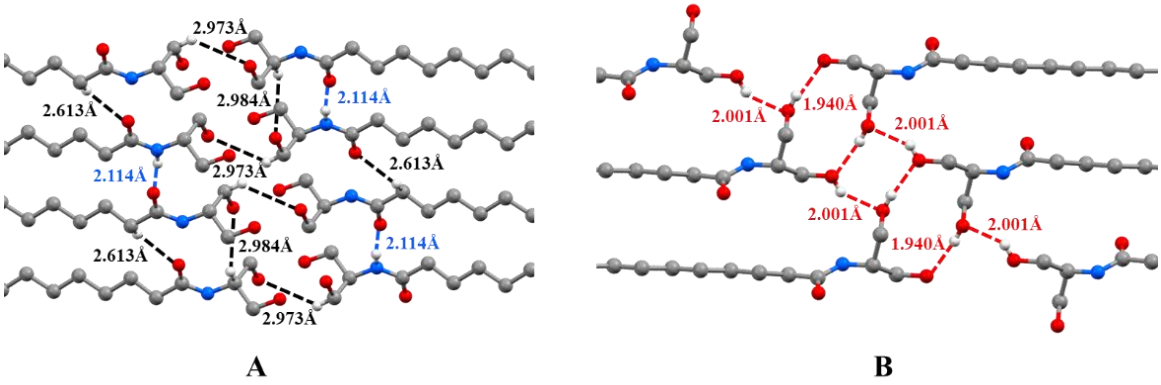

Fig. 5.9. Hydrogen bonding pattern in the crystal lattice of N15SOH. (**A**) N-H···O (----) and C-H···O (----) hydrogen bonds; (**B**) O-H···O (----) hydrogen bonds. Color code for atoms: gray, carbon; red, oxygen; blue, nitrogen. Hydrogen atoms not involved in H-bonds have been omitted for clarity.

5.4.4. Hydrogen bonding and intermolecular interaction

Molecular packing in the crystal structure of N9SOH and N15SOH was carefully examined to understand the intermolecular interactions, which revealed the presence of three types of hydrogen bonds: N-H···O, O-H···O and C-H···O. The H-bonds in N9SOH and N15SOH are shown in Fig. 5.8 and Fig. 5.9, respectively, and the bond distances and angles are listed in Table 5.3.

The H···O distance in the N-H···O bonds and the bond angles subtended at the hydrogen atom for N9SOH and N15SOH are 2.084 Å and 2.114 Å, and 169.9º and 171.1º, respectively. The distance between donor nitrogen and acceptor oxygen atoms for N9SOH and N15SOH are 2.934 and 2.967 Å, respectively. Similar N−H···O hydrogen bonds have been observed in several other amphiphiles bearing *N*-acyl chains, viz., *N*-acyl tris, *N*-acyl β-alaninols, *N*-acylethanolamines, *N*, *O*-diacylethanolamines (Ramakrishnan et al., 1999; Kamlekar et al., 2006, 2010; Sivaramakrishna et al., 2018, 2021a; Tarafdar et al., 2012; Reddy et al., 2021). Besides the N-H···O hydrogen bonds, two strong O-H···O hydrogen bonds are also observed between the hydroxyl O−H and hydroxyl oxygen of adjacent N9SOH molecules (Fig. 5.8). All these hydrogen bonds are identical, with an O−O distance of 2.669 and 2.715 Å, an H···O distance of 1.886 and 1.917 Å, and an O−H···O angle of 159.6 and 164.4º, respectively for N9SOH, whereas,

in N15SOH structure, two strong O-H···O hydrogen bonds are formed between adjacent and opposite N15SOH hydroxyl groups. Adjacent O-H···O hydrogen bonds have H···O distance of 2.001 Å, O···O distance of 2.681 Å, and bond angle at hydrogen atom of 139.8°. While O-H···O hydrogen bonds between opposite N15SOH molecules have H···O distance of 1.940 Å, O···O distance of 2.716 Å, and bond angle at hydrogen atom of 157.5^{o}. Similar O-H···O hydrogen bonds have been observed in the crystal structures of other amphiphiles bearing amide and hydroxy functionalities e.g., *N*-acylethanolamines, *N*-acyl tris and *N*-acyl β-alaninols (Ramakrishnan et al., 1999; Kamlekar et al., 2006; Sivaramakrishna et al., 2018, 2021a).

Table 5.3. Details of hydrogen bond distances and angles in the crystal structure of N9SOH and N15SOH.

Bond	H-O distance (Å)	Donor-acceptor distance (Å)	Bond angle at 'H' (°)
N9SOH			
N-H···O	2.084	2.934	169.9
C-H···O	2.554	3.402	146.0
"	2.881	3.614	132.3
"	2.904	3.554	125.3
O-H···O	1.886	2.669	159.6
"	1.917	2.715	164.4
N15SOH			
N-H···O	2.114	2.967	171.1
C-H···O	2.613	3.423	141.2
"	2.984	3.696	130.4
"	2.973	3.633	126.4
O-H···O	2.001	2.681	139.8
"	1.940	2.716	157.5

In addition to the N−H···O hydrogen bonds, several C−H···O hydrogen bonds are observed in the crystal structures of N9SOH and N15SOH (Fig. 5.8 and Fig. 5.9). In order

to identify the C−H···O hydrogen bonds, a cutoff of 3.7 Å was applied for the donor-acceptor distance (Horowitz and Trievel, 2012). Such an analysis revealed that each N9SOH or N15SOH molecule forms two C−H···O hydrogen bonds between adjacent N9SOH or N15SOH molecules and one C−H···O hydrogen bond with N9SOH or N15SOH molecules from the opposite layer (similar type/exactly same). The C−H···O H-bonds between adjacent N9SOH molecules have H···O distances of 2.554 and 2.881 Å (H-bond angles are 146.0 and 132.3 respectively; C·····O distances are 3.402 and 3.614 Å, respectively) and between opposite N9SOH molecules is 2.904 Å (H-bond angles is 125.2; and C·····O distances is 3.554 Å). Similarly, in N15SOH structure, C−H···O H-bonds between adjacent N15SOH molecules have H···O distances with 2.613 and 2.984 Å (H-bond angles are 141.2 and 130.4, respectively; the corresponding C·····O distances are 3.423 and 3.696 Å respectively) and between opposite N15SOH molecule the distance is 2.973 Å (H-bond angle is 126.4; and C·····O distances is 3.633 Å) (Fig. 5.8 and Fig. 5.9).

5.4.5. Structure and supramolecular organization of NAEs, NASOHs and NATs

It is pertinent to compare the structure and molecular packing of NASOHs with related single-chain amphiphiles such as NAEs and NATs; this is because while NASOHs have two hydroxy methyl (CH_2OH) groups attached to the C-atom adjacent to the amide N-H moiety, NAEs and NATs have one and three hydroxy methyl groups, respectively, at the same position (Fig. 5.10).

Molecular area: The area per molecule for N9SOH and N15SOH was determined as 29.17 and 29.23 $Å^2$, respectively. These values are considerably higher as compared to the NAEs with 14, 16, and 18 C-atoms in the acyl chain, which have molecular areas in the neighborhood of 22 $Å^2$ (Dahlen et al., 1977; Ramakrishnan & Swamy, 1999; Kamlekar & Swamy, 2006). On the other hand, the molecular areas of *N*-acyl tris with 10, 12 and 14 C-atoms are around 39 $Å^2$, which are significantly higher compared to the NASOHs (Sivaramakrishna et al., 2018; Megaranjan et al., 2018).

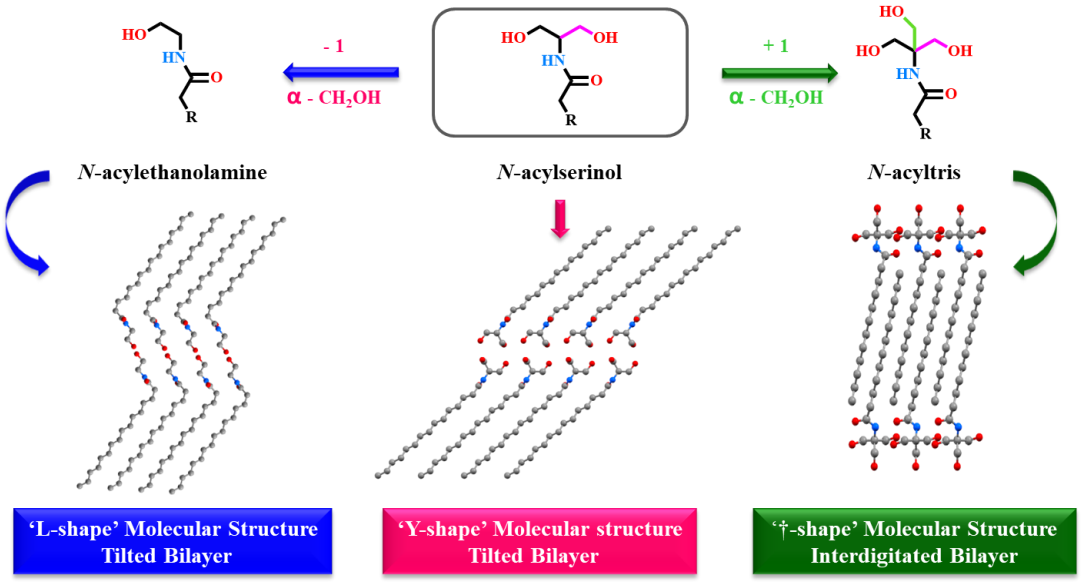

Fig. 5.10. Comparison of the molecular packing of NASOH with NAE and NAT. NASOH has two hydroxymethyl groups attached to the α-carbon atom (with respect to the amide nitrogen). Replacing one of these CH_2OH moieties with hydrogen atom gives NAE, whereas introducing one more CH_2OH moiety on the α-carbon gives NAT. While both NAE and NASOH adopt tilted bilayer structure, the larger head group of NAT due to the presence of an additional hydroxymethyl moiety induces it to adopt an interdigitated bilayer structure.

Molecular packing and chain tilt: Usually, when the headgroup area increases, the molecules of amphiphiles bearing long, saturated alkyl chains adopt a tilted orientation (with respect to the bilayer normal). For example, single crystal XRD studies have shown that *N*-acyl glycines pack in a bilayer with a very low tilt angle (<1°), PXRD measurements indicated that in *N*-acyl alanines, which have a larger head group, the acyl chains pack with a significant tilt (~41°) in the bilayer structure (Reddy et al., 2014; Sivaramakrishna et al., 2015a). It is interesting in this context to see that the presence of an additional hydroxymethyl (CH_2OH) group in NAT, as compared to NASOHs, which increases the head group area, induces the NAT molecules to adopt an interdigitated structure. Consequently, the tilt angle decreases significantly to 13-16° (for NATs) (Sivaramakrishna et al., 2018; Megarajan et al., 2018). On the other hand, in NAEs containing one less CH_2OH moiety, the molecules adopt an L-shaped geometry, leading

to a tilted orientation of the acyl chain with respect to the bilayer normal (Ramakrishnan & Swamy, 1999; Kamlekar & Swamy, 2006).

Chapter 6

General Discussion and Conclusion

The thesis titled *"Physiochemical Studies on Amphiphilic Conjugates of Amino Alcohols"* presents the findings derived from an examination of novel bioactive amino alcohol-based amphiphiles, including *O*-acyl-β-alaninols (OABAOHs), *O*-acyl-L-alaninols (OAAOHs), *N, O*-diacyl-L-alaninols (DAAOHs), and their effects on a stratum corneum model membrane. Additionally, the study delves into *N*-acyl serinols (NSOHs), recognized as an agonist of the G-Protein Coupled Receptor, GPR-119. The physicochemical properties of these compounds, both individually and in mixture with other amphiphilic molecules like sodium dodecyl sulfate (SDS), were investigated using a range of characterization techniques, encompassing single crystal X-ray diffraction (XRD), transmission electron microscopy (TEM), isothermal titration calorimetry (ITC), differential scanning calorimetry (DSC), powder X-ray diffraction (PXRD), nuclear magnetic resonance spectroscopy (NMR), Fourier-transform infrared spectroscopy (FTIR), high-resolution mass spectrometry (HRMS), fluorescence spectroscopy, UV-visible spectroscopy, and dynamic light scattering (DLS). The significant findings of Chapters 2-5 are succinctly outlined below.

In studies reported in Chapter 2, a homologous set of OABAOHs were synthesized, and differential scanning calorimetry was used to characterize their thermotropic phase transitions. The thermodynamic parameters ΔH_t and ΔS_t were found to be linearly dependent on the acyl chain length. Single crystal X-ray diffraction studies on *O*-myristoyl-β-alaninol and *O*-pamitoyl-β-alaninol revealed that these lipids adopt an extended, essentially linear geometry of the hydrophobic acyl chains which face one another, forming a head-to-head (and tail-to-tail) arrangement that is similar to a bilayer structure. The acyl chains are tilted away from the bilayer normal by a significant amount (35–42º). Studies on the interaction of *O*-myristoyl-β-alaninol with the anionic surfactant sodium dodecyl sulfate showed that these two amphiphiles combine to give an equimolar catanionic complex, which forms liposomes of ~150–160 nm diameter. Further research on how these molecules interact with other membrane lipids and therapeutic agents will be relevant for applying them in pharmaceutical applications, including their potential use in formulating liposomes for drug delivery applications.

In the work presented in Chapter 3, a series of OAAOHs have been synthesised, and their thermotropic phase behaviour was investigated using differential scanning

calorimetry. The thermodynamic parameters, ΔH_t and ΔS_t, were found to correlate linearly with the length of the acyl chain. Close analysis through single crystal XRD studies of *O*-pamitoyl-L-alaninol and *O*-heptadecanoyl-L-alaninol and PXRD studies on OAAOHs bearing 14-20 C-atoms revealed that the even- and odd chain length compounds are packed in different ways in the crystal lattice despite the similarity in the acyl chain packing. In both cases, the acyl chains are tilted with respect to the bilayer normal, with a tilt angle of ~55°. Investigation into the interaction between *O*-myristoyl-L-alaninol and the anionic surfactant SDS demonstrated the formation of an equimolar catanionic complex, which associates to yield liposomes with a diameter of 150-190 nm. The comparative study between OABAOHs and OAAOHs on phase behaviour and supramolecular organization is discussed. Future studies on the interaction of these molecules with other membrane lipids and therapeutic agents hold promise for their application in pharmaceutical contexts, especially in the development of liposomes for drug delivery.

In Chapter 4, studies on the synthesis and characterization of a homologous series of DAAOHs of matched acyl chains (n = 9–18) are reported. Similar to isomeric *N*-acyl-*L*-alanine esters (NAAEs), DAAOHs displayed an unusual odd-even alternation in transition enthalpies and entropies, with the odd chainlength compounds exhibiting higher values than the even chainlength ones. Odd-even alternation was also observed in the transition temperatures of DAAOHs, with the odd chainlength compounds exhibiting higher values. Powder XRD studies revealed that DAAOHs adopt tilted bilayer packing, which is similar to the isomeric NAAEs. However, DAAOHs were more tilted than NAAEs. Incorporation of *N, O*-dilauroylethanolamine (DLE) and *N, O*-dilauroyl-Lalaninol (DLAOH) into stratum corneum model membranes decreased the membrane fluidity more than that observed with *N*-acyl glycine lauryl ester (NAGE) and NAAE with lauroyl chains, suggesting that DAEs and DAAOHs would be better candidates than NAGEs and NAAEs as chemical enhancers in the design of transdermal drug delivery systems. However, further evaluation involving permeability studies is required in order to verify this possibility, which will be taken up in our future studies.

In Chapter 5, we report the crystal structures of two homologous *N*-acyl serinols, namely *N*-nonanoylserinol (N9SOH) and *N*-pentadecanoylserinol (N15SOH). Both

structures demonstrate that the NASOH molecules adopt a bilayer-type arrangement with head-to-head (and tail-to-tail) chain packing. This arrangement is stabilized by intermolecular hydrogen bonds between the hydroxy groups of NASOH molecules in the opposite leaflet and between the amide N-H and carbonyl oxygen of adjacent molecules in the same leaflet. Further stabilization is provided by the van der Waals' forces between the acyl chains. The influence of α-hydroxymethyl moieties in the molecular structure (shape) and supramolecular organization (packing) are discussed. These observations will be of considerable relevance in investigating the interaction of NASOHs in designing lipid-based drug delivery systems using them, as well as for understanding their interaction with membrane proteins. Additionally, the present results may provide clues to obtain a molecular-level understanding of their activity as GPR119 agonists.

In summary, the studies reported in this thesis investigated a series of OABAOHs, observing linear dependencies between thermodynamic parameters and acyl chain length. Crystallographic studies revealed a bilayer-like arrangement of hydrophobic acyl chains, forming catanionic complexes with sodium dodecyl sulfate and generating liposomes. Similarly, OAAOHs displayed thermodynamic correlations with acyl chain length, with crystallographic analyses highlighting packing differences between even- and odd-chain compounds. Interaction with SDS formed catanionic complexes, potentially applicable in drug delivery. DAAOHs exhibited odd-even alternation in thermodynamic parameters and transition temperatures, along with tilted bilayer packing and reduced membrane fluidity, suggesting utility as chemical enhancers in transdermal drug delivery systems. Crystallographic studies on NASOHs revealed bilayer-type arrangements stabilized by hydrogen bonding and van der Waals' forces, offering insights into lipid-based drug delivery. These findings lay essential groundwork for pharmaceutical applications and understanding molecular interactions in lipid-based systems.

References

Abrahamsson, S.; Dahlen, B.; Löfgren, H.; Pascher, I. Lateral packing of hydrocarbon chains. *Prog. Chem. Fats Other Lipids*, **1978,** 16, 125.

Abrahamsson, Z.; Kostarelos, K. Chemical Components for the Design of Temperature-Responsive Vesicles as Cancer Therapeutics. *Chem. Rev*. **2016**, 116, 3883–3918.

Al-Ahmady, Z.; Kostarelos, K. Chemical components for the design of temperature-responsive vesicles as cancer therapeutics. *Chem. Rev.* **2016**, 116, 3883–3918.

Allen, T. M.; Cullis, P. R. Liposomal drug delivery systems: from concept to clinical applications. *Adv. Drug Deliv. Rev.* **2013,** 65, 36–48.

Aryasomayajula, B.; Salzano, G.; Torchilin V. P. Multifunctional liposomes. *Methods Mol Biol.* **2017,** 1530: 41–61.

Bäckhed, F.; Crawford, P. A. Coordinated regulation of the metabolome and lipidome at the host-microbial interface. *Biochim. Biophys. Acta* **2010,** 1801, 240.

Bäckhed, F.; Ley, R. E.; Sonnenburg, J. L.; Peterson, D. A.; Gordon, J. I. Host-bacterial mutualism in the human intestine. *Science* **2005,** 307, 1915.

Bangham, A. D.; Standish, M. M.; Watkins, J. C. Diffusion of univalent ions across the lamellae of swollen phospholipids. *J. Mol. Biol.* **1965,** 13, 238–252.

Barenholz, Y. Doxil® - The first FDA-approved nano-drug: lessons learned. *J. Control Release.* **2012,** 160, 117–134.

Bastiaanse, E. M. L.; Hold, K. M.; Laarse, A. V. The effect of membrane cholesterol content on ion transport processes in plasma membranes. *Cardiovasc. Res.* **1997,** 33, 272–283.

Bhattacharya, S.; Haldar, S. Interactions between cholesterol and lipids in bilayer membranes. role of lipid headgroup and hydrocarbon chain-backbone linkage. *Biochem. Biophys. Acta* **2000,** 1467, 39–53.

Bieberich, E.; Hu, B.; Silva, J.; MacKinnon, S.; Yu, R. K.; Fillmore, H.; Broaddus, W. C.; Ottenbrite, R. M.; Synthesis and characterization of novel ceramide analogs for induction of apoptosis in human cancer cells. *Cancer Lett.,* **2002,** 181, 55–64.

Bieberich, E.; Kawaguchi, T.; Yu, R. K. *N*-acylated serinol is a novel ceramide mimic inducing apoptosis in neuroblastoma cells. *J. Biol. Chem.*, **2000,** 275, 177–181.

Bielawska, A.; Greenberg, M. S.; Perry, D.; Jayadev, S.; Shayman, J. A.; McKay, C.; Hannun, Y. A. (1*S*,2*R*)-D-*erythro*-2-(*N*-myristoylamino)-1-phenyl-1-propanol as an inhibitor of ceramidase. *J. Biol. Chem.*, **1996,** 271, 12646–12654.

Bielawska, A.; Linardic, C. M.; Hannun, Y. A. Ceramide-mediated biology. Determination of structural and stereospecific requirements through the use of *N*-acyl-phenylaminoalcohol analogs. *J. Biol. Chem.* **1992,** 267, 18493–18497.

Bijma, K.; Engberts, J. B. F. N.; Blandamer, M. J.; Cullis, P. M.; Last, P. M.; Irlam, K. D.; Soldi, L. G. Classification of calorimetric titration plots for alkyltrimethylammonium and alkylpyridinium cationic surfactants in aqueous solutions. *J. Chem. Soc. Faraday Trans.,* **1997,** 93, 1579–1584.

Bonte, F.; Pinguet, P.; Chevalier, J. M.; Meybeck, A. Analysis of all stratum corneum lipids by automated multiple development high-performance thin-layer chromatography. *J. Chromatography* **1995,** 664, 311.

Boscher, C.; Dennis, J. W.; Nabi, I. R. Glycosylation, galectins and cellular signaling. *Curr. Opin. Cell boil.* **2011,** 23, 383–392.

Bostwick, J. R.; Abbe, R.; Appel, S. H.; Modulation of acetylcholine release in rat hippocampus by amino alcohols and Bay K 8644. *Brain Res.,* **1993,** 629, 79-87.

Bostwick, J.R.; Abbe, R.; Sun, J.; Appel, S. H. Amino alcohol modulation of hippocampal acetylcholine release. *Nuroreport* **1992**, 3, 425-428

Bradshaw, H. B.; Rimmerman, N.; Hu, S. S. J.; Burstein, S.; Walker, J. M. Chapter 8 Novel endogenous *N*-acyl glycines: identification and characterization. *Vitam. Horm.* **2009**, 81, 191-205

Brady, J. E.; Evans, D. F.; Kacher, B.; Ninham, B. W.; Spontaneous vesicles, *J. Am.Chem. Soc.* **1984,** 106, 4279–4280.

Bramer, T.; Dew, N.; Edsman, K. Catanionic mixtures involving a drug: a rathergeneral concept that can be utilized for prolonged drug release from gels, *J.Pharm. Sci.*, **2006,** 95, 769–780.

Bramer, T.; Dew, N.; Edsman, K. Pharmaceutical applications for catanionic mixtures. *J. Pharm. Pharmacol.*, **2007,** 59, 1319–1334.

Brito, R. O.; Marques, E. F.; Gomes, P.; Falcão, S.; Söderman, O.; Self-assembly in a catanionic mixture with an aminoacid-derived surfactant: from mixed micelles to spontaneous vesicles, *J. Phys. Chem. B.* **2006,** 110, 18158–18165.

Calder, P. C. Functional roles of fatty acids and their effects on human health. *J. Parenter. Enter. Nutr.* **2015,** 39, 18S-32S.

Carreira, A. C.; Santos, T. C.; Lone, M. A.; Zupančič, E.; Lloyd-Evans, E.; de Almeida, R. F. M.; Hornemann, T.; Silva, L. C. Mammalian sphingoid bases: biophysical, physiological and pathological properties. *Prog Lipid Res.* **2019** 75, 100988

Carreira, A. C.; Santos, T. C.; Lone, M. A.; Zupančič, E.; Lloyd-Evans, E.; de Almeida, R. F. M.; Hornemann, T.; Silva, L. C. Mammalian sphingoid bases: biophysical, physiological and pathological properties. *Prog. Lipid Res.*, **2019,** 75, 100988.

Chatuphonprasert, W.; Jarukamjorn, K.; Ellinger, I. Physiology and pathophysiology of steroid biosynthesis, transport and metabolism in the human placenta. *Front. Pharmacol.* **2018,** 9, 1–29.

Cheng, X.; Smith, J. C. Biological membrane organization and cellular signaling. *Chem. Rev.* **2019,** 119, 5849–5880.

Choudhury, S. K.; Sivaramakrishna, D.; Swamy, M. J. Biophysical characterization of long chain *O*-acyl-β-alaninols and equimolar *O*-myristoyl-β-alaninol/sodium dodecyl sulfate complex, *Colloids Surfaces A: Physicochem. Eng. Aspects*, **2024,** 133483.

Choudhury, S. K.; Sivaramakrishna, D.; Swamy, M. J. Structure and supramolecular organization of *N*-acylserinols: agonists of the G-protein coupled receptor, GPR-119. *J. Chem. Sci.*, **2023,** 135, 1-9

Chu, C. J.; Huang, S. M.; Petrocellis, L. D.; Bisogno, T.; Ewing, S. A.; Miller, J. D.; Zipkin, R. E.; Daddario, N.; Appendino, G.; Marzo, V. D.; Walker, J. M. *N*-oleoyldopamine, a novel endogenous capsaicin-like lipid that produces hyperalgesia. *J. Biol. Chem.* **2003,** 278, 13633–13639.

Cohen, L. J.; Esterhazy, D.; Kim, S. H.; Lemetre, C.; Aguilar, R. R.; Gordon, E. A.; *et al.* Commensal bacteria make GPCR ligands that mimic human signalling molecules. *Nature* **2017,** 549, 48.

Connor, M.; Vaughan, C. W.; Vandenberg, R. J. *N*-acyl amino acids and *N*-acyl neurotransmitter conjugates: neuromodulators and probes for new drug targets. *Br. J. Pharmacol.* **2010,** 160, 1857–1871.

Cushman, S. W. Structure-function relationships in the adipose cell. I. Ultrastructure of the isolated adipose cell. *J Cell Biol*. **1970,** 46, 326–41.

Dahlén, B.; Pascher, I. The Crystal Structure of N-(2-Hydroxyethyl)-Octadecanoate. *Acta. Chim. Scand. A* **1977**, 31, 313–20.

Dahlen, B.; Pascher, I.; Sundell, S. The crystal structure of *N*-(2- ydroxyethyl)-octadecanoate. *Acta Chem. Scand. A* **1977,** 31, 313

Dhawan, V. V.; Nagarsenker, M. S. Catanionic systems in nanotherapeutics – biophysical aspects and novel trends in drug delivery applications. *J. Control. Release* **2017,** 266, 331–345.

di Gregorio, M. C.; Severoni, E.; Travaglini, L.; Gubitosi, M.; Sennato, S.; Mura, F.; Redondo-Gómez, C.; Jover, A.; Pavel, N. V.; Galantini, L. Bile acid derivative-based catanionic mixtures: versatile tools for superficial charge modulation of supramolecular lamellae and nanotubes. *Phys. Chem. Chem. Phys.* **2018,** 20, 18957–18969.

Ding, Y.; Wang, L.; Li, H.; Miao, F.; Zhang, Z.; Hu, C.; Yu, W.; Tang, Q.; Shao, G. Application of lipid nanovesicle drug delivery system in cancer immunotherapy. *J. Nanobiotechnology* **2022,** 20, 1–22.

Drulis-Kawa, Z.; Gubernator, J.; Dorotkiewicz-Jach, A.; Doroszkiewicz, W.; Kozubek, A. In vitro antimicrobial activity of liposomal meropenem against *pseudomonas aeruginosa* strains. *Int. J. Pharm.* **2006,** 315, 59–66.

Dubois, M.; Demé, B.; Gulik-Krzywicki, T.; Dedieu, J. -C.; Vautrin, C.; Désert, S.; Perez, E.; Zemb, T. Self-assembly of regular hollow icosahedra in salt-freecatanionic solutions, *Nature* **2001,** 411, 672–675.

Eeman, M.; Deleu, M. From biological membranes to biomimetic model membranes. *Biotechnol. Agron. Soc. Environ.* **2010,** 14, 691–708.

Eidelman, O.; BarNoy, S.; Razin, M.; Zhang, J.; McPhie, P.; Lee, G.; Huang, Z.; Sorscher, E. J.; Pollard, H. B. Role for phospholipid interactions in the trafficking defect of Δf508-CFTR†. *Biochem.* **2002**, 41, 11161–11170.

Elias, P. M. Epidermal lipids, barrier function, and desquamation. *J. Invest. Dermatol* **1983,** 80, 44s.

Fameau, A. -L.; Zemb, T. Self-assembly of fatty acids in the presence of amines and cationic components. *Adv. Colloid Interface Sci.* **2014,** 207, 43–64.

Fassbender, K.; Lütjohann, D.; Dik, M. G.; Bremmer, M.; König, J.; Walter, S.; Liu, Y.; Letièmbre, M.; Bergmann, K.; Jonker, C. Moderately elevated plant sterol levels are associated with reduced cardiovascular risk-The LASA study. *Atherosclerosis* **2008,** 196, 283–288.

Fernandis, A. Z.; Wenk, M. R. Membrane lipids as signaling molecules. *Curr. Opin. Lipidol.* **2007,** 18, 121–128.

Fujii, S.; Shimizu, K.; Hemmi, H.; Fukui, M.; Bonito, A. J.; Chen, G.; Franck, R. W.; Tsuji, M.; Steinman, R. M. Glycolipid α-C-galactosylceramide is a distinct inducer of dendritic cell function during innate and adaptive immune responses of mice. *Proc. Natl. Acad. Sci.* **2006,** 103, 11252-11257.

Ghosh, S.; Ray, A.; Pramanik, N.; Ambade, B. Can a catanionic surfactant mixture act as a drug delivery vehicle? *C. R. Chim.* **2016,** 19, 951–954.

Gimpl, G.; Wiegand, V.; Burger, K.; Fahrenholz, F. Chapter 4 Cholesterol and steroid hormones: Modulators of oxytocin receptor function. *Prog. Brain Res.* **2002,** 139, 43-55.

Gong, F.; Du, N.; Hou, W. Vesicle formation of single-tailed amphiphilic alkyltrimethylammonium bromides in water induced by dehydration-rehydration. *Soft Matter* **2022,** 18, 2072.

Gong, L.; Liao, G.; Luan, H.; Chen, Q.; Nie, X.; Liu, D.; Feng, Y. Oil solubilization in sodium dodecylbenzenesulfonate micelles: New insights into surfactant enhanced oil recovery. *J. Colloid Interface Sci.* **2020,** 569, 219-228.

Hannun, Y. A. Sphingolipid second messengers: tumor suppressor lipids. *Adv. Exp. Med. Biol.*, **1997,** 400, 305–312.

Hao, J.; Hoffmann, H. Self-assembled structures in excess and salt-free catanionic surfactant solutions. *Curr. Opin. Colloid Interface Sci.* **2004,** 9, 279–293.

Haque, T.; Talukder, M. M. U. Chemical enhancer: A simplistic way to modulate barrier function of the stratum corneum. *Adv. Pharm. Bull* **2018,** 8, 162.

Hazra, B.; Mondal, A.; Prasad, M.; Gayen, S.; Mandal, R.; Sardar, A.; Tarafdar, P. K. Lipidated lysine and fatty acids assemble into protocellular membranes to assist regioselective peptide formation: Correlation to the natural selection of lysine over nonproteinogenic lower analogues. *Langmuir* **2022,** 38, 15422–15432.

Heerklotz, H.; Seelig, J. Titration Calorimetry of Surfactant-Membrane Partitioning and Membrane Solubilization. *Biochim. Biophys. Acta Biomembranes* **2000**, 1508, 69–85.

Holleran, W. H.; Takagi, Y.; Uchida, Y. Epidermal sphingolipids: Metabolism, function, and roles in skin disorders. *FEBS Letters* **2006,** 580, 5456.

Horowitz, S.; Trievel, R. C. Carbon-oxygen hydrogen bonding in biological structure and function. *J. Biol. Chem.* **2012,** 287, 41576.

Huang, S. M.; Bisogno, T.; Petros, T. J.; Chang, S.Y.; Zavitsanos, P. A.; Zipkin, R. E.; Sivakumar, R.; Coop, A.; Maeda, D. Y.; De Petrocellis, L.; Burstein, S.; Di Marzo, V.; Walker, J. M. Identification of a new class of molecules, the arachidonyl amino acids, and characterization of one member that inhibits pain. *J. Biol. Chem.* **2001,** 276, 42639-42644.

Huang, S. M.; Bisogno, T.; Trevisani, M.; De Petrocellis, L.; Fezza, F.; Tognetto, M.; Petros, T. J.; Krey, J. F.; Chu, C. J.; Miller, J. D.; Davies, S. N.; Geppetti, P.; Walker, J. M.; Di Marzo, V. An endogenous capsaicin-like substance with high potency at recombinant and native vanilloid VR1 receptors. *Proc. Natl. Acad. Sci.* **2002,** 99, 8400-8405.

Innes, J. K.; Calder, P. C. Omega-6 fatty acids and inflammation. *Prostaglandins Leukot. Essent. Fat. Acids* **2018**, 132, 41-48.

Jain, S.; Kaur, A.; Puri, R.; Utreja, P.; Jain, A.; Bhide, M.; Ratnam, R.; Singh, V.; Patil, A. S.; Jayaraman, N.; Kaushik, G.; Yadav, S.; Khanduja, K. L. Poly Propyl Ether Imine (PETIM) Dendrimer: A Novel Non-Toxic Dendrimer for Sustained Drug Delivery. *Eur. J. Med. Chem.* **2010**, 45, 4997–5005.

Jia, J.; Chen, Y.; Xu, L.; Yang, Y.; Xu, X.; Ding, H.; *et al.* Screening for bacterial enzymes synthesizing gpr119 agonist in camp-responsive cells. *Acta Biochim. Biophys. Sin.* **2021,** 53, 121

Jungalwala, F. B. Expression and biological functions of sulfoglucuronyl glycolipids (SGGLs) in the nervous system-A review. *Neurochem. Res.* **1994,** 19, 945–957.

Kailash, V.; Pratibha, C.; Mahavir, G.; Ashwini, P.; Mangesh, K. Transdermal delivery: A recent trend in treatment of chronic diseases. *BioMedRx* **2013,** 1, 473.

Kaler, E. W.; Murthy, A. K.; Rodriguez, B. E.; Zasadzinski, J. A.; Spontaneous vesicleformation in aqueous mixtures of single-tailed surfactants, *Science* **1989,** 245, 1371–1374.

Kaler, E.W.; Herrington, K. L.; Iampietro, D. J.; Coldren, B. A.; Jung, H. -T.; Zasadzinski, J. A. Phase behavior and microstructure in aqueous mixtures of cationic and anionic surfactants, in: Abe, M.; Scamehorn J. F. (Eds.), Mixed Surfactant Systems, Second Ed, Marcel Dekker, New York, **2005**, pp. 289–338.

Kalhapure, R. S.; Akamanchi, K. G. Oleic acid based heterolipid synthesis, characterization and application in self-microemulsifying drug delivery system. *Int. J. Pharm.* **2012,** 425, 9-18.

Kalyanasundaram, K.; Thomas, J. K. Environmental Effects on Vibronic Band Intensities in Pyrene Monomer Fluorescence and Their Application in Studies of Micellar Systems. *J. Am. Chem. Soc.* **1977**, 99, 2039–2044.

Kamlekar, R. K.; Swamy, M. J. Molecular packing and intermolecular interactions in two structural polymorphs of *N*-palmitoylethanolamine, a type 2 cannabinoid receptor agonist. *J Lipid Res.*, **2006,** 47, 1424-33.

Kamlekar, R. K.; Tarafdar, P. K.; Swamy, M. J. Synthesis, calorimetric studies, and crystal structures of *N, O*-diacylethanolamines with matched chains. *J. Lipid Res*, **2010,** 51, 42–52.

Karande, P.; Mitragotri, S. Enhancement of transdermal drug delivery via synergistic action of chemicals. *Biochim. Biophys. Acta* **2009,** 1788, 2362.

Karmali, P. P.; Chaudhuri, A. Cationic liposomes as non-viral carriers of gene medicines: Resolved issues, open questions, and future promises. *Med. Res. Rev.* **2007,** 27, 696-722.

Komoroski, R. A.; Pearce, J. M.; Griffin, W. T.; Mrak, R. E.; Omori, M.; Karson, C. N. Phospholipid abnormalities in postmortem schizophrenic brains detected by ^{31}P nuclear magnetic resonance spectroscopy: A preliminary study. *Psychiatry Res.* **2001,** 106, 171-180.

Kovács, P.; Kõhidai, L.; Csaba, G. Effect of 3-amino-1-propanol on the phosphatidylinositol (PI) and glycosyl phosphatidylinositol (GPI) systems of *Tetrahymena. Comp. Biochem. Physiol.* **1997**, 118, 83-87.

Krendlinger, E. J.; Wolfmeier, U. H. Natural, and synthetic waxes: origin, production, technology, and application. John Wiley and Sons, **2022.**

Kume, G.; Gallotti, M.; Nunes, G. Review on anionic/cationic surfactant mixtures. *J. Surfact. Deterg.* **2008,** 11, 1–11.

Kume, G.; Gallotti, M.; Nunes, G. Review on anionic/cationic surfactant mixtures. *J. Surfact. Deterg.*, **2008,** 11, 1–11.

Kunitake, T. Synthetic bilayer membranes: molecular design, self-organization, and application. *Angew. Chem. Int. Ed. Engl.* **1992,** 31, 709.

Labaied, M.; Dagan, A.; Dellinger, M.; Gèze, M.; Egée, S.; Thomas, S. L.; Wang, C.; Gatt, S.; Grellier, P.; Anti-Plasmodium activity of ceramide analogs. *Malaria J.*, **2004,** 3, 49.

Landau, O.; Wasserman, L.; Deutsch, A. A.; Reiss, R.; Panet, H.; Novogrodsky, A.; Nordenberg, J. Amino acid alcohols: growth inhibition and induction of differentiated features in melanoma cells. *Cancer Lett.*, **1993,** 69, 203–208.

Lande, M, B.; Donovan, J. M.; Zeidel, M. L.; The relationship between membrane fluidity and permeabilities to water, solutes, ammonia, and protons. *J. Gen. Physiol.* **1995,** 106, 67

Larsson, K. The Lipid Handbook. Chapman and Hall, London, **1986**

Ley, R. E.; Hamady, M.; Lozupone, C.; Turnbaugh, P. J.; Ramey, R. R.; Bircher, J. S.; *et al.* Evolution of mammals and their gut microbes. *Science* **2008a,** 1647-1451.

Ley, R. E.; Lozupone, C. A.; Hamady, M.; Knight, R.; Gordon, J. I. Worlds within worlds: evolution of the vertebrate gut microbiota. *Nat. Rev. Microbiol.* **2008b,** 6, 776.

Li, Z.; Wu, H.; Hu, Y.; Chen, X.; Yuan, Y.; Luo, Y.; Hou, J.; Bai, B.; Kang, W. Ultra-low interfacial tension biobased and catanionic surfactants for low permeability reservoirs. *J. Mol. Liq.*, **2020,** 309, 113099.

Limin, Z.; Ganzuo, L.; Zhiwei, S. Spontaneous vesicle formation in aqueous solution of zwitterionic and anionic surfactant mixture. *Colloid Surf A: Physicochem. Eng. Asp*, **2001,** 190, 275-283.

Lioi, S. B.; Wang, X.; Islam, M. R.; Danoff, E. J.; English, D. S. Catanionic surfactant vesicles for electrostatic molecular sequestration and separation. *Phys. Chem. Chem. Phys.* **2009,** 11, 9315–9325.

Lísa, M.; Holčapek, M. Triacylglycerols profiling in plant oils important in food industry, dietetics and cosmetics using high-performance liquid chromatography–atmospheric pressure chemical ionization mass spectrometry. *J. Chromatogr. A* **2008,** 1198-1199, 115-130.

Liu, Y.; Xu, C.; Iqbal, S.; Yang, X.; Wang, J. Responsive nanocarriers as an emerging platform for cascaded delivery of nucleic acids to cancer. *Adv. Drug Deliv. Rev.* **2017,** 115, 98-114.

Lodish, H.: Berk, A.; Matsuddaira, P.; Kaiser, C. A.; Krieger, M.; Scott, M. P.; Zipursky, L.; Darnell, J. Molecular Cell Biology. 5th edition, **2008.**

Lodish, H.; Berk, A.; Zipursky, S. L.; et al. Molecular cell biology. 4th edition. New York: W. H. Freeman **2000**.

Lukyanov, A. N.; Elbayoumi, T. A.; Chakilam, A. R.; Torchilin, V. P. Tumor-targeted liposomes: Doxorubicin-loaded long-circulating liposomes modified with anti-cancer antibody. *J. Control. Release* **2004,** 100, 135-144.

Mahle, A.; Dashaputre, N.; DeShong, P.; Stein, D. C.; Catanionic surfactant vesicles as a new platform for probing glycan–protein interactions. *Adv. Funct. Mater.*, **2018,** 28, 1706215.

Manga, E. B.; Celik, P. A.; Cabuk, A.; Banat, I. M. Biosurfactants: opportunities for the development of a sustainable future. *Curr. Opin. Colloid Interface Sci.* **2021,** 56, 101514.

Mangraviti, A.; Tzeng, S.Y.; Kozielski, K.L.; Wang, Y.; Jin, Y.; Gullotti, D.; Pedone, M.; Buaon, N.; Liu, A.; Wilson, D.R.; Hansen, S.K.; Rodriguez, F.J.; Gao, G.-D.; DiMeco, F.; Berm, H.; Olivi, A.; Tyler, B.; Green, J.J. Polymeric nanoparticles for nonviral gene therapy extend brain tumor survival. *ACS Nano* **2015,** 9, 1236–1249.

Marqués, A. M.; Pérez, L.; Farfán, M.; Pinazo, A. Green surfactants: Production, properties, and application in advanced medical technologies, in: Sarma, H.; Prasad, M. N. V. (Eds.), Biosurfactants for a Sustainable Future: Production and Applications in the Environment and Biomedicine, Wiley, Hoboken, NJ, **2021**, 207–243.

Marques, E. F.; Regev, O.; Khan, A.; Lindman, B. Self-organization of double-chained and pseudodouble-chained surfactants: counterion and geometry effects. *Adv. Colloid Interface Sci.,* **2003,** 100, 83–104.

Marsh, D. Analysis of the chain length dependence of lipid phase transition temperatures: main and pretransitions of phosphatidylcholines; main and non-lamellar transitions of phosphatidylethanolamines. *Biochim. Biophys. Acta*, **1991,** 1062, 1–6.

Marsh, D. Biomembranes. *In:* Supramolecular structure and function. G. Pifat, J. N. Herak, Eds., Plenum Press: New York, **1982**, 127−178.

Marsh, D. Handbook of Lipid Bilayers. In CRC Press: Boca Raton, FL, **1990**

Marsh, D.; Swamy, M. J. Derivatized lipids in membranes. Physico-chemical aspects of *N*-biotinyl phosphatidylethanolamines, *N*-acyl phosphatidylethanolamines and *N*-acyl ethanolamines. *Chem. Phys. Lipids*, **2000,** 105, 43–69.

Martin, S.; Parton, R. G. Lipid droplets: a unified view of a dynamic organelle. *Nat Rev Mol Cell Biol.* **2006**, 7, 373-378.

Matosevic, S.; Paegel, B. M. Stepwise synthesis of giant unilamellar vesicles on a microfluidic assembly line. *J. Am. Chem. Soc.* **2011,** 133, 2798–2800.

Maulik. P. R.; Ruocco, M. J.; Shipley, G. G. Hydrocarbon chain packing modes in lipids: effect of altered sub-cell dimensions and chain rotation. *Chem. Phys. Lipids* **1990,** 56, 123.

Meer, S.; Tahir, M. A.; Abbasi, M. S. A. Formulation-based technology advancements in transdermal drug delivery system. *Asian J. Res. Derm. Sci.* **2020,** 3, 20.

Megarajan, S.; Subramaniyan, S. B.; Muthuswamy, S.; Anthony, S. P.; Arunachalam, J.; Moon, D. Veerappan, A. Synthesis, supramolecular organization and thermotropic phase behaviour of *N*-acyltris(hydroxymethyl) aminomethane. *RSC Adv.* **2018,** 8, 32823.

Milman, G.; Maor, Y.; Horowitz, M.; Gallily, R.; Batkai, S.; Mo, F.; Offertaler, L.; Pacher, P.; Kunos, G.; Mechoulam, R. *N*-arachidonoyl L-serine, an endocannabinoid-like brain constituent with vasodilatory properties. *Proc. Natl. Acad. Sci.*, **2006,** 103, 2428-2433.

Milshteyn, A.; Colosimo, D. A.; Brady, S. F.; Accessing bioactive natural products from the human microbiome. *Cell Host Microbe* **2018,** 23, 725.

Mouritsen, O. G. Model answers to lipid membrane questions. *Cold Spring Harb. Perspect. Biol.* **2011,** 3, 1–15.

Movassaghian, S.; Merkel, O. M.; Torchilin, V. P. Applications of polymer micelles for imaging and drug delivery. *Wiley Interdiscip. Rev. Nanomed. Nanobiotechnol.* **2015**, 7, 691-707.

Neish, A. S. Microbes in gastrointestinal health and disease. *Gastroenterology* **2009,** 136, 65.

Nelson, D. L.; Cox, M. M. Lehninger principles of biochemistry (7th ed.). W.H. Freeman. **2017.**

Niculescu-Duvaz, D.; Heyes, J.; Springer, C. J. Structure-activity relationship in cationic lipid mediated gene transfection. *Curr. Med. Chem.*, **2003**, 10, 1233-1261.

Nishimura, T.; Kitamura, H.; Iwakabe, K.; Yahata, T.; Ohta, A.; Sato, M.; Takeda, K.; Okumura, K.; Van Kaer, L.; Kawano, T.; Taniguchi, M.; Nakui, M.; Sekimoto, M.; Koda, T. The interface between innate and acquired immunity: Glycolipid antigen presentation by CD1d-expressing dendritic cells to NKT cells induces the differentiation of antigen-specific cytotoxic T lymphocytes. *Int. Immunol.* **2000,** 12, 987-994.

O'Driscoll, B. M. D.; Nickels, E. A.; Edler, K. J. Formation of robust, free-standingnanostructured membranes from catanionic surfactant mixtures andhydrophilic polymers, *Chem. Commun.* **2007,** 1068–1070.

O'Keefe, S. J. D. Nutrition and colonic health: the critical role of the microbiota. *Curr. Opin. Gastroen.* **2008,** 24, 51.

Ogura, M.; Handa, S. Induction of apoptosis by novel synthesized acylamides of human lymphocytes. *Biochim. Biophys. Acta* **2000,** 1483, 111–118.

Oliveira, I. S.; Pereira, C.; Borges, E.; do Vale, M. L.; Gomes, A. C.; Marques, E. F. Formation of catanionic vesicles by threonine-derived surfactants and gemini surfactants based on conventional or serine-derived headgroups: designing versatile and cytocompatible nanocarriers. *Soft Matter*, **2021,** 17, 7099–7110.

Packey, C. D.; Sartor, R. B. Interplay of commensal and pathogenic bacteria, genetic mutations, and immunoregulatory defects in the pathogenesis of inflammatory bowel diseases. *J. Intern. Med.* **2008,** 263, 597.

Parasassi, T.; Krasnowska, E. K.; Bagatolli, L.; Gratton, E. Laurdan and Prodan as polarity-sensitive fluorescent membrane probes. *J. Fluoresc.* **1998,** 8, 375.

Pascher, I.; Sundell, S. Molecular arrangements in sphingolipids. The crystal structure of the cerebroside. *Chem. Phys. Lipids* **1977,** 20, 175.

Pascher, I.; Sundell, S.; Harlos, K.; Eibl, H. Conformation and packing properties of membrane lipids: The crystal structure of sodium dimyristoylphosphatidylglycerol. *Biochim. Biophys. Acta* **1987,** 896, 77.

Penfold, J.; Thomas, R. K.; Recent developments and applications of the thermodynamics of surfactant mixing. *Mol. Phys.*, **2019,** 117, 3376–3388.

Peterson, D.; A.; Frank, D. N.; Pace, N. R.; Gordon, J. I. Metagenomic approaches or defining the pathogenesis of inflammatory bowel diseases. *Cell Host Microbe* **2008,** 3, 417.

Petkau-Milroy, K.; Brunsveld, L. Supramolecular chemical biology; bioactive synthetic self-assemblies. *Org. Biomol. Chem.* **2013,** 11, 219.

Pham, Q. D.; Bjorklund, S.; Engblom, J.; Topgaard, D.; Sparr, E. Chemical penetration enhancers in stratum corneum—Relation between molecular effects and barrier function. *J. Controlled Release* **2016,** 232, 175.

Rajkhowa, S.; Mahiuddin, S.; Dey, J.; Kumar, S.; Aswal, V. K.; Biswas, R.; Kohlbrecher, J.; Ismail, K. The effect of temperature, composition and alcohols on the microstructures of catanionic mixtures of sodium dodecylsulfate and cetyltrimethylammonium bromide in water. *Soft Matter*, **2017,** 13, 3556–3567.

Ramakrishnan, M.; Sheeba, V.; Komath, S. S.; Swamy, M. J. Differential scanning calorimetric studies on the thermotropic phase transitions of dry and hydrated forms of *N*-acylethanolamines of even chainlengths. *Biochim. Biophys. Acta* **1997**, 1329, 302–310.

Ramakrishnan, M.; Swamy, M. J. Differential scanning calorimetric studies on the thermotropic phase transitions of *N*-acylethanolamines of odd chainlengths. *Chem. Phys. Lipids* **1998**, 94, 43- 51.

Ramakrishnan, M.; Swamy, M. J. Molecular packing and intermolecular interactions in N-acylethanolamines: Crystal structure of *N*-myristoylethanolamine. *Biochim. Biophys. Acta* **1999,** 1418, 261-267.

Rang, M. J. Trend on development and application of high performancesurfactants for detergents. *Appl. Chem. Eng.,* **2009,** 20, 126–133.

Ravindar, C.; Reddy, S. T.; Sivaramakrishna, D.; Damera, D. P.; Swamy, M. J. Base-triggerable lauryl sarcosinate-dodecyl sulfate catanionic liposomes: Structure, biophysical characterization, and drug entrapment/release studies. *Soft Matter* **2022,** 18, 7814–7826.

Reddy, S. T.; Krovi, K. P.; Swamy, M. J. Structure and thermotropic phase behaviour of a homologous series of *N*-acylglycines: neuroactive and antinociceptive constituents of biomembranes. *Cryst. Growth Des.*, **2014,** 14, 4944-4954.

Reddy, S. T.; Sivaramakrishna, D.; Mamatha, K.; Sharma, M.; Swamy, M. J. Packing polymorphism, odd-even alternation and thermotropic phase transitions in *N*-, *O*-diacylethanolamines with varying *N*-Acyl Chains A combined experimental and computational study. *Phys. Chem. Chem. Phys.* **2021,** 23, 25264

Reddy, S. T.; Sivaramakrishna, D.; Swamy, M. J. Physicochemical characterization of lauryl glycinate-dodecyl sulfate equimolar complex: A base-triggerable catanionic liposomal system. *Colloid Surf A: Physicochem. Eng. Asp.* **2017,** 516, 139-146.

Reddy, S. T.; Swamy, M. J. Molecular structure, supramolecular organization, and thermotropic phase behavior of *N*-acylglycine alkyl esters with matched acyl and alkyl chains. *Chem. Phys. Lipids* **2017,** 208, 43.

Reddy, S. T.; Swamy, M. J.; Synthesis, physicochemical characterization and membrane interactions of a homologous series of *N*-acylserotonins: bioactive, endogenous conjugates of serotonin with fatty acids. *Biochim. Biophys. Acta*, **2015,** 1848, 95-103.

Reddy, S. T.; Tarafdar, P, K.; Kamlekar, R. K.; Swamy, M. J. Structure and Thermotropic Phase Behavior of a Homologous Series of Bioactive N-Acyldopamines. *J. Phys. Chem. B* **2013**, 117, 8747–8757.

Rimmerman, N.; Bradshaw, H. B.; Hughes, H. V.; Chen, J. S.; Hu S. S.; McHugh, D.; Vefring, E.; Jahnsen, J. A.; Thompson, E. L.; Masuda, K.; Cravatt, B. F.; Burstein, S.; Vasko, M. R.; Prieto, A. L.; O'Dell, D. K.; Walker, J. M. *N*-palmitoyl glycine, a novel endogenous lipid that acts as a modulator of calcium influx and nitric oxide production in sensory neurons. *Mol. Pharmacol.* **2008**, 74, 213-224.

Rubenstein, J. L.; Smith, B. A.; McConnell, H. M. Lateral diffusion in binary mixtures of cholesterol and phosphatidylcholines. *Proc. Natl. Acad. Sci.* **1979,** 76, 15-18.

Saghatelian, A.; McKinney, M. K.; Bandell, M.; Patapoutian, A.; Cravatt, B. F. A FAAH-regulated class of *N*-acyl taurines that activates TRP ion channels. *Biochemistry* **2006,** 45, 9007–9015.

Saghatelian, A.; Trauger, S. A.; Want, E. J.; Hawkins, E. G.; Siuzdak, G.; Cravatt, B. F. Assignment of endogenous substrates to enzymes by global metabolite profiling. *Biochemistry* **2004,** 43 14332–14339.

Sahle, F. F.; Gabre-Mariam, T.; Dobner, B.; Wohlrab, J.; Neubert, R. H. H. Skin diseases associated with the depletion of stratum corneum lipids and stratum corneum lipid substitution therapy. *Skin Pharmacol. Physiol.* **2015,** 28, 42.

Sakai, T.; Ikoshi, R.; Toshida, N.; Kagaya, M. Thermodynamically stable vesicle formation and vesicle-to-micelle transition of single-tailed anionic surfactant in water. *J. Phys. Chem. B.* **2013,** 117, 5081–508

Sardar, A.; Rout, N. K.; Nath, S.; Prasad, M.; Mahanti, J.; Mondal, S.; Tarafdar. P. K. A headgroup linker perturbs pK_a via acyl chain migration: designing base-labile supramolecular assemblies. *Chem. Commun.* **2018,** 54, 4282–85.

Scamehorn, J. F. An overview of phenomena involving surfactant mixtures. *ACS Symp. Ser.*, **1986,** 311, 1–27.

Schelero, N.; Lichtenfeld, H.; Zastrow, H.; Mohwald, H.; Dubois, M.; Zemb, T. Single particle light scattering method for studying aging properties of Pickering emulsions stabilized by catanionic crystals, *Colloid Surf.A: Physicochem. Eng. Asp.*, **2009,** 337, 146–153.

Šegota, S.; Težak, D. Spontaneous formation of vesicles, *Adv. Colloid InterfaceSci*. **2006**, 121, 51–75,

Serhan, C. N.; Levy, B. D. Resolvins in inflammation: Emergence of the pro-resolving superfamily of mediators. *J Clin. Invest.* **2018,** 128, 2657–2669.

Sharma, G.; Anabousi, S.; Ehrhardt, C.; Ravi Kumar, M. N. V. Liposomes as targeted drug delivery systems in the treatment of breast cancer. *J. Drug Target.* **2006,** 14, 301–310.

Shimizu, T.; Masuda, M.; Minamikawa, H. Supramolecular nanotube architectures based on amphiphilic molecules toshimi. *Chem. Rev.* **2005,** 105, 1401–1443.

Simons, K.; Ikonen, E. Functional rafts in cell membranes. *Nature* **1997,** 387, 569–572.

Simons, K.; Toomre, D. Lipid rafts and signal transduction. *Nat. Rev. Mol. Cell Biol.* **2000,** 1, 31–39.

Singer, S. J.; Nicolson, G. L. The fluid mosaic model of the structure of cell membranes. *Science* **1972,** 18, 720-31.

Sivaramakrishna, D.; Choudhury, S. K.; Cheppali, S. K.; Swamy, M. J. Structure, thermotropic phase behavior and membrane interaction of *N*-acyl-β-alaninols. Homologs of stress-combating *N*-acylethanolamines. *Chem. Phys. Lipids*, **2021a,** 236, 105056.

Sivaramakrishna, D.; Choudhury, S. K.; Swamy, M. J. Thermotropic phase behavior and supramolecular organization of *N, O*-diacyl-L-alaninols: effect on stratum corneum model membrane. *J. Chem. Sci.*, **2021b,** 133, 91.

Sivaramakrishna, D.; Prasad, M. D.; Swamy, M. J. A homologous series of apoptosis-inducing *N*-acylserinols: thermotropic phase behavior, interaction with cholesterol and characterization of cationic *N*-myristoylserinol-cholesterol-CTAB niosomes. *Biochim. Biophys. Acta.* **2019**, 1861, 504-513.

Sivaramakrishna, D.; Ravindar, C.; Swamy, M. J. Structure, supramolecular organization and thermotropic phase behavior of *N*-acyl tris homologs (n = 9-18): Structural analogs of apoptosis inducing ceramides. *Chem. Phys. Lipids.* **2018**, 217, 1-11.

Sivaramakrishna, D.; Reddy, S. T.; Nagaraju, T.; Swamy, M. J. Self-assembly, supramolecular organization, and phase transitions of a homologous series of *N*-acyl- L-alanines (n=8-20). *Colloids Surf. A: Physicochem. Eng. Asp.* **2015a,** 471, 108.

Sivaramakrishna, D.; Swamy, M. J. Differential scanning calorimetric and powder X-ray diffraction studies on a homologous series of *N*-acyl-L-alanine esters with matched Chains (n = 9-18). *J. Chem. Sci.* **2015b,** 127, 1627.

Sivaramakrishna, D.; Swamy, M. J. Self-Assembly, supramolecular organization, and phase behavior of L-alanine alkyl esters (n = 9-18) and characterization of equimolar L-alanine lauryl ester/lauryl sulfate catanionic complex. *Langmuir* **2015c**, 31, 9546-9556.

Sivaramakrishna, D.; Swamy, M. J. Structure, supramolecular organization and phase behavior of *N*-acyl-β-alanines: structural homologues of mammalian brain constituents *N*-acylglycine and N-acyl-GABA. *Chem. Phys. Lipids.* **2016a**, 201, 1-10.

Sivaramakrishna, D.; Swamy, M. J. Synthesis, characterization and thermotropic phase behavior of a homologous series of *N*-acyl-L-alaninols and interaction of *N*-myristoyl L-alaninol with dimyristoylphosphatidylcholine. *Chem. Phys. Lipids.* **2016b**, 196, 5-12.

Smith, J. D.; Barrows, L. J. Use of 3-aminopropanol as an ethanolamine analogue in the study of phospholipid metabolism in Tetrahymena. *Biochem. J.* **1988**, 254, 301–302.

Soussan, E.; Mille, C.; Blanzat, M.; Bordat, P.; Rico-Lattes, I. Sugar-derived tricatenar catanionic surfactant: synthesis, self-assembly properties, and hydrophilic probe encapsulation by vesicles. *Langmuir* **2008,** 24, 2326–2330.

Spiegel, S.; Foster, D.; Kolesnick, R. Signal transduction through lipid second messengers. *Curr. Opin. Cell Biol.* **1996,** *8*, 159-167.

Spitz, L. Sodeopec: Soaps, Detergents, Oleochemicals and Personal Care Products. *AOCS Press. Champaign,* **2004.**

Srinivas, R.; Samanta, S.; Chaudhuri, A. cationic amphiphiles: Promising carriers of genetic materials in gene therapy. *Chem. Soc. Rev.* **2009,** 38, 3326–3338.

Stocco, A.; Carriere, D.; Cottat, M.; Langevin, D. Interfacial behavior of catanionicsurfactants. *Langmuir,* **2010,** 26, 10663–10669.

Suleman, N.; Kalhapure, R. S.; Mocktar, C.; Rambharose, S.; Singh, M.; Govender, T. Silver salts of carboxylic acid terminated generation 1 poly (propyl ether imine) (PETIM) dendron and dendrimers as antimicrobial agents against S. aureus and MRSA. *RSC Adv.* **2015**, 5, 34967–34978.

Swamy, M. J.; Tarafdar, P. K.; Kamlekar, R. K. Structure, phase behaviour and membrane interactions of *N*-acylethanolamines and *N*-acylphosphatidylethanolamines. *Chem. Phys. Lipids.* **2010,** 163, 266-279.

Tan, B.; O'Dell, D. K.; Yu, Y. W.; Monn, M. F.; Hughes, H. V.; Burstein, S.; Walker, J. M. Identification of endogenous acyl amino acids based on a targeted lipidomics approach. *J. Lipid Res.* **2010,** 51, 112-119.

Tarafdar, P. K.; Reddy, S. T.; Swamy, M. J. A Base-Triggerable Catanionic Mixed Lipid System: Isothermal Titration Calorimetric and Single-Crystal X-Ray Diffraction Studies. *J. Phys. Chem.* B **2010a**, 114, 13710–13717.

Tarafdar, P. K.; Reddy, S. T.; Swamy, M. J. Effect of Hofmeister series anions on the thermotropic and chaotropic phase behavior of bioactive *O*-acylcholines. *J. Phys. Chem. B* **2013,** 117, 9900

Tarafdar, P. K.; Reddy, S. T.; Swamy, M. J. Nonclassical odd-even alternation in mixed-chain diacylethanolamines: implications of polymorphism. *Cryst. Growth Des.*, **2012,** 12, 1132–1140.

Tarafdar, P. K.; Swamy, M. J. Structure and phase behavior of *O*-stearoylethanolamine: A combined calorimetric, spectroscopic and X-ray diffraction study. *Biochem. Biophys. Acta* **2010b**, 1798, 872-881.

Tardieu, A.; Luzzati, V.; Reman, F. Structure and polymorphism of the hydrocarbon chains of lipids: A study of lecithin-water phases. *J. Mol. Biol.* **1973**, 75, 711-733.

Thomas, G. B.; Rader, L. H.; Park, J.; Abezgauz, L.; Danino, D.; DeShong, P.; English, D. S. Carbohydrate modified catanionic vesicles: probing multivalent binding at the bilayer interface. *J. Am. Chem. Soc.* **2009,** 131, 5471–5477.

Torchilin, V. P. Recent advances with liposomes as pharmaceutical carriers. *Nat. Rev. Drug Discov.*, **2005**, 4, 145-160.

Tsuchiya, K.; Nakanishi, H.; Sakai, H.; Abe, M. Temperature-dependent vesicleformation of aqueous solutions of mixed cationic and anionic surfactants, *Langmuir* **2004,** 20, 2117–2122,

Ueda, N.; Tsuboi, K.; Uyama, T. N-acylethanolamine metabolism with special reference to N-acylethanolamine-hydrolyzing acid amidase (NAAA). *Prog. Lipid Res.* **2010**, 49, 299–315.

Umlong, I. M.; Ismail, K. Micellization behaviour of sodium dodecyl sulfate in different electrolyte media. *Colloids Surf. A: Physicochem. Eng. Aspects,* **2007,** 299, 8–14.

van Meer, G.; Voelker, D. R.; Feigenson, G. W. Membrane lipids: Where they are and how they behave. *Nat. Rev. Mol. Cell Biol.* **2008,** 9, 112-124.

Vance, D. E. Chapter 8 Phospholipid biosynthesis in eukaryotes. *New Comprehensive Biochemistry* **2002,** 36, 205-232.

Varade, D.; Carriere, D.; Arriaga, L. R.; Fameau, A. L.; Rio, E.; Langevin, D.; Drenckhan W. On the origin of the stability of foams made from catanionicsurfactant mixtures. *Soft Matter*, **2011,** 7, 6557–6570.

Vavrova, K.; Hrabalek, A.; Dolezal, P.; Holas, T.; Zbytovska, J. L-serine and glycine-based ceramide analogs as transdermal permeation enhancers: Polar head size and hydrogen bonding. *Bioorg. Med. Chem. Lett.* **2003,** 13, 2351.

Viader, A.; Blankman, J. L.; Zhong, P.; Liu, X.; Schlosburg, J. E.; Joslyn, C. M.; Liu, Q.; Tomarchio, A. J.; Lichtman, A. H.; Selley, D. E.; Sim-Selley, L. J.; Cravatt, B. F. Metabolic interplay between astrocytes and neurons regulates endocannabinoid action. *Cell Rep.* **2015**, 12, 798-808.

Wang, C.; Liu, Y.; Wang, N.; Zhang, Y.; Zhang, L.; Zhao, S. Effects of catanionic surfactant mixture adsorption on the wettability of PTFE and PMMA (Art. No), *Colloids Surf. A: Physicochem. Eng. Asp*., **2021,** 631, 127659.

Welte, M. A. Expanding roles for lipid droplets. *Curr. Biol.* **2015**, 25, R470-R481.

Wenk, M. R. The emerging field of lipidomics. *Nat. Rev. Drug Discov.* **2005,** *4*, 594-610.

Weylandt, K. H.; Serini, S.; Chen, Y. Q.; Su, H. M.; Lim, K.; Cittadini, A.; Calviello, G. Omega-3 polyunsaturated fatty acids: The way forward in times of mixed evidence. *Biomed Res. Int.* **2015**, 143109

Xu, S.; Zhang, X.; Liu, P. Lipid droplet proteins and metabolic diseases. *Biochim. Biophys. Acta* **2018,** 1864, 1968-1983.

Yamano, Y.; Tsuboi, K.; Hozaki, Y.; Takahashi, K.; Jin, X. H. Lipophilic amines as potent inhibitors of N-acylethanolamine-hydrolyzing acid amidase. *Bioorg. Med. Chem.* **2012**, 20, 3658–3665.

Yin, H.; Huang, J.; Lin, Y.; Zhang, Y.; Qiu, S.; Ye, J. Heating-induced micelle tovesicle transition in the cationic-anionic surfactant systems: comprehensivestudy and understanding, *J. Phys. Chem. B.* **2005,** 109, 4104–4110.

Zhao, L.; Liu, J.; Zhang, L.; Gao, Y.; Zhang, Z.; Luan, Y. Self-assembly properties,aggregation behavior and prospective application for sustained drug deliveryof a drug-participating catanionic system. *Int. J. Pharm.*, **2013,** 452, 108–115.

Zhao, Y. Y.; Takahashi, M.; Gu, J. G.; Miyoshi, E.; Matsumoto, A.; Kitazume, S.; Taniguchi, N. Functional roles of *N*-glycans in cell signaling and cell adhesion in cancer. *Cancer Sci*. **2008,** 99, 1304–1310.

Zhi, D.; Bai, Y.; Yang, J.; Cui, S.; Zhao, Y.; Chen, H.; Zhang, S. A review on cationic lipids with different linkers for gene delivery. Adv. *Colloid Interface Sci.* **2018**, 253, 117–140.

Zhi, D.; Zhang, S.; Qureshi, F.; Zhao, Y.; Cui, S.; Wang, B.; Chen, H.; Yang, B.; Zhao, D. Structure-activity relationship of carbamate-linked cationic lipids bearing

hydroxyethyl headgroup for gene delivery. *Colloids Surf. B Biointerfaces* **2013**, 112, 537–541.

Supporting Information

Supporting Information to Chapter 2

Table S1. Assignment of resonances in the IR spectra of *O*-acyl-β-alaninols. Values given are in wavenumbers (cm^{-1}).

Acyl chain length	C=O stretch (ester)	C-H stretch	C-C-O stretch	O-C-C stretch	C-H scissoring	C-H rocking
14	~1732	~2955-2847	~1166	~1070	~1467	~720
15	~1735	~2951-2857	~1160	~1065	~1471	~719
16	~1739	~2951-2847	~1162	~1067	~1470	~718
17	~1735	~2951-2847	~1160	~1063	~1461	~719
18	~1739	~2951-2846	~1163	~1063	~1470	~717
19	~1734	~2952-2848	~1170	~1068	~1461	~720
20	~1739	~2914-2846	~1167	~1070	~1462	~729

Table S2. ^{1}H-NMR spectral data of *O*-acyl-β-alaninols in $CDCl_3$ solvent. Chemical shift values are given in ppm (δ scale).

Acyl chain length	CH_3-$(CH_2)_n$	$(CH_2)_n$	$(CH_2)n$-CH_2-CH_2-C=O	CH_2-CH_2-O	$(CH_2)n$-CH_2-C=O	CH_2-NH_3^+	CH_2-CH_2-O	NH_3^+
14	0.88, t	1.26, m	1.60, m	2.15, m	2.32, t	3.13, t	4.21, t	8.25
15	0.85, t	1.23, m	1.57, m	2.13, m	2.29, t	3.11, t	4.19, t	8.23
16	0.85, t	1.23, m	1.57, m	2.13, m	2.29, t	3.11, t	4.19, t	8.30
17	0.52, t	0.89, m	1.23, m	1.74, m	1.93, t	2.63, t	3.78, t	8.04
18	0.84, t	1.22, m	1.56, m	2.12, m	2.28, t	3.10, t	4.18, t	8.22
19	0.76, t	1.14, m	1.49, m	1.98, m	2.20, t	2.93, t	4.06, t	8.04
20	0.77, t	1.14, m	1.50, m	1.96, m	2.21, t	2.92, t	4.06, t	8.01

Table S3. ^{13}C-NMR spectral data of *O*-acyl-β-alaninols in $CDCl_3$ (solvent). Chemical shift values are given in ppm (δ scale).

Acyl chain length	CH_3-$(CH_2)_n$	CH_3-CH_2-$(CH_2)_n$	$(CH_2)_n$	CH_2-CH_2-C=O	CH_2-CH_2-C=O	CH_2-CH_2-O	CH_2-NH_3^+	CH_2-CH_2-O	O-C=O
14	14.07	22.67	29.20-29.67	24.86	34.18	31.91	37.14	60.98	174.10
15	14.09	22.67	29.42-29.92	24.87	34.18	31.91	37.14	60.98	174.13
16	14.32	22.90	29.22-29.68	25.10	34.40	32.14	37.31	61.03	174.29
17	13.53	21.99	28.64-28.98	24.20	33.45	31.22	36.33	60.50	172.95
18	13.68	22.17	28.82-29.17	24.38	33.63	31.40	36.53	60.66	173.18
19	14.07	22.70	29.31-29.72	24.87	34.14	31.95	37.03	60.67	174.20
20	14.07	22.71	29.32-29.73	24.89	34.15	31.96	37.04	61.05	174.34

Table S4. ESI-MS data of *O*-acyl-β-alaninols. Data (m/z values) are given for the more intense peaks of molecular ion and molecular ion dimer.

Acyl chain length	m/z values	assignment
14	286.2756, 571.5350,	$[M+H]^+$, $[2M+H]^+$
15	300.2888, 599.5682	$[M+H]^+$, $[2M+H]^+$
16	314.3059, 627.6138	$[M+H]^+$, $[2M+H]^+$
17	328.3214, 655.6468	$[M+H]^+$, $[2M+H]^+$
18	342.3372, 683.6740	$[M+H]^+$, $[2M+H]^+$
19	356.3527, 711.7253	$[M+H]^+$, $[2M+H]^+$
20	370.3685, 739.7212	$[M+H]^+$, $[2M+H]^+$

Table S5. Fractional atomic coordinates ($\times 10^4$) and equivalent isotropic displacement parameters ($Å^2 \times 10^3$) of OMBAOH. U(eq) is defined as one third of the trace of the orthogonalized Uij tensor. [U(eq) = ⅓ $\sum_i \sum_j U_{ij}\, a_{i*}\, a_{j*}\, a_i\, a_j \cos(ai, aj)$].

Atom	x	y	z	U(eq)
Cl1	14108(4)	7716(3)	5311.3(5)	60.6(7)
O1	6792(16)	14394(11)	6785.6(17)	96(2)
O2	8195(11)	12120(8)	6362.8(14)	68.0(15)
N1	10688(12)	12519(9)	5321.3(15)	57.1(16)
C1	6715(16)	12494(13)	6648(2)	58.3(18)
C2	5161(19)	10258(13)	6769(2)	70(2)
C3	3989(18)	10512(13)	7115(2)	66(2)
C4	2702(19)	8203(14)	7246(2)	72(2)
C5	1596(17)	8376(14)	7597(2)	65(2)
C6	393(19)	6006(14)	7722(2)	70(2)
C7	-699(19)	6094(14)	8075(2)	72(2)
C8	-1900(20)	3757(15)	8206(2)	76(2)
C9	-2930(20)	3882(14)	8559(2)	76(2)
C10	-4060(20)	1494(15)	8694(2)	75(2)
C11	-5120(20)	1623(16)	9038(2)	88(3)
C12	-6270(20)	-748(16)	9180(2)	88(3)
C13	-7250(30)	-591(17)	9528(3)	100(3)
C14	-8310(30)	-2960(20)	9669(3)	126(4)
C15	9906(17)	14180(13)	6246(2)	68(2)
C16	11311(15)	13469(14)	5931(2)	67(2)
C17	9173(14)	12928(12)	5644(2)	62(2)

Table S6. Bond lengths and bond angles of OMBAOH.

Bond lengths (Å)		**Bong angles (Degrees)**	
N(1)-C(17)	1.493(9)	N(1)-C(17)-C(16)	112.4(6)
O(2)- C(1)	1.356(9)	C(15)-C(16)-C(17)	113.7(6)
O(2)- C(15)	1.433(8)	C(1)-O(2)-C(15)	116.0(6)
O(1)- C(1)	1.167(9)	C(16)-C(15)-O(2)	108.9(6)
C(1)- C(2)	1.486(10)	O(1)-C(1)-O(2)	121.6(7)
C(2)- C(3)	1.497(11)	C(2)-C(1)-O(2)	113.3(6)
C(3)- C(4)	1.494(10)	C(2)-C(1)-O(1)	125.0(8)
C(4)- C(5)	1.503(11)	C(3)-C(2)-C(1)	114.7(6)
C(5)- C(6)	1.500(10)	C(4)-C(3)-C(2)	114.1(7)
C(6)- C(7)	1.505(11)	C(5)-C(4)-C(3)	115.6(7)
C(7)- C(8)	1.495(10)	C(6)-C(5)-C(4)	113.7(7)
C(8)- C(9)	1.498(11)	C(7)-C(6)-C(5)	115.5(7)
C(9)- C(10)	1.515(10)	C(8)-C(7)-C(6)	116.6(7)
C(10)- C(11)	1.469(12)	C(9)-C(8)-C(7)	115.7(7)
C(11)- C(12)	1.521(11)	C(10)-C(9)-C(8)	115.3(7)
C(12)- C(13)	1.472(13)	C(11)-C(10)-C(9)	115.3(7)
C(13)- C(14)	1.507(12)	C(12)-C(11)-C(10)	116.4(8)
C(15)- C(16)	1.480(11)	C(13)-C(12)-C(11)	115.7(8)
C(16)- C(17)	1.463(10)	C(14)-C(13)-C(12)	115.4(9)

Table S7. Torsion angles (degrees) for OMBAOH.

C15	O2	C1	O1	1(1)
C17	C16	C15	O2	69.7(8)
C16	C15	O2	C1	-178.8(6)
C15	O2	C1	C2	-175.9(6)
O2	C1	C2	C3	169.1(6)
O1	C1	C2	C3	-8(1)
C1	C2	C3	C4	-174.3(7)
C2	C3	C4	C5	178.1(7)
C3	C4	C5	C6	-178.5(7)
C4	C5	C6	C7	179.2(7)
C5	C6	C7	C8	-179.8(7)
C6	C7	C8	C9	179.1(7)
C7	C8	C9	C10	-178.3(7)
C8	C9	C10	C11	-179.0(7)
C9	C10	C11	C12	180.0(7)
C10	C11	C12	C13	178.5(8)
C11	C12	C13	C14	-178.5(9)

Table S8. Fractional atomic coordinates ($\times 10^4$) and equivalent isotropic displacement parameters ($Å^2 \times 10^3$) of OPBAOH. U(eq) is defined as one third of the trace of the orthogonalized Uij tensor. [U(eq) = ⅓ $\sum_i \sum_j U_{ij} a_{i*} a_{j*} a_i a_j \cos(ai, aj)$].

Atom	x	y	z	U(eq)
Cl1	9032(3)	2605(3)	7352.9(2)	51.3(6)
O1	940(14)	8603(11)	6681.4(7)	93(2)
O2	2533(10)	6462(9)	6870.2(6)	55.3(15)
N1	5570(11)	7364(10)	7347.0(6)	51.1(17)
C1	922(16)	6758(17)	6739.8(9)	57(2)
C2	-716(15)	4370(14)	6687.2(9)	60(2)
C3	-2100(16)	4470(15)	6526.2(9)	70(3)
C4	-3450(17)	2057(15)	6467.6(10)	71(3)
C5	-4743(17)	2123(15)	6307.5(10)	70(3)
C6	-5988(16)	-327(15)	6248.4(9)	64(2)
C7	-7261(19)	-333(15)	6090.1(10)	76(3)
C8	-8525(17)	-2814(16)	6034.2(9)	72(3)
C9	-9782(18)	-2856(16)	5872.4(10)	73(3)
C10	-10981(18)	-5343(16)	5815.5(10)	77(3)
C11	-12181(19)	-5340(17)	5657.0(11)	85(3)
C12	-13390(20)	-7780(17)	5595.8(11)	87(3)
C13	-14650(20)	-7860(20)	5433.2(10)	94(3)
C14	-15780(20)	-10314(18)	5368.7(13)	100(4)
C15	-16940(20)	-10270(20)	5210.4(13)	124(5)
C16	-18140(20)	-12730(20)	5150.4(12)	133(5)
C17	4303(15)	8651(13)	6922.9(8)	55(2)
C18	5949(13)	8041(13)	7066.8(8)	55(2)
C19	3885(12)	7653(13)	7201.9(8)	48(2)

Table S9. Bond lengths and bond angles of OPBAOH.

Bond lengths (Å)		**Bong angles (Degrees)**	
N(1)-C(19)	1.485(7)	N(1)-C(19)-C(18)	112.0(5)
O(2)- C(1)	1.360(8)	C(17)-C(18)-C(19)	112.5(6)
O(2)- C(17)	1.462(8)	C(1)-O(2)-C(17)	113.4(6)
O(1)- C(1)	1.156(9)	C(18)-C(17)-O(2)	107.2(6)
C(1)- C(2)	1.526(10)	O(1)-C(1)-O(2)	121.7(8)
C(2)- C(3)	1.533(9)	C(2)-C(1)-O(2)	110.3(7)
C(3)- C(4)	1.508(10)	C(2)-C(1)-O(1)	128.0(8)
C(4)- C(5)	1.508(9)	C(3)-C(2)-C(1)	113.0(6)
C(5)- C(6)	1.513(10)	C(4)-C(3)-C(2)	113.1(6)
C(6)- C(7)	1.488(9)	C(5)-C(4)-C(3)	113.5(6)
C(7)- C(8)	1.522(10)	C(6)-C(5)-C(4)	112.8(7)
C(8)- C(9)	1.513(9)	C(7)-C(6)-C(5)	114.3(7)
C(9)- C(10)	1.519(10)	C(8)-C(7)-C(6)	113.2(7)
C(10)- C(11)	1.478(10)	C(9)-C(8)-C(7)	113.8(7)
C(11)- C(12)	1.510(11)	C(10)-C(9)-C(8)	113.7(7)
C(12)- C(13)	1.520(10)	C(11)-C(10)-C(9)	112.7(8)
C(13)- C(14)	1.516(12)	C(12)-C(11)-C(10)	114.5(8)
C(14)- C(15)	1.472(11)	C(13)-C(12)-C(11)	116.3(8)
C(15)- C(16)	1.515(12)	C(14)-C(13)-C(12)	116.7(9)
C(17)- C(18)	1.508(8)	C(15)-C(14)-C(13)	113.9(9)
C(18)- C(19)	1.513(8)	C(16)-C(15)-C(14)	112.8(10)

Table S10. Torsion angles (degrees) for OPBAOH.

N1	C19	C18	C17	-172.6(5)
C17	O2	C1	O1	-1.9(1)
C19	C18	C17	O2	-71.7(6)
C18	C17	O2	C1	-179.9(5)
C17	O2	C1	C2	176.7(5)
O2	C1	C2	C3	-169.4(6)
O1	C1	C2	C3	9.1(1)
C1	C2	C3	C4	174.2(6)
C2	C3	C4	C5	-178.4(6)
C3	C4	C5	C6	177.9(6)
C4	C5	C6	C7	-179.5(6)
C5	C6	C7	C8	-179.4(6)
C6	C7	C8	C9	-179.0(6)
C7	C8	C9	C10	178.7(6)
C8	C9	C10	C11	-179.7(7)
C9	C10	C11	C12	179.8(7)
C10	C11	C12	C13	179.9(7)
C11	C12	C13	C14	178.1(8)
C12	C13	C14	C15	-179.4(8)
C13	C14	C15	C16	-178.2(8)

Supporting Information to Chapter 3

Table S1. Assignment of resonances in the IR spectra of *O*-acyl-L-alaninols. Values given are in wavenumbers (cm^{-1}).

Acyl chain length	C=O stretch (ester)	C-H stretch	C-C-O stretch	C-H scissoring	C-H rocking
14	~1736	~2848-2952	~1151	~1460	~719
15	~1731	~2848-2952	~1148	~1471	~719
16	~1731	~2848-2958	~1149	~1470	~718
17	~1730	~2848-2954	~1149	~1471	~718
18	~1730	~2848-2957	~1149	~1471	~717
19	~1742	~2849-2954	~1149	~1469	~718
20	~1730	~2848-2952	~1148	~1471	~720

Table S2. ^{1}H-NMR spectral data of *O*-acyl-L-alaninols in $CDCl_3$ solvent. Chemical shift values are given in ppm (δ scale).

Acyl chain length	CH_3-$(CH_2)_n$	$(CH_2)_n$	$(CH_2)_n$-CH_2-CH_2-C=O	CH_2-C=O	O-CH_2-CH(CH_3)-NH_3^+	O-CH_2-CH(CH_3)-NH_3^+	O-CH_2-CH(CH_3)-NH_3^+	O-CH_2-CH(CH_3)-NH_3^+
14	0.88, t	1.25, m	1.62, m	2.46, t	4.20, m	3.62, m	1.45, d	8.60
15	0.90, t	1.27, m	1.64, m	2.47, t	4.27, m	3.64, m	1.47, d	8.61
16	0.90, t	1.27, m	1.64, m	2.47, t	4.28, m	3.64, m	1.47, d	8.60
17	0.88, t	1.25, m	1.62, m	2.45, t	4.27, m	3.63, m	1.46, d	8.55
18	0.88, t	1.25, m	1.62, m	2.46, t	4.27, m	3.62, m	1.45, d	8.57
19	0.81, t	1.19, m	1.56, m	2.34, t	4.14, m	3.50, m	1.32, d	8.21
20	0.84, t	1.21, m	1.59, m	2.37, t	4.20, m	3.53, m	1.34, d	8.27

Table S3. ^{13}C-NMR spectral data of *O*-acyl-L-alaninols in $CDCl_3$ (solvent). Chemical shift values are given in ppm (δ scale).

Acyl chain length	CH_3-CH_2-CH_2-$(CH_2)_n$	CH_3-CH_2-CH_2-$(CH_2)_n$	CH_3-CH_2-CH_2-$(CH_2)_n$	$(CH_2)_n$	CH_2-CH_2-C=O	CH_2-CH_2-C=O	O-CH_2-CH(CH_3)-NH_3^+	O-CH_2-CH(CH_3)-NH_3^+	O-CH_2-CH(CH_3)NH_3^+	O-C=O
14	14.10	22.68	31.92	29.17-29.66	24.69	34.00	64.31	47.50	15.24	173.51
15	14.10	22.68	31.92	29.17-29.70	24.69	34.01	64.31	47.50	15.24	173.53
16	14.12	22.70	31.94	29.18-29.72	24.69	34.02	64.32	47.52	15.25	173.58
17	14.11	22.69	31.93	29.18-29.71	24.69	34.02	64.32	47.50	15.25	173.57
18	14.12	22.66	31.96	29.14-29.78	24.81	33.93	64.53	46.87	15.16	173.78
19	13.94	22.57	31.82	29.04-29.59	24.59	33.72	64.41	46.65	14.96	173.67
20	13.92	22.56	31.81	29.03-29.58	24.59	33.72	64.41	46.67	14.96	173.65

Table S4. ESI-MS data of *O*-acyl-L-alaninols. Data (m/z values) are given for the more intense peaks of molecular ion and Molecular ion dimer. In all cases, two peaks are seen/observed.

Acyl chain length	m/z values	Assignment
14	286.2748, 571.5338	$[M+H]^+$, $[2M+H]^+$
15	300.2906, 599.5615	$[M+H]^+$, $[2M+H]^+$
16	314.3059, 627.5918	$[M+H]^+$, $[2M+H]^+$
17	328.3217	$[M+H]^+$
18	342.3371	$[M+H]^+$
19	356.3526, 711.6858	$[M+H]^+$, $[2M+H]^+$
20	370.3684	$[M+H]^+$

Table S5. Fractional atomic coordinates ($\times 10^4$) and equivalent isotropic displacement parameters ($Å^2 \times 10^3$) of OPAOH. U(eq) is defined as one third of the trace of the orthogonalized Uij tensor. [U(eq) = ⅓ $\sum_i \sum_j U_{ij}\, a_{i*}\, a_{j*}\, a_i\, a_j \cos(ai, aj)$].

Atom	x	y	z	U(eq)
Cl1	-1920.2(11)	3953(2)	4540.1(3)	63.1(4)
O1	-545(5)	5185(7)	6552.1(18)	133(2)
O2	-692(4)	2572(5)	6268.7(9)	60.1(8)
N1	-1591(4)	2818(5)	5448.7(10)	53.6(9)
C1	51(5)	3826(9)	6482.1(14)	64.7(12)
C2	1664(5)	3317(7)	6586.6(14)	62.8(14)
C3	2339(5)	4394(7)	6934.2(14)	61.3(14)
C4	4012(5)	3972(9)	7016.3(13)	61.4(11)
C5	4724(6)	4982(8)	7366.9(14)	65.5(14)
C6	6387(5)	4489(7)	7453.5(15)	65.3(14)
C7	7125(6)	5452(8)	7805.6(15)	67.2(14)
C8	8788(6)	4982(8)	7885.9(16)	69.5(15)
C9	9520(6)	5916(9)	8239.5(15)	72.6(15)
C10	11182(6)	5452(9)	8319.2(15)	75.1(16)
C11	11915(6)	6397(9)	8674.3(16)	77.1(16)
C12	13567(6)	5911(9)	8758.6(17)	80.5(17)
C19	-4083(5)	4040(11)	5629.5(15)	74.4(14)
C18	-2408(4)	3877(8)	5757.2(12)	54.0(10)
C13	14278(6)	6858(9)	9118.8(17)	86.2(19)
C14	15938(7)	6370(10)	9212.3(19)	92(2)
C15	16651(7)	7331(13)	9560.7(19)	119(3)
C16	18281(8)	6856(16)	9660(2)	145(4)
C17	-2269(5)	2940(8)	6153.7(14)	62.9(13)

Table S6. Bond lengths and bond angles of OPAOH.

Bond lengths (Å)		Bong angles (Degrees)	
N(1)-C(18)	1.495(5)	N(1)-C(18)-C(19)	108.7(4)
O(2)- C(1)	1.345(7)	N(1)-C(18)-C(17)	108.5(4)
O(2)- C(17)	1.446(5)	O(2)-C(17)-C(18)	112.4(4)
O(1)- C(1)	1.181(7)	O(2)-C(1)-C(2)	112.3(5)
C(1)- C(2)	1.490(6)	O(1)-C(1)-C(2)	126.6(5)
C(2)- C(3)	1.523(6)	O(1)-C(1)-O(2)	120.9(4)
C(3)- C(4)	1.511(5)	C(1)-O(2)-C(17)	116.5(4)
C(4)- C(5)	1.516(6)	C(1)-C(2)-C(3)	112.6(4)
C(5)- C(6)	1.517(6)	C(2)-C(3)-C(4)	112.2(4)
C(6)- C(7)	1.511(6)	C(3)-C(4)-C(5)	114.1(4)
C(7)- C(8)	1.511(6)	C(4)-C(5)-C(6)	113.2(4)
C(8)- C(9)	1.503(7)	C(5)-C(6)-C(7)	114.6(4)
C(9)- C(10)	1.507(7)	C(6)-C(7)-C(8)	114.4(5)
C(10)- C(11)	1.511(7)	C(7)-C(8)-C(9)	114.6(5)
C(11)- C(12)	1.506(7)	C(8)-C(9)-C(10)	114.6(5)
C(12)- C(13)	1.517(7)	C(9)-C(10)-C(11)	114.5(5)
C(13)- C(14)	1.519(7)	C(10)-C(11)-C(12)	114.5(5)
C(14)- C(15)	1.493(8)	C(11)-C(12)-C(13)	113.7(5)
C(15)- C(16)	1.494(9)	C(12)-C(13)-C(14)	114.6(5)
C(17)- C(18)	1.500(7)	C(13)-C(14)-C(15)	114.7(6)
C(18)- C(19)	1.516(5)	C(14)-C(15)-C(16)	115.5(7)
		C(17)-C(18)-C(19)	110.1(4)

Table S7. Torsion angles (degrees) for OPAOH.

N1	C18	C17	O2	54.6(5)
C19	C18	C17	O2	173.5(4)
C18	C17	O2	C1	89.0(5)
C17	O2	C1	O1	-3.6(7)
C17	O2	C1	C2	179.8(4)
O2	C1	C2	C3	-161.0(4)
O1	C1	C2	C3	22.6(8)
C1	C2	C3	C4	-175.4(4)
C2	C3	C4	C5	-178.6(4)
C3	C4	C5	C6	177.9(4)
C4	C5	C6	C7	-179.1(4)
C5	C6	C7	C8	-178.9(4)
C6	C7	C8	C9	-179.1(4)
C7	C8	C9	C10	-179.8(5)
C8	C9	C10	C11	179.8(5)
C9	C10	C11	C12	178.9(5)
C10	C11	C12	C13	-179.4(5)
C11	C12	C13	C14	179.3(5)
C12	C13	C14	C15	178.6(5)
C13	C14	C15	C16	179.4(6)

Table S8. Fractional atomic coordinates ($\times 10^4$) and equivalent isotropic displacement parameters ($Å^2 \times 10^3$) of OHDAOH. U(eq) is defined as one third of the trace of the orthogonalized Uij tensor. [U(eq) = ⅓ $\sum_i \sum_j U_{ij} a_{i*} a_{j*} a_i a_j \cos(ai, aj)$].

Atom	x	y	z	U(eq)
Cl1	1662.5(8)	-7508.1(14)	4527.5(3)	57.4(3)
O1	867(3)	-5147(4)	6318.3(11)	90.8(11)
O2	3091(3)	-6278(4)	6259.1(9)	69.4(9)
N1	1727(3)	-6395(4)	5420.1(9)	52.2(8)
C1	2172(4)	-5019(5)	6377.9(12)	54.4(10)
C2	3004(4)	-3524(5)	6585.6(13)	60.6(11)
C3	2059(4)	-2098(5)	6755.5(12)	59.6(12)
C4	2967(4)	-704(5)	6992.2(12)	58.3(10)
C5	2097(4)	798(5)	7157.5(13)	62.8(11)
C6	3019(4)	2180(5)	7393.1(13)	62.1(11)
C7	2154(4)	3685(5)	7568.0(14)	65.3(11)
C8	3101(4)	5055(6)	7804.5(14)	67.3(12)
C9	2236(4)	6548(6)	7980.0(14)	68.5(12)
C10	3184(4)	7914(5)	8216.1(14)	69.7(13)
C11	2343(4)	9387(6)	8399.7(14)	72.5(13)
C12	3283(5)	10751(6)	8635.6(14)	76.2(13)
C13	2439(5)	12249(7)	8818.3(14)	78.6(13)
C14	3383(6)	13565(6)	9061.2(15)	86.9(15)
C15	2563(6)	15083(7)	9243.1(16)	89.0(15)
C16	3512(6)	16367(8)	9488.9(19)	117(2)
C17	2710(7)	17831(8)	9681(2)	144(3)
C18	2469(5)	-7835(5)	6059.3(13)	64.7(12)
C19	2680(3)	-7788(5)	5630.7(11)	49.9(9)
C20	4274(3)	-7487(7)	5544.6(12)	67.6(10)

Table S9. Bond lengths and bond angles of OHDAOH.

Bond lengths (Å)		**Bong angles (Degrees)**	
N(1)-C(19)	1.487(4)	N(1)-C(19)-C(20)	109.0(3)
O(2)-C(1)	1.338(4)	N(1)-C(19)-C(18)	111.6(3)
O(2)-C(18)	1.427(5)	O(2)-C(18)-C(19)	111.6(3)
O(1)-C(1)	1.185(4)	O(2)-C(1)-C(2)	111.2(3)
C(1)- C(2)	1.482(5)	O(1)-C(1)-O(2)	122.1(4)
C(2)- C(3)	1.510(5)	O(1)-C(1)-C(2)	126.7(4)
C(3)- C(4)	1.507(5)	C(1)-O(2)-C(18)	118.5(3)
C(4)- C(5)	1.504(5)	C(1)-C(2)-C(3)	115.1(3)
C(5)- C(6)	1.505(5)	C(2)-C(3)-C(4)	112.5(3)
C(6)- C(7)	1.517(5)	C(3)-C(4)-C(5)	115.3(3)
C(7)- C(8)	1.512(5)	C(4)-C(5)-C(6)	114.7(3)
C(8)- C(9)	1.511(5)	C(5)-C(6)-C(7)	115.3(3)
C(9)- C(10)	1.510(5)	C(6)-C(7)-C(8)	114.4(3)
C(10)- C(11)	1.501(5)	C(7)-C(8)-C(9)	114.3(3)
C(11)- C(12)	1.505(5)	C(8)-C(9)-C(10)	114.2(3)
C(12)- C(13)	1.514(6)	C(9)-C(10)-C(11)	115.0(3)
C(13)- C(14)	1.495(6)	C(10)-C(11)-C(12)	115.2(3)
C(14)- C(15)	1.512(6)	C(11)-C(12)-C(13)	115.4(3)
C(15)- C(16)	1.487(6)	C(12)-C(13)-C(14)	114.9(3)
C(16)- C(17)	1.492(7)	C(13)-C(14)-C(15)	115.7(4)
C(18)- C(19)	1.493(5)	C(14)-C(15)-C(16)	115.2(4)
C(19)- C(20)	1.518(4)	C(15)-C(16)-C(17)	115.6(5)
		C(18)-C(19)-C(20)	113.8(3)

Table S10. Torsion angles (degrees) for OHDAOH.

N1	C19	C18	O2	-71.2(4)
C20	C19	C18	O2	52.7(4)
C19	C18	O2	C1	107.5(4)
C18	O2	C1	O1	-0.9(6)
C18	O2	C1	C2	178.9(3)
O2	C1	C2	C3	-175.9(3)
O1	C1	C2	C3	3.8(6)
C1	C2	C3	C4	175.1(3)
C2	C3	C4	C5	177.8(3)
C3	C4	C5	C6	177.8(3)
C4	C5	C6	C7	-178.9(3)
C5	C6	C7	C8	179.8(3)
C6	C7	C8	C9	-179.7(3)
C7	C8	C9	C10	179.9(3)
C8	C9	C10	C11	-178.8(3)
C9	C10	C11	C12	179.9(3)
C10	C11	C12	C13	179.4(4)
C11	C12	C13	C14	178.3(4)
C12	C13	C14	C15	179.4(4)
C13	C14	C15	C16	179.1(4)
C14	C15	C16	C17	-177.9(5)

Supporting Information to Chapter 4

Table S1. Assignment of resonances in the IR spectra of DAAOHs. Values are given in wavenumbers (cm^{-1}).

Acyl chain length	**C=O stretch (ester)**	**C=O stretch (amide)**	**N-H stretch**	**C-H stretch**	**C-O stretch**	**N-H bending**	**C-H scissoring**	**C-H rocking**
9	~1736	~1638	~3309	~2958-2860	~1050-1265	~1534	~1463	~717
10	~1730	~1637	~3309	~2958-2848	~1073-1259	~1533	~1467	~722
11	~1725	~1648	~3309	~2964-2848	~1018-1232	~1544	~1473	~717
12	~1734	~1640	~3302	~2958-2849	~1038-1268	~1549	~1464	~719
13	~1725	~1648	~3309	~2964-2859	~1013-1260	~1544	~1478	~722
14	~1742	~1638	~3309	~2964-2849	~1046-1260	~1545	~1463	~723
15	~1720	~1643	~3309	~2958-2849	~1019-1271	~1539	~1473	~717
16	~1736	~1638	~3309	~2964-2854	~1052-1260	~1539	~1468	~717
17	~1720	~1637	~3309	~2964-2848	~1046-1226	~1544	~1478	~722
18	~1741	~1625	~3309	~2958-2854	~1023-1254	~1544	~1473	~717

Table S2. ^{1}H-NMR spectral data of DAAOHs in $CDCl_3$ solvent. Chemical shift values are given in ppm (δ scale).

Acyl chain length	CH_3-$(CH_2)_n$	$(CH_2)_n$	$(CH_2)_n$-CH_2-CH_2-CO-O-	CH_2-CO-O-CH_2	O=C-O-CH_aH_b-CH-	-CH-CH_3	-CH-CH_3	NH-CO-CH_2-CH_2	-CH-NH-C=O
9	0.88, t	1.27, m	1.62, m	2.32, t	3.99, dd 4.02, dd	4.12, m	1.16. d	2.16, t	5.75, d
10	0.88, t	1.26, m	1.62, m	2.32, t	3.98, dd 4.01, dd	4.29, m	1.15, d	2.15, t	5.67, d
11	0.84, t	1.22, m	1.58, m	2.28, t	3.98, dd 4.06, dd	4.24, m	1.12, d	2.11, t	5.88, d
12	0.88, t	1.26, m	1.60, m	2.32, t	3.99, dd 4.02, dd	4.28, m	1.16, d	2.16, t	5.82, d
13	0.88, t	1.26, m	1.61, m	2.32, t	4.00, dd 4.12, dd	4.29, m	1.16, d	2.15, t	5.69, d
14	0.88, t	1.26, m	1.61, m	2.32, t	3.99, dd 4.01, dd	4.12, m	1.16, d	2.15, t	5.67, d
15	0.88, t	1.26, m	1.61, m	2.32, t	4.01, dd 4.11, dd	4.28, m	1.16, d	2.17, t	5.85, d
16	0.88, t	1.25, m	1.62, m	2.32, t	4.00, dd 4.12, dd	4.29, m	1.16, d	2.17, t	5.86, d
17	0.90, t	1.27, m	1.62, m	2.34, t	4.01, dd 4.14, dd	4.31, m	1.17, d	2.16, t	5.57, d
18	0.90, t	1.27, m	1.62, m	2.34, t	4.01, dd 4.14, dd	4.31, m	1.17, d	2.18, t	5.75, d

Table S3. ^{13}C-NMR spectral data of DAAOHs in $CDCl_3$ solvent. Chemical shift values are given in ppm (δ scale).

Acyl chain length	**CH_3-$(CH_2)_n$**	**$(CH_2)_n$**	**$(CH_2)_n$-CH_2-CO-O-**	**CH_2-CO-O-CH_2**	**O=C-O-CH_aH_b-CH-**	**-CH-CH_3**	**-CH-CH_3**	**NH-CO-CH_2-CH_2**	**NH-CO-CH_2**
9	14.07	22.63-31.81	34.19	172.77	66.71	44.42	17.39	174.02	36.85
10	14.08	22.65-31.85	34.18	172.70	66.72	44.37	17.40	174.00	36.87
11	14.03	22.62-31.84	34.13	172.67	66.66	44.27	17.31	173.86	36.78
12	14.09	22.66-31.89	34.17	172.83	66.67	44.44	17.36	173.98	36.79
13	14.10	22.68-31.91	34.19	172.73	66.71	44.40	17.39	174.00	36.86
14	14.10	22.68-31.91	34.18	172.67	66.71	44.37	17.40	173.99	36.87
15	14.10	22.68-31.92	34.18	172.87	66.66	44.47	17.35	173.98	36.78
16	14.10	22.69-31.92	34.18	172.88	66.67	44.48	17.36	173.98	36.78
17	14.11	22.69-31.93	34.20	172.64	66.74	44.41	17.43	174.03	36.92
18	14.12	22.70-31.93	34.20	172.88	66.69	44.53	17.38	174.05	36.81

Table S4. ESI-MS data of DAAOHs. Data (m/z values) are given for the molecular ion peaks ($[M+H]^+$, and $[M+Na]^+$).

Acyl chain length	m/z values	assignment
9	356.3173, 378.2990	$[M+H]^+$, $[M+Na]^+$
10	384.3479, 406.3264	$[M+H]^+$, $[M+Na]^+$
11	412.3794, 434.3612	$[M+H]^+$, $[M+Na]^+$
12	440.4103, 462.3910	$[M+H]^+$, $[M+Na]^+$
13	468.4416, 490.4216	$[M+H]^+$, $[M+Na]^+$
14	496.4732, 518.4552	$[M+H]^+$, $[M+Na]^+$
15	524.5047, 546.4860	$[M+H]^+$, $[M+Na]^+$
16	552.5359, 574.5179	$[M+H]^+$, $[M+Na]^+$
17	580.5668, 602.5495	$[M+H]^+$, $[M+Na]^+$
18	608.5982, 630.5812	$[M+H]^+$, $[M+Na]^+$

Supporting Information to Chapter 5

Table S1. Fractional atomic coordinates ($\times 10^4$) and equivalent isotropic displacement parameters ($Å^2 \times 10^3$) of N9SOH. U(eq) is defined as one third of the trace of the orthogonalized Uij tensor. [$U(eq) = \frac{1}{3} \sum_i \sum_j U_{ij} a_{i*} a_{j*} a_i a_j \cos(ai, aj)$].

Atom	X	Y	Z	U (eq)
O1	2848 (3)	3337 (2)	3230 (1)	30.6 (4)
O2	8757 (3)	2972 (2)	4382 (1)	29.2 (4)
O3	9607 (3)	2460 (2)	4591 (1)	26.0 (4)
N1	7410 (3)	2303 (2)	3501 (1)	22.7 (4)
C1	5336 (3)	3419 (3)	3162 (1)	21.5 (4)
C2	6289 (4)	4721 (3)	2683 (1)	23.9 (4)
C3	4122 (4)	7082 (3)	2560 (1)	25.3 (4)
C4	5115 (4)	8226 (3)	2049 (1)	25.8 (4)
C5	2964 (4)	10534 (3)	1885 (1)	26.1 (4)
C6	4021 (4)	11638 (3)	1373 (1)	26.7 (4)
C7	1914 (4)	13959 (3)	1200 (1)	28.0 (5)
C8	2993 (4)	15041 (3)	0691 (1)	32.3 (5)
C9	889 (5)	17360 (4)	521 (1)	41.3 (6)
C10	6906 (4)	894 (3)	3973 (1)	22.3 (4)
C11	9201 (4)	1503 (3)	3936 (1)	24.4 (4)
C12	6853 (4)	2161 (3)	4516 (1)	24.6 (4)

Table S2. Bond lengths and bond angles of N9SOH.

Bond lengths (Å)		**Bond angles (degrees)**	
O1-C1	1.229 (19)	**O1-C1-N1**	122.45 (17)
O2-C11	1.422 (2)	**O1-C1-C2**	122.02 (16)
O3-C12	1.433 (2)	**O2-C11-C10**	110.86 (15)
N1-C1	1.349 (2)	**O3-C12-C10**	110.90 (14)
N1-C10	1.455 (2)	**N1-C1-C2**	115.50 (14)
C1-C2	1.506 (2)	**N1-C10-C11**	108.69 (14)
C2-C3	1.521 (2)	**N1-C10-C12**	110.64 (13)
C3-C4	1.520 (2)	**C1-N1-C10**	123.11 (14)
C4-C5	1.521 (2)	**C1-C2-C3**	114.18 (14)
C5-C6	1.521 (3)	**C2-C3-C4**	111.60 (14)
C6-C7	1.523 (2)	**C3-C4-C5**	114.19 (15)
C7-C8	1.514 (3)	**C4-C5-C6**	112.95 (15)
C8-C9	1.520 (3)	**C5-C6-C7**	114.09 (15)
C10-C11	1.525 (2)	**C6-C7-C8**	113.57 (15)
C10-C12	1.520 (3)	**C7-C8-C9**	113.45 (16)
		C11-C10-C12	112.70 (15)

Table S3. Torsion angles (degrees) for N9SOH.

Atom1	Atom2	Atom3	Atom4	Torsion
O1	C1	N1	C10	0.5 (3)
O1	C1	C2	C3	41.6 (3)
O2	C11	C10	C12	58.5 (2)
O3	C12	C10	C11	57.7 (2)
N1	C1	C2	C3	140.1 (2)
N1	C10	C11	O2	178.5 (2)
N1	C10	C12	O3	-64.2 (2)
C1	N1	C10	C12	107.0 (2)
C1	N1	C10	C11	128.8 (2)
C1	C2	C3	C4	176.0 (2)
C2	C1	N1	C10	177.9 (2)
C2	C3	C4	C5	176.8 (2)
C3	C4	C5	C6	179.9 (2)
C4	C5	C6	C7	179.8 (2)
C5	C6	C7	C8	179.9 (2)
C6	C7	C8	C9	179.8 (2)

Table S4. Fractional atomic coordinates ($\times 10^4$) and equivalent isotropic displacement parameters ($Å^2 \times 10^3$) of N15SOH. U(eq) is defined as one third of the trace of the orthogonalized Uij tensor. [$U(eq) = \frac{1}{3} \sum_i \sum_j U_{ij} a_{i*} a_{j*} a_i a_j \cos(ai, aj)$].

Atom	X	Y	Z	U(eq)
O1	7538(5)	11538(5)	6230.6(8)	89.2(11)
O2	1328(7)	17852(4)	5423.6(8)	83.7(10)
O3	539(5)	12449(5)	5292.9(7)	76.0(9)
N1	2977(6)	12553(5)	6039.9(9)	66.2(10)
C1	5101(7)	11406(6)	6267.8(11)	62.8(11)
C2	4308(7)	10027(7)	6594.1(12)	70.8(12)
C3	6533(7)	7809(7)	6709.8(12)	71.8(12)
C4	5669(7)	6525(7)	7041.5(12)	74.0(12)
C5	7864(7)	4351(7)	7184.4(13)	78.8(13)
C6	6977(7)	3103(7)	7517.9(12)	76.8(13)
C7	9157(8)	936(7)	7667.5(13)	81.9(14)
C8	8221(8)	-293(8)	7997.1(13)	83.8(14)
C9	10385(8)	-2451(8)	8156.0(13)	89.1(15)
C10	9414(8)	-3684(8)	8481.8(13)	91.5(15)
C11	11567(9)	-5813(8)	8646.1(14)	97.8(16)
C12	10605(9)	-7018(9)	8973.7(15)	101.4(16)
C13	12728(10)	-9142(9)	9143.6(16)	108.1(18)
C14	11737(11)	-10334(11)	9465.7(17)	137(2)
C15	13852(12)	-12487(10)	9638.6(18)	156(3)
C16	3312(7)	14028(7)	5718.1(11)	61.0(11)
C17	1036(8)	16354(7)	5733.4(12)	71.2(12)
C18	3275(7)	12802(7)	5348.3(12)	74.6(13)

Table S5. Bond lengths and bond angles of N15SOH.

Bond lengths (Å)		**Bond angles (degrees)**	
O1-C1	1.225(4)	**O1-C1-N1**	122.9(4)
O2-C17	1.420(4)	**O1-C1-C2**	121.2(3)
O3-C18	1.433(4)	**O2-C17-C16**	110.8(3)
N1-C1	1.326(4)	**O3-C18-C16**	110.3(3)
N1-C16	1.449(4)	**N1-C1-C2**	115.9(3)
C1-C2	1.505(5)	**N1-C16-17**	109.4(3)
C2-C3	1.495(5)	**N1-C16-C18**	110.6(3)
C3-C4	1.500(5)	**C1-N1-C16**	123.8(3)
C4-C5	1.498(5)	**C1-C2-C3**	115.7(3)
C5-C6	1.498(5)	**C2-C3-C4**	113.7(3)
C6-C7	1.500(5)	**C3-C4-C5**	116.4(3)
C7-C8	1.491(5)	**C4-C5-C6**	115.7(3)
C8-C9	1.504(5)	**C5-C6-C7**	116.5(3)
C9-C10	1.490(5)	**C6-C7-C8**	115.6(3)
C10-C11	1.498(5)	**C7-C8-C9**	116.6(3)
C11-C12	1.484(6)	**C8-C9-C10**	116.1(3)
C12-C13	1.496(5)	**C9-C10-C11**	116.6(3)
C13-C14	1.471(6)	**C10-C11-C12**	116.4(3)
C14-C15	1.510(6)	**C11-C12-C13**	117.3(4)
C16-C17	1.505(5)	**C12-C13-C14**	116.7(4)
C17-C18	1.512(5)	**C13-C14-C15**	117.3(4)
		C17-C16-C18	112.5(3)

Table S6. Torsion angles (degrees) for N15SOH.

Atom1	Atom2	Atom3	Atom4	Torsion
O1	C1	N1	C16	1.7 (569)
O1	C1	C2	C3	-37.0 (517)
O2	C17	C16	C18	-57.4 (427)
O3	C18	C16	C17	-57.9 (416)
N1	C1	C2	C3	146.5 (346)
N1	C16	C17	O2	179.3 (299)
N1	C16	C18	O3	64.8 (391)
C1	N1	C16	C18	104.6 (399)
C1	N1	C16	C17	-131.0 (366)
C1	C2	C3	C4	178.7 (326)
C2	C1	N1	C16	178.1 (325)
C2	C3	C4	C5	-176.9 (338)
C3	C4	C5	C6	179.4 (340)
C4	C5	C6	C7	-179.4 (346)
C5	C6	C7	C8	-179.4 (357)
C6	C7	C8	C9	-179.1 (363)
C7	C8	C9	C10	-179.2 (376)
C8	C9	C10	C11	-179.1 (384)
C9	C10	C11	C12	179.2 (401)
C10	C11	C12	C13	-179.7 (420)
C11	C12	C13	C14	-179.4 (460)
C12	C13	C14	C15	179.7 (481)

Curriculum Vitae

Suman Kumar Choudhury

School of Chemistry
University of Hyderabad
Hyderabad- 500046
Email: Sumankumar3394@gmail.com

Suman Kumar Choudhury was born in Rangiamunda village [Tangarpali (Block), Sundargarh (Dist.), Odisha, India] on 3rd March 1994. After finishing high school in Saraswati Sishu Vidya Mandir, Sundargarh, he completed his intermediate (XI & XII) in 2011 from Gayatri +2 Science College, Bhubaneswar. Then he finished his B.Sc degree [Chemistry (Hons), Physics, and Mathematics] in 2014 from Ispat Autonomous College, Rourkela, Sundargarh (Dist). He completed his M.Sc degree (Chemistry) in 2017 from the Central University of Karnataka, Gulbarga (Dist). After that, he joined the Ph.D. program under the supervision of Prof. Musti J. Swamy at the School of Chemistry, University of Hyderabad in 2018. His major research focus is on "**Physiochemical Studies on Amphiphilic Conjugates of Amino Alcohols**".

List of Publication

1. **Choudhury, S. K.,** Sivaramakrishna, D., Ravindar C., Swamy, M. J.* (2024) Biophysical characterization of long chain *O*-acyl-β-alaninols and equimolar *O*-myristoyl-β-alaninol/sodium dodecyl sulfate complex, ***Colloids Surfaces A: Physicochem. Eng. Aspects*.** 133483.

2. **Choudhury, S. K.**[$]**,** Sivaramakrishna, D.[$], Swamy, M. J.* (2023) Structure and supramolecular organization of *N*-acylserinols: agonists of the G-protein coupled receptor, GPR-119. ***J. Chem. Sci.*** 135, 1-9. ([$]These authors contributed equally)

3. Sivaramakrishna, D.; **Choudhury, S. K.;** Swamy, M. J.* (2021) Thermotropic phase behavior and supramolecular organization of *N*, *O*-diacyl-L-alaninols: effect on stratum corneum model membrane, ***J. Chem. Sci.*** 133, 91.

4. Sivaramakrishna, D., **Choudhury, S. K.**, Kumar, C. S. and Swamy, M. J.* (2021) Structure, thermotropic phase behavior and membrane interaction of N-acyl-β-alaninols. Homologs of stress-combating N-acylethanolamines. ***Chem. Phys. Lipids*** 236, 105056.

5. Ravindar C., Sivaramakrishna D., **Choudhury S. K.,** Manasa K., Cheppali S. K., Swamy M. J.* (2024) Structure, self-assembly, and phase behavior of neuroactive N-acyl GABAs: Doxorubicin encapsulation in NPGABA/DPPC liposomes and release studies, ***Langmuir*** **(Accepted for publication)**

6. **Choudhury, S. K.,** Manasa, K., Swamy, M. J.*, Long chain *O*-acyl-L-alaninols: Synthesis, biophysical characterization and formation of equimolar catanionic liposomes with sodium dodecyl sulfate. **(Manuscript under preparation)**

7. Choudhury S. K., Sivaramakrishna D., Swamy M. J.*, Cholesterol interaction with isomeric chiral and achiral N-acyl alaninols. Impact on thermotropic phase behavior, fluidity, and niosomes. (**Manuscript under preparation)**

8. Choudhury S. K., Manasa K., Swamy M. J.*, Structure, synthesis, biophysical characterization and application of N-acyl neurotransmitters: A review. (**Manuscript under preparation)**

Presentation in Symposia and Conferences

1. Poster presentation at **"International Conference on Frontier Area of Science and Technology (ICFACT-2022)",** 12th India-Japan Science and Technology Seminar organized by Indian JSPS Alumni Association (IJAA), University of Hyderabad, Hyderabad.

2. Oral presentation at **"CHEMFEST-2023"** Annual in-house Symposium, organized by School of Chemistry, University of Hyderabad, Hyderabad.

3. Poster presentations at **"CHEMFEST-2020 and 2023"** organized by School of Chemistry, University of Hyderabad, Hyderabad.

Colloids and Surfaces A: Physicochemical and Engineering Aspects 687 (2024) 133483

Contents lists available at ScienceDirect

Colloids and Surfaces A: Physicochemical and Engineering Aspects

journal homepage: www.elsevier.com/locate/colsurfa

Biophysical characterization of long chain *O*-acyl-β-alaninols and equimolar *O*-myristoyl-β-alaninol/sodium dodecyl sulfate complex

Suman Kumar Choudhury, Dokku Sivaramakrishna, Chinapaka Ravindar, Musti J. Swamy *,1

School of Chemistry, University of Hyderabad, Hyderabad 500 046, India

HIGHLIGHTS

- *O*-Acyl-β-alaninols (OABAOHs) inhibit *N*-acylethanolamine hydrolyzing acid amidase (NAAA).
- Biophysical and structural studies were carried out on long-chain OABAOHs.
- Phase transition enthalpy and entropy of OABAOHs exhibit odd-even alternation.
- The odd-even alternation originates from differences in crystal packing.
- Equimolar mixtures of OMBAOH and SDS form catanionic liposomes.

GRAPHICAL ABSTRACT

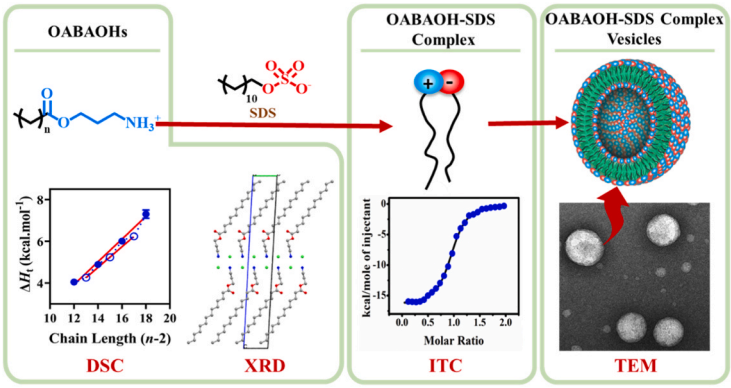

ARTICLE INFO

Keywords:
O-acyl-β-alaninol
Critical micellar concentration
Differential scanning calorimetry
X-ray diffraction
Tilted bilayer
Odd-even alternation

ABSTRACT

O-Acyl-β-alaninols (OABAOHs) are interesting amphiphiles in view of their ability to strongly inhibit *N*-acylethanolamine hydrolyzing acid amidase. In the present work, we synthesized and characterized long-chain OABAOHs bearing 14–20 C atoms in the acyl chain. Differential scanning calorimetric (DSC) studies showed that OABAOHs exhibit odd-even alternation in the solid-liquid phase transition enthalpies (ΔH_t) and entropies (ΔS_t). However, the odd- and even- chain length series independently showed linear dependence on the chain length (n) and values for the even chain length series are slightly higher than for the odd chain length series. Such odd-even alternation was not observed upon hydration, although ΔH_t and ΔS_t exhibited linear dependence on the chain length. Crystal structures of *O*-myristoyl-β-alaninol and *O*-palmitoyl-β-alaninol have been solved in triclinic crystal system with P-1 space group. In both structures, hydrocarbon chains of the amphiphiles are organized in a tail-to-tail format in a tilted bilayer. Powder X-ray diffraction data revealed odd-even alternation

Abbreviations: ΔG_b, Gibbs free energy of binding; ΔH_o, end contribution to transition enthalpy; ΔH_b, enthalpy of binding; ΔH_{inc}, incremental contribution of each CH_2 group to transition enthalpy; ΔH_t, transition enthalpy; ΔS_o, end contribution to transition entropy; ΔS_b, entropy of binding; ΔS_{inc}, incremental contribution of each CH_2 group to transition entropy; ^{13}C NMR, carbon-13 nuclear magnetic resonance; ^1H NMR, proton nuclear magnetic resonance; Boc, tert-butyloxycarbonyl; CMC, critical micellar concentration; DCC, *N,N'*-dicyclohexylcarbodiimide; DCM, dichloromethane; DLS, dynamic light scattering; DMAP, 4-dimethylaminopyridine; DNA, deoxyribonucleic acid; DSC, differential scanning calorimetry; ESI-MS, electrospray ionisation mass spectrometry; FTIR, Fourier transform infrared.

* Corresponding author.
E-mail address: mjswamy@uohyd.ac.in (M.J. Swamy).
[1] Website: http://www.uohyd.ac.in.

https://doi.org/10.1016/j.colsurfa.2024.133483
Received 5 January 2024; Received in revised form 4 February 2024; Accepted 13 February 2024
Available online 15 February 2024

in the *d*-spacings of all OABAOHs, suggesting that the odd-even alternation observed in the thermodynamic properties most likely originates from differences in the crystal packing. A number of C-H···O and N-H···Cl hydrogen bonds between OABAOH molecules from adjacent and opposite layers stabilize the overall supramolecular organization of the self-assembled bilayer system. In aqueous solution, turbidimetric and isothermal titration calorimetric studies established that *O*-myristoyl-β-alaninol and sodium dodecyl sulfate form an equimolar complex. Transmission electron microscopic, dynamic light scattering and DSC studies indicate that the complex forms unilamellar liposomes of ~150–160 nm diameter, which undergo a sharp thermotropic phase transition. These results provide a thermodynamic and structural basis for further investigations on OABAOHs including biomedical applications, e.g. in developing liposomal drug-delivery systems.

1. Introduction

3-Amino-1-propanol, or β-alaninol, is a compound derived by the reduction of β-alanine, a nonessential amino acid present in carnosine (a dipeptide of β-alanine and L-histidine). Supplementation of β-alaninol to *Tetrahymena* (a model organism used in biomedical research) led to the formation of phosphatidylpropanolamine and reduction of other phospholipids [1,2]. Studies show that the *O*-acyl derivatives of β-alaninol, i.e., *O*-acyl-β-alaninols (OABAOHs), are potent inhibitors of *N*-acylethanolamine-hydrolyzing acid amidase (NAAA), which play a central role in the degradation of endogenous lipid mediators like *N*-acylethanolamines (NAEs) [3,4]. Several derivatives (polymeric, dendritic, etc) of β-alaninol have been employed as drug carriers, as non-viral gene carriers to treat brain tumours, and as antimicrobial agents [5–7].

Phospholipids form vesicular structures, and when they are kept for a long time, their metastable nature and thermodynamic instability often lead to precipitation as solid aggregates [8,9]. Conversely, the spontaneous formation of thermodynamically stable vesicles is observed in aqueous dispersions of mixed cationic and anionic single-chain lipids with simple structures [9–14]. This phenomenon was observed across various single-tailed charged lipids and mixtures of cationic and anionic amphiphiles, which are also referred to as ion pair amphiphiles (IPA) or catanionic systems [11,15,16]. Mixing aqueous solutions of cationic and anionic amphiphiles can result in spontaneous formation of catanionic vesicles, and these vesicles exhibit enhanced stability and improved efficiency in drug encapsulation compared to other types of vesicles. This is evidenced by numerous reports underscoring the versatility and promise of catanionic surfactant mixtures for various applications [17–22]. Notably, these mixtures have demonstrated efficacy in diverse areas, including membrane applications, drug delivery, detergents, foaming processes, emulsions, wetting and others [19,23–28].

OABAOHs are structural isomers of *N*-acyl-β-alaninols (NABAOHs) and share structural similarity with *O*-acylethanolamines (OAEs) [29,30]. While NABAOHs are non-ionic and contain an amide linkage, OABAOHs are cationic under physiological conditions and contain an ester linkage (see Fig. 1 for representative structures of these compound classes). Cationic lipids have been recognized as highly versatile agents in drug delivery, particularly for transporting DNA and RNA in therapeutic applications as interaction of the positively charged head groups of cationic lipids with the negatively charged phosphate groups of nucleic acids results in the formation of condensed complexes [31–33]. The length and composition of the aliphatic chain in these amphiphiles can impact the fluidity of the hydrophobic region of the assembly [34–36]. Transfection efficiency, biodegradability, stability, and cytotoxicity of cationic lipids depend on the length, number, type, and relative alignment of the linker group that joins the polar head group and the hydrophobic tail [37–39].

The foregoing shows that OABAOHs represent a novel family of amphiphiles with application potential in creating drug formulations and delivery systems. Direct interaction of these amphiphiles with membrane proteins may also affect their conformation and dynamics. Additionally, the ester linkage is base labile and can result in *O*- to *N*-acyl migration of the hydrocarbon chain, which could be used to design base labile nanocarriers for drug delivery applications [34,35]. Cationic lipids can also interact with anionic lipids and form catanionic mixed lipid systems which exhibit high stability and versatile physicochemical properties [40,41]. In this context, it is imperative to conduct systematic investigations on their self-assembly, phase transition characteristics, molecular structure and supramolecular organization and the knowledge obtained from such studies will be highly useful in designing lipid-based drug delivery systems employing these amphiphiles. In this direction, in the present study, we have synthesized a homologous series of *O*-acyl-β-alaninols (n = 14–20) bearing saturated acyl chains and characterized their self-assembly, supramolecular organization and phase behavior using various spectroscopic, calorimetric and crystallographic techniques. Additionally, complex formation between *O*-myristoyl-β-alaninol with sodium dodecyl sulphate was investigated and the catanionic liposomes formed by the complex were characterized with respect to size, stability and polydispersity. The results obtained are discussed in this manuscript.

2. Materials and methods

2.1. Materials

Fatty acids, *N,N′*-dicyclohexylcarbodiimide (DCC), 4-dimethylaminopyridine (DMAP) and sodium dodecyl sulphate (SDS) were purchased from Sigma Aldrich (India). 3-(Tert-butoxycarbonylamino)−1-propanol was purchased from TCI Chemicals (India). 1,4-Dioxane, dichloromethane (DCM), chloroform and tetrahydrofuran (THF) were purchased from Sisco Research Laboratories (India). All other chemicals

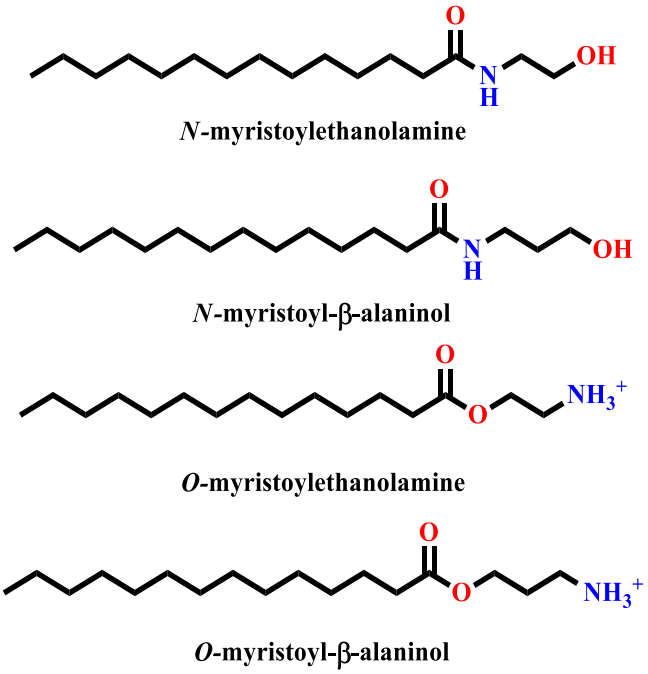

Fig. 1. Molecular structures of *N*-myristoylethanolamine, *N*-myristoyl-β-alaninol, *O*-myristoylethanolamine and *O*-myristoyl-β-alaninol.

and solvents required were obtained from local vendors and were of the highest purity available. Milli-Q water was used for preparing buffers and other aqueous solutions.

2.2. Synthesis of O-acyl-β-alaninols

DCC (5.5 mmol), DMAP (1 mmol) and fatty acid of appropriate chain length (5 mmol) were dissolved in anhydrous DCM or chloroform. For reactions with C14-C16 fatty acids DCM was used as the solvent, whereas chloroform was used in reactions involving fatty acids bearing 17–20 C-atoms. After stirring for about 10 minutes, a solution of 3-(tert-butoxycarbonylamino)−1-propanol in THF (5 mmol) was added to the reaction mixture. The reaction mixture was kept under reflux with stirring for 5 hours at 40°C and 60°C for compounds bearing acyl chains with 14–16 and 17–20 C-atoms, respectively. The mixture was then cooled, filtered through celite, and concentrated to yield a transparent oil that was purified using flash column chromatography. N-Boc protected *O*-acyl-β-alaninols were then deprotected using 4 M HCl in 1,4-dioxane for 30 minutes affording white coloured hydrochlorides of *O*-acyl-β-alaninols. The final product was refined through two recrystallizations at −18°C from DCM and chloroform for compounds with acyl chains bearing 14–16 and 17–20 C-atoms, respectively. The purified products were characterized by Fourier transform infrared (FTIR), ^{1}H NMR, and ^{13}C NMR spectroscopy and high-resolution mass spectrometry (HRMS) Scheme 1.

2.3. Isothermal titration calorimetry

Critical micellar concentrations (CMC) of OABAOHs were determined by isothermal titration calorimetry. Experiments were carried out on a MicroCal PEAQ-ITC from Malvern Instruments (Worcestershire, United Kingdom). In order to calculate the CMC of OABAOHs (C14–C16), small aliquots of the surfactant were injected into the water from a 5–25 mM stock solution. A gap of 150 seconds was given between successive injections, with each 1.5 μL injection taking place over 3 sec. Throughout the titration, the solution in the reaction cell was constantly stirred at a rate of 750 rpm. As previously mentioned, an abrupt shift in enthalpy (ΔH_i) brought on by the injections was observed and used to calculate the CMC [30,42]. The first injection was usually found to be inaccurate, so the resulting point was eliminated before the rest of the data was analyzed to a "dissociation" model using the MicroCal PEAQ-ITC Analyser software provided by the ITC manufacturer.

The interaction between SDS and *O*-myristoyl-β-alaninol (OMBAOH) was investigated by ITC in the following manner. A 0.5 mM solution of OMBAOH in water was prepared. Using a rotating stirrer syringe, 1.5 μL aliquots of the solution were added sequentially to a sample cell containing 280 μL of a 50 μM aqueous solution of SDS. Concentrations of the cationic and anionic amphiphiles were kept well below their respective CMCs [43]. Each injection was performed over a period of 3 seconds, and a time gap of 150 seconds was maintained between successive injections. Throughout the titration, the reaction cell contents were continuously stirred at a speed of 750 rpm. To address the potential inaccuracy of the first injection, a preliminary 1 μL injection was made, and the corresponding data point was excluded from the analysis. The remaining data were analyzed using the MicroCal PEAQ-ITC Analyser provided by MicroCal, as previously described [42]. The analysis allowed the determination of the stoichiometry of binding (n), binding constant (K_b), and enthalpy of binding (ΔH_b). Additionally, based on these values, the free energy of binding (ΔG_b) and entropy of binding (ΔS_b) were calculated using the fundamental thermodynamic Eqs. (1) and (2).

$$\Delta G_b = -RT \ln K_b \quad (1)$$

$$\Delta G_b = \Delta H_b - T\Delta S_b \quad (2)$$

.

2.4. Fluorescence spectroscopy

The CMCs of OABAOHs were also determined by fluorescence spectroscopy using pyrene as the fluorescent probe. A Horiba Jobin-Yvon Fluoromax-4 spectrofluorometer was used for the fluorescence measurements. In these experiments, small aliquots of OABAOHs from a 5–25 mM stock solution were added to a 1.0 mL solution of 2 μM pyrene. The fluorescence spectra were recorded between 350 and 500 nm keeping the excitation wavelength at 335 nm. The scan rate was set at 200 nm/min and 2.5 nm slits were used on both excitation and emission monochromators. The emission spectrum of the pyrene monomer displays five bands [44]. Intensity ratio of bands one and three in the emission spectrum of pyrene (I_1/I_3), also known as the polarity ratio, was calculated for each spectrum and plotted as a function of amphiphile concentration. The concentration at which a clear break in the slope was observed was taken as the CMC.

2.5. Turbidimetry

The interaction between OMBAOH and SDS was also studied by turbidimetry using a JASCO V-750 UV-Vis spectrophotometer. Aqueous solutions of OMBAOH and SDS, each with a concentration of 0.2 mM (which is well below their critical micellar concentration), were mixed in various proportions and incubated for 30 minutes. The resulting turbidity was analysed at room temperature by measuring the optical density (OD) between 320 and 450 nm. Data was collected at a scanrate of 200 nm/min. The turbidity at 340 nm was selected for subsequent analysis.

2.6. Differential scanning calorimetry

A DSC-250 differential scanning calorimeter from TA instruments (New Castle, Delaware, USA) was used for studies on dry (solid) samples. Thermograms were collected between 25°C and 120°C with a scan rate of 2°/min by taking 2–3 mg of each sample in an aluminum sample pan, whereas the reference pan was prepared without any sample [29]. For each sample, three heating and two cooling scans were recorded in alternate heating and cooling cycles. All heating scans were reproducible with only minor decreases in the enthalpies in the second and third heating scans. Therefore, the first thermal scans were taken for further analysis.

For studies with hydrated samples, a lipid film was prepared on the inner walls of a test tube using 2–5 mg of each OABAOH dissolved in dichloromethane/methanol (1:1, v/v) followed by slow evaporation of the solvent and vacuum desiccation for several hours. The film was then hydrated with 1 mL of 150 mM NaCl and put through 5–6 freeze-thaw cycles. A Nano-DSC differential scanning calorimeter from TA instruments (New Castle, Delaware, USA) was used to perform DSC studies on these samples. The sample compartment was filled with 0.3 mL of the lipid suspension and the reference cell was filled with 150 mM NaCl.

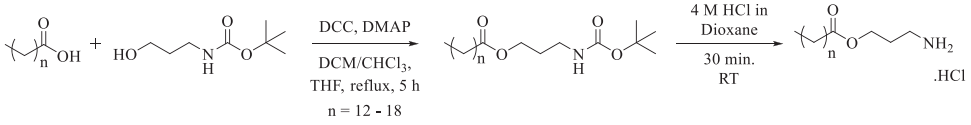

Scheme 1. Synthesis of *O*-acyl-β-alaninols.

Three heating and two cooling thermograms were recorded for each sample between 0 and 100°C at a scan rate of 60°/h. Although the temperature and enthalpy of the major transition peak are reproducible in repeat scans, the minor transition peaks were not seen in the subsequent heating cycles. Therefore, the second heating thermogram was considered for further analysis.

DSC measurements on hydrated OMBAOH-SDS equimolar catanionic mixtures were also performed by preparing a thin film of the sample on the inner walls of a test tube by evaporation from a solution in dichloromethane/methanol (1:1, v/v) and hydrating it with water to yield 10 mM concentration each of OMBAOH and SDS (20 mM total surfactant concentration). The sample was then subjected to a couple of freeze-thaw cycles (heating to ~60 °C) after which it was loaded into the DSC sample cell. Each sample was subjected to three heating and two cooling scans. Data obtained from repeat scans were found to be essentially identical and data obtained from the first heating scan were used for further analysis.

For all DSC experiments, peak area under the transition curve was integrated to obtain the enthalpy of the phase transition (ΔH_t) and peak point of the transition curve was taken as the transition temperature (T_t). Transition entropy (ΔS_t) values were derived from transition enthalpy and transition temperature under the assumption of a first-order transition [45]:

$$\Delta S_t = \Delta H_t / T_t \quad (3)$$

where T_t, ΔH_t and ΔS_t refer to the transition temperature, enthalpy and entropy, respectively.

2.7. Crystallization, structure solution and refinement

Thin plate type, colourless single crystals of OMBAOH and *O*-palmitoyl-β-alaninol (OPBAOH) were grown at room temperature from dichloromethane containing trace amounts of methanol. X-ray diffraction data was collected at room temperature (~293 K) on a Xtlab Synergy Rigaku Oxford diffractometer with HyPix – 3000 detector, equipped with a graphite monochromator giving Mo Kα radiation (λ =0.7107 Å). The 2θ range for data collection was 2–25° for both samples. CrysAlisPro, Xtlab Synergy Rigaku Oxford Diffraction, Version 171.39.exe, and absorption correction based on the multi-scan approach were used to analyze the data interpretations. Olex2–1.2 programme was used to solve and refine the crystal structures. Both structures were solved in P-1 space group in the triclinic crystal system. For OMBAOH the refinement was carried out using 3500 observed [>2σ (F0)] reflections, which converged into final $R_1 = 0.1262$, w$R_2 = 0.3742$ and goodness of fit = 1.065. For OPBAOH the refinement was carried out using 7677 observed [>2σ (F0)] reflections, which converged into final $R_1 = 0.1295$, w$R_2 = 0.3317$ and goodness of fit = 1.086.

2.8. Powder X-ray diffraction studies

Powder X-ray diffraction (PXRD) patterns of all OABAOHs (C14-C20) were captured using a Bruker SMART D8 Advance powder X-ray diffractometer (Bruker-AXS, Karlsruhe, Germany) with Cu-K radiation (λ = 1.5406 Å) at 40 kV and 30 mA as described earlier [46]. The circular spinning disk of the instrument sample holder was loaded with fine powders of the OABAOHs. A LynxEye PSD data collector was used to record diffraction patterns at room temperature over a 2θ range of 5–50° with a step size of 0.0198° and a measurement duration of 1.5 s for each step. *d*-Spacings were determined using Bragg's equation from the diffraction peaks.

2.9. Dynamic light scattering

Dynamic light scattering (DLS) experiments were conducted to investigate the particle size and stability of catanionic vesicles made up of OMBAOH and SDS, prepared as described in Section 2.5, with minor modifications as indicated below. The lipid film containing the two amphiphiles in equimolar ratio was hydrated with water, sonicated in a bath sonicator at room temperature (~25 °C) for ~2 minutes, and then incubated at 10 °C for 12 hours to facilitate vesicle formation.

For DLS measurements, the samples were taken in a 1 mL quartz cuvette and placed securely in the sample chamber of a Horiba SZ-100 nanoparticle analyser [41]. Multiple measurements were performed for each sample, and average values from three independent measurements are reported. The acquired data were analyzed using the built-in software of the instrument, which utilizes autocorrelation analysis to determine the particle size distribution and polydispersity index (PDI) of the vesicles. To ensure the reliability of the results, the entire experiment was repeated with different batches of OMBAOH–SDS catanionic vesicles, and the measurements were found to be consistent and reproducible.

2.10. Transmission electron microscopy

The morphology of OMBAOH-SDS vesicles was investigated using transmission electron microscopy (TEM) with the aid of a JEOL JEM-F200/F2 multipurpose electron microscope [41]. A 0.5 mM catanionic vesicle suspension was prepared for TEM analysis following the same procedure as described above for DLS studies. A microsyringe was employed to load a 5–10 μL sample volume onto a carbon-coated copper grid, and any excess solution was removed by blotting with filter paper. Subsequently, the sample on the grid was air-dried, and a stratified layer of 1.0% uranyl acetate solution was applied. Excess solution was removed with the aid of a blotting paper. The samples were then allowed to dry at room temperature (~25 °C) for a few minutes before examination by TEM.

3. Results and discussion

3.1. Synthesis and characterization of OABAOHs

In the current study, a homologous series of OABAOHs have been synthesized by condensation of 3-(tert-butoxycarbonylamino)−1-propanol with fatty acids bearing saturated acyl chains (with 14–20 C atoms), followed by deprotection with the help of 4 M HCl in 1,4-dioxane. The structure and purity of the products obtained were characterized by FTIR, ^{1}H NMR and ^{13}C NMR spectroscopy and HRMS and representative spectra corresponding to OMBAOH are shown in Figs. S1-S4. Additionally, the FTIR, ^{1}H NMR and ^{13}C NMR spectra of the remaining OABAOHs are given in Figs. S7-S24. The spectral data are also presented in Tables S1-S4 and details of the spectral analysis for the entire homologous series are given in the supporting information. The spectral data are fully consistent with the molecular structures of the OABAOHs bearing different acyl chains and confirm that all the compounds synthesized in this study are highly pure.

3.2. Critical micellar concentration of OABAOHs

To determine the CMCs of OABAOHs (C14-C16) from ITC measurements, change in the enthalpy is monitored when each OABAOH was added from a stock solution (5–25 mM concentration) to water. The top panel of Fig. 2A shows an ITC profile depicting the heat changes caused by the injection of small amounts of OMBAOH from a 25 mM stock solution. Fig. 2B shows a plot of incremental heat changes as a function of surfactant concentration. The heat changes decrease gradually for successive injections, but display a steep decrease after about 7–8 injections, and after another 4–5 injections the heat changes again become gradual. Since this is a thermodynamically favourable process, the endothermic changes must be accompanied by positive entropy changes, which most likely result from the disruption of water structure around the micelles [30,47]. The steep drop in the peak height observed

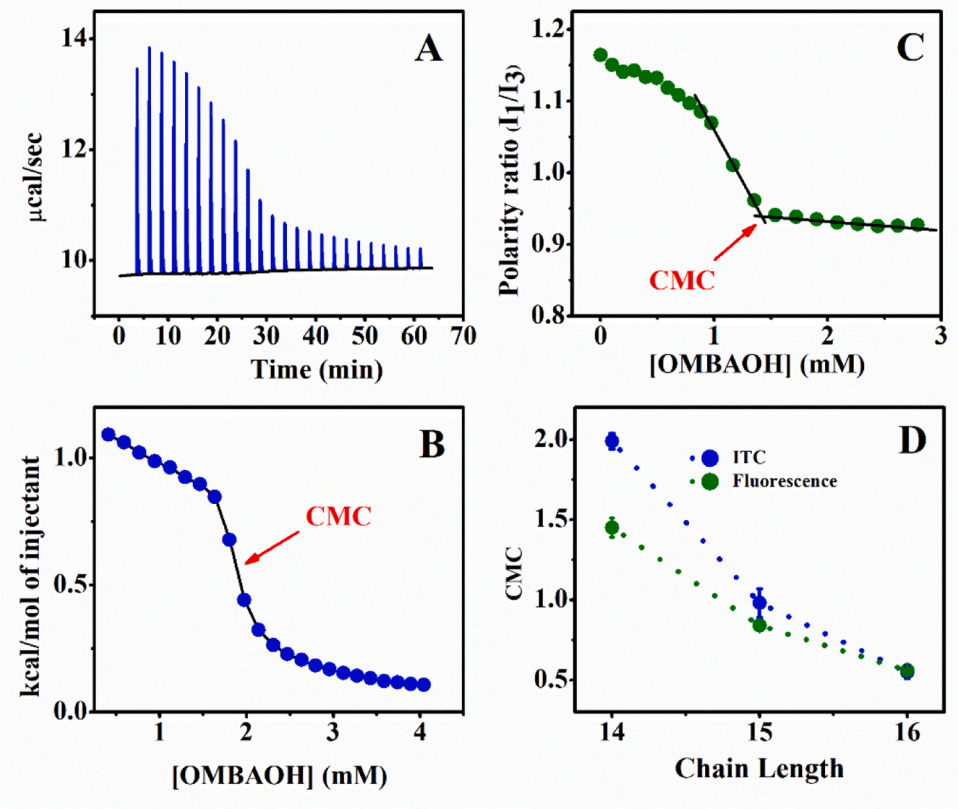

Fig. 2. Determination of the CMC of OMBAOH. (**A**) ITC profile obtained when aliquots were injected from a concentrated OMBAOH solution into water. (**B**) Integrated heats of dilution from the raw data shown in **A**. The CMC is obtained as 2.0 (±0.1) mM from the midpoint of the steeply decreasing part of the ΔH_i *vs* [OMBAOH] plot shown in **B**. (**C**) Determination of CMC by fluorescence spectroscopy using pyrene as a probe. The plot depicts the variation of the pyrene polarity ratio as a function of added OMBAOH concentration. The CMC is determined as 1.5 (±0.1) mM from the intercept of two linear fits. (**D**) Chain-length dependence of CMC.

in the middle of the titration indicates that the surfactant concentration in the reaction cell exceeded the CMC and that the micelles added subsequently to the reaction cell do not dissociate further. Therefore, the only cause of the enthalpy shift above the CMC is the effects of micelle dilution. From the inflection point in the ΔH_i versus lipid concentration plots, the CMC of OMBAOH, OPDBAOH, and OPBAOH was calculated as 2.0 (±0.1) mM, 1.0 (±0.1) mM, and 0.55 (±0.04) mM, respectively.

Fluorescence spectroscopy was also used to estimate the CMC of OABAOHs by following changes in the fluorescence emission properties of pyrene probe when the concentration of the amphiphiles is altered [48]. The polarity ratio of the probe showed a steady decrease when the OABAOH concentration in solution was increased, but showed a steep change in the slope at a particular point. The CMC was calculated from the intercept of the linear least squares fits of the two sections of such plots. Such a plot for the determination of CMC of OMBAOH is shown in Fig. 2C. The CMC values obtained by this approach for OMBAOH, *O*-pentadecanoyl-β-alaninol (OPDBAOH) and OPBAOH are 1.5 (±0.1) mM, 0.84 (±0.02) mM and 0.56 (±0.01) mM, respectively. While the values for C14 and C15 compounds show 20–25% variation with the CMC values obtained from the ITC studies, the values obtained for C16 compound by both methods are nearly identical (Fig. 2D). Similar observations were made in earlier studies where ITC and fluorescence techniques were employed for estimating the CMC of other amphiphiles [40,41].

3.3. DSC of dry and hydrated OABAOHs

First heating thermograms for dry OABAOHs with even and odd numbers of C-atoms in the acyl chain are shown in Figs. 3A and 3B, respectively. Each thermogram displays a prominent transition peak corresponding to the capillary melting point of the compound. In addition, one or two minor transitions are seen before the major transition peak and these can be interpreted as arising from solid−solid transitions, indicating polymorphism. In most cases these minor transitions were reproduced in repeat scans. Similar minor transitions have also been observed in other homologous series of single-chain amphiphiles such as *N*-acylethanolamines (NAEs) and *N*-acyl-β-alaninols (NABAOHs) [29,49]. In the case of NAEs, the crystal structures of two different polymorphs of *N*-palmitoylethanolamine were solved and it was shown that a simple 180° rotation of a lipid layer in one polymorph could yield the other polymorph [50]. It is possible that the minor transitions observed in OABAOHs also arise due to the presence of different polymorphic structures in the solid state. Thermograms that are essentially indistinguishable were obtained in the second and third heating scans. Thus, data obtained from the initial heating scans were selected for further analysis, and the transition temperature (T_t), transition enthalpy (ΔH_t) and transition entropy (ΔS_t) values are presented in Table S5.

In a previous study it was shown that the presence of salt, such as NaCl stabilizes the lamellar structure of *O*-stearoylethanolamine even at elevated temperatures [36]. To investigate the effect of salt on the phase transitions of OABAOHs, we hydrated OABAOHs with 150 mM NaCl and carried out DSC studies on them. The thermograms obtained with the even and odd chain-length compounds are shown in Figs. 3C and 3D, respectively. The values of transition temperature, transition enthalpy and transition entropy for hydrated OABAOHs, obtained from analyzing the DSC thermograms, are presented in Table S5.

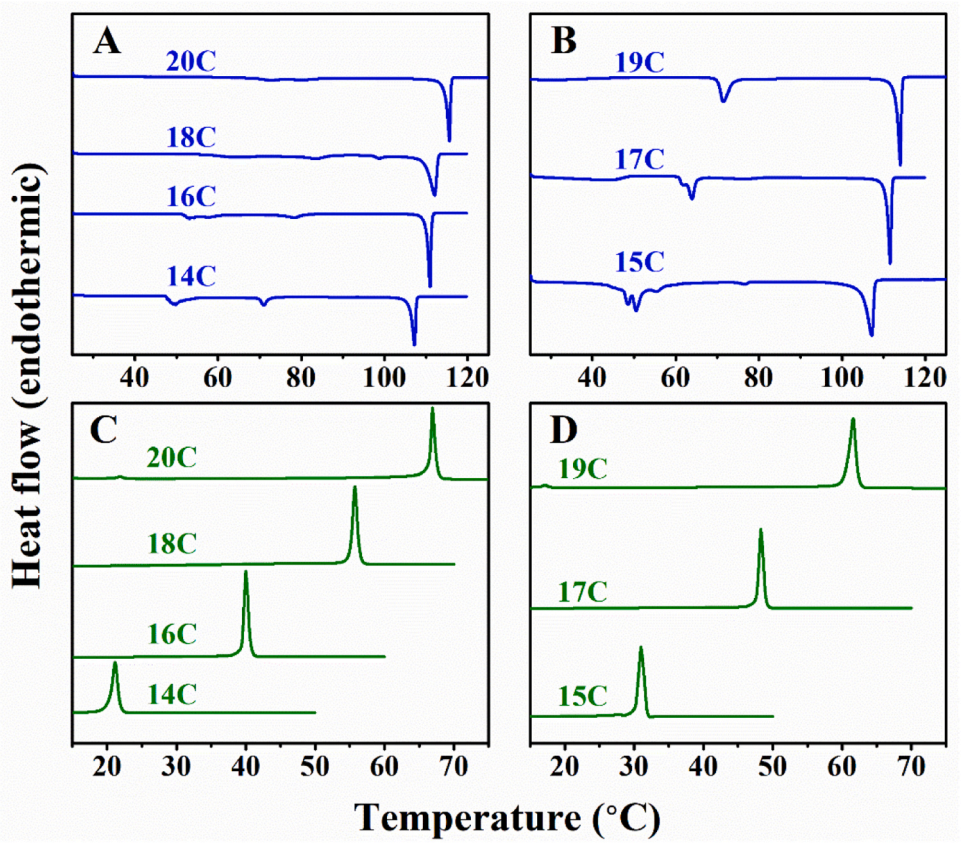

Fig. 3. DSC thermograms of dry and hydrated OABAOHs. (**A**, **B**) dry samples; (**C**, **D**) hydrated samples. The left panels (**A**, **C**) correspond to compounds with an even number of C atoms in the acyl chains, and the right panels (**B**, **D**) correspond to those with an odd number of C atoms. The number of carbon atoms in the acyl chain is indicated against each thermogram.

3.4. Chain length dependence of transition enthalpy and entropy

Figs. 4A and 4B present the relationship between acyl chain length of the OABAOHs in the solid state and the transition enthalpy (ΔH_t) and transition entropy (ΔS_t), respectively. The corresponding plots for the hydrated samples are shown in Figs. 4C and 4D, respectively. For solid OABAOHs, a linear dependence of ΔH_t and ΔS_t on the chain length is independently seen for the even and odd acyl chain length compounds, with the enthalpy and entropy values for the odd acyl chain length compounds being slightly lower than those for the even acyl chain length ones. Thus, when the data obtained for the entire series are examined together, a zig-zag pattern is observed. On the other hand, for the hydrated samples a linear dependence was observed for the transition enthalpies and entropies for the entire chain length series. The chain length dependent ΔH_t and ΔS_t values could be fit to expressions 4 and 5, respectively [51]:

$$\Delta H_t = \Delta H_o + (n-2)\,\Delta H_{inc} \quad (4)$$

$$\Delta S_t = \Delta S_o + (n-2)\,\Delta S_{inc} \quad (5)$$

where ΔH_o and ΔS_o are the end contributions to ΔH_t and ΔS_t resulting from the terminal methyl group and the polar component of the molecule, and n is the number of C atoms in the acyl chains. The average incremental contributions of each CH_2 group to the overall ΔH_t and ΔS_t are ΔH_{inc} and ΔS_{inc}, respectively. It was previously noted that the transition enthalpies and entropies of several homologous series of single/double chain amphiphiles with saturated acyl/alkyl chains including diacyl phosphatidylcholines and phosphatidylethanolamines with matched, saturated acyl chains fit well to Eqs. 4 and 5 [49,52–56]. The incremental values (ΔH_{inc} and ΔS_{inc}) and end contributions (ΔH_o and ΔS_o) obtained from the linear least-squares analysis of ΔH_t and ΔS_t for the OABAOHs investigated here (for both solid samples and hydrated suspensions) are given in Table 1.

The fact that both transition entropy and enthalpy are linearly dependent on chain length suggests that the solid-state structures of OABAOHs with various even chain lengths exhibit high similarity. In addition, the results indicate that structures of all odd-chain OABAOHs are also likely to be very similar. This conclusion is supported by the molecular packing and intermolecular interactions observed in the 3-dimensional structures of OMBAOH and OPBAOH, which will be further discussed below.

3.5. Chain length dependence of transition temperature

The transition temperatures of dry and hydrated OABAOHs increase with chain length (Fig. 5). However, in both situations, the magnitude of the shift gets smaller as the chains get longer. Fig. 5A shows that compounds in the even chain length series exhibit slightly higher transition temperatures than the odd chain length compounds. This alternation was not seen with the hydrated samples (Fig. 5B). A similar trend was observed previously for several long-chain amphiphiles such as *N*-acylethanolamines, *N*-acyldopamines, *N*-acylserotonins, and *N*, *O*-diacylethanolamines [53,56–58]. However, in a few cases, e.g., *N*-acyl-L-alanines, *N*-acyl-L-alanine alkyl esters with matched chains, and L-alanine alkyl esters, the T_t values for the odd chain length series were found to be greater than those for the even chain length series [46,48,59].

For a range of single-chain amphiphiles and two-chain lipids that exhibit linear dependence of ΔH_t and ΔS_t on the chain length, it has been shown that the values of ΔH_t and ΔS_t could be fitted to the equation below [60]:

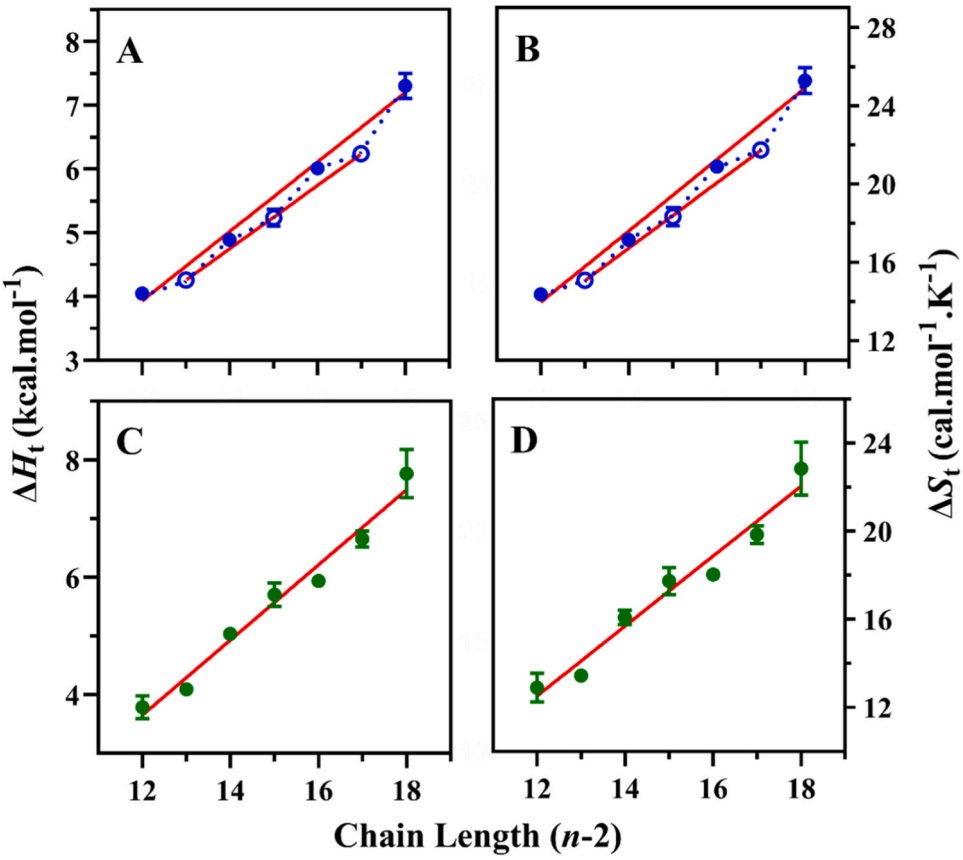

Fig. 4. Chain length dependence of transition enthalpy and transition entropy of OABAOHs in the dry state (**A**, **B**) and upon hydration with water (**C**, **D**). (**A**, **C**) Transition enthalpy; (**B**, **D**) transition entropy. For dry samples: open circles, (○) odd chain length; filled circles (●) even chain length. For hydrated samples: filled circles (●) both even- and odd- chain length. Values of ΔH_t and ΔS_t were plotted against the number of methylene (CH_2) units in the *N*-acyl chain (*n*-2). The solid lines in **A** and **B** represent linear least squares fits of the data for even and odd chain length series separately. The solid line in **C** and **D** represents the linear least-squares fit of the data.

Table 1
Incremental values (ΔH_{inc} and ΔS_{inc}) of chain length dependence and end contributions (ΔH_o and ΔS_o) of the phase transition enthalpy and entropy of OABAOHs.[a]

Thermodynamic parameter	Dry OABAOHs		Hydrated OABAOHs (odd- & even chain lengths)
	Even chain length	Odd chain length	
ΔH_{inc} (kcal/mol)	0.54 (0.02)	0.49 (0.02)	0.64 (0.03)
ΔH_o (kcal/mol)	-2.59 (0.30)	-2.18 (0.29)	-4.03 (0.46)
ΔS_{inc} (cal/mol/K)	1.82 (0.07)	1.66 (0.07)	1.59 (0.09)
ΔS_o (cal/mol/K)	-7.92 (1.07)	-6.60 (1.04)	-6.54 (1.42)

[a] Average values of ΔH_t and ΔS_t given in Table S5 have been used for linear fitting of the data. Errors shown in parentheses are fitting errors obtained from the linear least-squares analysis.

$$T_t = \Delta H_t/\Delta S_t = T_t^{\infty}\,[1-(n_o - n_o')/(n - n_o')] \quad (6)$$

where n_o(= - $\Delta H_o/\Delta H_{inc}$) and n_o' (= - $\Delta S_o/\Delta S_{inc}$) are the values of *n* at which the ΔH_t and ΔS_t extrapolate to zero. Figs. 5A and 5B show that the T_t values of dry OABAOHs with even and odd acyl chains independently fit rather well to Eq. (6). The nonlinear least-squares fitting of T_t values of all the hydrated OABAOHs to Eq. (6) was quite satisfactory, as is evident in Fig. 5B. The T_t^{∞} values for even and odd chain length OABAOHs in the dry state were 398 and 389 K, respectively, and 432 K, for the hydrated OABAOHs.

3.6. Description of structure

ORTEPs presented in Fig. 6A and Fig. S5A depict the molecular structures of OMBAOH and OPBAOH determined by single-crystal X-ray diffraction. The atom numbering for all non-hydrogen atoms is shown in these ORTEPs. Table 2 lists the crystal parameters for these two compounds, and Tables S6-S8 (OMBAOH) and S9-S11 (OPBAOH) provide the corresponding atomic coordinates, equivalent isotropic displacement parameters, bond lengths and torsion angles.

These results demonstrate that the hydrocarbon portion of the acyl chains of OMBAOH (C2-C14) and OPBAOH (C2-C16) exist in an *all-trans* conformation (Fig. 6A and Fig. S5A) with all the torsion angles being ~180°. The torsion angle corresponding to the O2-C1-C2-C3 linkage in OMBAOH and OPBAOH is 169.1° and −169.4°, respectively. The molecular structures of OMBAOH and OPBAOH are very similar. The torsion angles observed for C17-C16-C15-O2 and O2-C17-C18-C19 linkages in OMBAOH and OPBAOH are −69.7° and −71.7°, respectively. The gauche conformation at the C15-C16 bond in OMBAOH and C17-C18 bond in OPBAOH results in a bending of the molecule, giving it an ice hockey stick like shape. In NAEs bearing saturated acyl chains such as *N*-myristoylethanolamine, *N*-palmitoylethanolamine and *N*-stearoylethanolamine similar bending of the molecule due to gauche conformation at a single C-C bond was reported earlier which gave them a bent structure resembling the letter 'L' [50,61,62]. Interestingly, in the isomeric *O*-acylethanolamines (OAEs) such as *O*-stearoylethanolamine a significant difference is observed in the acyl chain conformation, due to which the molecular geometry changes from a bent structure in the NAEs to an essentially linear structure in OAEs [36,50,62]. It is pertinent

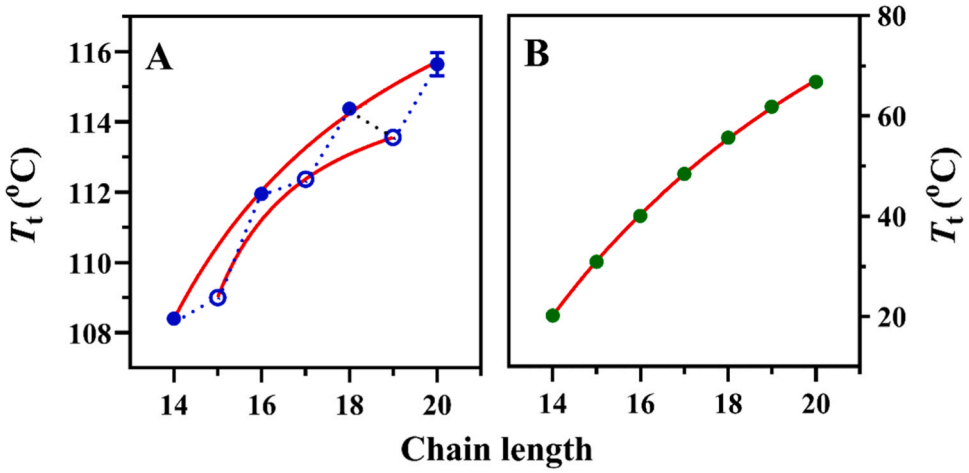

Fig. 5. Chain length dependence of chain-melting phase transition temperatures of OABAOHs. (**A**) Dry samples: (○) even chain-length compounds; (●) odd chain-length compounds. (**B**) fully hydrated samples. The solid lines correspond to nonlinear least-squares fits of the transition temperatures to Eq. 6.

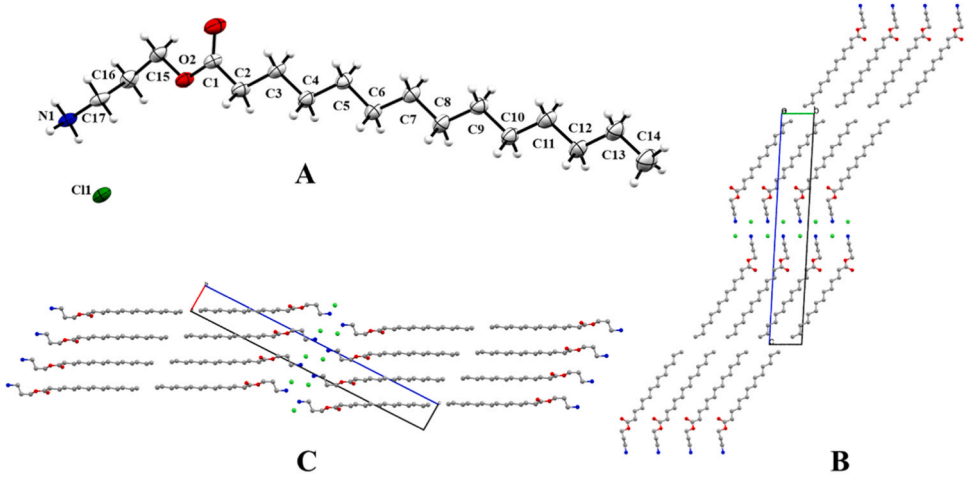

Fig. 6. Molecular and crystal structures of *O*-myristoyl-β-alaninol. (**A**) ORTEP; (**B**, **C**) packing diagrams along the *a*-axis and *b*-axis, respectively. Hydrogen atoms were omitted in the packing diagrams for clarity.

to note here that OAEs are also structural homologues of OABAOHs. Similarly, the acyl chain conformations in NPBAOH exhibits distinct differences from its isomer OPBAOH [29].

3.7. Molecular packing

Packing diagrams of OMBAOH, viewed along the *a*-axis and *b*-axis, are shown in Figs. 6B and 6C, respectively. Similarly, the packing diagrams of OPBAOH, viewed along the *a*-axis and *b*-axis, are shown in Figs. S5B and S5C, respectively. These diagrams show that in OMBAOH, each unit cell contains two molecules, whereas in OPBAOH, each unit cell contains four molecules. In both cases the molecules are packed in a head-to-head (and tail-to-tail) manner in stacked bilayers. The hydrocarbon chains in the two leaflets of the bilayer are at an angle of 180° with each other, resulting in a collinear arrangement of the chains, similar to that seen in NAEs [50,61,62]. The methyl ends of the stacked bilayers are in van der Waals contact, with the closest methyl-methyl contact distance (C14-C14 in OMBAOH and C16-C16 in OPBAOH) between the opposing layers and within the same layer being 3.84 Å and 4.49 Å for OMBAOH and 3.83–3.88 and 4.48 Å for OPBAOH, respectively. The bilayer thickness (i.e., Me − Me distance) in the crystal lattices of OMBAOH and OPBAOH are 37.08 Å and 41.02 Å, respectively, and the monolayer (single leaflet) thickness (O3 − C12 distance) for OMBAOH is 17.26 Å. For OPBAOH (O3-C14 distance), it is 19.28 Å. The repeat distance (*d*-spacing) is 39.71 Å and 43.64 Å for OMBAOH and OPBAOH, respectively. Area per molecule of OMBAOH and OPBAOH is 25.1 $Å^2$ and 25.0 $Å^2$, respectively. The *O*-acyl chains are tilted by 35.0° in OMBAOH and 34.9° in OPBAOH with respect to the bilayer normal.

3.8. Subcell structure

The different lateral packing modes observed in hydrocarbon chains of lipid crystal are usually described in terms of subcells which specify the relations between equivalent positions within the chain and its neighbours. Such chain packing modes have been classified into a small number of subcells on the basis of symmetry considerations such as triclinic, monoclinic etc. Further, within each category, the polymethylene planes of the chains can be parallel or perpendicular with respect to their neighbours [63,64]. Analysis of the acyl chain packing in OMBAOH and OPBAOH indicated that the subcells in their crystals belong to the classic triclinic parallel ($T_{\parallel}$) type (Fig. S6). The unit cell dimensions of these subcells are given in Table S12.

3.9. Hydrogen bonding and intermolecular interaction

Close examination of the molecular packing in the crystal structure

Table 2
Crystallographic data for OMBAOH and OPBAOH.

Crystal parameter	OMBAOH	OPBAOH
Formula	$C_{17}H_{35}NO_2$. HCl	$C_{19}H_{40}NO_2$. HCl
Formula wt.	321.92	349.97
Crystal system	Triclinic	Triclinic
T, K	295.9(8)	297(1)
Space group	P-1	P-1
a (Å)	4.4857(4)	4.4763(2)
b (Å)	5.5889(8)	5.5917(2)
c (Å)	39.797(4)	87.300(3)
α	92.847(12)	90.768(3)
β	92.314(9)	90.651(3)
γ	95.143(29	95.270(4)
z	2	4
V (Å3)	991.47(19)	2175.52(14)
Dx (g cm-3)	1.078	1.068
μ (mm^{-1})	0.198	0.185
F(000)	356.0	776.0
Reflections collected	3500	7677
Independent reflections	2108	2412
Parameters	192	419
GOF	1.065	1.086
R indices (all data)	$R_1 = 0.1671$, $wR_2 = 0.4004$	$R_1 = 0.2365$, $wR_2 = 0.4064$
Final R indices	$R_1 = 0.1262$, $wR_2 = 0.3742$	$R_1 = 0.1295$, $wR_2 = 0.3317$

of OMBAOH and OPBAOH revealed that the intermolecular interactions in these compounds involve two types of hydrogen bonds: C-H···O and N-H···Cl. The H-bonds in OMBAOH and OPBAOH are shown in Figs. 7A and 7B, respectively and the bond distances and angles are listed in Table 3. Each ammonium group forms hydrogen bonds with three chloride ions, with two of these N-H···Cl hydrogen bonds bridging adjacent molecules in the same leaflet, whereas the third N-H···Cl H-bond connects the molecules from opposite layers. Details of the three types of N–H···Cl H-bonds observed in the crystal structures of OMBAOH and OPBAOH are listed in Table 3, including the hydrogen bond distance (H···Cl), donor-acceptor distance, and bond angle at the H atom.

In addition to the N–H···Cl interactions, a C-H···O interaction was also seen between a carbonyl oxygen (O1) from a neighbouring molecule and an H-atom on the C2 and C4 carbon atoms (at α- and γ- positions with respect to the ester carbonyl) (Figs. 7A and 7B). Two types of C–H···O bonds are seen in the crystal structures of OMBAOH and OPBAOH. In OPBAOH, same kind of C-H···O and N-H···Cl bonds in opposite layers show minor differences in the H-bond characteristics. The corresponding H-bond distance, donor-acceptor distance and the bond angle at 'H' atom are given in Table 3.

3.10. Powder X-ray diffraction studies

Powder X-ray diffraction (PXRD) experiments provided additional details on the molecular packing of OABAOHs with various acyl chain lengths. Figs. 8A and 8B display the PXRD data obtained at room temperature for OABAOHs with even and odd chain lengths, respectively. All OABAOHs ($n = 14–20$) produced a number of distinct peaks in the 2θ range of 5−50°. The *d*-spacing was determined from the position of these diffraction peaks. For each compound, the *d*-spacing was estimated using 4−5 peaks and the values obtained are presented in Table S13. Fig. 8C displays a plot of the *d*-spacings of OABAOHs as a function of acyl chain length. From this plot it is seen that the even chain-length OABAOHs exhibit higher *d*-spacings than the odd chain-length ones, indicating a clear odd-even alternation.

The slopes of the two separate linear dependences seen for the even and odd acyl chain length series in Fig. 8C are 1.974 and 1.882 Å/CH_2, respectively, and indicate increases of 0.987 and 0.941 Å per additional CH_2 moiety. Since in a typical bilayer with all-trans acyl chains oriented perpendicular to the bilayer plane, increase in the acyl chain length by one CH_2 unit raises the *d*-spacing by 1.27 Å for each layer (2.54 Å for the bilayer), the incremental increase in the *d*-spacings estimated here indicate that the acyl chains must be tilted with respect to the bilayer normal. The larger deviation of the incremental *d*-spacing observed with the odd chain-length OABAOHs from the ideal value indicates that they are more tilted as compared to those with even chain lengths. From the incremental *d*-spacings the tilt angles (with respect to the bilayer normal) could be estimated as 39° and 42.2° for the even- and odd chain-length series, respectively. The value obtained for the even chain length series is in fairly good agreement with the value of 35° determined from the crystal structures of OMBAOH and OPBAOH ($n = 14, 16$).

3.11. Interaction between OMBAOH and SDS: Turbidimetric, ITC and DSC studies

The investigation of several systems of catanionic mixed amphiphiles revealed that they form unilamellar liposomes with considerable potential for application in developing drug delivery systems [23,30,40,41,48]. In this study, we focused on examining the interaction between the cationic amphiphile OMBAOH and sodium dodecyl sulphate (SDS), using turbidimetry, isothermal titration calorimetry and DSC. The results obtained from all three methods consistently indicate the formation of an equimolar complex between these two surfactants.

OMBAOH forms an optically clear solution in water. Upon the addition of small aliquots of SDS solution, the optically clear sample becomes turbid, suggesting the formation of larger aggregates. This can

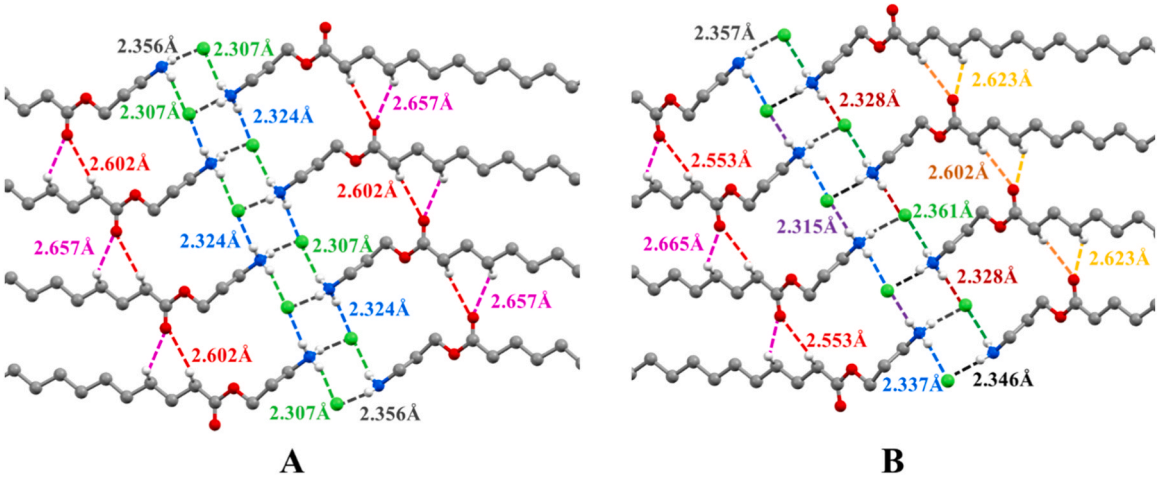

Fig. 7. Hydrogen bonding pattern in the crystal lattice of OMBAOH (**A**) and OPBAOH (**B**). Similar colours have been used for similar bonds. Colour code for atoms: grey, carbon; red, oxygen; blue, nitrogen. Hydrogen atoms not involved in H-bonds have been omitted for clarity.

Table 3
Details of hydrogen bond distances and angles in the crystal structures of OMBAOH and OPBAOH.

Bond	H-bond distance (Å)	Donor-acceptor distance (Å)	Bond angle at 'H' (°)
OMBAOH			
C-H···O	2.602	3.425	142.79
,	2.657	3.441	138.17
N-H···Cl	2.324	3.208	172.29
,	2.356	3.235	169.40
,	2.307	3.164	161.48
OPBAOH			
C-H···O	2.553	3.374	142.52
,	2.665	3.433	136.42
,	2.623	3.415	138.92
,	2.602	3.436	144.27
N-H···Cl	2.315	3.201	173.46
,	2.346	3.234	175.20
,	2.328	3.207	169.37
,	2.337	3.186	159.72
,	2.361	3.171	151.37
,	2.357	3.239	170.98

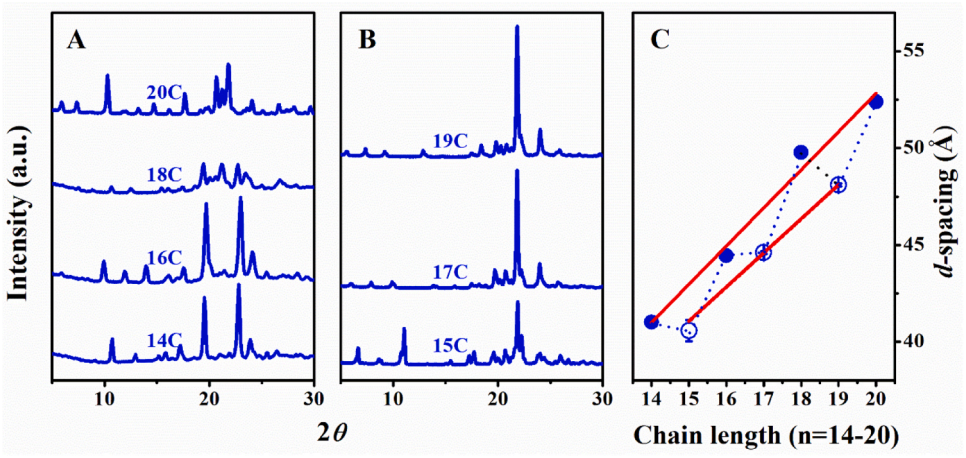

Fig. 8. Powder X-ray diffraction patterns of OABAOHs. Data for compounds with even acyl chain length (**A**) and odd acyl chain length (**B**) are shown. (**C**) Dependence of *d*-spacing on the acyl chain length. The number of C-atoms in the saturated, unbranched acyl chains is indicated against each PXRD profile. Solid lines in C represent linear fits of the data for even- and odd-chain length series, separately. Filled circles (•), even chain length; open circles (O) odd chain-length.

be attributed to the interaction between the cationic OMBAOH and the negatively charged dodecyl sulfate, leading to the formation of larger aggregates compared to those formed by OMBAOH or SDS alone. To investigate this phenomenon, we carried out turbidimetric experiments according to Job's method. The total surfactant concentration was held constant throughout the experiments, and the optical density at 340 nm, of the mixtures are presented in Fig. 9A. The plot reveals that the turbidity of the mixed surfactant solution initially increases with increasing SDS content until an X_{SDS} value of 0.5, but decreases with further increase in SDS content. The higher turbidity observed at $X_{SDS} = 0.5$ suggests the formation of large aggregates comprising the two components in an equimolar ratio.

Thermodynamic factors governing the interaction between OMBAOH and SDS were characterized by ITC, and the results are presented in Figs. 9C and 9D. Concentrations of the two surfactants were kept well below their CMC in order to avoid complications from the presence of micelles. Fig. 9C shows that the exothermic heat of binding remains relatively constant for the initial injections of OMBAOH into SDS present in the reaction cell, but gradually decreases as more OMBAOH is added until saturation is achieved. Fig. 9D depicts a plot of incremental heat changes against the OMBAOH/SDS ratio, and analysis of this data employing the 'one set of sites' binding model (solid line in the lower panel) yielded the following thermodynamic parameters: stoichiometry of binding (n) = 0.94 ± 0.01, binding (association) constant (K_b) = 9.74 (± 1.27) × 10^5 M^{-1}, enthalpy of binding (ΔH_b) = −17.4 ± 1.1 kcal.mol^{-1}, and entropy of binding (ΔS_b) = −29.9 ± 3.5 cal.mol^{-1} K^{-1}. From these values the free energy of binding (ΔG_b) was estimated to be −8.30 kcal mol^{-1}. The stoichiometry of binding (n = 0.94) obtained from the ITC analysis is in excellent agreement with the results obtained from Job's experiment, further confirming that the interaction between OMBAOH and SDS leads to the formation of an equimolar complex between the two surfactants.

The thermal stability of the OMBAOH-SDS catanionic mixed system in water was investigated by differential scanning calorimetry. DSC thermograms of equimolar complex of OMBAOH and SDS exhibited a single, well-defined endothermic peak centered at 59.0 °C indicating that the complex undergoes a clear-cut phase transition (Fig. 9B). Repeat scans confirmed the reversibility and reproducibility of the thermal behavior. The transition enthalpy (ΔH_t) and entropy (ΔS_t) were found to be 14.84 (±0.14) kcal.mol^{-1} and 44.70 (±0.42) cal.mol^{-1}.K^{-1} respectively. In comparison, OMBAOH alone displayed a single, sharp endothermic peak centered at 14.1 °C with a transition enthalpy (ΔH_t) of 3.51 (±0.17) kcal.mol^{-1} and transition entropy (ΔS_t) of 12.3 (±0.64) cal.mol^{-1}.K^{-1}. On the other hand, SDS did not exhibit any thermal transition under similar conditions (not shown), which is consistent with its existence as micelles under these conditions [65]. In the mixture, the samples appeared turbid at room temperature but became optically clear above the phase transition temperature, indicating that the mixture most likely exists in a micellar form above T_t. These observations indicate that the equimolar mixture of NMBAOH and SDS forms

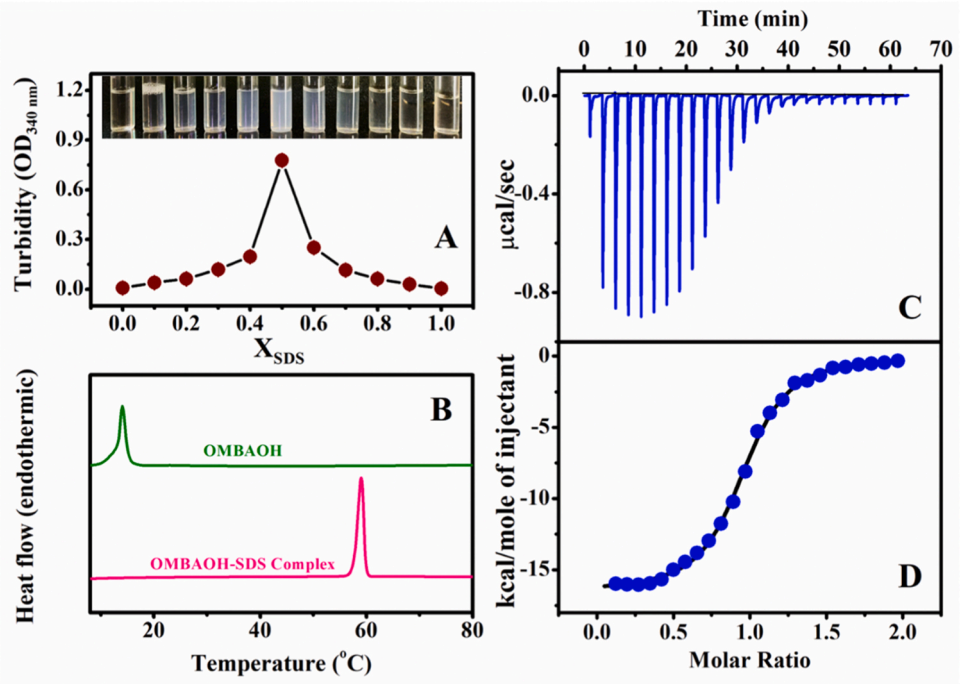

Fig. 9. Interaction of OMBAOH with SDS studied by Job's method and ITC. (**A**) Job's experiment measuring the turbidity of various mixtures of OMBAOH and SDS. The photo at the top shows turbidity of the samples and the plot below shows the optical density of the individual samples at 340 nm. (**B**) DSC thermograms of OMBAOH and equimolar OMBAOH-SDS complex in water. (**C, D**) Interaction of OMBAOH and SDS studied by ITC. (**C**) Raw heats released upon successive injections. (**D**) Integrated heats obtained from the titration data shown in **C** after correcting for dilution effects. The solid line represents the best curve fit of the experimental data to the 'one set of sites' binding model in MicroCal PEAQ-ITC data analysis software. See text for more details.

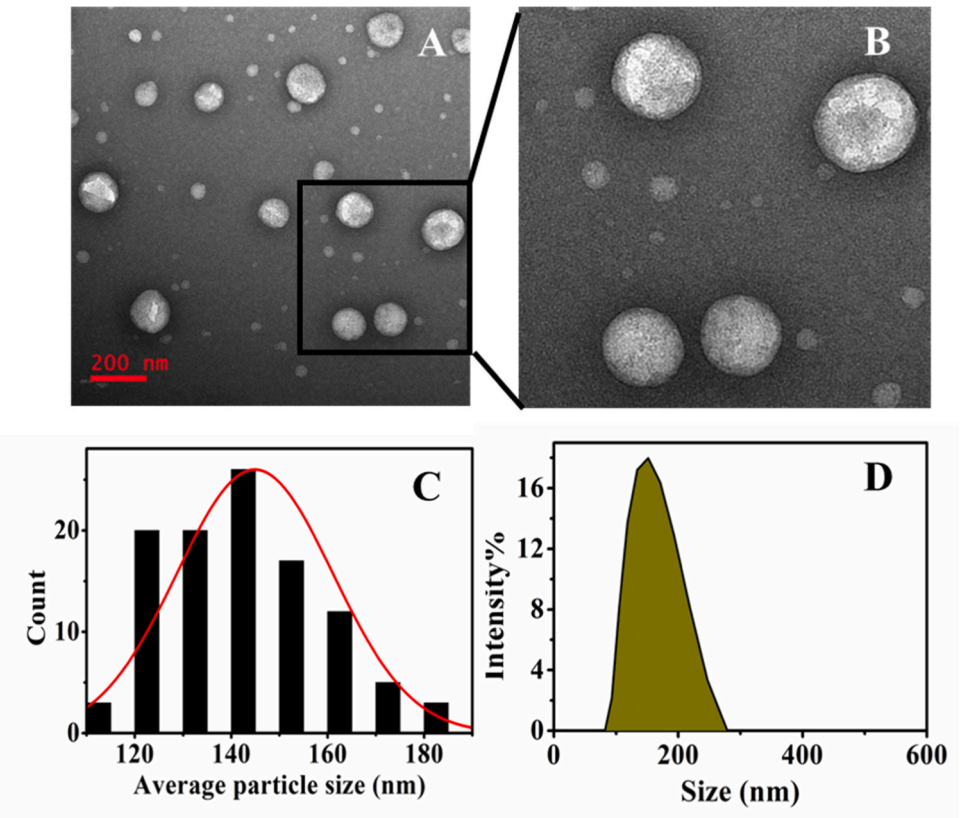

Fig. 10. Characterization of liposomes formed by OMBAOH-SDS equimolar mixture. (**A**) A TEM image of vesicles consisting of OMBAOH-SDS equimolar mixture. (**B**) A zoomed-in image of some of the vesicles shown in **A**. (**C**) A graphical representation of the average particle size measured from the TEM images. (**D**) Graphical representation of the particle-size distribution obtained from DLS measurements.

stable liposomes, which undergo a reversible transition from a lamellar gel phase to a micellar phase.

3.12. Characterization of the size and shape of liposomes by TEM and DLS

The above observations indicate that catanionic aggregates are formed by mixing OMBAOH and SDS in equimolar ratio. The morphology and size of these ensembles were further investigated by transmission electron microscopy (TEM). A TEM images of the equimolar mixture is shown in Fig. 10A and an enlarged view of a part of this image is shown in Fig. 10B. These images provide evidence for the spherical morphology of the ensembles, which are most likely catanionic vesicles. The average size of these vesicles was estimated as 144 (±16) nm (Fig. 10C). Size of the OMBAOH-SDS catanionic vesicles was also measured using dynamic light scattering (DLS), which yielded the vesicle size as 160 (±11) nm (Fig. 10D). The minor difference (~10%) in the size obtained from these two techniques could possibly be due to the fact that in TEM studies, the sample is dried whereas vesicles that are fully hydrated in aqueous medium are used in the DLS measurements. Previous TEM and DLS studies have shown that catanionic vesicles made up of equimolar complexes of SDS with lauryl sarcosinate (~300 nm), lauryl alaninate (300–600 nm) and lauroyl glycinate (700–1000 nm) are about 2–6 times larger in size [40,41,48].

4. Conclusion

In this study, a homologous set of *O*-acyl-β-alaninols were synthesized, and differential scanning calorimetry was used to characterize their thermotropic phase transitions. The thermodynamic parameters ΔH_t and ΔS_t were found to be linearly dependent on the acyl chain length. Single crystal X-ray diffraction studies on *O*-myristoyl-β-alaninol and *O*-pamitoyl-β-alaninol revealed that these lipids adopt an extended, essentially linear geometry of the hydrophobic acyl chains which face one another, forming a head-to-head (and tail-to-tail) arrangement that is similar to a bilayer structure. The acyl chains are tilted away from the bilayer normal by a significant amount (35–42°). Studies on the interaction of *O*-myristoyl-β-alaninol with the anionic surfactant sodium dodecyl sulphate showed that these two amphiphiles combine to give an equimolar catanionic complex, which forms liposomes of ~150–160 nm diameter. Further research on how these molecules interact with other membrane lipids and therapeutic agents will be relevant for applying them in pharmaceutical applications, including their potential use in formulating liposomes for drug delivery applications.

CRediT authorship contribution statement

Swamy Musti J.: Writing – review & editing, Supervision, Resources, Project administration, Funding acquisition, Conceptualization. **Sivaramakrishna Dokku:** Writing – review & editing, Validation, Methodology, Investigation, Formal analysis, Data curation. **Choudhury Suman Kumar:** Writing – original draft, Methodology, Investigation, Formal analysis, Data curation. **Ravindar Chinapaka:** Validation, Methodology, Data curation.

Declaration of Competing Interest

The authors declare that they have no known competing financial interests or personal relationships that could have appeared to influence the work reported in this paper.

Data availability

Data will be made available on request.

Acknowledgements

This work was supported by Grant No. UOH-IOE-RC3–21–015 to MJS from the Institution of Eminence project of University of Hyderabad sanctioned by UGC (India). DS was supported by a Senior Research Fellowship from the CSIR (India). SKC was supported by a non-NET fellowship from University Grants Commission (UGC). DS acknowledges GITAM SRG (F.No. 2023/0256) for financial support. We thank Mr. Mahesh S. Rathod for help in X-ray data collection and crystal structure analysis. UGC is acknowledged for their support through the UPE and CAS programs to the University of Hyderabad and School of Chemistry.

Notes

The authors declare no competing financial interest.

APPENDIX or Supplementary Information

Thirteen tables (S1−S13) and 24 figures (S1−S24) as well as analysis of FTIR, ^{1}H- and ^{13}C NMR and HRMS spectral data are given as supplementary material related to this article, which can be found in the online version. In addition, CCDC deposition numbers 2323182 and 2323183 contain the supplementary crystallographic data for this paper.

Appendix A. Supporting information

Supplementary data associated with this article can be found in the online version at doi:10.1016/j.colsurfa.2024.133483.

References

[1.] P. Kovács, L. Kõhidai, G. Csaba, Effect of 3-amino-1-propanol on the phosphatidylinositol (PI) and glycosyl phosphatidylinositol (GPI) systems of *Tetrahymena*, Comp. Biochem. Physiol. 118 (1997) 83–87, https://doi.org/10.1016/S0742-8413(97)00001-7.
[2.] J.D. Smith, L.J. Barrows, Use of 3-aminopropanol as an ethanolamine analogue in the study of phospholipid metabolism in *Tetrahymena*, Biochem. J. 254 (1988) 301–302, https://doi.org/10.1042/bj2540301.
[3.] Y. Yamano, K. Tsuboi, Y. Hozaki, K. Takahashi, X.-H. Jin, N. Ueda, A. Wada, Lipophilic amines as potent inhibitors of *N*-acylethanolamine-hydrolyzing acid amidase, Bioorg. Med. Chem. 20 (2012) 3658–3665, https://doi.org/10.1016/j.bmc.2012.03.065.
[4.] N. Ueda, K. Tsuboi, T. Uyama, *N*-acylethanolamine metabolism with special reference to *N*-acylethanolamine-hydrolyzing acid amidase (NAAA), Prog. Lipid Res. 49 (2010) 299–315, https://doi.org/10.1016/j.plipres.2010.02.003.
[5.] S. Jain, A. Kaur, R. Puri, P. Utreja, A. Jain, M. Bhide, R. Ratnam, V. Singh, A. S. Patil, N. Jayaraman, G. Kaushik, S. Yadav, K.L. Khanduja, Poly propyl ether imine (PETIM) dendrimer: A novel non-toxic dendrimer for sustained drug delivery, Eur. J. Med. Chem. 45 (2010) 4997–5005, https://doi.org/10.1016/j.ejmech.2010.08.006.
[6.] A. Mangraviti, S.Y. Tzeng, K.L. Kozielski, Y. Wang, Y. Jin, D. Gullotti, M. Pedone, N. Buaron, A. Liu, D.R. Wilson, S.K. Hansen, F.J. Rodriguez, G.-D. Gao, F. DiMeco, H. Brem, A. Olivi, B. Tyler, J.J. Green, Polymeric nanoparticles for nonviral gene therapy extend brain tumor survival in *vivo*, ACS Nano 9 (2015) 1236–1249, https://doi.org/10.1021/nn504905q.
[7.] N. Suleman, R.S. Kalhapure, C. Mocktar, S. Rambharose, M. Singh, T. Govender, Silver salts of carboxylic acid terminated generation 1 poly (propyl ether imine) (PETIM) dendron and dendrimers as antimicrobial agents against *S. aureus* and MRSA, RSC Adv. 5 (2015) 34967–34978, https://doi.org/10.1039/C5RA03179F.
[8.] Z. Limin, L. Ganzuo, S. Zhiwei, Spontaneous vesicle formation in aqueous solution of zwitterionic and anionic surfactant mixture, Colloids Surf. A: Physicochem. Eng. Asp. 190 (2001) 275–283, https://doi.org/10.1016/S0927-7757(01)00693-8.
[9.] T. Sakai, R. Ikoshi, N. Toshida, M. Kagaya, Thermodynamically stable vesicle formation and vesicle-to-micelle transition of single-tailed anionic surfactant in water, J. Phys. Chem. B. 117 (2013) 5081–5089.
[10.] J.E. Brady, D.F. Evans, B. Kacher, B.W. Ninham, Spontaneous vesicles, J. Am. Chem. Soc. 106 (1984) 4279–4280, https://doi.org/10.1021/ja00327a044.
[11.] E.W. Kaler, A.K. Murthy, B.E. Rodriguez, J.A.N. Zasadzinski, Spontaneous vesicle formation in aqueous mixtures of single-tailed surfactants, Science 245 (1989) 1371–1374. ⟨https://www.science.org/doi/10.1126/science.2781283⟩.
[12.] K. Tsuchiya, H. Nakanishi, H. Sakai, M. Abe, Temperature-dependent vesicle formation of aqueous solutions of mixed cationic and anionic surfactants, Langmuir 20 (2004) 2117–2122, https://doi.org/10.1021/la0302908.
[13.] H. Yin, J. Huang, Y. Lin, Y. Zhang, S. Qiu, J. Ye, Heating-induced micelle to vesicle transition in the cationic-anionic surfactant systems: comprehensive study and understanding, J. Phys. Chem. B. 109 (2005) 4104–4110, https://doi.org/10.1021/jp045158a.

[14.] R.O. Brito, E.F. Marques, P. Gomes, S. Falcão, O. Söderman, Self-assembly in a catanionic mixture with an aminoacid-derived surfactant: from mixed micelles to spontaneous vesicles, J. Phys. Chem. B. 110 (2006) 18158–18165, https://doi.org/10.1021/jp061946j.
[15.] E.W. Kaler, K.L. Herrington, D.J. Iampietro, B.A. Coldren, H.-T. Jung, J. A. Zasadzinski, Phase behavior and microstructure in aqueous mixtures of cationic and anionic surfactants, in: M. Abe, J.F. Scamehorn (Eds.), Mixed Surfactant Systems, Second Ed, Marcel Dekker, New York, 2005, pp. 289–338.
[16.] M. Dubois, B. Demé, T. Gulik-Krzywicki, J.-C. Dedieu, C. Vautrin, S. Désert, E. Perez, T. Zemb, Self-assembly of regular hollow icosahedra in salt-free catanionic solutions, Nature 411 (2001) 672–675. ⟨https://www.nature.com/articles/35079541⟩.
[17.] J.F. Scamehorn, An overview of phenomena involving surfactant mixtures, ACS Symp. Ser. 311 (1986) 1–27. ⟨https://pubs.acs.org/doi/pdf/10.1021/bk-1986-0311.ch001⟩.
[18.] S. Šegota, D. Težak, Spontaneous formation of vesicles, Adv. Colloid Interface Sci. 121 (2006) 51–75, https://doi.org/10.1016/j.cis.2006.01.002.
[19.] T. Bramer, N. Dew, K. Edsman, Catanionic mixtures involving a drug: a rather general concept that can be utilized for prolonged drug release from gels, J. Pharm. Sci. 95 (2006) 769–780, https://doi.org/10.1002/jps.20582.
[20.] B.M.D. O'Driscoll, E.A. Nickels, K.J. Edler, Formation of robust, free-standing nanostructured membranes from catanionic surfactant mixtures and hydrophilic polymers, Chem. Commun. (2007) 1068–1070, https://doi.org/10.1039/B614224A.
[21.] G. Kume, M. Gallotti, G. Nunes, Review on anionic/cationic surfactant mixtures, J. Surfactants Deterg. 11 (2008) 1–11, https://doi.org/10.1007/s11743-007-1047-1.
[22.] S.B. Lioi, X. Wang, M.R. Islam, E.J. Danoff, D.S. English, Catanionic surfactant vesicles for electrostatic molecular sequestration and separation, Phys. Chem. Chem. Phys. 11 (2009) 9315–9325, https://doi.org/10.1039/B908523H.
[23.] L. Zhao, J. Liu, L. Zhang, Y. Gao, Z. Zhang, Y. Luan, Self-assembly properties, aggregation behavior and prospective application for sustained drug delivery of a drug-participating catanionic system, Int. J. Pharm. 452 (2013) 108–115, https://doi.org/10.1016/j.ijpharm.2013.04.072.
[24.] M.-J. Rang, Trend on development and application of high performance surfactants for detergents, Appl, Chem. Eng. 20 (2009) 126–133. ⟨https://koreascience.kr/article/JAKO200910103461964.page⟩.
[25.] A. Stocco, D. Carriere, M. Cottat, D. Langevin, Interfacial behavior of catanionic surfactants, Langmuir 26 (2010) 10663–10669, https://doi.org/10.1021/la100954v.
[26.] D. Varade, D. Carriere, L.R. Arriaga, A.-L. Fameau, E. Rio, D. Langevin, W. Drenckhan, On the origin of the stability of foams made from catanionic surfactant mixtures, Soft Matter 7 (2011) 6557–6570, https://doi.org/10.1039/C1SM05374D.
[27.] N. Schelero, H. Lichtenfeld, H. Zastrow, H. Möhwald, M. Dubois, T. Zemb, Single particle light scattering method for studying aging properties of Pickering emulsions stabilized by catanionic crystals, Colloid Surf. A: Physicochem. Eng. Asp. 337 (2009) 146–153, https://doi.org/10.1016/j.colsurfa.2008.12.013.
[28.] C. Wang, Y. Liu, N. Wang, Y. Zhang, L. Zhang, S. Zhao, Effects of catanionic surfactant mixture adsorption on the wettability of PTFE and PMMA (Art. No), Colloids Surf. A: Physicochem. Eng. Asp. 631 (2021) 127659, https://doi.org/10.1016/j.colsurfa.2021.127659.
[29.] D. Sivaramakrishna, S.K. Choudhury, S.K. Cheppali, M.J. Swamy, Structure, thermotropic phase behavior and membrane interaction of *N*-acyl-β-alaninols. Homologs of stress-combating *N*-acylethanolamines, Chem. Phys. Lipids 236 (2021) 105056, https://doi.org/10.1016/j.chemphyslip.2021.105056.
[30.] P.K. Tarafdar, S.T. Reddy, M.J. Swamy, A base-triggerable catanionic mixed lipid system: Isothermal titration calorimetric and single-crystal X-ray diffraction studies, J. Phys. Chem. B 114 (2010) 13710–13717, https://doi.org/10.1021/jp104841k.
[31.] D. Zhi, S. Zhang, F. Qureshi, Y. Zhao, S. Cui, B. Wang, H. Chen, B. Yang, D. Zhao, Structure-activity relationship of carbamate-linked cationic lipids bearing hydroxyethyl headgroup for gene delivery, Colloids Surf. B: Biointerfaces 112 (2013) 537–541, https://doi.org/10.1016/j.colsurfb.2013.08.040.
[32.] D. Niculescu-Duvaz, J. Heyes, C.J. Springer, Structure-activity relationship in cationic lipid mediated gene transfection, Curr. Med. Chem. 10 (2003) 1233–1261, https://doi.org/10.2174/0929867033457476.
[33.] Y. Liu, C.-F. Xu, S. Iqbal, X.-Z. Yang, J. Wang, Responsive nanocarriers as an emerging platform for cascaded delivery of nucleic acids to cancer, Adv. Drug Deliv. Rev. 115 (2017) 98–114, https://doi.org/10.1016/j.addr.2017.03.004.
[34.] A. Sardar, N.K. Rout, S. Nath, M. Prasad, J. Mahanti, S. Mondal, P.K. Tarafdar, A headgroup linker perturbs pKa via acyl chain migration: Designing base-labile supramolecular assemblies, Chem. Commun. 54 (2018) 4282–4285, https://doi.org/10.1039/C8CC00776D.
[35.] B. Hazra, A. Mondal, M. Prasad, S. Gayen, R. Mandal, A. Sardar, P.K. Tarafdar, Lipidated lysine and fatty acids assemble into protocellular membranes to assist regioselective peptide formation: Correlation to the natural selection of lysine over nonproteinogenic lower analogues, Langmuir 38 (2022) 15422–15432, https://doi.org/10.1021/acs.langmuir.2c02849.
[36.] P.K. Tarafdar, M.J. Swamy, Structure and phase behavior of *O*-stearoylethanolamine: A combined calorimetric, spectroscopic and X-ray diffraction study, Biochim. Biophys. Acta 1798 (2010) 872–881, https://doi.org/10.1016/j.bbamem.2010.01.012.
[37.] D. Zhi, Y. Bai, J. Yang, S. Cui, Y. Zhao, H. Chen, S. Zhang, A review on cationic lipids with different linkers for gene delivery, Adv. Colloid Interface Sci. 253 (2018) 117–140, https://doi.org/10.1016/j.cis.2017.12.006.
[38.] P.P. Karmali, A. Chaudhuri, Cationic liposomes as non-viral carriers of gene medicines: Resolved issues, open questions, and future promises, Med. Res. Rev. 27 (2007) 696–722, https://doi.org/10.1002/med.20090.
[39.] R. Srinivas, S. Samanta, A. Chaudhuri, Cationic amphiphiles: Promising carriers of genetic materials in gene therapy, Chem. Soc. Rev. 38 (2009) 3326–3338, https://doi.org/10.1039/B813869A.
[40.] S.T. Reddy, D. Sivaramakrishna, M.J. Swamy, Physicochemical characterization of lauryl glycinate-dodecyl sulfate equimolar complex: A base-triggerable catanionic liposomal system, Colloids Surf. A: Physicochem. Eng. Asp. 516 (2017) 139–146, https://doi.org/10.1016/j.colsurfa.2016.12.012.
[41.] C. Ravindar, S.T. Reddy, D. Sivaramakrishna, D.P. Damera, M.J. Swamy, Base-triggerable lauryl sarcosinate-dodecyl sulfate catanionic liposomes: Structure, biophysical characterization, and drug entrapment/release studies, Soft Matter 18 (2022) 7814–7826, https://doi.org/10.1039/D2SM00965J.
[42.] H. Heerklotz, J. Seelig, Titration calorimetry of surfactant-membrane partitioning and membrane solubilization, Biochim. Biophys. Acta 1508 (2000) 69–85, https://doi.org/10.1016/S0304-4157(00)00009-5.
[43.] I.M. Umlong, K. Ismail, Micellization behaviour of sodium dodecyl sulfate in different electrolyte media, Colloids Surf. A: Physicochem. Eng. Asp. 299 (2007) 8–14, https://doi.org/10.1016/j.colsurfa.2006.11.010.
[44.] K. Kalyanasundaram, J.K. Thomas, Environmental effects on vibronic band intensities in pyrene monomer fluorescence and their application in studies of micellar systems, J. Am. Chem. Soc. 99 (1977) 2039–2044. ⟨https://pubs.acs.org/doi/pdf/10.1021/ja00449a004⟩.
[45.] D. Marsh, Handbook of Lipid Bilayers, CRC Press, Boca Raton, FL, 1990.
[46.] D. Sivaramakrishna, S.T. Reddy, T. Nagaraju, M.J. Swamy, Self-assembly, phase transitions and supramolecular organization of a homologous series of *N*-acyl-L-alanines (n = 8–20), Colloids Surf. A: Physicochem. Eng. Asp. 471 (2015) 108–116, https://doi.org/10.1016/j.colsurfa.2015.02.025.
[47.] K. Bijma, J.B.F.N. Engberts, M.J. Blandamer, P.M. Cullis, P.M. Last, K.D. Irlam, L. G. Soldi, Classification of calorimetric titration plots for alkyltrimethylammonium and alkylpyridinium cationic surfactants in aqueous solutions, J. Chem. Soc. Faraday Trans. 93 (1997) 1579–1584, https://doi.org/10.1039/A607596G.
[48.] D. Sivaramakrishna, M.J. Swamy, Self-assembly, supramolecular organization, and phase behavior of L-alanine alkyl esters (n = 9-18) and characterization of equimolar L-alanine lauryl ester/lauryl sulfate catanionic complex, Langmuir 31 (2015) 9546–9556, https://doi.org/10.1021/acs.langmuir.5b02475.
[49.] M. Ramakrishnan, V. Sheeba, S.S. Komath, M.J. Swamy, Differential scanning calorimetric studies on the thermotropic phase transitions of *N*-acylethanolamines of even chainlengths, Biochim. Biophys. Acta 1329 (1997) 302–310, https://doi.org/10.1016/S0005-2736(97)00120-X.
[50.] R.K. Kamlekar, M.J. Swamy, Molecular packing and intermolecular interactions in two structural polymorphs of *N*-palmitoylethanolamine, a type 2 cannabinoid receptor agonist, J. Lipid Res. 47 (2006) 1424–1433, https://doi.org/10.1194/jlr.M600043-JLR200.
[51.] K. Larsson, The lipid hand-book, Chapman and Hall, London, 1986.
[52.] P.K. Tarafdar, S.T. Reddy, M.J. Swamy, Nonclassical odd-even alternation in mixed-chain diacylethanolamines: Implications of polymorphism, Cryst. Growth Des. 12 (2012) 1132–1140, https://doi.org/10.1021/cg200698t.
[53.] S.T. Reddy, M.J. Swamy, Synthesis, physicochemical characterization and membrane interactions of a homologous series of *N*-acylserotonins: Bioactive, endogenous conjugates of serotonin with fatty acids, Biochim. Biophys. Acta 1848 (2015) 95–103, https://doi.org/10.1016/j.bbamem.2014.09.012.
[54.] D. Marsh, Analysis of the chainlength dependence of lipid phase transition temperatures: Main and pretransitions of phosphatidylcholines; main and non-lamellar transitions of phosphatidylethanolamines, Biochim. Biophys. Acta 1062 (1991) 1–6, https://doi.org/10.1016/0005-2736(91)90326-4.
[55.] D. Marsh, M.J. Swamy, Derivatized lipids in membranes. Physico-chemical aspects of *N*-biotinyl phosphatidylethanolamines, *N*-acyl phosphatidylethanolamines and *N*-acyl ethanolamines. Chem. Phys. Lipids 105 (2000) 43–69, https://doi.org/10.1016/S0009-3084(99)00132-2.
[56.] R.K. Kamlekar, P.K. Tarafdar, M.J. Swamy, Synthesis, calorimetric studies, and crystal structures of *N, O*-diacylethanolamines with matched chains, J. Lipid Res. 51 (2010) 42–52, https://doi.org/10.1194/jlr.M900105-JLR200.
[57.] M. Ramakrishnan, M.J. Swamy, Differential scanning calorimetric studies on the thermotropic phase transitions of *N*-acylethanolamines of odd chainlengths, Chem. Phys. Lipids 94 (1998) 43–51.
[58.] S.T. Reddy, P.K. Tarafdar, R.K. Kamlekar, M.J. Swamy, Structure and Thermotropic Phase Behavior of a Homologous Series of Bioactive *N*-Acyldopamines, J. Phys. Chem. B. 117 (2013) 8747–8757.
[59.] D. Sivaramakrishna, M.J. Swamy, Differential scanning calorimetric and powder X-ray diffraction studies on a homologous series of *N*-acyl-L-alanine esters with matched chains (*n* = 9-18), J. Chem. Sci. 127 (2015) 1627–1635.
[60.] D. Marsh, Biomembranes, in: G. Pifat, J.N. Herak (Eds.), Supramolecular structure and function, Plenum Press, New York, 1982, pp. 127–178.
[61.] B. Dahlén, I. Pascher, S. Sundell, The crystal structure of *N*-(2-Hydroxyethyl)-octadecanoate, Acta Chim. Scand. A 31 (1977) 313–320. ⟨http://actachemscand.org/pdf/acta_vol_31a_p0313-0320.pdf⟩.
[62.] M. Ramakrishnan, M.J. Swamy, Mol. Pack. Intermol. Interact. *N.*-acylethanolamines: Cryst. Struct. *N.*-myristoylethanolamine 1418 (1999) 261–267.

[63.] S. Abrahamsson, B. Dahlen, H. Löfgren, I. Pascher, Lateral packing of hydrocarbon chains, Prog. Chem. Fats Other Lipids 16 (1978) 125–143, https://doi.org/10.1016/0079-6832(78)90039-3.
[64.] P.R. Maulik, M.J. Ruocco, G.G. Shipley, Hydrocarbon chain packing modes in lipids: Effect of altered sub-cell dimensions and chain rotation, Chem. Phys. Lipids 56 (1990) 123–133, https://doi.org/10.1016/0009-3084(90)90095-9.
[65.] S. Rajkhowa, S. Mahiuddin, J. Dey, S. Kumar, V.K. Aswal, R. Biswas, J. Kohlbrecher, K. Ismail, The effect of temperature, composition and alcohols on the microstructures of catanionic mixtures of sodium dodecylsulfate and cetyltrimethylammonium bromide in water, Soft Matter 13 (2017) 3556–3567, https://doi.org/10.1039/C7SM00342K.

J. Chem. Sci. (2021)133:91
https://doi.org/10.1007/s12039-021-01951-0

REGULAR ARTICLE

Special Issue on Beyond Classical Chemistry.

Thermotropic phase behavior and supramolecular organization of *N*,*O*-diacyl-L-alaninols: effect on stratum corneum model membrane

DOKKU SIVARAMAKRISHNA, SUMAN KUMAR CHOUDHURY and MUSTI J SWAMY*
School of Chemistry, University of Hyderabad, Hyderabad 500 046, India
E-mail: mjswamy@uohyd.ac.in; mjswamy1@gmail.com

MS received 15 April 2021; revised 3 June 2021; accepted 8 June 2021

Abstract. In recent years, chemical enhancers that increase the permeability of stratum corneum (SC) attracted the attention of clinicians and researchers due to their utility in developing transdermal drug delivery systems. *N*-Lauroyl glycine lauryl ester (NLGLE) was reported to induce higher SC permeability than *N*-lauroyl serine lauryl ester (NLSLE). Earlier, we proposed a similar activity could be obtained by *N*-acyl-L-alanine esters (NAAEs) towards SC, which are homologous to NLGLE. In this study, we synthesized a homologous series of *N*,*O*-diacyl-L-alaninols (DAAOHs) (which are isomers of NAAEs) with saturated acyl chains. We investigated their thermotropic phase behavior and supramolecular organization, and the results are discussed with the properties of isomeric NAAEs. Most DAAOHs exhibited one polymorphic phase transition (solid-solid transition) before the melting transition in the first heating thermogram. The solid-solid transition disappeared in further heating thermograms. Odd chainlength DAAOHs exhibited higher transition enthalpy and transition entropy values than even chainlength DAAOHs. Interestingly, the even chainlength DAAOHs exhibited higher transition temperature and *d*-spacing values than odd chainlength DAAOHs. Further, Laurdan fluorescence studies revealed that *N*,*O*-dilauroyl-L-alaninol increases the fluidity of SC model membrane more efficiently as compared to NLGLE, suggesting that DAAOHs can potentially be used as chemical enhancers in developing transdermal drug delivery systems.

Keywords. *N*,*O*-diacyl alaninols; stratum corneum; Differential scanning calorimetry; powder X-ray diffraction; Laurdan fluorescence; generalized polarization; membrane fluidity.

1. Introduction

Transdermal drug delivery (TDD) is a convenient and safe approach compared to conventional drug delivery methods of subcutaneous/intravenous injection, and oral administration. TDD avoids the hepatic first-pass effect, especially for drugs with low bioavailability through conventional administration, and when high doses of medication are necessary for a longer duration to get effective bioavailability.[1] Several anti-dermal, anti-ischemic, anti-hypertensive and hypoglycemic drugs, as well as some others are widely delivered in a transdermal form.[1,2] However, due to the low permeability of drugs through the stratum corneum (SC), the use of TDD is considerably restricted. SC or epidermis is the outer layer of skin, which serves as the primary barrier between the environment and the body. SC consists of dead cells (Corneocytes) without nuclei and cell organelles and contains cytoplasm with filamentous keratin. The major lipid components of the SC are ceramides (40-60%), sterols (20-33%), and fatty acids (7-13%), whereas cholesterol-3-sulphate and cholesteryl esters are minor components.[3–5] However, the lipid composition varies based on a variety of parameters, e.g., location (depth of the skin), age, sex, race, and health of the individual. The ceramides in SC are complex and contain primarily saturated fatty acids, due to which permeability of drugs through SC is rather low.[4,6]

*For correspondence

Supplementary Information: The online version contains supplementary material available at https://doi.org/10.1007/s12039-021-01951-0.

Published online: 03 September 2021

Several chemical enhancers (CEs) have been investigated with the objective of improving the permeability of SC to drugs and therapeutic agents. These CEs include short and long-chain alcohols, propylene glycol and its esters, benzoic acid esters, fatty acid esters, cyclic amides, unsaturated fatty acids, etc. However, the exact mechanism of how CEs enhance SC's permeability is not well understood. It is assumed that most CEs enhance the permeability by changing the SC lipid organization and protein hydration by their bent structure, hydration capabilities and partition differences.[7–9] Earlier, *N*-acyl glycine alkyl esters (NAGEs) and *N*-acyl serine alkyl esters (NASEs), which are structurally similar to ceramides, have been reported to enhance the permeability of SC. NAGEs have shown a significant enhancement of permeability as compared to NASEs. The reduced/low ability of NASEs has been explained as due to the higher hydrophilic nature of the head group, which improves hydrogen bonding between adjacent lipid molecules, which results in improved resistance to the passage of the drug through SC.[10] In previous work, we synthesized and characterized *N*-acyl-L-alanine alkyl esters (NAAEs), which are homologous to NAGEs and hydrophobic analogs of NASEs, and proposed them as potential CEs for enhancing the permeability of SC given their reduced hydrogen bonding capacity.[11] With the objective of identifying other CEs for application in TDD, in the present study we synthesized and characterized a homologous series of *N*, *O*-diacyl-L-alaninols (DAAOHs) (see Figure 1 for the structures of the above classes of compounds). The ability of these 4 classes of compounds to modulate the fluidity of stratum corneum model membrane (SCM) was investigated by monitoring Laurdan fluorescence properties, considering that membrane fluidity provides a good correlation to membrane permeability.[12] The results obtained have been presented here and their potential for use in developing transdermal drug delivery systems has been discussed.

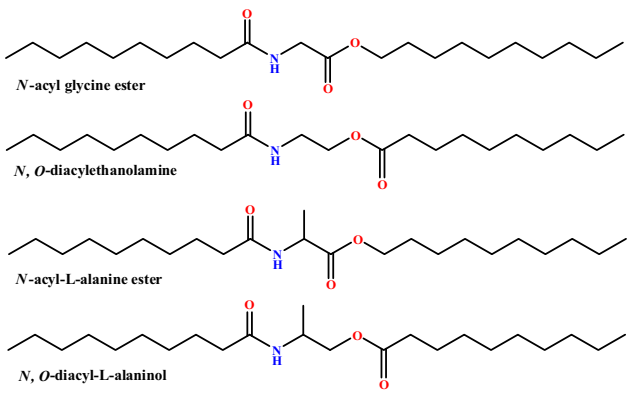

Figure 1. Molecular structure of *N*-acyl glycine ester (NAGE), *N, O*-diacylethanolamine (DAE), *N*-acyl-L-alanine ester (NAAE), and *N, O*-diacyl-L-alaninol (DAAOH) with matched acyl-alkyl/acyl-acyl chains.

The above introduction indicates that *N*-acyl amino acid esters are a new class of compounds that may find use as CEs in formulating TDD systems. Recent studies on the structure and supramolecular organization of NAGEs revealed that these amphiphilic molecules are packed in an untitled, normal bilayer mode.[13] This raised a question as to how the untilted NAGEs improve the permeability of the tightly packed SC lipid membrane. Further, how do the *N*, *O*-diacylethanolamines (DAEs), which adopt a bent structure,[14] influence the SC permeability? Additionally, how do isomeric NAAEs and DAAOHs differ from one another with respect to modulating SC permeability? How do isomeric NAGEs and DAEs, and homologous NAAEs and DAAOHs show their impact on SCM? We attempt to address these questions in the present study.

2. Materials and methods

2.1 *Materials*

Fatty acids (C9-C18) and L-alaninol were obtained from Sigma-Aldrich (Bangalore, India). Oxalyl chloride was purchased from Merck (Germany), and the remaining chemicals and solvents were obtained from Sisco Research Laboratories (Mumbai, India).

2.2 *Synthesis of DAAOHs*

DAAOHs of matched acyl chains were synthesized by a two-step procedure (Scheme 1). In the first step, *N*-acyl-L-alaninols (NAAOHs) were prepared as described earlier.[15] In the second step, the NAAOHs were *O*-acylated to yield DAAOHs. Briefly, the fatty acid (1 mmol) was converted to the acid chloride by mixing with oxalyl chloride (4 mmol) in dichloromethane (DCM) under a dry N_2 atmosphere. After two hours, excess oxalyl chloride was removed by passing dry N_2 gas. The acid chloride thus obtained was added to L-alaninol (4 mmol) in DCM at low temperature (0-5 °C), and the mixture was kept under stirring for 3 h. The crude NAAOH obtained after removing the excess DCM was then *O*-acylated as follows. Acid chloride of matched acyl chain length, prepared as mentioned above (1.1 mmol), was added to NAAOH (1 mmol) in DCM at room temperature, and the

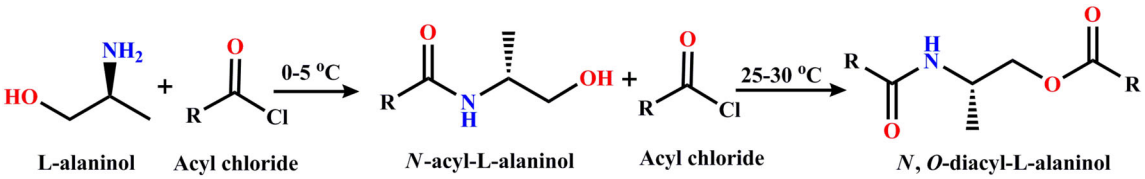

Scheme 1. Synthesis of *N*, *O*-diacyl-L-alaninols.

reaction mixture was kept under continuous stirring overnight. After removing excess solvent, the reaction mixture was washed with water and brine solution, which yielded the crude DAAOH. Crude DAAOHs thus obtained were purified by silica gel column chromatography. Ethyl acetate/n-hexane mixtures of varying ratios were used for elution. Finally, pure products were obtained in 70-80% yield after recrystallization from DCM containing trace amounts of acetone solvent at low temperature (ca. -20 °C). The purified DAAOHs were characterized using IR, NMR (^{1}H and ^{13}C), and high-resolution mass spectrometry (HRMS).

2.3 *Differential scanning calorimetry*

DSC experiments with dry DAAOHs were carried out on a Perkin Elmer Diamond differential scanning calorimeter as described earlier.[11] About 2 mg of each dry DAAOH was weighed accurately into an aluminum sample pan, covered with an aluminum lid and sealed with the aid of crimper. Another pan, prepared similarly but without any sample in it was used as the reference. For every sample, alternate heating (3) and cooling (2) scans were collected at a scan rate of 2 °C/min. Most of the compounds showed minor transitions in the first heating scan which disappeared in the subsequent heating scans; therefore, the first heating scans were considered for further analysis. Transition temperatures (T_t) were determined from the peak of the transition curve and transition enthalpies (ΔH_t) were determined by integrating the area under the transition curve, whereas transition entropies (ΔS_t) were obtained from the ΔH_t values assuming a first-order transition, indicated by Eq. (1):[16]

$$\Delta S_t = \Delta H_t / T_t \quad (1)$$

2.4 *Powder X-ray diffraction studies*

Powder X-ray diffraction measurements on DAAOHs were carried out using a Bruker SMART D8 Advance powder X-ray diffractometer (Bruker-AXS, Karlsruhe, Germany) with Cu-Kα radiation operating at 40 kV and 30 mA. Finely powdered samples were placed in the instrument sample holder and diffraction data were collected using a LynxEye PSD data collector over a 2θ range of 1–50° at room temperature with a step size of 0.0198° and a measuring time of 1.5 s for each step. Peaks corresponding to $2\theta \leq 20°$ were used to calculate d-spacings employing Bragg's equation.

2.5 *Stratum corneum model membrane preparation and Laurdan fluorescence*

Stratum corneum model membrane (SCM) was prepared from *N*–acetyl ceramide (C2-ceramide) (60 mol%), cholesterol (30 mol%), and palmitic acid (10 mol%). Twenty mol% of *N, O*-dilauroyl-L-alaninol (DLAOH), *N*-lauroyl-L-alanine lauryl ester (NLALE), *N, O*-dilauroylethanolamine (DLE), and *N*-lauroyl glycine lauryl ester (NLGLE) were added to the above lipid mixture in separate experiments to check their ability to modulate the fluidity of SCM. The final lipid composition in these samples was C2-ceramide (50 mol%), cholesterol (25 mol%), palmitic acid (8.3 mol%), DLAOH/DLE/NLGLE/NLALE (16.7 mol%). Stock solutions of C2-ceramide, cholesterol, palmitic acid, DLAOHs, NLALE, DLE, and NLGLE were prepared by dissolving in a mixture of chloroform and methanol (1:1, v/v). Samples with the above-mentioned lipid composition were obtained by mixing appropriate aliquots of the stock solutions of each lipid component. Similarly, a stock solution of the fluorescent dye Laurdan was prepared in ethanol, and an aliquot from it was added to the lipid mixture in chloroform-methanol to give a final probe concentration of 1 μM [1 mM lipid and 1 μM probe (1:1000 dilution)]. Then the solvent was evaporated by gently blowing dry nitrogen gas over the sample, and the remaining traces of solvent were removed by vacuum desiccation. Each sample was hydrated with 20 mM sodium phosphate buffer (pH 7.4) and subjected to 4-5 freeze-thaw cycles to get a homogeneous mixture. Laurdan fluorescence spectra were collected as reported earlier,[17] and generalized

polarization (GP) values were calculated using equation 2.[18]

$$GP = (I_{433} - I_{503})/(I_{433} + I_{503}) \quad (2)$$

where I_{433}, I_{503} are the emission intensities at 433 and 490 nm, respectively.

3. Results and Discussion

The homologous series of DAAOHs synthesized in the current study were characterized comprehensively by FTIR, ^{1}H- and ^{13}C-NMR spectroscopy and by high resolution mass spectrometry. Details of the spectral data and their analysis are given in Supporting Information (Tables S1-S4 and Figures S1-S4, Supplementary Information). These data are fully consistent with the structures of DAAOHs and show that they are all highly pure.

3.1 *Thermotropic phase behavior of DAAOHs*

Heating thermograms of dry DAAOHs bearing matched odd- and even acyl chains are given in Figure 2A and B, respectively, and the corresponding cooling thermograms are shown in Figure S5A (SI) and B. DAAOHs bearing different acyl chains (12-18 C-atoms) show two transitions, whereas those with 9-11 C-atoms show a single transition (Figure 2). The minor transitions most likely correspond to solid-solid phase transitions and suggest polymorphism in the solid-state structures of the compounds. The minor transition in even-chain DAAOHs are relatively less intense than those observed with odd-chain DAAOHs. The minor transition of C15 DAAOH is shifted towards a major transition compared to C13 DAAOH, whereas it is partially merged with a major transition in C17 DAAOH. It is interesting to note that minor transitions are not observed in the case of NAAEs and NAGEs (which are structural analogs and homologs of DAAOHs), while homologous DAEs showed minor transitions in the first heating thermograms.[11,13,14] *N*-Acyl derivatives of alanine and alaninol, namely *N*-acyl-L-alanines (NAAs) and *N*-acyl-L-alaninols (NAAOHs) also did not show any minor transitions, whereas even-chain ester derivatives of L-alanine (AEs) showed one minor transition in the first heating thermogram.[15,19,20]

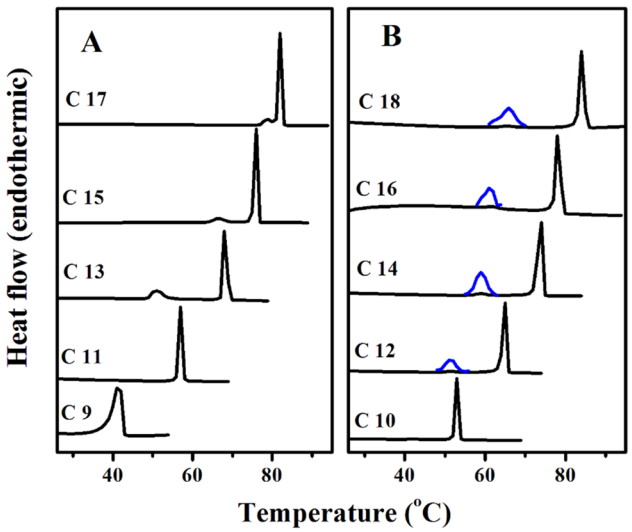

Figure 2. DSC first heating thermograms of dry DAAOHs with odd (A) and even (B) number of C-atoms in the acyl chain. The number of C-atoms is indicated against each thermogram. Less-intense minor transitions of even-chain DAAOHs are vertically expanded 15 times and shown in blue color.

The sharp transition temperatures of DAAOHs matched very well with the capillary melting points of the compounds. When the same samples were subjected to further heating scans, minor transitions for both even- and odd DAAOHs (C12-18) completely disappeared in the second and subsequent heating cycles and a slight decrease in the transition enthalpies was noticed in the second heating scans (Figure S6 (SI), Table 1). The minor transition were not seen in the first cooling scans also (Figure S5, SI). Similar behavior was noticed earlier in several single-chain and double-chain amphiphiles.[14,17,20–24] Interestingly, the minor transitions were also seen in the second heating scans in the case of *N*-acyl-β-alanines.[25] Values of T_t, ΔH_t, and ΔS_t of DAAOHs determined from the first and second heating thermograms are given in Table 1.

3.2 *Chainlength dependence of ΔH_t and ΔS_t*

The chainlength dependence of ΔH_t and ΔS_t corresponding to the phase transitions of DAAOHs in the first and second heating thermograms is shown in Figures 3A and B, and Figures S7A (SI) and B, respectively. In Figure 3, the ΔH_t and ΔS_t values of odd chainlength DAAOHs are somewhat higher as compared to the even chainlength compounds, except for the C10 compound. A similar pattern was observed earlier in NAAEs, which are structural isomers of DAAOHs. Besides, a similar pattern was noticed in the case of NAAs, while such pattern is missing in

Table 1. Average values of transition temperatures (T_t), transition enthalpies (H_t), and transition entropies (S_t) of DAAOHs from first and second heating thermograms. Values in parentheses correspond to standard deviations from three independent measurements.

	1st Heating			2nd Heating		
Acyl chain length (n)	T_t (°C)	ΔH_t (kcal mol^{-1})	ΔS_t (cal mol^{-1} K^{-1})	T_t (°C)	ΔH_t (kcal mol^{-1})	ΔS_t (cal mol^{-1} K^{-1})
9	41.8 (0.1)	7.55 (0.19)	24.0 (0.6)	41.8 (0.1)	7.55 (0.19)	24.0 (0.6)
10	53.2 (0.1)	10.39 (0.13)	31.8 (0.4)	53.1 (0.1)	10.31 (0.12)	31.6 (0.4)
11	57.4 (0.1)	12.17 (0.22)	36.8 (0.7)	56.9 (0.1)	11.39 (0.22)	34.5 (0.7)
12	64.8 (0.2)	13.28 (0.09)	39.3 (0.2)	64.7 (0.2)	13.19 (0.46)	39.1 (1.4)
13	68.4 (0.1)	18.37 (0.36)	53.7 (1.1)	67.6 (0.1)	14.64 (0.32)	43.0 (0.9)
14	73.5 (0.3)	17.43 (0.27)	50.3 (0.8)	73.3 (0.2)	16.29 (0.33)	47.0 (1.0)
15	76.0 (0.1)	22.17 (0.35)	63.5 (0.9)	75.3 (0.1)	17.65 (0.32)	50.7 (0.9)
16	79.4 (0.1)	20.64 (0.35)	58.5 (1.0)	78.9 (0.1)	19.55 (0.39)	55.5 (1.1)
17	82.5 (0.2)	26.91 (0.66)	75.8 (1.9)	81.8 (0.1)	21.09 (0.60)	59.2 (1.8)
18	84.8 (0.1)	24.06 (1.04)	67.2 (2.9)	84.2 (0.1)	22.39 (0.71)	62.7 (2.0)

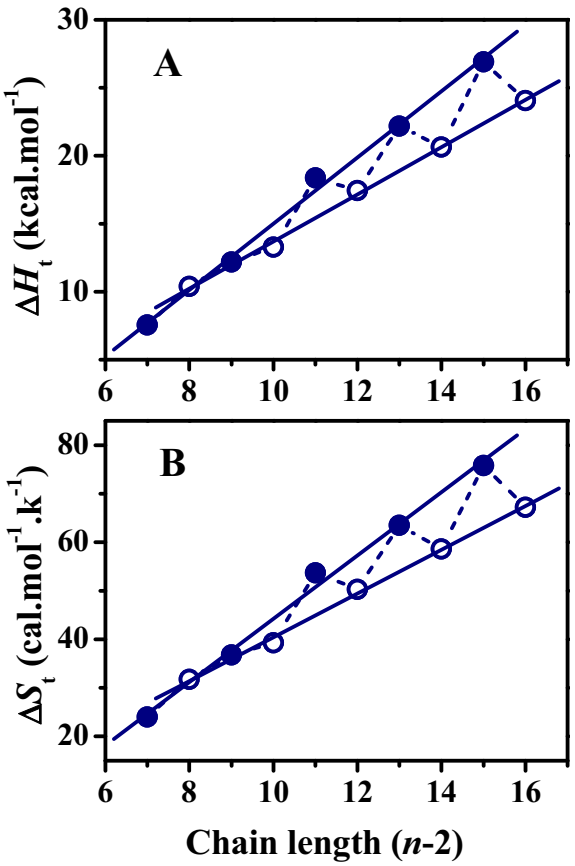

Figure 3. Chainlength dependence of transition enthalpy (A) and transition entropy (B) of dry DAAOHs from the first heating scans. Values of ΔH_t and ΔS_t were plotted against the number of methylene units (n-2). Filled symbols, odd chainlength compounds; open symbols, even chainlength compounds. Solid lines correspond to linear least-squares fits of the data.

NAAOHs.[11,15,19] The values of ΔH_t and ΔS_t obtained for odd- and even chainlength DAAOHs independently exhibit linear dependence on the chainlength. In contrast, ΔH_t and ΔS_t of second heating thermograms (Figure S7, SI) show linear dependence for all DAAOHs, except C9 DAAOH. The ΔH_t and ΔS_t values of first and second heating scans could be fit well to expressions (3) and (4).

$$\Delta H_t = \Delta H_o + (n-2)\Delta H_{inc} \quad (3)$$

$$\Delta S_t = \Delta S_o + (n-2)\Delta S_{inc} \quad (4)$$

Similar linear dependence of the transition enthalpies and entropies was observed previously in several single- and double-chain amphiphiles such as NAAEs, NAAOHs, NAGEs, DAEs, and NAAs.[11–15,19,24] The linear fits yielded incremental values of transition enthalpy and transition entropy (ΔH_{inc}, ΔS_{inc}) from polymethylene groups, and end contributions (ΔH_o, ΔS_o) arising from the terminal methyl group of the acyl chains and the head group. These values obtained from the first and second heating thermograms are given in Table 2.

The linear chainlength dependence of ΔH_t and ΔS_t values, observed here, indicates that molecular packing of the compounds with odd- and even chains would be similar initially (obtained after crystallization from the solvent) within each group, whereas upon going through the melting transition, all DAAOHs (even chain compounds as well as odd chain compounds) might adopt a similar molecular packing. Therefore, molecular packing and intermolecular interactions in the solid-state of all the even-chain

Table 2. Incremental values (H_{inc}, S_{inc}) and end contributions (H_o, S_o) arising from the phase transition enthalpies and entropies of DAAOHs. Values in parentheses correspond to fitting errors obtained from the least-squares analysis.

Thermodynamic parameter	1st Heat		2nd Heat
	Odd chain length	Even chain length	
ΔH_{inc} (kcal/mol)	2.44 (0.09)	1.74 (0.05)	1.55 (0.02)
ΔH_o (kcal/mol)	− 9.36 (1.11)	− 3.66 (0.59)	− 2.35 (0.28)
ΔS_{inc} (cal/mol/k)	6.52 (0.30)	4.50 (0.14)	3.98 (0.05)
ΔS_o (cal/mol/k)	− 20.91 (3.46)	− 4.62 (1.69)	− 0.77 (0.62)

DAAOHs are likely to be somewhat similar (initially), and determination of the 3-dimensional structure of any one of them can give a reasonably good idea of the molecular packing and intermolecular interactions present in the crystal lattice of DAAOHs in the particular series. Interestingly, incremental and end contribution values obtained from second heating thermograms are significantly lower compared to the incremental and end contributions of first heating thermograms (both odd- and even chainlength compounds), which could be due to changes in the molecular packing after the first heating cycle.

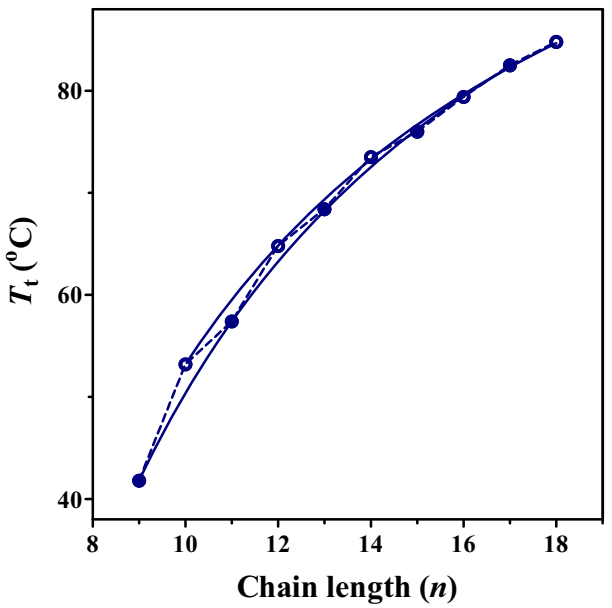

Figure 4. Chainlength dependence of solid-liquid phase transition temperatures (T_t) of DAAOHs. Solid lines correspond to a nonlinear least-squares fit of the transition temperatures to Eq. 8. Filled symbols, odd chainlength compounds; open symbols, even chainlength compounds.

3.3 *Chain length dependence of T_t*

The change in the melting phase transition temperatures (T_t) of DAAOHs in the first heating thermograms is given in Figure 4. The even chainlength DAAOHs have higher T_t values as compared to the odd-chain compounds and within each series, the T_t of DAAOHs increases in a smooth progression with the acyl chainlength, but the differences between the two series decrease with increasing chainlength and after C15 the differences become very small such that the odd-even alternation is not detectable. In general, for many single-chain amphiphiles, T_t values of even chainlength compounds were found to be higher than the odd chainlength compounds,[21,26,27] although some exceptions were reported, e.g., NAAs and L-alanine alkyl esters (AEs).[19,20] The odd-even alternation in the T_t values, enthalpies and entropies in DAAOHs is unusual in that while the even chainlength compounds have higher T_t values, the ΔH_t and ΔS_t values are higher for the odd chainlength compounds. Similar unusual behavior was noticed earlier in AEs.[20]

For compounds with long acyl chains, the end contribution from terminal methyl and the polar head group can be neglected compared to the polymethylene chain portion towards ΔH_t and ΔS_t. Thus, at infinite acyl chainlength, Eqs. (3) and (4) can be reduced to Eqs. (5) and (6), respectively:

$$\Delta H_t = (n-2)\,\Delta H_{inc} \tag{5}$$

$$\Delta S_t = (n-2)\,\Delta S_{inc} \tag{6}$$

Then the T_t for infinite chain length, T_t^{∞}, can be obtained from:

$$T_t^{\infty} = \Delta H_{inc}/\Delta S_{inc} \tag{7}$$

T_t^{∞} values for the NAAOHs have been estimated from the ΔH_{inc} and ΔS_{inc} values presented in Table 2. The

obtained T_t^{∞} for odd- and even chainlength DAAOHs are 101.2 °C (374.2 K) and 113.7 °C (386.7 K), respectively, whereas the T_t^{∞} values obtained for the second heating scans is 116.4 °C (389.4 K).

For many single- and double chain amphiphiles, which show a linear dependence of ΔH_{inc} and ΔS_{inc} on the chain-length, it has been shown that the ΔH_t and ΔS_t values can be fit to the following equation:[28]

$$T_t^{\infty} = \Delta H_t/\Delta S_t = T_t\left[1\left(n_o - n'_o\right)/(n - n_o)\right] \quad (8)$$

where $n_o(= -\Delta H_o/\Delta H_{inc})$ and $n'_o(= -\Delta S_o/\Delta S_{inc})$ are the values of n at which the ΔH_t and ΔS_t are extrapolated to zero. Figure 4 indicates that the T_t values of both odd- and even chainlength DAAOHs obtained from first heating scans fit well to Eq. (8). The T_t^{∞} values obtained for odd- and even chain DAAOHs are 128.9 °C (401.9 K) and 126 °C (399 K), respectively. Similarly, the T_t^{∞} values obtained for odd- and even-chain DAAOHs from second heating thermograms are 130.6 °C (403.6 K) and 122.2 °C (395.2 K), respectively. The T_t^{∞} values obtained for both first and second heating scans of DAAOHs from fitting to Eq. (8) are in good agreement with the T_t^{∞} values estimated using Eq. (7).

3.4 *Comparison of thermodynamic properties of DAAOHs with other diacyl compounds*

It is instructive to compare the thermodynamic parameters associated with the phase transitions of DAAOHs with isomeric NAAEs, as well as with those of homologous DAEs and their isomers, namely the NAGEs. The ΔH_t values of isomeric pair DAAOHs and NAAEs are shown in Figure 5A, and those of the other isomeric pair, namely NAGEs and DAEs are given in Figure 5B. As can be seen from this figure, ΔH_t values of DAAOHs and DAEs are low as compared to the isomeric NAAEs and NAGEs, respectively (although minor differences are observed in even chainlength DAEs at higher chainlength). This indicates that the functional group position plays a key role in the phase transition properties between the isomeric compounds. The ΔH_t values show clear distinction among the four series at lower chainlength. However, the distinction is reduced at higher chainlength due to partial overlap. This complex nature can be understood by comparing their incremental values (ΔH_{inc}) and end contributions (ΔH_o) given in Table 3. If the partial overlap at higher chainlengths is ignored, the ΔH_t values of four series follows the order: NAGEs

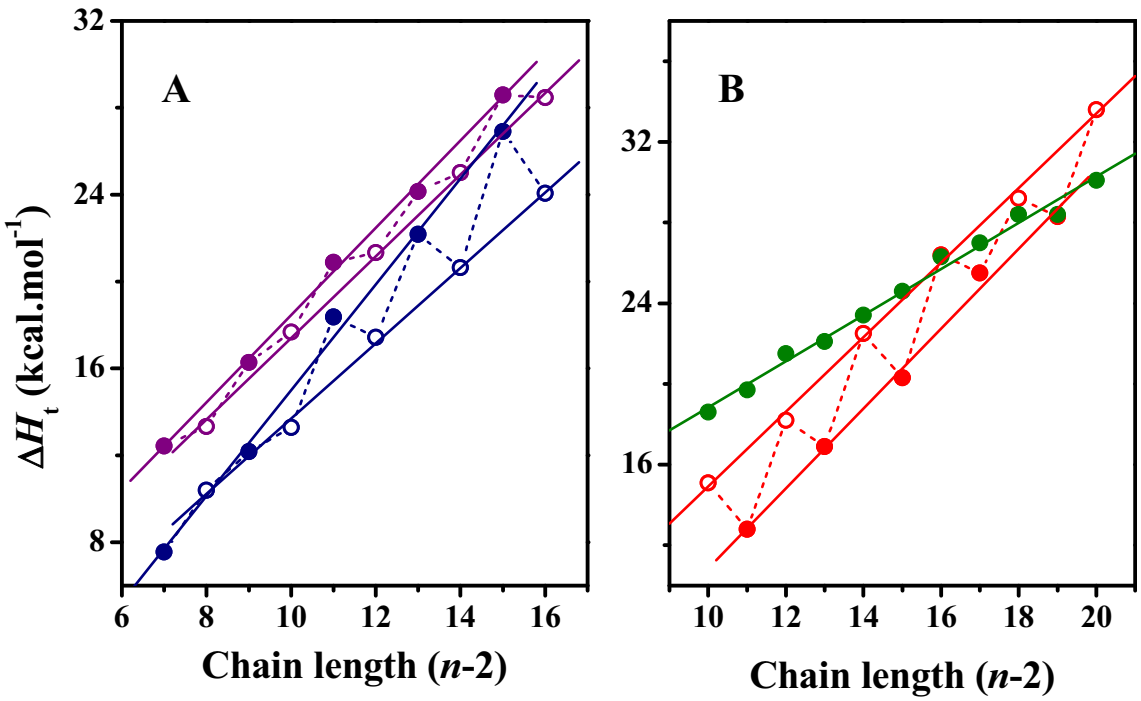

Figure 5. Chain length dependence of transition enthalpies. (**A**) NAAEs (●) and DAAOHs (●). (**B**) NAGEs (●) and DAEs (●). Filled circles, odd chainlength compounds; open circles, even chainlength compounds. Values of ΔH_t were plotted against the number of CH_2 groups in the acyl chains (n-2). Solid lines correspond to linear least-squares fits of the data. For more details, see the text.

Table 3. Incremental values of transition enthalpies (ΔH_{inc}), end contribution (ΔH_o), and transition temperature at infinite chainlength (T_t^{∞}) for NAGEs, DAEs, NAAEs, and DAAOHs.

Lipid	ΔH_{inc} (kcal/mol)	ΔH_o (kcal/mol)	T_t^{∞} (K) Eq. 7	T_t^{∞} (K) Eq. 8	References
NAGEs	1.19 (0.03)	10.16 (0.38)	442.4	409.8	[13]
DAEs (even chainlength)	1.84 (0.04)	0.13 (0.66)	402.6	407.2	[14]
DAEs (odd chainlength)	1.98 (0.09)	− 4.98 (1.19)	396.0	407.2	[14]
NAAEs (odd chainlength)	2.01 (0.05)	− 1.64 (0.59)	400.4	404.8	[11]
NAAEs (even chainlength)	1.88 (0.05)	− 1.39 (0.57)	406.9	402	[11]
DAAOHs (odd chainlength)	2.44 (0.09)	− 9.36 (1.11)	374.2	401.9	Present study
DAAOHs (even chainlength)	1.74 (0.05)	− 3.66 (0.59)	386.7	399	Present study

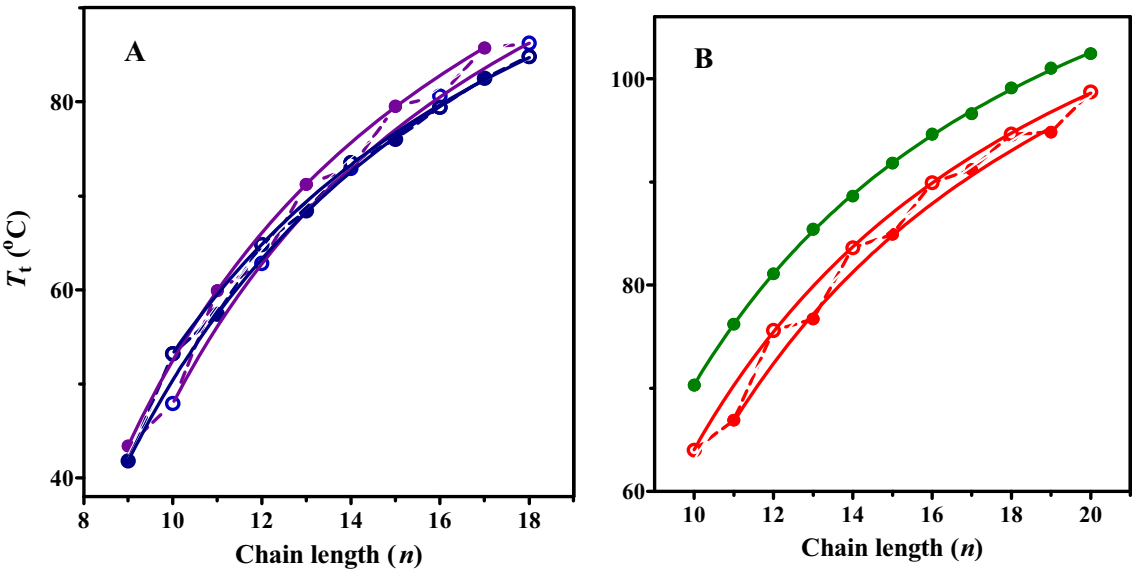

Figure 6. Chainlength dependence of transition temperatures, T_t of different two-chain amphiphiles. (**A**) NAAEs (●) and DAAOHs (●). (**B**) NAGEs (●) and DAEs (●). Filled symbols, odd chainlength compounds; open symbols, even chainlength compounds. Solid lines correspond to nonlinear least-squares fits of the data. For more details, see the text.

> $DAEs_{even}$ = $NAAEs_{odd}$ > $NAAEs_{even}$ > $DAAOHs_{odd}$ > $DAEs_{odd}$ > $DAAOHs_{even}$.

Similarly, a comparison of T_t values of the four series is shown in Figure 6. Chainlength dependence of T_t values of isomeric NAAEs and DAAOHs is shown in Figure 6A, whereas the corresponding plots of NAGEs and DAEs are given in Figure 6B. Similar to the transition enthalpies, the transition temperatures of NAGEs and NAAEs are higher compared to isomeric DAEs and DAAOHs. The difference in T_t values is more distinct at all chainlengths between NAGEs and DAEs, but less so between NAAEs and DAAOHs. The T_t values of the four series are in the following order: NAGEs > $DAEs_{even}$ > $DAEs_{odd}$ > $NAAEs_{odd}$ > $DAAOHs_{even}$ ~ $NAAEs_{even}$ ~ $DAAOHs_{odd}$. The noticed differences could be due to the differential contributions arising from polyethylene chains and end contributions. The T_t^{∞} calculated from Equations 7 and 8 are given in Table 3. Although the T_t^{∞} values obtained show good agreement with the order mentioned above, few differences are observed in case of $DAEs_{odd}$ (Eq. 7) and $DAAOHs_{odd}$ (Eq. 8). These exceptions can be rationalized in terms of molecular packing and intermolecular interactions if crystal structures of several compounds (of both odd and even chainlengths) are determined from each series.

Further, odd-even alternation in ΔH_t (as well as ΔS_t and T_t) of homologous series of single and double chain lipids was explained by differences in the packing of terminal methyl groups of odd- and even chainlength compounds.[27] If the hydrocarbon chains are aligned perpendicular to the plane of the terminal methyl groups, such alteration is not observed. On the

other hand, if the acyl/alkyl chains are tilted with respect to the plane of the terminal methyl groups, the packing is different for the odd- and even-chain compounds and thus leads to changes in the physical properties. This can be seen in Table 3, where the end contribution (ΔH_o) is much different for the four series. Although incremental values of NAGEs are low as compared to isomeric DAEs, due to the significant contribution of terminal methyl groups and the central polar moiety of NAGEs (0-1° tilt angle, untilted bilayer packing), NAGEs have shown higher ΔH_t than isomeric DAEs (32-33° tilt angle, tilted bilayer packing).[13,14] Similarly, though incremental values of NAAEs and DAAOHs are comparable, due to lesser end contributions in DAAOHs, NAAEs have higher ΔH_t than isomeric DAAOHs.

3.5 *PXRD and molecular packing*

Since we could not obtain crystals of DAAOHs that are suitable for single-crystal X-ray diffraction studies, we carried out PXRD studies to derive structural information on these compounds. The PXRD data obtained for odd- and even-chain DAAOHs are shown in Figures 7A and B, except for the C9 compound. All the other DAAOHs (C10−C18) gave several sharp diffraction peaks in the 2θ range of 1−30°. From the diffraction peak positions, the average *d*-spacings were calculated using 3−4 peaks for each DAAOH. The average *d*-spacings obtained are given in Table S5 (SI), and the chainlength dependence of the *d*-spacing is shown in Figure 7C. The *d*-spacing data exhibit a linear dependence on the chainlength, independently for the even- and odd acyl chainlength series with slopes of 0.82 and 0.79Å/CH_2, respectively. The C11 compound which is an outlier was omitted from the fit of the odd chainlength series. Since the estimated increment in the *d*-spacing for each C−C bond in an untilted chain is 1.27 Å/CH_2, the smaller incremental values obtained for DAAOHs suggest that the acyl chains are tilted with respect to the bilayer normal. The value of 0.82 Å for an increase in *d*-spacing per CH_2 for DAAOH is lower than the value of 0.88 Å/CH_2 obtained for the isomeric NAAEs,[11] and suggests that the acyl chains in DAAOHs are more tilted as compared to the chains in NAAEs. While NAGEs are packed in a normal, untilted bilayer packing with the *d*-spacing increment of 1.28 Å/CH_2,[13] the isomeric DAEs are packed in a tilted bilayer.[14] Similar to

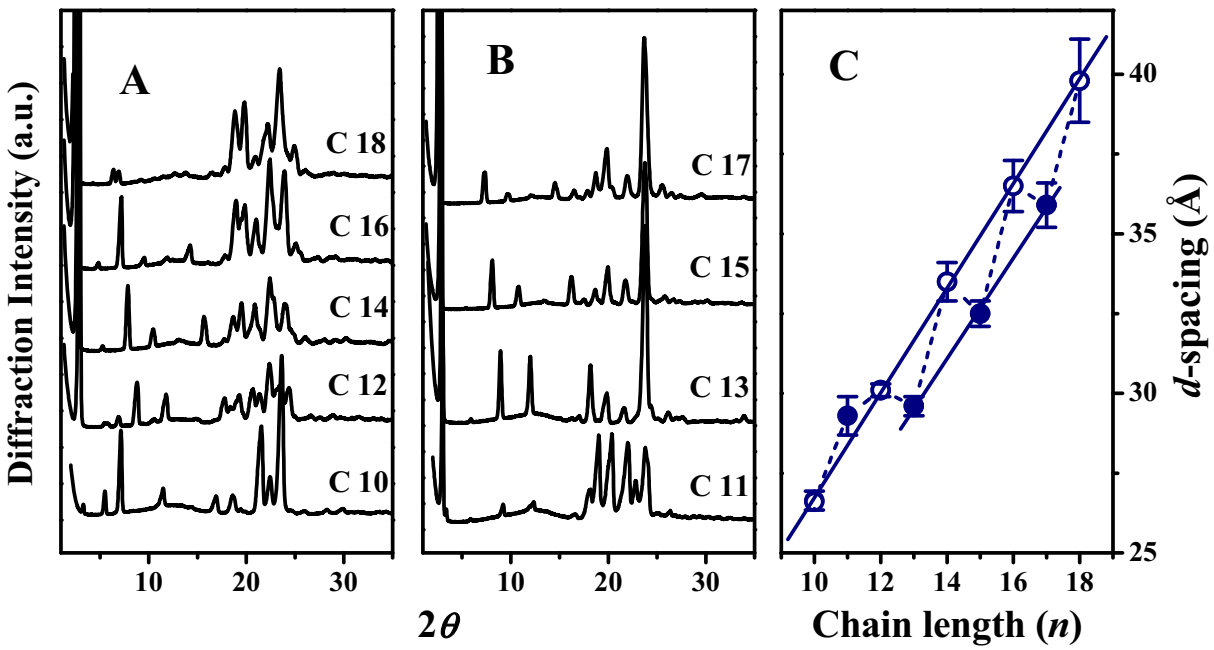

Figure 7. Powder X-ray diffraction patterns of DAAOHs with different saturated acyl chains (**A**, **B**) and dependence of *d*-spacings on the chain length (**C**). The number of C-atoms in the acyl chain is indicated against each PXRD profile. Filled symbols, odd chainlength compounds; open symbols, even chainlength compounds. The solid lines in C represent linear least-squares fit of the data. Data corresponding to C11 compound was omitted from the linear fit as it is an outlier.

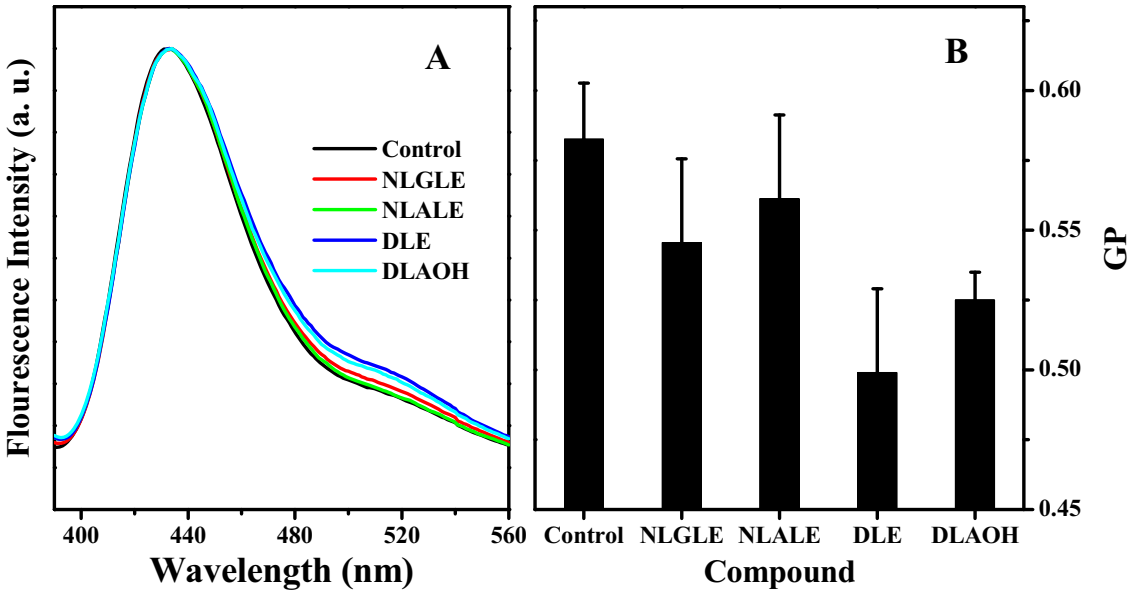

Figure 8. (**A**) Emission spectra of Laurdan in stratum corneum model (SCM) lipid mixture and SCM containing 20 mol% NLGLE, NLALE, DLE, or DLAOH. (**B**) Comparison of Laurdan GP values for the different samples. See text for details.

DAAOHs, DAEs, and NAAEs, dimyristoylphosphatidylglycerol (DMPG) and cerebroside also have tilted bilayer packing.[29,30]

3.6 *Laurdan GP studies on stratum corneum model membranes*

To monitor the change in fluidity, we determined the generalized polarization (GP) of Laurdan for SCM lipid mixture and SCM lipid mixtures to which 20 mol% of DLAOH, DLE, NLALE, or NLGLE was added, which results in 16.7% mol% of the added lipid while the relative proportion of the SCM lipids remains constant. Laurdan is a phase-sensitive dye and shows distinct emission maxima in the gel phase (430-440 nm) and fluid phase (>470 nm).[18] Since the decrease in GP indicates increase in fluidity, which can be correlated to the permeability of the membrane. In the present case, SCM and SCM containing DLAOH, DLE, NLALE, or NLGLE have shown emission maximum at 433 nm (Figure 8A). Upon addition of any of these to the SCM lipid mixture, we noticed a small to moderate decrease in emission intensity at ~490 nm in both cases. Values of laurdan GP calculated from the fluorescence spectral data using eq. 2 are shown in Figure 8B. The results presented in Figs. 8A and 8B reveal that the SCM fluidity is lower for membranes containing DLE and DLAOH compared to isomeric NLGLE and NLALE, respectively. Although, as discussed above, the general trends in the physical properties of these four classes of compounds are broadly similar, the present results on their interaction with stratum corneum model membranes suggest that they may exhibit important differences in their specific interaction with other membrane lipids, which in turn modulate the membrane fluidity. Importantly, these results also indicate that membranes containing *N*, *O*-diacylethanolamines (DAEs) and *N*, *O*-diacyl-L-alaninols (DAAOHs) exhibit higher potential as chemical enhancers for increasing the permeability of SC membranes.

4. Conclusions

In the present work, we report the synthesis and characterization of a homologous series of *N*-, *O*-diacyl alaninols (DAAOHs) of matched acyl chains (n = 9–18). Similar to isomeric NAAEs, DAAOHs displayed an unusual odd-even alternation in transition enthalpies and entropies, with the odd-chainlength compounds exhibiting higher values than the even-chainlength ones. Odd-even alternation was also observed in the transition temperatures of DAAOHs, with the odd-chainlength compounds exhibiting higher values. Powder XRD studies revealed that DAAOHs adopt tilted bilayer packing, which is similar to the isomeric NAAEs. However, DAAOHs were more tilted than NAAEs. Incorporation of *N*, *O*-dilauroylethanolamine (DLE) and *N*, *O*-dilauroyl-L-alaninol (DLAOH) into stratum corneum model membranes decreased the membrane fluidity more than that observed with NAGE and NAAE with

lauroyl chains, suggesting that DAEs and DAAOHs would be better candidates than NAGEs and NAAEs as chemical enhancers in the design of transdermal drug delivery systems. However, further evaluation by permeability studies is required in order to verify this possibility, which will be taken up in our future studies.

Supplementary Information (SI)

Representative FTIR, ^{1}H-NMR, ^{13}C-NMR, and HRMS spectra of *N*, *O*-dilauroyl-L-alaninol (DLAOH) are given in Figures S1–S4. Corresponding spectral data for all DAAOHs (n = 9-18) are given in Tables S1–S4. DSC thermograms for the first cooling scan and second heating scan are given in Figure S5 and S6, respectively. Chain-length dependence of transition enthalpies and entropies are given in Figure S7, and chainlength dependence of transition temperatures from second heating thermograms is given in Figure S8. Supplementary Information is available online at www.ias.ac.in/chemsci.

Acknowledgments

This work was supported by a research Grant from the DST (India) to MJS. DS was supported by a Senior Research Fellowship from the CSIR (India). SKC acknowledges a non-NET fellowship from University Grants Commission (UGC) (India). UGC is acknowledged for their support through the UPE and CAS programs to the University of Hyderabad and School of Chemistry. University of Hyderabad is an Institution of Eminence of the UGC (India).

Declaration

Conflict of interest The authors declare no conflict of interest for this work.

References

1. Kailash V, Pratibha C, Mahavir G, Ashwini P and Mangesh K 2013 Transdermal delivery: A recent trend in treatment of chronic diseases *BioMedRx* **1** 473
2. Meer S, Tahir M A and Abbasi M S A 2020 Formulation-based technology advancements in transdermal drug delivery system *Asian J. Res. Derm. Sci.* **3** 20
3. Elias P M 1983 Epidermal lipids, barrier function, and desquamation *J. Invest. Dermatol.* **80** 44s
4. Sahle F F, Gabre-Mariam T, Dobner B, Wohlrab J and Neubert R H H 2015 Skin diseases associated with the depletion of stratum corneum lipids and stratum corneum lipid substitution therapy *Skin Pharmacol. Physiol.* **28** 42
5. Bonte F, Pinguet P, Chevalier J M and Meybeck A 1995 Analysis of all stratum corneum lipids by automated multiple development high-performance thin-layer chromatography *J. Chromatogr.* **664** 311
6. Holleran W H, Takagi Y and Uchida Y 2006 Epidermal sphingolipids: Metabolism, function, and roles in skin disorders *FEBS Lett.* **580** 5456
7. Haque T and Talukder M M U 2018 Chemical enhancer: A simplistic way to modulate barrier function of the stratum corneum *Adv. Pharm. Bull.* **8** 162
8. Pham Q D, Bjorklund S, Engblom J, Topgaard D and Sparr E 2016 Chemical penetration enhancers in stratum corneum—Relation between molecular effects and barrier function *J. Control. Rel.* **232** 175
9. Karande P and Mitragotri S 2009 Enhancement of transdermal drug delivery via synergistic action of chemicals *Biochim. Biophys. Acta* **1788** 2362
10. Vavrova K, Hrabalek A, Dolezal P, Holas T and Zbytovska J 2003 L-serine and glycine based ceramide analogs as transdermal permeation enhancers: Polar head size and hydrogen bonding *Bioorg. Med. Chem. Lett.* **13** 2351
11. Sivaramakrishna D and Swamy M J 2015 Differential scanning calorimetric and powder X-ray diffraction studies on a homologous series of *N*-acyl-L-alanine esters with matched chains (n = 9–18) *J. Chem. Sci.* **127** 1627
12. Lande M B, Donovan J M and Zeidel M L 1995 The relationship between membrane fluidity and permeabilities to water, solutes, ammonia, and protons *J. Gen. Physiol.* **106** 67
13. Reddy S T and Swamy M J 2017 Molecular structure, supramolecular organization, and thermotropic phase behavior of *N*-acylglycine alkyl esters with matched acyl and alkyl chains *Chem. Phys. Lipid.* **208** 43
14. Kamlekar R K, Tarafdar P K and Swamy M J 2010 Synthesis, calorimetric studies and crystal structures of N, O-diacylethanolamines with matched chains *J. Lipid. Res.* **51** 42
15. Sivaramakrishna D and Swamy M J 2016 Synthesis, characterization and thermotropic phase behavior of a homologous series of N-acyl-L-alaninols and interaction of N-myristoyl L-alaninol with dimyristoylphosphatidylcholine *Chem. Phys. Lipid.* **196** 5
16. Marsh D 1990 *Handbook of Lipid Bilayers* (Boca Raton, FL: CRC Press)
17. Sivaramakrishna D, Prasad M D and Swamy M J A 2019 homologous series of apoptosis-inducing N-acylserinols: Thermotropic phase behavior, interaction with cholesterol and characterization of cationic N-myristoylserinol-cholesterol-CTAB niosomes *Biochim. Biophys. Acta* **1861** 504
18. Parasassi T, Krasnowska E K, Bagatolli L and Gratton E 1998 Laurdan and Prodan as polarity-sensitive fluorescent membrane probes *J. Fluoresc.* **8** 375
19. Sivaramakrishna D, Reddy S T, Nagaraju T and Swamy M J 2015 Self-assembly, supramolecular organization, and phase transitions of a homologous series of *N*-acyl-L-alanines (n = 8–20) *Colloid Surf. A: Physicochem. Eng. Asp.* **47** 108
20. Sivaramakrishna D and Swamy M J 2015 Self-assembly, supramolecular organization and phase behavior of L-alanine alkyl esters (n = 9-18) and characterization of equimolar L-alanine lauryl ester/Lauryl sulphate catanionic complex *Langmuir* **31** 9546

21. Ramakrishnan M and Swamy M J 1998 Differential scanning calorimetric studies on the thermotropic phase transitions of N-acylethanolamines of odd chain lengths *Chem. Phys. Lipids* **94** 43
22. Kamlekar RK and Swamy M J 2006 Molecular packing and intermolecular interactions in two structural polymorphs of N-palmitoylethanolamide, a type 2 cannabinoid receptor agonist *J. Lipid Res.* **47** 1424
23. Reddy S T, Krovi K P and Swamy M J 2014 Structure and thermotropic phase behavior of a homologous series of N-acylglycines: Neuroactive and antinociceptive constituents of biomembranes *Cryst. Growth Des.* **14** 4944
24. Tarafdar P K, Reddy S T and Swamy M J 2012 Nonclassical odd-even alternation in mixed chain diacylethanolamines: Implications of polymorphism *Cryst. Growth. Des.* **12** 1132
25. Sivaramakrishna D and Swamy M J 2016 Structure, supramolecular organization and phase behavior of *N*-Acyl-β-Alanines: Structural homologs of mammalian brain constituents N-acylglycine and N-acyl-GABA *Chem. Phys. Lipid.* **201** 1
26. Reddy ST, Tarafdar PK, Kamlekar RK and Swamy MJ 2013 Structure and thermotropic phase behavior of a homologous series of bioactive *N*-acyldopamines *J. Phys. Chem. B* **117** 8747
27. Larsson K 1986 Physical properties–structural and physical characteristics In *The Lipid Handbook* F D Gunstone, J L Harwood and F B Padley (Eds.) (London: Chapman and Hall) pp. 321–384
28. Marsh D 1982 Biomembranes. In: *Supramolecular Structure and Function* G Pifat and J N Herak (Eds.) (New York: Plenum Press) pp. 127–178
29. Pascher I, Sundell S, Harlos K and Eibl H 1987 Conformation and packing properties of membrane lipids: The crystal structure of sodium dimyristoylphosphatidylglycerol *Biochim. Biophys. Acta* **896** 77
30. Pascher I and Sundell S 1977 Molecular arrangements in sphingolipids. The crystal structure of the cerebroside *Chem. Phys. Lipid.* **20** 175

J. Chem. Sci. (2023) 135:103
https://doi.org/10.1007/s12039-023-02222-w

REGULAR ARTICLE

Structure and supramolecular organization of *N*-acylserinols: agonists of the G-protein coupled receptor, GPR-119

SUMAN K CHOUDHURY[a], D SIVARAMAKRISHNA[a,b] and MUSTI J SWAMY[a,*]
[a]School of Chemistry, University of Hyderabad, Hyderabad 500 046, India
[b]Department of Chemistry, School of Science, GITAM (Deemed to be University), Visakhapatnam 530 045, India
E-mail: mjswamy@uohyd.ac.in

Suman K Choudhury and D Sivaramakrishna contributed equally to this study.

MS received 22 June 2023; revised 17 August 2023; accepted 6 September 2023

Abstract. *N*-acyl serinols, the amphiphilic molecules produced by gastrointestinal bacteria regulate metabolic hormone production and glucose homeostasis in the host species, and also exhibit anti-cancer activity. In this study, molecular structure, supramolecular organization and intermolecular interactions of two *N*-acylserinols (NASOHs), *viz.*, *N*-nonanoylserinol (N9SOH) and *N*-pentadecanoylserinol (N15SOH), are determined by single-crystal X-ray diffraction. The molecular structure and packing are compared and discussed with the structurally related molecules, *N*-acylethanolamine (NAE) and *N*-acyl tris (NAT) as NASOHs and NATs are derived by substituting one/two α-hydrogen(s) (with respect to amide N-H) of NAE with hydroxymethyl group(s). Structures of N9SOH and N15SOH were solved in the triclinic system in the *P-1* space group and both molecules are organized in a tilted head-to-head (and tail-to-tail) manner, resembling a bilayer membrane. The acyl chains in N9SOH and N15SOH are tilted by 20.43° and 18.12°, respectively, with respect to the bilayer normal. Several N—H···O, O—H···O, and C—H···O hydrogen bonds between the hydroxyl and amide moieties of the head groups of NASOH molecules belonging to adjacent and opposite layers stabilize the overall supramolecular organization. These results suggest that the α-hydroxymethyl groups exhibit considerable influence on the crystal structure, molecular packing, and phase structure of these amphiphiles.

Keywords. *N*-acylserinol; single-crystal X-ray diffraction; molecular packing; hydrogen bonding.

1. Introduction

Mammals have co-evolved along with diverse microbial species that colonize cutaneous and mucosal surfaces of the gastrointestinal tract, which are supported by diet.[1,2] Many (patho)physiological processes of the mammalian hosts are profoundly affected by the gut microbiota, such as mucosal immunity, vitamin biosynthesis, inflammatory bowel disease, and colorectal cancer.[3–7] Recently, the expression of *N*-acyl amide synthase genes has been reported in gastrointestinal bacteria, and the lipids encoded by these genes interact with G protein-coupled receptors (GPCRs) that regulate the physiology of the gastrointestinal tract.[8] *N*-acylserinols are one of the six *N*-acyl amide families isolated from gastrointestinal bacteria.[9,10]

In an interesting study, Brady and co-workers discovered that bacterial lipid products can modulate the activity of host GPCRs: for instance, *N*-oleoyl serinol is a GPR119 agonist able to modulate glucagon-like peptide 1 (GLP1) secretion and glucose homeostasis.[9] They also identified several *N*-acyl synthase (NAS) genes and cloned and expressed them in *E. coli*. *N*-oleoyl serinol derived from bacteria such as *Gemella spp*. was shown to activate GPR119 with similar potency to the endogenous ligand, oleoylethanolamide.

*For correspondence

Supplementary Information: The online version contains supplementary material available at https://doi.org/10.1007/s12039-023-02222-w.

Published online: 13 October 2023

In this direction, Hu and co-workers identified a new bacterial NAS that could effectively synthesize *N*-acylserinols, which exhibit GPR119 agonist activity in the bacterium *E. coli* Nissle1917.[11] GPR119 is an attractive therapeutic target for diabetes and obesity because this receptor affects, among others, glucose homeostasis through the release of GLP1.

In recent times, synthetic single-tailed amphiphiles have gained importance due to their ability to form various supramolecular assemblies, including vesicles with high application potential in various fields.[12–14] The bilayer thickness or mode of packing in these assemblies can be affected by both the head and tail groups of amphiphiles and modulated by various additives. Researchers have observed differences in bilayer thickness for amphiphiles, which differ in the head group structure but have identical hydrocarbon chains. Similarly, changes in the head group may affect the molecular packing by modulating the chain tilt and/or adopting interdigitated chain packing.[15–30] In this study, we discuss the structural analysis of two *N*-acylserinols (with 9 and 15 C-atoms in the acyl chain) and compare the results with those obtained with *N*-acylethanolamines[31] and *N*-acyltris[19] with the objective of understanding the influence of α-hydroxymethyl groups on the molecular structure and supramolecular organization (Figure 1). Previous work on the preparation and characterization of niosomes containing NASOHs suggests that these compounds could be useful in developing nanocarriers for the delivery of drugs and therapeutics.[20] In view of this, the precise structure of NASOHs at the atomic level will be helpful for a better understanding of the physicochemical properties and molecular assembly of these bioactive amphiphiles with potential applications.

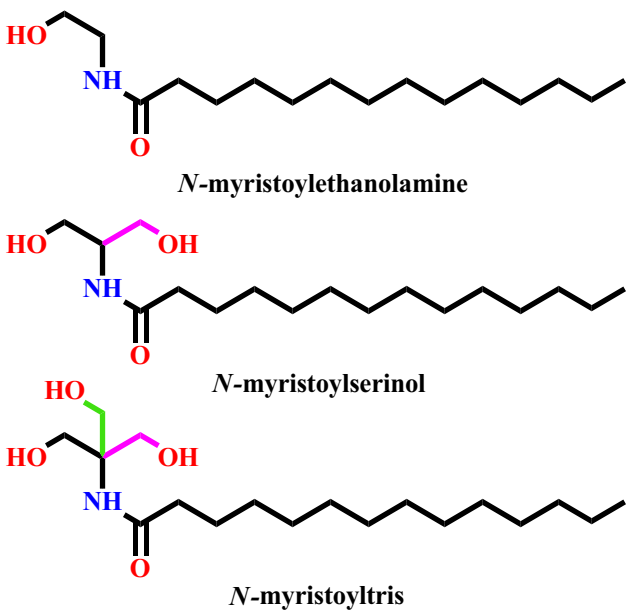

Figure 1. Structures of *N*-myristoylethanolamine, *N*-myristoylserinol and *N*-myristoyltris.

2. Materials and methods

2.1 *Materials*

Serinol and long-chain fatty acids (n = 9, 15) were purchased from Sigma-Aldrich (St. Louis, MO, USA). Oxalyl chloride was purchased from Merck (Mumbai, India). Solvents and other reagents were obtained from Sisco Research Laboratories (Mumbai, India) and were of the highest purity.

2.2 *Synthesis of N-acylserinols*

N-nonanoylserinol (N9SOH) and *N*-pentadecanoylserinol (N15SOH) were prepared as reported in our previous study.[20] Briefly, the fatty acids were converted to corresponding acid halides by reacting with oxalyl chloride. Then, the acid chloride was added to the solution containing serinol (1.1 mmol) and triethylamine (1.1 mmol) in a mixture of methanol:dichloromethane (1:3 v/v) at 0 °C and the reaction mixture was stirred continuously for 3 h. The solvent was removed by reduced pressure, and the final product was obtained by recrystallization followed by column chromatography. The purified products were characterized by various spectroscopic techniques (FT-IR, ^{1}H and ^{13}C-NMR) as well as by high-resolution mass spectrometry, and the results were consistent with those reported in our previous study.[20]

2.3 *Crystallization*

Thin plate-type, colorless single crystals of N9SOH and N15SOH were grown at room temperature from dichloromethane containing a trace of methanol. X-ray diffraction data was collected at liquid nitrogen temperature (~112 K) for N9SOH and at room temperature (~293 K) for N15SOH on an Xtlab Synergy Rigaku Oxford diffraction system equipped with a HyPix – 3000 CCD plate detector. Mo-Kα radiation (λ = 0.7107 Å) was used, and the diffraction data were collected in the 2θ range of 2-27° for both samples.

2.4 *Structure solution and refinement*

The X-ray diffraction data of N9SOH and N15SOH were processed using CrysAlisPro Version 171.39, XtLAB Synergy Rigaku Oxford Diffraction, and absorption correction was done based on the multi-scan method. The crystal structures were solved and refined using the Olex2-1.3/1.2 program. Both structures were solved in the triclinic crystal system with the *P-1* space group. The corresponding CIF files (deposition numbers 2243212 and 2243213) have been deposited in the Cambridge Crystallographic Data Centre (CCDC).

3. Results and Discussion

Given the interesting biological properties of *N*-acylserinols and their potential in developing lipid-based drug delivery systems such as niosomes, as mentioned in the Introduction, we have taken up biophysical and structural investigations on these amphiphiles. In this direction, in a previous study, we reported on the thermotropic phase behaviour of a homologous series of *N*-acylserinols and the preparation and characterization of niosomes containing these non-ionic lipids.[20] In this study, we report the crystal structures of two *N*-acylserinols, namely N9SOH and N15SOH, and the molecular packing and intermolecular interactions in the solid state.

3.1 *Description of the structure*

Molecular structures of N9SOH and N15SOH, determined by single-crystal X-ray diffraction, are shown in the ORTEPs given in Figures 2A and 2B, respectively, along with the atom numbering for all non-hydrogen atoms. Crystal parameters for these two compounds are given in Table 1. The corresponding atomic coordinates, equivalent isotropic displacements, bond lengths, bond angles, and torsion angles are given in Tables S1-S3 (N9SOH) and S4-S6 (N15SOH).

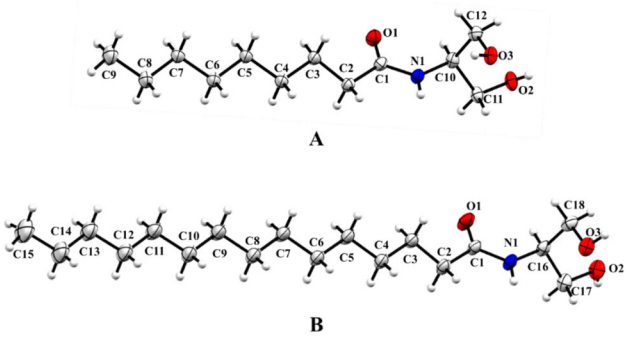

Figure 2. ORTEP diagrams showing the structures of N9SOH (A) and N15SOH (B).

Table 1. Crystallographic data for N9SOH and N15SOH.

Crystal parameter	**N9SOH**	**N15SOH**
Formula	$C_{12}H_{25}NO_3$	$C_{18}H_{37}NO_3$
Formula wt.	231.33	315.49
Crystal system	triclinic	triclinic
T, K	112 (18)	300 (3)
Space group	P-1	P-1
a (Å)	4.8800 (1)	4.8994 (3)
b (Å)	5.9777 (1)	5.9650 (6)
c (Å)	24.1131 (7)	35.1240 (3)
α	88.925 (2)	88.322 (7)
β	86.003 (2)	89.359 (5)
γ	72.207 (2)	72.914 (7)
Z	2	2
V ($Å^3$)	668.13 (3)	980.77 (14)
D_{calc} (g cm^{-3})	1.150	1.065
μ (mm^{-1})	0.081	0.071
F(000)	256	352
Total Reflections	3006	3465
Used Reflections	2161	1460
Parameters	148	202
GOF	1.018	0.973
R indices	R1 = 7.69	R1= 18.04
(all data)	wR2 = 18.52	wR2 = 33.49
Final *R* indices	R1 = 5.19	R1 = 9.63
	wR2 = 16.51	wR2 = 33.49

These data show that the hydrocarbon portions of the acyl chains of both N9SOH (C2-C9) and N15SOH (C2-C15) are in *all-trans* conformation (Figure 2A and 2B), with all the torsion angles being ~180°. The torsion angles corresponding to the N1-C1-C2-C3 unit in N9SOH and N15SOH are 140.1° and 146.5°, respectively. The amide N–H and carbonyl groups are also in trans geometry. The molecular structures of N9SOH and N15SOH are very similar to each other. In the structure of N9SOH, the torsion angles of C1-N1-C10-C11 and C1-N1-C10-C12 linkage are 128.8° and 107°, respectively, and the torsion angles for N1-C10-C11-O2 and N1-C10-C12-O3 units are 178.5° and -64.2°, respectively. Similarly, torsion angles for C1-N1-C16-C17 and C1-N1-C16-C18 linkage in N15SOH are -131° and 104.6°, respectively, and for N1-C16-C17-O2 and N1-C16-C18-O3 units are 179.3° and 64.8°, respectively. This suggests that the additional hydroxymethyl groups of N9SOH (C12-O3) and N15SOH (C18-O3) adopt a particular conformation, resulting in a "Y-like" shape by the NASOHs, whereas NAEs (which do not have any α-hydroxymethyl moiety) adopt an "L-shaped" structure, and NATs (which

have two α-hydroxymethyl moieties) have a "dagger (†) shaped" structure.[19,31]

3.2 *Molecular packing*

Packing diagrams of N9SOH and N15SOH, viewed along the *a*-axis are shown in Figures 3A and 3B, respectively, and those viewed along the *c*-axis are given in Figures S1A and S1B, respectively. Corresponding diagrams viewed along the *b*-axis, are given in Figure S2A and S2B. These diagrams show that N9SOH and N15SOH are packed in a head-to-head (and tail-to-tail) format in stacked bilayers, with each unit cell containing two molecules. Several O-H····O and C-H····O hydrogen bonds that connect adjacent bilayers, as well as and N-H····O, O-H····O and C-H····O hydrogen bonds between adjacent molecules stabilize the molecular packing (see Figure 5 and Figure S4; discussed in detail in Section 3.4). The methyl ends of stacked bilayers are in van der Waals' contacts, with the closest methyl − methyl distance between opposite layers being 3.915 and 3.786 Å in the crystal lattices of N9SOH and N15SOH, respectively. The van der Waals' distances between the methyl groups in the same leaflet are 4.880 and 4.899 Å for N9SOH and N15SOH, respectively. The bilayer thickness (*i.e.*, Me − Me distance) in the crystal lattices of N9SOH and N15SOH are 21.55 Å and 32.57 Å, respectively, and the monolayer (single leaflet) thickness (O3−C12 distance) for N9SOH is 9.79 Å, and for N15SOH (O3-C14 distance) it is 15.26 Å. The repeat distance (*d*-spacing) is 24.05 Å and 35.11 Å for N9SOH and N15SOH, respectively. The *N*-acyl chains are tilted by 20.43° in N9SOH and 18.13° in N15SOH with respect to the bilayer normal (Figure S3, SI). The *N*-acyl/*O*-acyl chains of several other single-chain amphiphiles such as *N*-acyl-β-alanines, *N*-acyl-β-alaninols, and *O*-stearoylethanolamine were also found to be tilted with respect to the bilayer normal.[19,21,27] Interestingly, in the crystal structures of *N*-myristoylglycine and *N*-palmitoylglycine, the acyl chains were found to be essentially parallel to the bilayer normal with tilt angles <1°, which was attributed to the very small head group size in the *N*-acylglycines.[23]

3.3 *Subcell structure and area per molecule*

Hydrocarbon chains in lipid crystals adopt different lateral packing modes, generally described in subcells that specify the relations between equivalent positions within the chain and its neighbors. Based on symmetry considerations, the modes of chain packing have been classified into a small number of subcells: triclinic, monoclinic, orthorhombic, and hexagonal. Within each of these categories the polymethylene planes of the chains can be mutually parallel or perpendicular with respect to their neighbors.[32,33] Careful examination of the acyl chain packing in N9SOH and N15SOH revealed that the subcells in the crystals of both these compounds are of the classic triclinic parallel ($T_{\|}$) type (Figure 4). The unit cell dimensions of these subcells are given in Table 2.

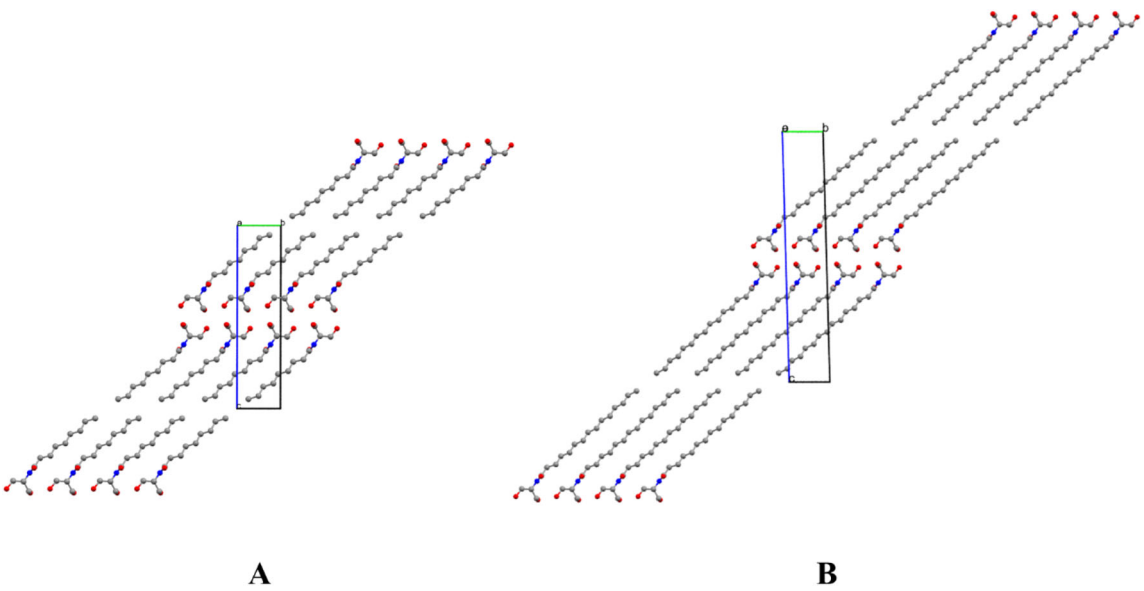

Figure 3. Molecular packing diagrams of N9SOH (A) and N15SOH (B) viewed along the *a*-axis.

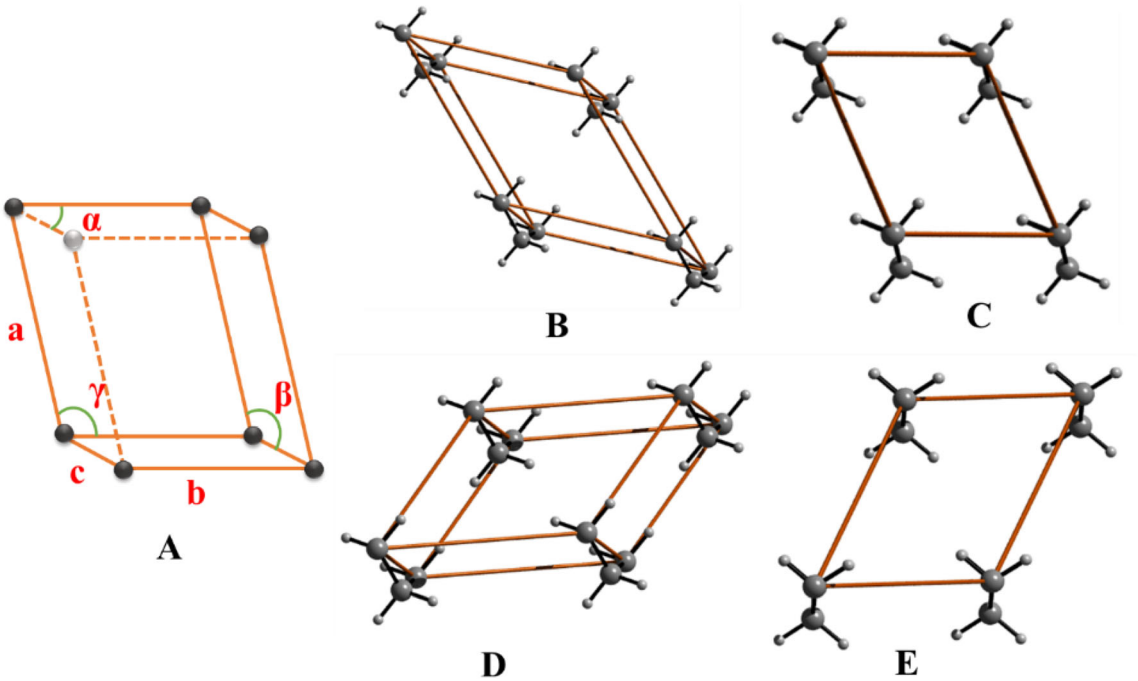

Figure 4. (A) General representation of triclinic unit cell. Subcell packing of (B, C) N9SOH and (D, E) N15SOH. Both subcells belong to the classic triclinic parallel ($T_{\|}$) type.

Table 2. Subcell dimensions of N9SOH and N15SOH.

Cell parameter	N9SOH	N15SOH
a (Å)	6.46	6.51
b (Å)	5.98	5.96
c (Å)	2.54	2.53

3.4 *Hydrogen bonding and intermolecular interaction*

Molecular packing in the crystal structure of N9SOH and N15SOH was carefully examined to understand the intermolecular interactions, which revealed the presence of three types of hydrogen bonds: N-H···O, O-H···O and C-H···O. The H-bonds in N9SOH and N15SOH are shown in Figures 5 and Figure S4, respectively and the bond distances and angles are listed in Table 3.

The H···O distance in the N-H···O bonds and the bond angles subtended at the hydrogen atom for N9SOH and N15SOH are 2.084 Å and 2.114 Å, and 169.9° and 171.1°, respectively. The distance between donor nitrogen and acceptor oxygen atoms for N9SOH and N15SOH are 2.934 and 2.967 Å, respectively. Similar N−H···O hydrogen bonds have been observed in several other amphiphiles bearing *N*-acyl chains, *viz.,* *N*-acyl tris, *N*-acyl β-alaninols, *N*-acylethanolamines and *N*, *O*-diacylethanolamines.[19,21,29,34–36] Besides the N-H···O hydrogen bonds, two strong O-H···O hydrogen bonds are also observed between the hydroxyl O−H and hydroxyl oxygen of adjacent N9SOH molecules (Figure 5). All these hydrogen bonds are identical, with an O−O distance of 2.669 and 2.715 Å, an H···O distance of 1.886 and 1.917 Å, and an O−H···O angle of 159.6 and 164.4°, respectively, for N9SOH, whereas, in N15SOH structure, two strong O-H···O hydrogen bonds are formed between adjacent and opposite N15SOH hydroxyl groups. Adjacent O-H···O hydrogen bonds have H···O distance of 2.001 Å, O···O distance of 2.681 Å, and a bond angle of 139.8° at the hydrogen atom. While O-H···O hydrogen bonds between opposite N15SOH molecules have H···O distance of 1.940 Å, O···O distance of 2.716 Å, and bond angle of 157.5° at the hydrogen atom. Similar O-H···O hydrogen bonds have been observed in the crystal structures of other amphiphiles bearing amide and hydroxy functionalities, e.g., *N*-acylethanolamines, *N*-acyl tris and *N*-acyl-β-alaninols.[19,21,31,34]

In addition to the N−H···O hydrogen bonds, several C−H···O hydrogen bonds are observed in the crystal structures of N9SOH and N15SOH (Figure 5 and Figure S4). In order to identify the C−H···O hydrogen bonds, a cutoff of 3.7 Å was applied for the donor-acceptor distance.[36] Such an analysis revealed that each N9SOH or N15SOH molecule forms two

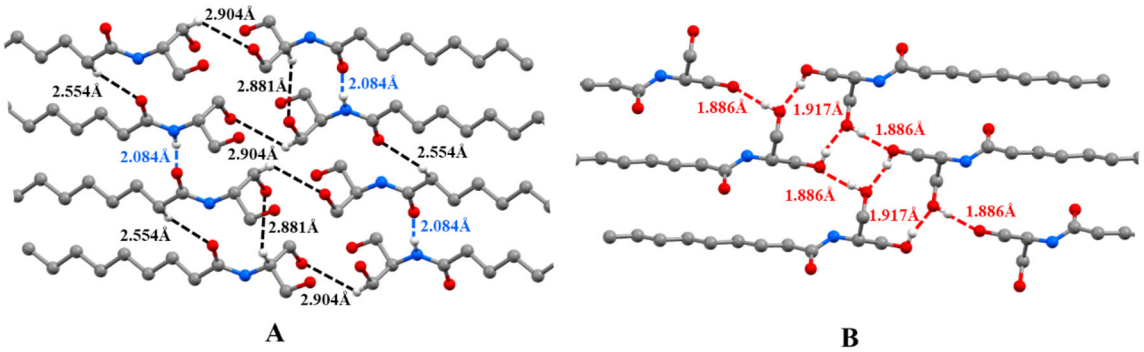

Figure 5. Hydrogen bonding pattern in the crystal lattice of N9SOH. (**A**) N-H···O (----) and C-H···O (----) hydrogen bonds; (**B**) O-H···O (----) hydrogen bonds. In **A**, only alternate N-H···O and C-H···O hydrogen bonds are shown for the sake of clarity. Color code for atoms: gray, carbon; red, oxygen; blue, nitrogen. Hydrogen atoms not involved in H-bonds have been omitted for clarity.

Table 3. Details of hydrogen bond distances and angles in the crystal structures of N9SOH and N15SOH.

Bond	H-O distance (Å)	Donor-acceptor distance (Å)	Bond angle at 'H' (°)
N9SOH			
N-H···O	2.084	2.934	169.9
C-H···O	2.554	3.402	146.0
”	2.881	3.614	132.3
”	2.904	3.554	125.3
O-H···O	1.886	2.669	159.6
”	1.917	2.715	164.4
N15SOH			
N-H···O	2.114	2.967	171.1
C-H···O	2.613	3.423	141.2
”	2.984	3.696	130.4
”	2.973	3.633	126.4
O-H···O	2.001	2.681	139.8
”	1.940	2.716	157.5

C−H···O hydrogen bonds between adjacent N9SOH or N15SOH molecules and one C−H···O hydrogen bond with N9SOH or N15SOH molecules from the opposite layer (similar type/exactly same). The C−H···O H-bonds between adjacent N9SOH molecules have H···O distances of 2.554 and 2.881 Å (H-bond angles are 146.0° and 132.3°, respectively; C·····O distances are 3.402 and 3.614 Å, respectively) and between opposite N9SOH molecules the distance is 2.904 Å (H-bond angle is 125.2°; and C·····O distance is 3.554 Å). Similarly, in N15SOH structure, C−H···O H-bonds between adjacent N15SOH molecules have H···O distances of 2.613 and 2.984 Å (H-bond angles are 141.2° and 130.4°, respectively; the corresponding C·····O distances are 3.423 and 3.696 Å, respectively) and between opposite N15SOH molecule the distance is 2.973 Å (H-bond angle is 126.4°; and C·····O distance is 3.633 Å) (Figure 5 and Figure S4).

3.5 *Structure and supramolecular organization of NAEs, NASOHs, and NATs*

It is pertinent to compare the structure and molecular packing of NASOHs with related single-chain amphiphiles such as NAEs and NATs; this is because while NASOHs have two hydroxy methyl (CH_2OH) groups attached to the C-atom adjacent to the amide N-H moiety, NAEs and NATs have one and three hydroxy methyl groups, respectively, at the same position (Figure 6).

Molecular area: The area per molecule for N9SOH and N15SOH was determined as 29.17 and 29.23 $Å^2$, respectively. These values are considerably higher as compared to the NAEs with 14, 16, and 18 C-atoms in the acyl chain, which have molecular areas in the neighborhood of 22 $Å^2$.[31,34,37] On the other hand, the molecular areas of *N*-acyl tris with 10, 12 and 14 C-atoms are around 39 $Å^2$, which are significantly higher compared to the NASOHs.[19,38]

Molecular packing and chain tilt: Usually, when the headgroup area increases, the molecules of amphiphiles bearing long, saturated alkyl chains adopt a tilted orientation (with respect to the bilayer normal). For example, single crystal XRD studies have shown that *N*-acyl glycines pack in a bilayer with a very low tilt angle (<1°), whereas PXRD measurements indicated that in *N*-acyl alanines, which have a larger head group, the acyl chains pack with a significant tilt (∼41°) in the bilayer structure.[15,23] It is interesting in this context to see that the presence of an additional hydroxymethyl (CH_2OH) group in NAT as compared to NASOHs, which increases the head group area, induces the NAT molecules to adopt an interdigitated structure. Consequently, the tilt angle decreases significantly to 13-16° (for NATs).[19] On the other hand, in NAEs containing one less CH_2OH moiety, the

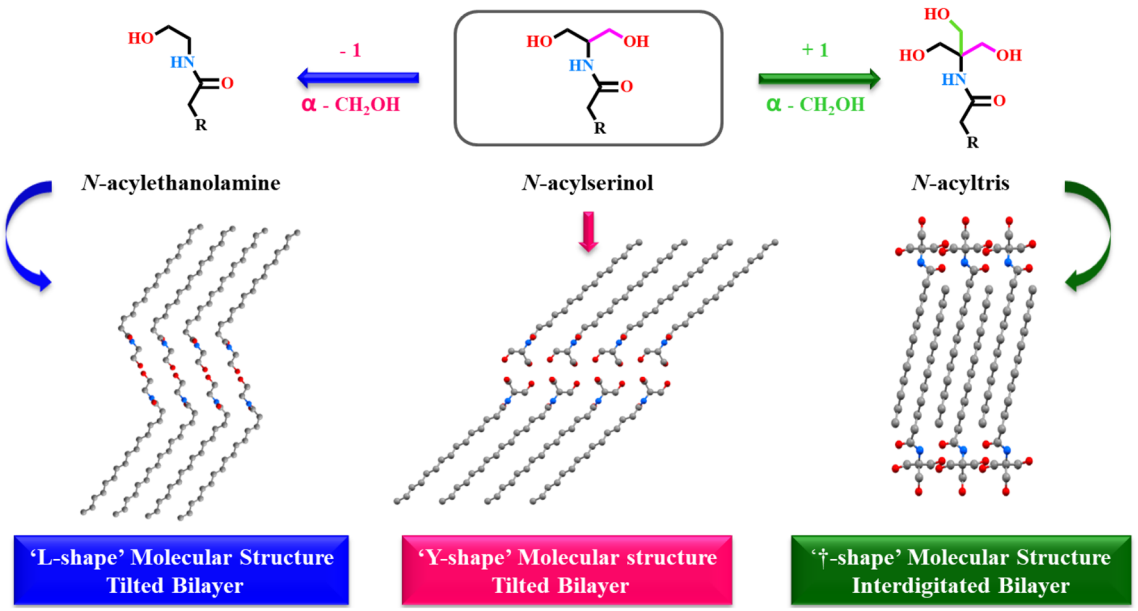

Figure 6. Comparison of the molecular packing of NASOH with NAE and NAT. NASOH has two hydroxymethyl groups attached to the α-carbon atom (with respect to the amide nitrogen). Replacing one of these CH_2OH moieties with a hydrogen atom gives NAE, whereas introducing one more CH_2OH moiety on the α-carbon gives NAT. While both NAE and NASOH adopt a tilted bilayer structure, the larger head group of NAT induces it to adopt an interdigitated bilayer structure due to the presence of an additional hydroxymethyl moiety.

molecules adopt an L-shaped geometry, leading to a tilted orientation of the acyl chain with respect to the bilayer normal.[31,34]

4. Conclusions

In the present study, we report the crystal structures of two homologous *N*-acyl serinols: *N*-nonanoylserinol (N9SOH) and *N*-pentadecanoylserinol (N15SOH). Both structures demonstrate that the NASOH molecules adopt a bilayer-type arrangement with head-to-head (and tail-to-tail) chain packing. This arrangement is stabilized by intermolecular hydrogen bonds between the hydroxy groups of NASOH molecules in the opposite leaflet and between the amide N-H and carbonyl oxygen of adjacent molecules in the same leaflet. Further stabilization is provided by the van der Waals' forces between the acyl chains. The influence of α-hydroxymethyl moieties in the molecular structure (shape) and supramolecular organization (packing) are discussed. These observations will be of considerable relevance in investigating the interaction of NASOHs in designing lipid-based drug delivery systems using them as well as for understanding their interaction with membrane proteins and may provide clues to obtain a molecular-level understanding of their activity as GPR119 agonists.

Supplementary Information (SI)

Four Figures (S1−S4) and six Tables (S1−S6) are given as supplementary material related to this article and are available at www.ias.ac.in/chemsci. In addition, CCDC deposition numbers 2243212 and 2243213 contain the supplementary crystallographic data for this paper.

Acknowledgements

This work was supported by Grant No. UOH-IOE-RC3-21-015 to MJS from the Institution of Eminence project of the University of Hyderabad sanctioned by UGC (India). SKC acknowledges a non-NET fellowship from UGC (India). DS was supported by Senior Research Fellowships from the CSIR (India). UGC (India) is acknowledged for support through the UPE and CAS programs to the University of Hyderabad and the School of Chemistry.

Declarations

Conflict of interest The authors do not have any competing interests in this work.

References

1. Ley R E, Hamady M, Lozupone C, Turnbaugh P J, Ramey R R, Bircher J S, *et al.* 2008 Evolution of mammals and their gut microbes *Wild* **1647** 1647
2. Ley R E, Lozupone C A, Hamady M, Knight R and Gordon J I 2008 Worlds within worlds: evolution of the vertebrate gut microbiota *Nat. Rev. Microbiol.* **6** 776

3. Bäckhed F, Ley R E, Sonnenburg J L, Peterson D A and Gordon J I 2005 Host-bacterial mutualism in the human intestine *Science* **307** 1915
4. Packey C D and Sartor R B 2008 Interplay of commensal and pathogenic bacteria, genetic mutations, and immunoregulatory defects in the pathogenesis of inflammatory bowel diseases *J. Intern. Med.* **263** 597
5. O'Keefe S J D 2008 Nutrition and colonic health: the critical role of the microbiota *Curr. Opin. Gastroen.* **24** 51
6. Peterson D A, Frank D N, Pace N R and Gordon J I 2008 Metagenomic approaches for defining the pathogenesis of inflammatory bowel diseases *Cell Host Microbe* **3** 417
7. Neish A S 2009 Microbes in gastrointestinal health and disease *Gastroenterology* **136** 65
8. Backhed F and Crawford P A 2010 Coordinated regulation of the metabolome and lipidome at the host-microbial interface *Biochim. Biophys. Acta* **1801** 240
9. Cohen L J, Esterhazy D, Kim S H, Lemetre C, Aguilar R R, Gordon E A, *et al.* 2017 Commensal bacteria make GPCR ligands that mimic human signalling molecules *Nature* **549** 48
10. Milshteyn A, Colosimo D A and Brady S F 2018 Accessing bioactive natural products from the human microbiome *Cell Host Microbe* **23** 725
11. Jia J, Chen Y, Xu L, Yang Y, Xu X, Ding H, *et al.* 2021 Screening for bacterial enzymes synthesizing gpr119 agonist in camp-responsive cells *Acta Biochim. Biophys. Sin.* **53** 121
12. Kunitake T 1992 Synthetic bilayer membranes: molecular design, self-organization, and application *Angew. Chem. Int. Ed. Engl.* **31** 709
13. Petkau-Milroy K and Brunsveld L 2013 Supramolecular chemical biology; bioactive synthetic self-assemblies *Org. Biomol. Chem.* **11** 219
14. Gong F, Du N and Hou W 2022 Vesicle formation of single-tailed amphiphilic alkyltrimethylammonium bromides in water induced by dehydration-rehydration *Soft Matter* **18** 2072
15. Sivaramakrishna D, Reddy S T, Nagaraju T and Swamy M J 2015 Self-assembly, supramolecular organization, and phase transitions of a homologous series of *N*-acyl-*L*-alanines (n=8-20) *Colloids Surf. A: Physicochem. Eng. Asp.* **471** 108
16. Sivaramakrishna D and Swamy M J 2015 Self-assembly, supramolecular organization, and phase behavior of *L*-alanine alkyl esters (n = 9-18) and characterization of equimolar *L*-alanine lauryl ester/lauryl sulfate catanionic complex *Langmuir* **31** 9546
17. Sivaramakrishna D and Swamy M J 2016 Structure, supramolecular organization and phase behavior of *N*-acyl-β-alanines: structural homologues of mammalian brain constituents *N*-acylglycine and *N*-acyl-GABA *Chem. Phys. Lipids* **201** 1
18. Sivaramakrishna D and Swamy M J 2016 Synthesis, characterization and thermotropic phase behavior of a homologous series of *N*-acyl-L-alaninols and interaction of *N*-myristoyl-*L*-alaninol with dimyristoylphosphatidylcholine *Chem. Phys. Lipids* **196** 5
19. Sivaramakrishna D, Ravindar C and Swamy M J 2018 Structure, supramolecular organization and thermotropic phase behavior of *N*-acyl tris homologs (n = 9–18): structural analogs of apoptosis inducing ceramides *Chem. Phys. Lipids* **217** 1
20. Sivaramakrishna D, Prasad M D and Swamy M J 2019 A homologous series of apoptosis-inducing *N*-acylserinols: thermotropic phase behavior, interaction with cholesterol and characterization of cationic *N*-myristoylserinol-cholesterol-CTAB niosomes *Biochim. Biophys. Acta* **1861** 504
21. Sivaramakrishna D, Choudhury S K, Cheppali S K and Swamy M J 2021 Structure, thermotropic phase behavior and membrane interaction of *N*-acyl-*β*-alaninols. homologs of stress-combating N-acylethanolamines *Chem. Phys. Lipids* **236** 105056
22. Sivaramakrishna D, Choudhury S K and Swamy M J 2021 Thermotropic phase behavior and supramolecular organization of *N, O*-diacyl-*L*-alaninols: effect on stratum corneum model membrane *J. Chem. Sci.* **133** 91
23. Reddy S T, Krovi K P and Swamy M J 2014 Structure and thermotropic phase behavior of a homologous series of *N*-acylglycines: neuroactive and antinociceptive constituents of biomembranes *Cryst. Growth Des.* **14** 4944
24. Reddy S T and Swamy M J 2015 Synthesis, physicochemical characterization and membrane interactions of a homologous series of *N*-acylserotonins: bioactive, endogenous conjugates of serotonin with fatty acids *Biochim. Biophys. Acta* **1848** 95
25. Reddy S T and Swamy M J 2017 Molecular structure, supramolecular organization and thermotropic phase behavior of *N*-acylglycine alkyl esters with matched acyl and alkyl chains *Chem. Phys. Lipids* **208** 43
26. Reddy S T, Sivaramakrishna D, Mamatha K, Sharma M and Swamy M J 2021 Packing polymorphism, odd-even alternation and thermotropic phase transitions in N-, O-diacylethanolamines with varying *N*-Acyl Chains A combined experimental and computational study *Phys. Chem. Chem. Phys.* **23** 25264
27. Tarafdar P K and Swamy M J 2010 Structure and phase behavior of O-stearoylethanolamine: a combined calorimetric, spectroscopic and X-ray diffraction study *Biochim. Biophys. Acta* **1798** 872
28. Tarafdar P K, Reddy S T and Swamy M J 2013 Effect of Hofmeister series anions on the thermotropic and chaotropic phase behavior of bioactive *O*-acylcholines *J. Phys. Chem. B* **117** 9900
29. Kamlekar R K, Tarafdar P K and Swamy M J 2010 Synthesis, calorimetric studies, and crystal structures of *N*, *O*-diacylethanolamines with matched chains *J. Lipid Res.* **51** 42
30. Swamy M J, Tarafdar P K and Kamlekar R K 2010 Structure, phase behaviour and membrane interactions of *N*-acylethanolamines and *N*-acylphosphatidylethanolamines *Chem. Phys. Lipids* **163** 266
31. Ramakrishnan M and Swamy M J 1999 Molecular packing and intermolecular interactions in *N*-acylethanolamines: crystal structure of *N*-myristoylethanolamine *Biochim. Biophys. Acta* **1418** 261

32. Abrahamsson S, Dahlen B, Löfgren H and Pascher I 1978 Lateral packing of hydrocarbon chains *Prog. Chem. Fats Other Lipids* **16** 125
33. Maulik P R, Ruocco M J and Shipley G G 1990 Hydrocarbon chain packing modes in lipids: effect of altered sub-cell dimensions and chain rotation *Chem. Phys. Lipids* **56** 123
34. Kamlekar R K and Swamy M J 2006 Molecular packing and intermolecular interactions in two structural polymorphs of *N*-palmitoylethanolamine, a type 2 cannabinoid receptor agonist *J. Lipid Res.* **47** 1424
35. Tarafdar P K, Reddy S T and Swamy M J 2012 Non-classical odd-even alternation in mixed-chain diacylethanolamines: Implications of polymorphism *Cryst. Growth Des.* **12** 1132
36. Horowitz S and Trievel R C 2012 Carbon-oxygen hydrogen bonding in biological structure and function *J. Biol. Chem.* **287** 41576
37. Dahlen B, Pascher I and Sundell S 1977 The crystal structure of N-(2-hydroxyethyl)-octadecanoate *Acta Chem. Scand. A* **31** 313
38. Megarajan S, Subramaniyan S B, Muthuswamy S, Anthony S P, Arunachalam J, Moon D and Veerappan A 2018 Synthesis, supramolecular organization and thermotropic phase behaviour of *N*-acyltris(hydroxymethyl)aminomethane *RSC Adv.* **8** 32823

Physicochemical Studies on Amphiphilic Conjugates of Amino Alcohols

by Suman Kumar Choudhury

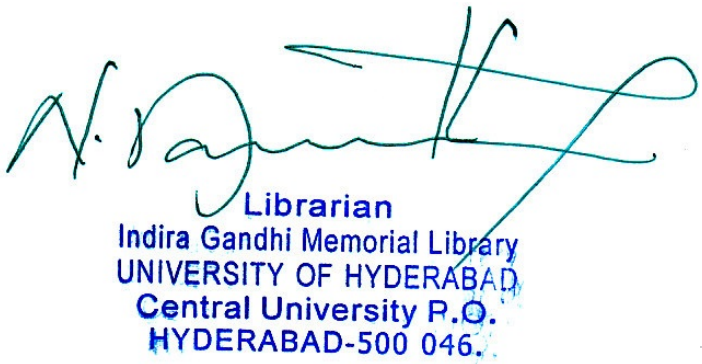

Submission date: 05-Apr-2024 05:15PM (UTC+0530)
Submission ID: 2340673279
File name: chemical_Studies_on_Amphiphilic_Conjugates_of_Amino_Alcohols.pdf (6.88M)
Word count: 33896
Character count: 179898

Physicochemical Studies on Amphiphilic Conjugates of Amino Alcohols

ORIGINALITY REPORT

59%	29%	57%	10%
SIMILARITY INDEX	INTERNET SOURCES	PUBLICATIONS	STUDENT PAPERS

PRIMARY SOURCES

1	Suman Kumar Choudhury, Dokku Sivaramakrishna, Chinapaka Ravindar, Musti J. Swamy. "Biophysical characterization of long chain O-acyl-β-alaninols and equimolar O-myristoyl-β-alaninol/sodium dodecyl sulfate complex", Colloids and Surfaces A: Physicochemical and Engineering Aspects, 2024 Publication	25%
2	www.ias.ac.in Internet Source	14%
3	Suman K Choudhury, D Sivaramakrishna, Musti J Swamy. "Structure and supramolecular organization of N-acylserinols: agonists of the G-protein coupled receptor, GPR-119", Journal of Chemical Sciences, 2023 Publication	9%
4	Submitted to University of Hyderabad, Hyderabad Student Paper	2%

own publication

Prof. Musti J. Swamy
School of Chemistry
University of Hyderabad
Hyderabad – 500 046, India

own publication

Prof. Musti J. Swamy
School of Chemistry
University of Hyderabad
Hyderabad – 500 046, India

own publication

Prof. Musti J. Swamy
School of Chemistry
University of Hyderabad
Hyderabad – 500 046, India

own publication

Prof. Musti J. Swamy
School of Chemistry
University of Hyderabad
Hyderabad – 500 046, India

5	Dokku Sivaramakrishna, Suman Kumar Choudhury, Sudheer K. Cheppali, Musti J. Swamy. "Structure, thermotropic phase behavior and membrane interaction of N-acyl-β-alaninols. Homologs of stress-combating N-acylethanolamines", Chemistry and Physics of Lipids, 2021 Publication	1 %
6	dspace.uohyd.ac.in Internet Source	1 %
7	silo.pub Internet Source	1 %
8	s3.amazonaws.com Internet Source	1 %
9	D. Sivaramakrishna, Musti J. Swamy. " Self-Assembly, Supramolecular Organization, and Phase Behavior of -Alanine Alkyl Esters (= 9–18) and Characterization of Equimolar -Alanine Lauryl Ester/Lauryl Sulfate Catanionic Complex ", Langmuir, 2015 Publication	<1 %
10	S. Thirupathi Reddy, Krishna Prasad Krovi, Musti J. Swamy. " Structure and Thermotropic Phase Behavior of a Homologous Series of -Acylglycines: Neuroactive and Antinociceptive Constituents of Biomembranes ", Crystal Growth & Design, 2014	<1 %

own publication

Prof. Musti J. Swamy
School of Chemistry
University of Hyderabad
Hyderabad – 500 046, India

	Publication	
11	link.springer.com Internet Source	<1 %
12	daneshyari.com Internet Source	<1 %
13	www.jlr.org Internet Source	<1 %
14	D. Sivaramakrishna, Musti J. Swamy. "Structure, supramolecular organization and phase behavior of N-acyl-β-alanines: Structural homologues of mammalian brain constituents N-acylglycine and N-acyl-GABA", Chemistry and Physics of Lipids, 2016 Publication	<1 %
15	S. Thirupathi Reddy, Pradip K. Tarafdar, Ravi Kanth Kamlekar, Musti J. Swamy. " Structure and Thermotropic Phase Behavior of a Homologous Series of Bioactive - Acyldopamines ", The Journal of Physical Chemistry B, 2013 Publication	<1 %
16	Sivaramakrishna D., Ravindar Chinapaka, Musti J. Swamy. "Structure, supramolecular organization and thermotropic phase behavior of N-acyl tris homologs (n = 9–18): Structural analogs of apoptosis inducing	<1 %

ceramides", Chemistry and Physics of Lipids, 2018
Publication

17	www.coursehero.com Internet Source	<1 %
18	D. Sivaramakrishna, Musti J. Swamy. "Synthesis, characterization and thermotropic phase behavior of a homologous series of N-acyl-l-alaninols and interaction of N-myristoyl l-alaninol with dimyristoylphosphatidylcholine", Chemistry and Physics of Lipids, 2016 Publication	<1 %
19	Sanaullah Khan, Deborah S. Teitz, Mohammed Jemal. " Kinetic Analysis by HPLC–Electrospray Mass Spectrometry of the pH-Dependent Acyl Migration and Solvolysis as the Decomposition Pathways of Ifetroban 1- -Acyl Glucuronide ", Analytical Chemistry, 1998 Publication	<1 %
20	ibdigital.uib.cat Internet Source	<1 %
21	Pradip K. Tarafdar, S. Thirupathi Reddy, Musti J. Swamy. " Effect of Hofmeister Series Anions on the Thermotropic Phase Behavior of Bioactive -Acylcholines ", The Journal of Physical Chemistry B, 2013	<1 %

	Publication	
22	id.scribd.com Internet Source	<1 %
23	S. Thirupathi Reddy, Musti J. Swamy. "Molecular Structure, Supramolecular Organization and Thermotropic Phase Behavior of N -Acylglycine Alkyl Esters with Matched Acyl and Alkyl Chains", Chemistry and Physics of Lipids, 2017 Publication	<1 %
24	repositorio.ufjf.br Internet Source	<1 %
25	Submitted to University of Sydney Student Paper	<1 %
26	rupress.org Internet Source	<1 %
27	Submitted to Glendale Union High School District Student Paper	<1 %
28	mafiadoc.com Internet Source	<1 %
29	docksci.com Internet Source	<1 %
30	Chinapaka Ravindar, S. Thirupathi Reddy, Dokku Sivaramakrishna, Deepthi Priyanka Damera, Musti J. Swamy. "Base-triggerable	<1 %

	lauryl sarcosinate–dodecyl sulfate catanionic liposomes: structure, biophysical characterization, and drug entrapment/release studies", Soft Matter, 2022 Publication	
31	sipeg.unj.ac.id Internet Source	<1 %
32	vbook.pub Internet Source	<1 %
33	vdoc.pub Internet Source	<1 %
34	fastercapital.com Internet Source	<1 %
35	idoc.pub Internet Source	<1 %
36	studymind.co.uk Internet Source	<1 %
37	Submitted to Universidad TecMilenio Student Paper	<1 %
38	S. Thirupathi Reddy, Dokku Sivaramakrishna, Keerthi Mamatha, Manju Sharma, Musti J Swamy. "Packing polymorphism, odd-even alternation and thermotropic phase transitions in N-, O-diacylethanolamines with varying N-acyl chains. A combined	<1 %

experimental and computational study", Physical Chemistry Chemical Physics, 2021
Publication

39 D SIVARAMAKRISHNA, MUSTI J SWAMY. "Differential scanning calorimetric and powder X-ray diffraction studies on a homologous series of N-acyl-L-alanine esters with matched chains (n = 9-18)", Journal of Chemical Sciences, 2015 <1%
Publication

40 www.jove.com <1%
Internet Source

41 Dokku Sivaramakrishna, Suman Kumar Choudhury, Musti J Swamy. "Thermotropic phase behavior and supramolecular organization of N,O-diacyl-l-alaninols: effect on stratum corneum model membrane", Journal of Chemical Sciences, 2021 <1%
Publication

42 S. Thirupathi Reddy, D. Sivaramakrishna, Musti J. Swamy. "Physicochemical characterization of lauryl glycinate-dodecyl sulfate equimolar complex: A base-triggerable catanionic liposomal system", Colloids and Surfaces A: Physicochemical and Engineering Aspects, 2017 <1%
Publication

pureadmin.uhi.ac.uk

43	Internet Source	<1%
44	smkxxy.hutc.zj.cn Internet Source	<1%
45	www.repositorio.ufop.br Internet Source	<1%
46	D. Sivaramakrishna, S. Thirupathi Reddy, Thejaswi Nagaraju, Musti J. Swamy. "Self-assembly, supramolecular organization, and phase transitions of a homologous series of N-acyl-l-alanines (n=8–20)", Colloids and Surfaces A: Physicochemical and Engineering Aspects, 2015 Publication	<1%
47	David Dunér, Christophe Malaterre, Wolf Geppert. "The history and philosophy of the Origin of Life", International Journal of Astrobiology, 2016 Publication	<1%
48	repository.guildhe.ac.uk Internet Source	<1%
49	Sengan Megarajan, Siva Bala Subramaniyan, Sureshan Muthuswamy, Savarimuthu Philip Anthony et al. " Synthesis, supramolecular organization and thermotropic phase behaviour of -	<1%

acyltris(hydroxymethyl)aminomethane ", RSC Advances, 2018
Publication

50	huggingface.co Internet Source	<1 %
51	ndl.ethernet.edu.et Internet Source	<1 %
52	open.library.ubc.ca Internet Source	<1 %
53	www.scielo.br Internet Source	<1 %
54	Fabíola Silva Garcia Praça, Wanessa Silva Garcia Medina, Josimar O. Eloy, Raquel Petrilli et al. "Evaluation of critical parameters for in vitro skin permeation and penetration studies using animal skin models", European Journal of Pharmaceutical Sciences, 2018 Publication	<1 %
55	Submitted to Miva Open University Student Paper	<1 %
56	Santanu Bhattacharya, Saubhik Haldar. "Interactions between cholesterol and lipids in bilayer membranes. Role of lipid headgroup and hydrocarbon chain–backbone linkage", Biochimica et Biophysica Acta (BBA) - Biomembranes, 2000 Publication	<1 %

57	Submitted to University of Sheffield Student Paper	<1%
58	berlmathges.de Internet Source	<1%
59	core.ac.uk Internet Source	<1%

Exclude quotes	On	Exclude matches	< 14 words
Exclude bibliography	On		